



**HAL**  
open science

## Ca<sup>2+</sup> handling in a mice model of CPVT

Yueyi Wang

► **To cite this version:**

Yueyi Wang. Ca<sup>2+</sup> handling in a mice model of CPVT. Cardiology and cardiovascular system. Université Paris-Saclay, 2016. English. NNT: 2016SACLS156 . tel-01552304v1

**HAL Id: tel-01552304**

**<https://theses.hal.science/tel-01552304v1>**

Submitted on 2 Jul 2017 (v1), last revised 6 Jul 2017 (v2)

**HAL** is a multi-disciplinary open access archive for the deposit and dissemination of scientific research documents, whether they are published or not. The documents may come from teaching and research institutions in France or abroad, or from public or private research centers.

L'archive ouverte pluridisciplinaire **HAL**, est destinée au dépôt et à la diffusion de documents scientifiques de niveau recherche, publiés ou non, émanant des établissements d'enseignement et de recherche français ou étrangers, des laboratoires publics ou privés.

NNT : 2016SACLS156

THESE DE DOCTORAT  
DE  
L'UNIVERSITE PARIS-SACLAY  
PREPAREE A  
L'UNIVERSITE PARIS SUD EN CHATENAY-MALABRY

ECOLE DOCTORALE N° 569  
Innovation Thérapeutique : du fondamental à l'appliqué

Physiopathologie Moléculaire et Cellulaire

Par

**Mme YueYi WANG**

Ca<sup>2+</sup> handling in a mouse model of  
Catecholaminergic Polymorphic Ventricular Tachycardia

**Thèse présentée et soutenue à Châtenay-Malabry, le 7 juillet 2016 :**

**Composition du Jury :**

M Pous Christian, Professeur, Université Paris-Saclay, Châtenay-Malabry, France, Président du Jury

M Mangoni Matteo E., Directeur de Recherche, CNRS, Montpellier, France, Rapporteur

M Egger Marcel, Professeur, University of Bern, Suisse, Rapporteur

M Charpentier Flavien, Directeur de Recherche, Inserm, Nantes, Examinateur

Mme Zorio Esther, MD, Hospital Universitario y Politécnico La Fe, Valencia, Spain, Examinatrice

Mme Gomez Ana-Maria, Directrice de Recherche, Inserm, Châtenay-Malabry, France, Directeur de thèse

# Acknowledgment

My PhD is an amazing experience and it would not have been possible without the support and guidance that I received from many people.

I would like to express my deepest gratitude to my supervisor Dr. Ana Maria Gomez for her professional guidance, patience, constant encouragement and support. Her guidance helped me in all the time of research and writing of this thesis. Her advices on research, my career and my personal life have been priceless. I have learnt a great deal from her and I could not imagine having a better supervisor.

I sincerely thank Dr. Jean-Pierre Benitah and Dr. Rodolphe Fischmeister, who opened the door and accepted me into this big family about five years ago, making all these life-changing experiences possible. I also thank Dr. Jean-Pierre Benitah for the guidance, valuable comments and suggestions for my research, and help that he kindly offered during my PhD.

I greatly appreciate the contribution to my project by the authors in my paper. I thank Pietro Mesirca and Matteo Mangoni for the patch-clamp experiments and analysis, Elena Marqués-Sulé for the ECG arrhythmia analysis, Alexandra Zahradnikova Jr for the first ECGs implant surgery, recording and analysis, Olivier Villejouvert for some ECG recording and analysis, Esther Zorio for the clinical data and arrhythmia analysis, Jean-Pierre Benitah for supervising the work, and Ana Maria Gomez for supervising the work and writing the IDL programs. I also thank all the authors for edited the manuscript of the paper.

I am grateful to Alexandra Zahradnikova Jr and Ana Llach for their help in my experiments and my life. I am also grateful to Riccardo Rizzetto, Elena Marqués-Sulé, Olivier Villejouvert and Thassio Mesquita for their support and being great friends. I also thank Francoise Boussac for administrative assistance.

Many thanks to all my wonderful colleagues for offering precious help and letting my PhD life enjoyable.

I gratefully acknowledge the financial support of China Scholarship Council (CSC) for the past four years.

Last but not the least, I would like to thank my family: my Mum Guirong Li, my Dad Xingxu WANG, my husband Yongchao XU, my mother-in-law Dongfeng HUANG and my father-in-law Jinxiang Xu.

## **Ca<sup>2+</sup> manutention dans un model de souris de CPVT**

La tachycardie ventriculaire catécholergique (CPVT) est une maladie héréditaire qui se manifeste par des syncopes voire une mort subite, lors de stress émotionnel ou physique en absence d'altération morphologique du cœur. Bien qu'étant une maladie rare, qui touche 1 à 5 personnes sur 10 000 en Europe, cette maladie n'est malheureusement diagnostiquée qu'après le décès d'un enfant ou jeune adulte dans une famille avec des causes inconnues. Une syncope ou la mort subite peuvent apparaitre dès l'âge de 7 ans. Pour 10-20% des patients, la première manifestation est la mort subite. Les arythmies les plus fréquentes sont la tachycardie ventriculaire bidirectionnelle, mais aussi la tachycardie supraventriculaire, la fibrillation atriale, et la dysfonction sinusale. Au repos, ces patients ont un électrocardiogramme normal, mais une tendance plus importante à la bradycardie.

Des mutations dans 4 gènes ont été identifiées comme étant à l'origine de la CPVT. La plupart des mutations autosomiques dominantes identifiées (~60%, CPVT1) concernent le récepteur de la ryanodine type 2 (RyR<sub>2</sub>), canal de libération du Ca<sup>2+</sup> du réticulum sarcoplasmique (RS) cardiaque. D'autres mutations concernent des gènes codant pour des protéines régulatrices du RyR<sub>2</sub> : la calséquestrine (CPVT2, autosomique récessive, qui apparait dans environ 2% de cas), la triadine (autosomique récessive) et la calmoduline1 (autosomique dominante).

Nos collaborateurs ont identifié la mutation RyR<sub>2</sub><sup>R420Q</sup> chez une famille espagnole atteinte de CPVT. Ces patients ont une dysfonction du *pacemaker* (nœud sinusal, NSA) avec une bradycardie. Nous avons construit une souris portant cette mutation, et étudié l'activité du NSA en analysant le calcium intracellulaire, afin d'élucider les mécanismes impliqués dans cette bradycardie.

Toutes les expériences ont été faites sur des souris, mâles et femelles, d'environ 6 mois, hétérozygotes pour la mutation (KI), et sur leurs frères et sœurs ne portant pas la mutation (WT).

Tout d'abord, pour caractériser les souris, des électrocardiogrammes (ECG) ont été enregistrés en

télémetrie. Des capteurs ont été implantés chez la souris en subcutanée sous anesthésie sous isofluorane. Les enregistrements ont été faits au moins une semaine après la chirurgie, pour que les animaux récupèrent de l'opération. Une injection d'épinéphrine et de caféine (2+120 mg/Kg) en intra-péritonéal a été réalisée, afin de vérifier leur phénotype. Ceci a induit une tachycardie bidirectionnelle chez toutes les souris KI et aucune chez les WT, validant ainsi le modèle. Le rythme cardiaque était similaire pendant la période d'activité (nuit) chez les souris KI et WT, mais plus lent pendant la période de repos (jour) chez les femelles KI. Une stimulation sympathique avec injection d'isoprénaline (ISO 1 mg/kg) a accéléré le rythme de toutes les souris, mais de manière plus importante chez les souris KI. D'autre part, la stimulation parasympathique avec injection de carbachol (CCH 0,25 mg/kg) ralentit le rythme cardiaque de façon similaire chez toutes les souris. En présence d'ISO, un plus grand nombre de souris présentent des échappements jonctionnels, indiquant que l'absence d'activité du NSA durant ces battements.

Afin d'analyser les mécanismes, nous avons disséqué le NSA et l'avons chargé avec un indicateur fluorescent du  $\text{Ca}^{2+}$  (le fluo-4) puis analysé les mouvements calciques spontanés par microscopie confocale. Cette technique, développée dans le laboratoire, est très délicate mais nous permet d'étudier les mouvements du  $\text{Ca}^{2+}$  dans la cellule du NSA dans son contexte naturel, sans dissocier le tissu. Ces données *in-vitro* ont montré une différence basale du rythme cardiaque entre mâles et femelles, avec une fréquence de transitoires  $[\text{Ca}^{2+}]_i$  plus lente chez les femelles. La présence de la mutation ralentit la fréquence des transitoires  $[\text{Ca}^{2+}]_i$  chez les deux sexes (WT : mâle  $0,66 \pm 0,03$  s ; femelle  $0,76 \pm 0,03$  s ; KI : mâle  $0,76 \pm 0,04$  s ; femelle  $0,94 \pm 0,04$  s). De plus, ces transitoires  $[\text{Ca}^{2+}]_i$  ont une plus faible amplitude et une prolongation du temps au pic (amplitude : WT  $3,82 \pm 0,11$  ; KI  $3,55 \pm 0,10$  ; temps au pic : WT  $46,95 \pm 1,63$  ms ; KI  $52,41 \pm 1,50$  ms).

Afin d'évaluer l'activité du  $\text{RyR}_2$ , nous avons analysé les *sparks*  $\text{Ca}^{2+}$ , qui sont des événements élémentaires produits par l'activation d'un cluster de  $\text{RyR}_2$ s. Nos analyses en microscopie confocale sur des NSA disséqués ont montré que la fréquence des *sparks*  $\text{Ca}^{2+}$  n'était que légèrement augmentée (WT : mâle  $5,92 \pm 1,33 \text{ sparks} \times \text{s}^{-1} \times 100 \mu\text{m}^{-1}$ ; femelle  $6,30 \pm 1,07 \text{ sparks} \times \text{s}^{-1} \times 100 \mu\text{m}^{-1}$ ;

KI : mâle  $13,07 \pm 2,32 \text{ sparks} \times \text{s}^{-1} \times 100 \mu\text{m}^{-1}$ ; femelle  $8,03 \pm 1,26 \text{ sparks} \times \text{s}^{-1} \times 100 \mu\text{m}^{-1}$ ). Par contre, la durée de ces *sparks* est fortement prolongée dans les cellules KI par rapport aux *sparks*  $\text{Ca}^{2+}$  enregistrés dans les cellules WT (WT : mâle  $42,69 \pm 0,47 \text{ ms}$  ; femelle  $36,52 \pm 0,37 \text{ ms}$  ; KI : mâle  $52,98 \pm 0,38 \text{ ms}$  ; femelle  $58,17 \pm 0,47 \text{ ms}$ ). Ceci produit une libération plus importante de  $\text{Ca}^{2+}$  dans chaque *spark* en moyenne. Ainsi, les cellules KI ont une fuite de  $\text{Ca}^{2+}$  par unité du temps pendant la diastole plus importante que les cellules WT (WT : mâle  $1749,06 \pm 28,01 \text{ Ca}^{2+} \text{ release} \times \text{s}^{-1} \times 100 \mu\text{m}^{-1}$ ; femelle  $1679,65 \pm 25,09 \text{ Ca}^{2+} \text{ release} \times \text{s}^{-1} \times 100 \mu\text{m}^{-1}$ ; KI : mâle  $5091,91 \pm 56,82 \text{ Ca}^{2+} \text{ release} \times \text{s}^{-1} \times 100 \mu\text{m}^{-1}$ ; femelle  $3300,64 \pm 36,91 \text{ Ca}^{2+} \text{ release} \times \text{s}^{-1} \times 100 \mu\text{m}^{-1}$ ). Pour analyser la conséquence que cette augmentation de la libération du  $\text{Ca}^{2+}$  peut avoir, nous avons évalué la charge calcique du RS, qui était réduite, ceci pouvant ainsi réduire l'automatisme. De plus, les canaux calciques de type L du sarcolemme, aussi impliqués dans l'automatisme, sont inactivés par le calcium intracellulaire. L'analyse de ce courant par *patch-clamp* montre que les cellules isolées du NSA des souris KI ont une amplitude de courant plus faible. En revanche, cette diminution était dépendante du  $\text{Ca}^{2+}$  intracellulaire car elle disparaît lorsqu'on tamponne le  $\text{Ca}^{2+}$  intracellulaire par le BAPTA.

En résumé, la mutation  $\text{RyR}_2^{\text{R420Q}}$  produit des *sparks*  $\text{Ca}^{2+}$  plus longs dans le temps, suggérant des ouvertures du canal plus longues, ce qui est directement impliqué dans la bradycardie du fait de la vidange du réservoir RS et l'inactivation des canaux calciques type L. En conséquence, les thérapies en cours d'étude qui favoriseraient la stabilisation du  $\text{RyR}_2$  à l'état fermé pourraient ne pas être efficaces, et il faudrait plutôt essayer des thérapies qui faciliteraient la fermeture du canal, une fois qu'il est ouvert.

# Table of contents

|  |    |
|--|----|
| <b>Chapter 1 Introduction</b> .....  | 1  |
| <b>1.1 Overview of heart function, action potentials and CICR</b> .....      | 1  |
| Action potentials.....   | 2  |
| <b>1.2 Sinoatrial node (SAN) automaticity</b> .....                          | 5  |
| <b>1.2.1 Membrane clock theory</b> .....                                     | 5  |
| 1.2.1.1 Ion channels.....  | 5  |
| 1.2.1.2 Membrane clock.....  | 18 |
| <b>1.2.2 Ca<sup>2+</sup> clock theory</b> .....                              | 18 |
| 1.2.2.1 Sodium-calcium exchanger (NCX).....                                  | 18 |
| 1.2.2.2 RyR <sub>2</sub> in Ca <sup>2+</sup> clock.....                      | 20 |
| 1.2.2.3 Ca <sup>2+</sup> clock.....  | 20 |
| <b>1.2.3 Coupled clock theory</b> .....                                      | 22 |
| <b>1.2.4 Autonomic regulation of cardiac automaticity</b> .....              | 23 |
| 1.2.4.1 Sympathetic regulation of cardiac automaticity .....                 | 24 |
| 1.2.4.2 Parasympathetic regulation of cardiac automaticity.....              | 31 |
| 1.2.4.3 Additional regulator of cardiac automaticity .....                   | 33 |
| <b>1.3 CPVT and CPVT related sinus dysfunction</b> .....                     | 42 |
| RyR <sub>2</sub> related CPVT mutations.....                                 | 43 |
| <b>1.4 Ryanodine receptors (RyRs)</b> .....                                  | 45 |
| <b>1.4.1 RyR isoforms and tissue distribution</b> .....                      | 46 |
| <b>1.4.2 RyR structure</b> .....   | 48 |
| 1.4.2.1 Overall mammalian RyR structure.....                                 | 48 |
| 1.4.2.2 RyR <sub>2</sub> structure.....                                      | 49 |
| 1.4.2.3 Membrane topology and pore region.....                               | 50 |
| 1.4.2.4 Ion permeation .....   | 52 |
| 1.4.2.5 Gating.....  | 53 |
| 1.4.2.6 N-terminal region and R420 site.....                                 | 54 |
| 1.4.2.7 RyR <sub>2</sub> Ca <sup>2+</sup> release events .....               | 57 |
| 1.4.2.8 RyR regulation by endogenous effectors .....                         | 58 |
| <b>1.4.3 RyR accessory proteins</b> .....                                    | 63 |
| 1.4.3.1 FK506-binding proteins (FKBP) .....                                  | 63 |
| 1.4.3.2 Calmodulin (CaM) .....   | 64 |
| 1.4.3.3 Calsequestrin (CASQ) .....   | 65 |
| <b>1.4.4 Clinical characterization of RyR<sup>R420Q</sup> mutation</b> ..... | 66 |



|  |            |
|--|------------|
| 1.5 Objectives.....  | 68         |
| <b>Chapter 2 Materials and methods .....</b>   | <b>69</b>  |
| <b>2.1 Generation of RyR2 (R420Q) mutation mice (Performed by Institut Clinique de la Souris) and etics statement .....</b>                | <b>69</b>  |
| <b>Ethics statement .....</b>  | <b>70</b>  |
| <b>2.2 Genotyping.....</b>   | <b>71</b>  |
| <b>2.3 Telemetry .....</b>   | <b>74</b>  |
| <b>2.3.1 ECG and telemetry .....</b>   | <b>74</b>  |
| <b>2.3.2 ECG analysis .....</b>  | <b>76</b>  |
| <b>2.4 Ca<sup>2+</sup> handling recording by confocal microscopy .....</b>   | <b>78</b>  |
| <b>2.4.1 SAN dissection .....</b>  | <b>78</b>  |
| <b>2.4.2 Ca<sup>2+</sup> handling recording by confocal microscopy .....</b>   | <b>79</b>  |
| <b>2.4.3 Confocal microscope recording analysis.....</b>   | <b>82</b>  |
| <b>2.5 Protein measurement.....</b>  | <b>83</b>  |
| <b>2.6 SAN cell dissociation and patch clamp (Performed by Pietro Mesirca).....</b>  | <b>89</b>  |
| <b>2.6.1 SAN cell dissociation.....</b>  | <b>89</b>  |
| <b>2.6.2 SAN cell patch clamp (Performed by Pietro Mesirca) .....</b>  | <b>89</b>  |
| <b>2.7 Statistics .....</b>  | <b>91</b>  |
| <b>2.8 Materials .....</b>   | <b>91</b>  |
| <b>Chapter 3 Results .....</b>   | <b>92</b>  |
| <b>3.1.1- Manuscript .....</b>   | <b>92</b>  |
| <b>Mechanisms of bradycardia in RyR<sub>2</sub><sup>R420Q</sup> Catecholaminergic Polymorphic Ventricular Tachycardia mutation.....</b>    | <b>92</b>  |
| <b>3.1.2. Additional data on RyR<sub>2</sub><sup>R420Q</sup> SAN.....</b>  | <b>93</b>  |
| <b>Chapter 4 Discussion .....</b>  | <b>102</b> |
| <b>Reference: .....</b>  | <b>109</b> |
| <b>Anexe .....</b>   | <b>147</b> |
| <b>Reconciling depressed Ca<sup>2+</sup> sparks occurrence with enhanced RyR<sub>2</sub> activity in failing mice cardiomyocytes .....</b> | <b>147</b> |

# Chapter 1 Introduction

The heart rhythm is initiated by the activity of sinoatrial node (SAN), which generates electrical impulses and spreads to the heart inducing heart contraction. Arrhythmias occur when SAN or spreading system has anomalies, or when the contraction is driven by a stimulus in another area (ectopic foci), referring abnormal rhythm of the heart beats.<sup>1</sup> At intracellular levels, calcium ( $\text{Ca}^{2+}$ ) plays a key role in maintaining normal heart function, such as automatic pacing, action potential generation, excitation-contraction coupling (EC coupling). Thus, sick intracellular  $\text{Ca}^{2+}$  release in heart could cause cardiac arrhythmias.

This thesis seeks to elucidate the relationship between  $\text{Ca}^{2+}$  handling and cardiac arrhythmias, specifically, focusing on the role of the pathological changes in the intracellular  $\text{Ca}^{2+}$  regulation through  $\text{Ca}^{2+}$  release channel (ryanodine receptor 2,  $\text{RyR}_2$ ) modification contributing to the abnormal SAN function.

## 1.1 Overview of heart function, action potentials and CICR

The human heart beats about  $10^5$  times a day resulting in 2 billion heartbeats during a lifetime.<sup>2</sup> Sinoatrial node (SAN) is described as the primary and physiological pacemaker since its discovery more than a century ago.<sup>3</sup> Under physiological condition, it spontaneously initiates regular electricity. SAN anticipates to atrioventricular (AV) node and Purkinje fibers network (PFN) electrical activity, considering that the two can also generate pacemaker activity, although they only drive the heart when the SAN is in pathological condition.<sup>4-6</sup> For instance, AV node can become dominant during SAN block or heart failure, and PFN can also lead a viable rhythm during AV block. Thereby this system can maintain heartbeat when the SAN fails.

SAN is located near the entrance of the superior vena cava (SCV) in the right atrium (Figure 1), bordered by the crista terminalis. As the impulse-generating tissue, it initiates the electrical impulse, which spreads across both right and left atrium and induces the atria depolarization and contraction, known as atrial systole. This process corresponds to P wave ( $\sim 0.08\text{s}$  in humans) on the surface electrocardiogram (ECG) (Figure 2). When the impulse reaches the AV node (located near the AV valve, in the interatrial septum), it slows down because of the conduction property of AV node. This delay makes sure all the blood has been ejected to the ventricles before ventricular contraction. It corresponds to PR segment ( $\sim 0.04\text{s}$  in humans), a flat line following the P wave, while the PR interval ( $\sim 0.12\text{s}$  in humans) represents the duration from the beginning of atrial depolarization until ventricular depolarization. The AV node passes the signal to AV bundles (also known as His bundles), which bifurcates into left and right bundle branches. The signal then passes to Purkinje fibers and through both ventricles, inducing ventricular depolarization and contraction, known as

ventricle systole. Thereby the blood is pumped throughout the body. On the ECG, it is represented by QRS complex (~0.12s in humans). Meanwhile, the atrial repolarization occurs, although it's buried in the QRS complex. The Q wave depicts the septum depolarization, from left to right. When the depolarization travels throughout the ventricles, the R wave and S wave show up. Then another flat line, ST segment (~0.08s in humans), indicates no large electrical vector, while ventricle is contracting. The ventricle repolarization represented by T wave (0.16s in humans). As the epicardial cells repolarize before the endocardial cells, the T wave reflects positively.

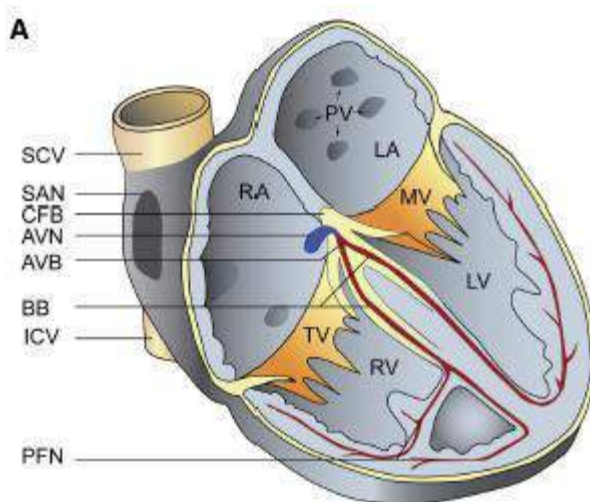


Figure 1 The mammalian heart with the cardiac conduction system. SAN, sinoatrial node; SCV, superior vena cava; RA, right atrium; AVN, atrioventricular node; ICV, inferior vena cava; CFB, central fibrous body; TV, tricuspid valve; AVB, atrioventricular bundle; BB, bundle branches; PFN, Purkinje fibers network; LA, left atrium; PV, pulmonary veins; MV, mitral valve; RV, right ventricle; LV, left ventricle. (Panel A is adapted from Mangoni and Nargeot, 2008<sup>6</sup>)

## Action potentials

The cardiac action potential (AP) is the membrane potential ( $E_m$ ) waveform that is determined by a complex interplay of many ion channels and transporters, and the  $[Ca^{2+}]_i$  transient itself.<sup>7</sup> The cardiac AP morphology between cardiomyocytes varies dramatically in different regions of the heart according to the physiological characteristics (Figure 2).

In order to maintain the heart rate, the SAN cells spontaneously generate regular and cyclic AP. Then, the electrical impulse propagates to atrium, AV node, Purkinje fiber and ventricle (Figure 2).

In ventricular myocytes, the AP contains four phases. Between 2 consecutives AP, the resting membrane is maintained by  $I_{K1}$  of the  $K_{ir}2.1$  potassium channels. When a ventricular myocyte is excited by adjacent cells, voltage-dependent  $Na_v1.5$  sodium channels are activated resulting in a rapid inward  $Na^+$  current ( $I_{Na}$ ) and concomitantly rapid membrane depolarization constituting the upstroke of the AP (phase 0). The membrane depolarization induces the slow deactivation of  $Na_v1.5$  channel and activation of voltage-dependent  $K^+$  channels ( $K_v4.3$  and  $K_v1.4$ ), which generates a rapid repolarizing current ( $I_{to}$ ) (phase 1). Then, the voltage-dependent  $Ca^{2+}$  channels

(Ca<sub>v</sub>1.2) are activated, producing an inward Ca<sup>2+</sup> current (I<sub>Ca,L</sub>). The activation of outward rectifying K<sup>+</sup> currents (I<sub>Kur</sub>, I<sub>Kr</sub> and I<sub>Ks</sub> via K<sub>V</sub>1.4, K<sub>V</sub>11.1 and K<sub>V</sub>7.1, respectively) and I<sub>Ca,L</sub> are at similar voltages, result in the plateau phase of AP (phase 2). Deactivation of Ca<sub>v</sub>1.2 induces the predominance of K<sup>+</sup> currents and further membrane depolarization (phase 3). In the end, K<sub>ir</sub>2.1 is re-activated, which generates the I<sub>K1</sub> current and push the membrane potential back to the resting level.<sup>6, 8-10</sup>

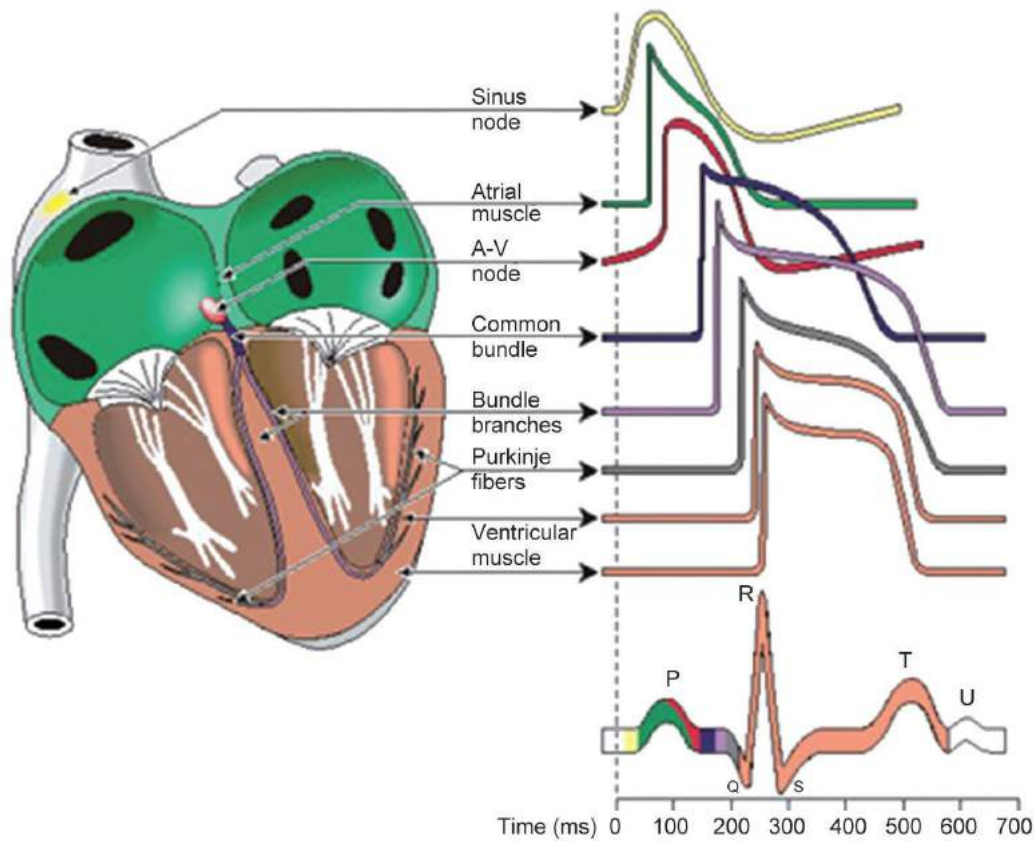


Figure 2 Electro-activity of the adult heart. Top: schematic of a human heart with illustration of typical action potential waveforms in different regions of the heart. Bottom: schematic of a surface electrocardiogram. (Adapted from Weisbrod et al., 2016<sup>11</sup>)

In myocytes, the membrane (including transverse tubules, t-tubules) depolarization during the action potential activates I<sub>Ca,L</sub> inducing SR Ca<sup>2+</sup> release through ryanodine receptor 2 (RyR<sub>2</sub>), which is known as calcium induced calcium release (CICR) leading to myocytes and heart contraction.<sup>12, 13</sup> This process from electrical excitation of the myocytes to contraction of the heart is termed cardiac excitation-contraction coupling (EC coupling).<sup>7</sup> The action potential and the following contraction are well studied in ventricular myocytes. However, the generation of electrical impulse in SAN cells is still under debate. As many ion channels expressed in ventricular myocytes are also expressed in SAN cell, the studies about SAN cells are always in comparison to ventricular myocytes.

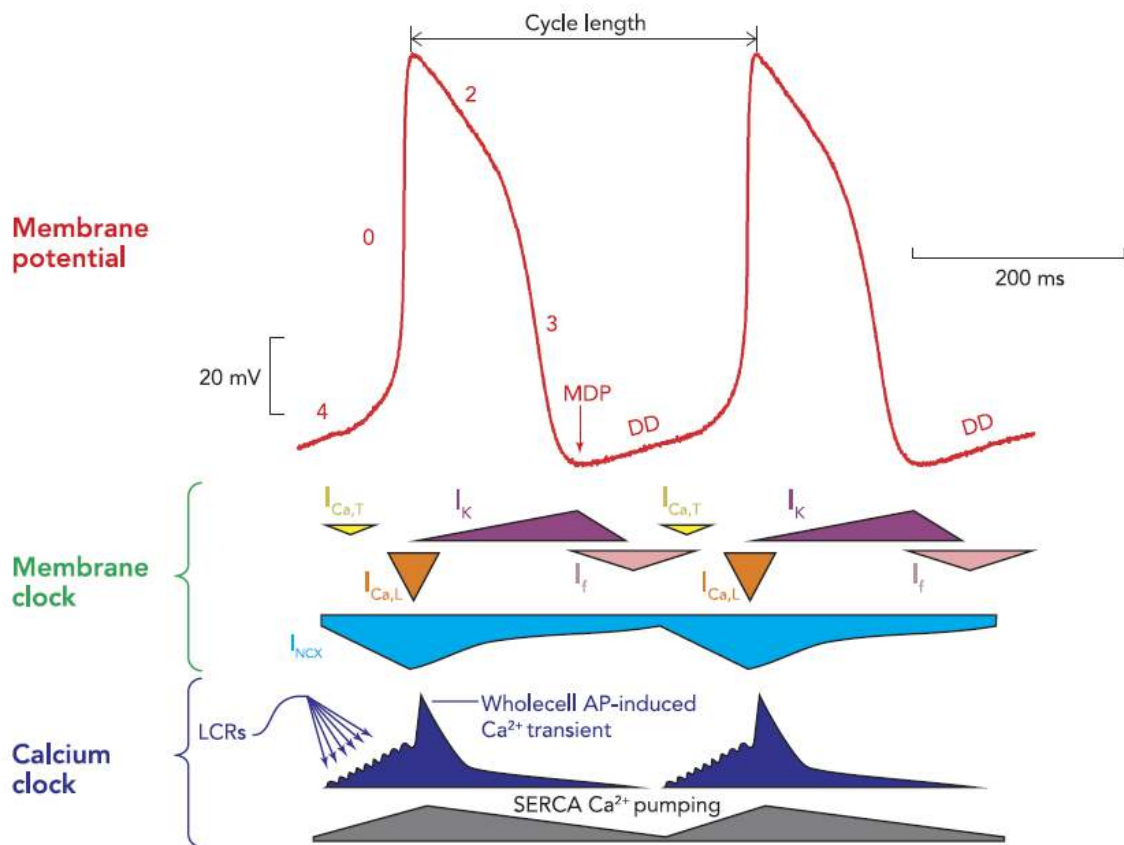


Figure 3 Schematic of membrane clock and calcium clock mechanisms. Top: the red trace shows an example of a typical action potential of spontaneously beating rabbit SANC. The different phases of the AP are labeled, while phase 4 also represents diastolic depolarization (DD). MDP, maximum diastolic potential. Middle: schematic representation of the timing and magnitude of the different components of the “membrane clock”. Bottom: the timing and magnitude of the important components of the “Ca<sup>2+</sup> clock” are shown at the bottom. LCRs, local Ca<sup>2+</sup> releases. L-type Ca<sup>2+</sup> current, I<sub>Ca,L</sub>. T-type Ca<sup>2+</sup> current, I<sub>Ca,T</sub>. Potassium current, I<sub>K</sub>. NCX current, I<sub>NCX</sub>. (Adapted from Monfredi et al., 2013<sup>14</sup>)

In automatic cells there is an additional phase of the AP, which is the slow depolarization (phase 4), which slowly depolarizes the membrane, until reaching threshold and producing another AP. In ventricular and atrial myocytes this phase does not exist and the myocytes are not automatic, as they need to be excited by other cells to generate an AP. The AP of SAN includes diastolic depolarization (DD, Figure 3, also referred to as phase 4), rapid depolarizing upstroke (phase 0) and repolarization (phase 2 and 3).<sup>15</sup> Major ion currents involved in the AP are depicted in Figure 3, and further introduced in the next session. The morphology of AP in SAN cells is different from that of ventricular myocytes (Figure 3). The SAN cell doesn't have real resting membrane potential. The more negative potential reached is named maximum diastolic potential. The phase 4 includes the slow increase in membrane potential toward an excitation threshold, at which the action potential fires.<sup>14, 16</sup> Regarding the mechanisms of DD, one important factor involved is the funny current (I<sub>f</sub>) carried by hyperpolarization-activated cyclic nucleotide-gated channels (HCN channels), which

depolarizes the membrane. Other currents also contribute to the progression of depolarization, such as  $I_{Ca,T}$ ,  $I_{NCX}$  and  $I_{Ca,L}$  carried respectively by T-type  $Ca^{2+}$  channel ( $Ca_v3.1$ ,  $Ca_v3.2$ ), sodium-calcium exchanger (NCX), L-type  $Ca^{2+}$  channel ( $Ca_v1.2$ ,  $Ca_v1.3$ ). The phase 4 consists of two components, a linear component (the first two-thirds of DD) and a nonlinear, exponentially rising component (the last third of DD). The nonlinear component is proposed to occur along with the subsequent cytosolic  $Ca^{2+}$  increase induced by local  $Ca^{2+}$  release by SR and concomitant inward NCX activation.<sup>17</sup> The rapid upstroke (phase 0, Figure 3) of SAN AP is much faster than diastolic depolarization, but still slower than that of ventricular myocytes as it's carried out by slow  $Ca^{2+}$  current in SAN instead of the fast  $Na^+$  current in ventricular myocytes. The initial repolarization phase (phase 1) in ventricular myocytes is completely absent, and the plateau of phase 2 is replaced by a slow velocity repolarization phase. In the end, the  $E_m$  is driven to maximum diastolic potential (MDP) by potassium channels. The AP of SAN has a relatively positive MDP of around -50mV due to the absence of  $I_{K1}$ .<sup>6, 8, 9, 14, 16, 18</sup>

## **1.2 Sinoatrial node (SAN) automaticity**

This session serves to introduce SAN action potential and the generation of pacemaker activity. For now, the mysterious ability of SAN generating the spontaneous rhythm is still under debate. There are two theories that can explain the SAN automaticity, the membrane clock theory,  $Ca^{2+}$  clock theory and the subsequent coupled clock theory, which are reviewed in this session.

### **1.2.1 Membrane clock theory**

Before introducing the membrane clock, we will simply discuss the ion channels involved in membrane clock.

#### **1.2.1.1 Ion channels**

##### **1.2.1.1.1 HCN channels**

#### **HCN channels and $I_f$ current**

The hyperpolarization-activated cyclic nucleotide-gated (HCN) channels belong to the superfamily of voltage-gated pore loop channels, expressed widely in nervous system and in heart. They are located on plasma membrane. As a voltage-gated channel, HCNs can sense the changes of the electrical membrane potential, be activated by membrane hyperpolarization (around -50/-65 mV) and generate a unique inward current. Their activation could be facilitated by direct interaction with cyclic adenosine monophosphate (cAMP), via binding with the C-terminus of the channel. Other regulators have also been described, including phosphatidylinositol 4,5-bisphosphate ( $PIP_2$ ), kinases and phosphatases.<sup>19-22</sup>

HCN channels are tetramers (four subunits), and homologous to voltage-gated potassium channels. Like  $K^+$  channels, HCN channels are blocked by millimolar concentration of  $Cs^+$ , and activated by extracellular  $K^+$ .<sup>23-27</sup> But unlike  $K^+$  channels, they are not sensitive to  $Ba^{2+}$ , tetraethylammonium (TEA) and 4-aminopyridine (4-AP), which are strong blockers of potassium channel.<sup>26</sup>

Each HCN channel subunit consists of six transmembrane helices (S1-S6), including the voltage sensor (S4) and a glycine-tyrosine-glycine (GYG) sequence in the P loop between S5-S6. In potassium channels, the GYG sequence forms the highly selective filter for  $K^+$ . However, HCN channels conduct both  $Na^+$  and  $K^+$ , in spite of the greater permeability for  $K^+$ , and even display a small permeability for  $Ca^{2+}$ .<sup>28-30</sup> Until now, the mechanisms about the specific permeation properties of HCN channels are still unclear. It has been found that the sequences in the P-loop and before GYG are different in  $K^+$  channels and in HCN channels, which are TT-V/I-GYG and LC-I-GYG respectively.<sup>31-33</sup> D'Avanzo et al. changed the residues closed to the selectivity filter in the HCN4 channel to match the  $K^+$  channels, and failed to increase  $K^+$  selectivity, suggesting the differences are outside the P-loop region.<sup>34</sup> Macri et al. further investigated, showing that the cysteine doesn't contribute to permeation.<sup>35</sup> It was also proposed that the GYG sequence is coordinated in a less rigid model in HCN channels than in  $K^+$  channels, allowing the entrance of cations of different sizes.<sup>36</sup>

Upon membrane hyperpolarization, HCN channels generate a unique and mixed inward current (termed  $I_h/I_f$ , Figure 3).<sup>26, 36-39</sup>  $I_f$  is first described in 1979, and referred by some researchers as pacemaker current, in respect that it plays an important role in control of cardiac and neuronal rhythmicity.<sup>28, 40-42</sup>  $I_f$  current widely presents in cardiac pacemaker cells of most species. However, it is absent in some SAN cells from monkey and rat, although it is questioned that this could be artificial effect produced by dialysis of the intracellular medium with the pipette solution.<sup>43, 44</sup>

The physiological contribution of  $I_f$  current in SAN pacemaker activity is still under debate.  $I_f$  is activated upon membrane hyperpolarization at the end of the repolarization phases of an action potential. When  $I_f$  is activated, it shifts the current flow from outward to inward (Figure 3), which reverses the action potential at maximum diastolic potential (MDP). It ends the repolarization process, and initiates the first part of depolarization process until the activation of voltage-dependent  $Ca^{2+}$  channels is achieved ( $\sim -40mV$ ). The fact that blockade of  $I_f$  causes the prolongation of cycle length in SAN cells indicates that  $I_f$  participates to the generation of pacemaker activity.<sup>45, 46</sup> For instance,  $Cs^+$  (2mM) decreases beating rate of rabbit SAN cells by 30%.<sup>45</sup> In human SAN cells, 2mM  $Cs^+$  is sufficient to slow DD slope and pacemaker activity (26% cycle length increase).<sup>47</sup>

However, it is notable that blockade of  $I_f$  only results in a modest prolongation of cycle length in SAN cell.<sup>48</sup> The presence of  $Cs^+$  only induces slightly decrease of pacing rate, which has been seen as an indication that  $I_f$  is not the unique determinant for SAN automaticity.<sup>45, 49</sup> Yet, this idea is challenged by DiFrancesco and his coworkers, who mentioned that  $Cs^+$  does not fully block  $I_f$  and the blockage is voltage dependent. Thus the partially unblocked  $I_f$  would still be able to drive the automaticity, and the membrane potential changes further unblock  $I_f$ .<sup>25</sup> Although,  $Cs^+$  is also a  $K^+$  channel blocker which could indirectly affect  $I_f$ .<sup>25</sup>

Additions of other  $I_f$  blockers are also used to quantify whether this current is necessary for SAN automaticity generation, in which ivabradine is a specific organic blocker of  $I_f$ .<sup>50</sup> The blockers access to the binding site within the open pore of HCN channel and cannot leave the binding site when the channel is closed.<sup>51-54</sup> A low concentration of ivabradine ( $<3 \mu M$ ) specifically inhibits  $I_f$  without suppressing  $I_{Ca,L}$  or other membrane ion currents.<sup>55, 56</sup> Ivabradine slows automaticity by  $\sim 20\%$  at concentration of  $3 \mu M$  in isolated rabbit SAN cells, and reduces the heart rate in vivo in mice and conscious dogs, but doesn't block pacemaking.<sup>46, 57-59</sup> Therefore, these data again suggest that  $I_f$  is probably not an absolute prerequisite for SAN automaticity. However, some researchers point out that the block/unblock by the blockers (ivabradine, UL-FS 49, etc) is coupled to ionic flow rather than voltage alone.<sup>51-54</sup> The blockers are removed from the blocking site by strong hyperpolarization inducing inward large  $I_f$ .<sup>51-54</sup> It is also noticeable that  $3 \mu M$  ivabradine also perturbs  $Ca^{2+}$  clock with reduced SR  $Ca^{2+}$  load, slowed intracellular  $Ca^{2+}$  cycling kinetics, and prolonged the period of spontaneous LCRs occurrence during diastolic depolarization.<sup>60</sup> A higher concentration of ivabradine ( $10 \mu M$ ) also suppresses  $I_{Ca,L}$ .<sup>55</sup>

The low activation voltage of  $I_f$  may also protect SAN cells from hyperpolarizing, bradycardiac effect of surrounding atrial myocardium.<sup>14</sup> Thus, it was also proposed that  $I_f$  is responsible for a slower DD in the pacemaker range of  $< -65$  mV of subsidiary pacemaker cells rather than of SAN cells, due to its low activation voltage and slow activation kinetics.<sup>61, 62</sup>

The activation of  $I_f$  could be facilitated by direct interaction with cyclic adenosine monophosphate (cAMP), produced at the sarcolemma from adenosine triphosphate (ATP) by adenylate cyclases (ACs) in basal condition and during sympathetic/ parasympathetic stimulation. Activation or inhibition of ACs/cAMP is a consequence of sympathetic and parasympathetic response of the autonomic nervous system controlling the pacemaker activity. A small augmentation of cAMP increases  $I_f$  open probability. Besides, the  $I_f$  activation curve shifts positively under  $\beta$ -adrenergic stimulation (or a rise in cAMP), and negatively upon muscarinic stimulation.<sup>6, 50, 63</sup> The shift indirectly indicates the important role of  $I_f$  on pacemaking and during sympathetic/ parasympathetic activation. However, the responses are questioned by the evidence that the full range of responses to autonomic agonists is possible in the partial absence of  $I_f$  or when



$I_f$  function is deficient.<sup>64, 65</sup> Cytosolic  $Ca^{2+}$  concentration and CaM (Calmodulin) are also reported to regulate  $I_f$ , but not CaMKII ( $Ca^{2+}$ /CaM activates  $Ca^{2+}$ /calmodulin-dependent protein kinase II).<sup>66</sup> BAPTA ( $Ca^{2+}$  chelator) loading significantly decreases the amplitude of  $I_f$  in guinea-pig SAN cells, and shifts the voltage-dependent activation to more negative potentials.<sup>66</sup> Three CaM antagonists (W7, Calmidazolium and ophiobolin A) cause the same effect as BAPTA.<sup>66</sup>

### **Kinetics and contributions to SAN automaticity of HCN isoforms**

Four members of this family (HCN 1-4) have been cloned so far.<sup>26, 27, 33, 67-69</sup> HCN channels can be assembled into either homotetramers by identical (homomeric) type of subunits, or heterotetramers by different (heteromeric) types.<sup>70-75</sup>

HCN channels present distinct biophysical properties, such as activation kinetics, sensitivity to cyclic nucleotides.<sup>6, 37, 67, 69</sup> HCN1 channel shows fastest opening kinetics and the lowest sensitivity to cAMP.<sup>37, 38</sup> However, HCN4 channel is the most slowly activation isoform, and markedly sensitive to cAMP.<sup>27, 33, 37, 67</sup> HCN2 and HCN3 represent intermediate properties between HCN1 and HCN4.<sup>27, 37, 76</sup>

All four HCN channel isoforms have been detected in the heart.<sup>77, 78</sup> In the SAN, HCN4 is the predominant isoform and account for 80% of  $I_f$ , whereas the expression of HCN1 and HCN2 are also found and responsible for the remaining 20%.<sup>77, 79-81</sup> HCN3 was recently observed in rodent ventricular myocytes.<sup>78</sup> Both heteromeric HCN1-HCN4 and heteromeric HCN2-HCN4 channel exist in native SAN tissues.<sup>70, 74</sup>

In rabbit and mouse SAN, HCN1 was detected.<sup>77, 79, 80</sup> HCN1 held >18% of the total HCN mRNA in rabbit SAN, although only a low level of HCN1 was found in mouse SAN.<sup>79, 81</sup> Mice lacking HCN1 channel display congenital SAN dysfunction, characterized by bradycardia, sinus dysrhythmia, increased heart rate variability, prolonged sinoatrial node recovery time, increased sinoatrial conduction time, and recurrent sinus pauses.<sup>82</sup> Therefore, HCN1 is required for stable heart rate and regular beat-to-beat variation.<sup>82</sup>

HCN2 is the dominant ventricular isoform.<sup>77</sup> Only a detectable amount of HCN2 was found in rabbit SAN (HCN4>>HCN1>>HCN2), but a moderate level was found in mouse SAN (HCN4>>HCN2>>HCN1).<sup>79, 81</sup> Overexpression of HCN2 leads to elevation of  $I_f$  current and increase in spontaneous firing rate, but it is not clear whether overexpression of any other inward current generator would produce the similar result.<sup>83, 84</sup> HCN2-deficient mice display modest cardiac dysrhythmia, in which the mean heart rate is not changed, but the heart rate variability is increased.<sup>85</sup> Isolated SAN cells from HCN2-deficient mice present reduced  $I_h$  and slightly hyperpolarized maximum diastolic potential.<sup>85</sup> These data suggest that HCN2 may provide a safety mechanism for the correct setting of the MDP.<sup>85, 86</sup> Besides, the heart rate in response to

isoproterenol is increased similarly in HCN2-deficient and wildtype mice, indicating HCN2 is not required for sympathetic stimulation. It is also proposed that HCN2 and HCN1 probably are not essential for the development of cardiac conduction system and generation of automaticity, but for prevention of arrhythmias.<sup>85, 87</sup>

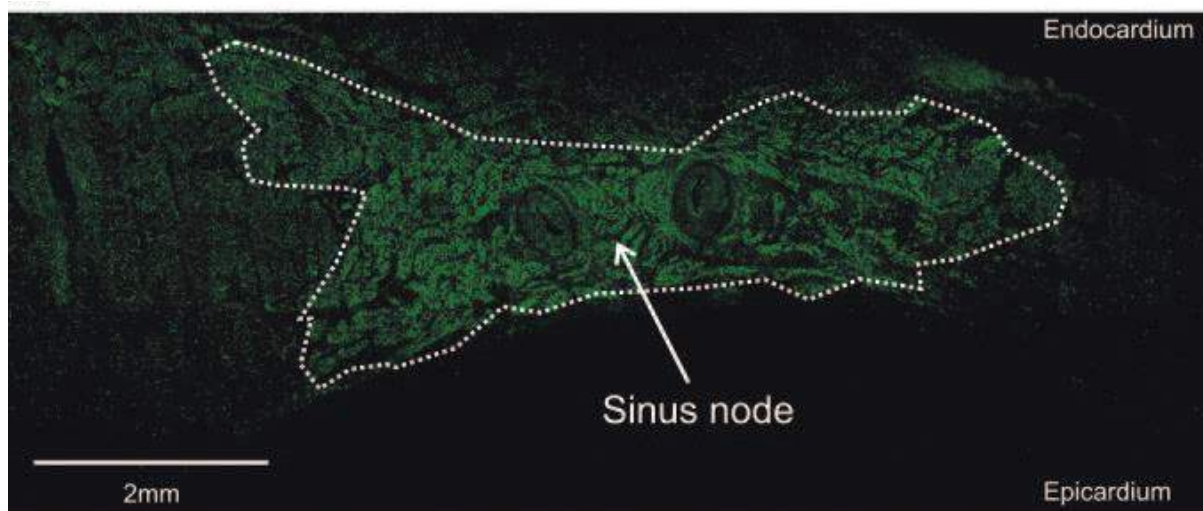


Figure 4 Expression of HCN4 protein in human SAN. Low-power montage of immunolabeling of HCN4 protein (green signal). White dashed line highlights SAN. (Adapted from Chandler et al., 2009<sup>88</sup>)

HCN4 is the predominant isoform in human, rabbit, dog and rodent SAN, and is often used as a marker of pacemaking tissue (Figure 4).<sup>88</sup> It plays an important role in SAN pacemaker activity. Firstly, global or heart-specific deletion of HCN4 channels induced embryonic lethality, while mice died from embryonic days 5.<sup>89, 90</sup> HCN4-deficient embryos had significantly slower heart rate, suppression of  $I_f$  and AV block compared with wild type, which also indicates the essential role of HCN4 for the development of cardiac conduction system.<sup>89, 90</sup> Secondly, to overcome the embryonic lethality, Herrmann et al. used temporally controlled deletion of HCN4.<sup>64</sup> Cells isolated from HCN4 deletion mice showed reduced  $I_f$  (about 75%) and a slight response to isoproterenol.<sup>64</sup> The mutant mice also presented cardiac arrhythmia characterized by recurrent sinus pauses.<sup>64</sup> But the heart rate challenged by isoproterenol had no change.<sup>64</sup> This result was then confirmed by Hoesl et al. who used temporally controlled HCN4 gene deletion technique, and found that application of isoproterenol accelerate the knock-out mice and wild-type mice to similar levels.<sup>65</sup> Thus, it was proposed that HCN4 is necessary for generating and maintaining a stable cardiac rhythm, but not critical for acceleration of the heart rate.<sup>6, 64, 90</sup> Moreover, HCN4 gene mutations are associated with arrhythmias.<sup>42, 91, 92</sup> For instance, patient carrying HCN4 mutation L573X exhibits severe sinus bradycardia and intermittent episodes of atrial fibrillation, chronotropic incompetence during exercise.<sup>93</sup> Up to date, 13 HCN4 mutations from 14 families were reported.<sup>42, 91, 92</sup> In summary, all these evidences indicate the important contribution of HCN4 to SAN pacemaker activity.

#### 1.2.1.1.2 L-type $Ca^{2+}$ channel (LTCC)

L-type  $\text{Ca}^{2+}$  channel is a voltage gated channel on sarcolemmal membrane expressed all over the heart.<sup>6, 13, 14, 94</sup> LTCC is activated when membrane potential reaches  $\sim -50\text{mV}$ , and generates L-type  $\text{Ca}^{2+}$  current ( $I_{\text{Ca,L}}$ ). It exhibits fast  $\text{Ca}^{2+}$ - and slow voltage-dependent inactivation.<sup>95, 96</sup> The fast  $\text{Ca}^{2+}$  dependent inactivation produces a negative feedback and limits its own  $\text{Ca}^{2+}$  entry, whereas the slow voltage-dependent inactivation results in a time dependent behavior and prevents the premature  $\text{Ca}^{2+}$  entry when cytosolic  $\text{Ca}^{2+}$  decreases.<sup>97</sup>  $I_{\text{Ca,L}}$  is also regulated by PKA, CaMKII. The low activation voltage implicates the important role of  $I_{\text{Ca,L}}$  in generation and regulation of SAN automaticity by contributing to the diastolic depolarization, although  $I_{\text{Ca,L}}$  also participates in the rapid upstroke of the action potential (Figure 3).<sup>6, 98-101</sup>

LTCCs are highly sensitive to dihydropyridines (DHPs), such as nifedipine and BAY K8644.<sup>6, 102, 103</sup> Blockade of  $I_{\text{Ca,L}}$  by nifedipine abolishes the spontaneous activity in both isolated SAN cells and in SAN center tissue without affecting T-type  $\text{Ca}^{2+}$  channel, but not in SAN periphery tissue.<sup>101, 104</sup> In contrast, blockade of  $\text{Na}^+$  current by tetrodotoxin has no effect on SAN center tissue, but slows spontaneous activity in periphery tissue.<sup>101</sup> These results indicate the obligatory role of L-type  $\text{Ca}^{2+}$  current in generation of SAN automaticity in SAN center region, while  $\text{Na}^+$  current plays a major role in pacemaking in periphery. Indeed, LTCC antagonist nifedipine could induce bradycardia in anesthetized mice in vivo.<sup>105</sup> A recent research showed colocalization between  $\text{RyR}_2$  and LTCC ( $\text{Ca}_v1.2$  or  $\text{Ca}_v1.3$ ) in the SAN, which may be relevant to the functional role of  $\text{RyR}$ -mediated  $\text{Ca}^{2+}$  release in pacemaking, in respect that  $I_{\text{Ca,L}}$  could induce  $\text{Ca}^{2+}$  release through  $\text{RyR}_2$  in ventricular myocytes (CICR).<sup>12, 13</sup> In ventricular myocytes from failing heart, structural alterations, such as altered T-tubular structure and increased orphaned  $\text{RyRs}$ , contribute to the defect on the efficacy of  $I_{\text{Ca,L}}$  to release  $\text{Ca}^{2+}$ .<sup>106, 107</sup> These results indicate the crucial role of LTCC to CICR and EC coupling in ventricular myocytes, and also suggest the potential importance of colocalization between  $\text{RyR}_2$  and LTCC in SAN.

LTCCs are formed by five subunits,  $\alpha_1$ ,  $\beta$ , and  $\gamma$ ,  $\alpha_2$ ,  $\delta$ .<sup>6, 7, 13</sup> The  $\alpha_1$  subunit forms the ion conducting pore and bears the main functional characteristics.<sup>7, 13</sup> The architecture of  $\alpha_1$  subunit is similar to tetrameric  $\text{K}^+$  channels and voltage-dependent  $\text{Na}^+$  channel. Each  $\alpha_1$  subunit consists of four homologous domains (I-IV), and each domain contains six transmembrane helices (S1-S6) and a P-loop between S5 and S6. The charged S4 contributes as a voltage sensor, and the  $\alpha_2$ ,  $\delta$ ,  $\beta$  and  $\gamma$  are auxiliary subunits.

Four  $\alpha_1$  subunits have been cloned for LTCC (termed  $\text{Ca}_v1.1$ ,  $\text{Ca}_v1.2$ ,  $\text{Ca}_v1.3$  and  $\text{Ca}_v1.4$ , corresponding to  $\alpha_{1S}$ ,  $\alpha_{1C}$ ,  $\alpha_{1D}$  and  $\alpha_{1F}$ ).<sup>108</sup>  $\text{Ca}_v1.1$  subunit is expressed in the skeletal muscle, while  $\text{Ca}_v1.4$  is widely expressed in the retina, adrenal gland, bone marrow, spinal cord, muscle, spleen and immune cells.<sup>13</sup>  $\text{Ca}_v1.2$  and  $\text{Ca}_v1.3$  are expressed in the brain, cardiovascular system and neuroendocrine cells.<sup>12, 13, 88, 109, 110</sup>  $\text{Ca}_v1.2$  is highly expressed in the whole heart, and  $\text{Ca}_v1.3$  is

preferentially expressed in supraventricular regions, although the expression of  $Ca_v1.3$  in SAN is lower than  $Ca_v1.2$ .<sup>80, 111</sup> Isolated SAN cells from  $Ca_v1.3$  gene inactivation mice showed a ~70% reduction in  $I_{Ca,L}$  density, demonstrating the major contribution of  $Ca_v1.3$  to total  $I_{Ca,L}$  in mouse SAN cells.<sup>6, 98, 112</sup>  $Ca_v1.2$ -mediated  $I_{Ca,L}$  accounts for the residual  $I_{Ca,L}$ .<sup>6</sup>

The electrical characteristics of  $Ca_v1.2$  and  $Ca_v1.3$  mediated L-type  $Ca^{2+}$  currents are also different (Table 1).  $Ca_v1.3$  mediated current is activated at more negative voltage and more rapidly, while inactivation during depolarization is slower than  $Ca_v1.2$  mediated current<sup>113</sup> and the dihydropyridine sensitivity for  $Ca_v1.3$  is lower than  $Ca_v1.2$ .<sup>113</sup>

Table 1 Characteristics of the LTCC and TTCC isoforms involved in SAN automaticity. (Adapted from Mesirca et al., 2015<sup>13</sup>)

|                              | L-type VGCC ( $Ca_v1$ )  |   | T-type VGCC ( $Ca_v3$ )  |   |
|------------------------------|--|---|--|---|
|                              | $Ca_v1.2$  | $Ca_v1.3$   | $Ca_v3.1$  | $Ca_v3.2$   |
| Expression time              | Embryonic stage  | Embryonic stage   | Start to increase in the perinatal period and becomes predominant in the adulthood | High in Embryonic heart tissue and then decrease and disappear in adult heart |
| Cardiac tissues expression   | SAN, AVN, atria, PF networks, Ventricles                           | SAN, AVN, atria, PF networks, poorly or not expressed in ventricular    | SAN, AVN, atria, PF networks, poorly or not expressed in ventricular tissue        | SAN, AVN, atria, PF networks, poorly expressed in ventricular tissue          |
| Voltage dependent activation | High threshold of activation (~ -40 mV)<br>Fast activation         | Lower threshold of activation than $Ca_v1.2$ (~ -55 mV) Fast activation | Lower threshold of activation (~ -70 mV) Slow activation                           |   |
| Inactivation properties      | $Ca^{2+}$ and voltage dependent inactivation                       | $Ca^{2+}$ and voltage dependent inactivation                            | Fast voltage dependent inactivation  |   |
| DHP sensitivity              | High   | Lower than $Ca_v1.2$  | Low and very low   |   |
| Role in pacemaking           | Control the $Ca^{2+}$ dependent upstroke phase of action potential | Diastolic pacemaker current   | Diastolic pacemaker current  |   |
| Knock-out mice phenotype     | Lethal   | Strong bradycardia, SAN arrhythmia, conduction system dysfunction       | Mild bradycardia AV conduction disorders   | No phenotype  |

Genetically modified mice are used to examine the role of  $Ca_v1.3$   $Ca^{2+}$  channel in SAN automaticity.  $Ca_v1.3$  deficient mice show SAN dysfunction, including bradycardia and arrhythmia.<sup>114</sup> Consistent with that, Matthes et al. also found bradycardia in isolated heart of  $Ca_v1.3$ -knockout mice.<sup>115</sup> Isolated SAN cells from  $Ca_v1.3$  deficient mice exhibit decreased pacemaking rate with shift in activation threshold of  $I_{Ca,L}$ .<sup>116</sup> Similarly, Mangoni et al. investigated SAN cells from  $Ca_v1.3$  gene inactivation mice, and found slower pacemaker activity and arrhythmia.<sup>98</sup> Moreover, Torrente et al. further found slower pacemaker activity in SAN cells from genetic  $Ca_v1.3$  knock-out mice, associated with impaired  $[Ca^{2+}]_i$  dynamics, reduced local  $[Ca^{2+}]_i$  release events, and deficient synchronization.<sup>112</sup> These results indicate that in SAN cells  $Ca_v1.3$  accounts for regulation of  $[Ca^{2+}]_i$  dynamics, triggering local  $[Ca^{2+}]_i$  release, and thus controlling

pacemaker activity. In the other hand, DHP (isradipine) reduced the heart rate in knock-in  $\text{Ca}_v1.2^{\text{DHP-/-}}$  mice, in which the DHP sensitivity in  $\text{Ca}_v1.2 \alpha 1$  was eliminated without effecting channel function and expression, indicating  $\text{Ca}_v1.3$  is an important component of LTCC in SAN.<sup>117</sup> The stronger colocalization of  $\text{Ca}_v1.3$  with  $\text{RyR}_2$  also suggests the major impact of  $\text{Ca}_v1.3$  on SAN.<sup>12</sup> Besides SAN automaticity,  $\text{Ca}_v1.3$  also plays functional roles in AVN pacemaking activity and conduction, and in atrial tissues.<sup>111, 115, 118, 119</sup> AV conduction abnormalities were reported in  $\text{Ca}_v1.3$ -deficient mice.<sup>115</sup> In support of that, Marger et al. also reported that  $\text{Ca}_v1.3$  is required for AVN cells spontaneous automaticity.<sup>119</sup> Zhang et al. isolated AV node from  $\text{Ca}_v1.3$  null mice, and found a significant decrease in the firing rate and a depolarizing shift in  $I_{\text{Ca,L}}$ , but no significant difference in density peak indicating the potential existence of compensatory changes.<sup>118</sup> In atrial myocytes, the lack of  $\text{Ca}_v1.3$  channels in null mutant mice results in a depolarizing shift in the voltage-dependent activation of  $I_{\text{Ca,L}}$ .<sup>111</sup>

$\text{Ca}_v1.2$  also contributes the L-type  $\text{Ca}^{2+}$  current in SAN.<sup>12</sup> BayK induced heart rate increase is absent in  $\text{Ca}_v1.2^{\text{DHP-/-}}$  mice, indicating the contribution of  $\text{Ca}_v1.2$  to SAN automaticity regulation.<sup>117</sup> However, more research is needed.

### 1.2.1.1 3 T-type $\text{Ca}^{2+}$ channel (TTCC)

T-type  $\text{Ca}^{2+}$  channel (TTCC) is also a voltage gated channel on sarcolemmal membrane as LTCC. It is activated at more negative voltage ( $\sim -70$  mV) than LTCC, and generates T-type  $\text{Ca}^{2+}$  current ( $I_{\text{Ca,T}}$ , Figure 3).<sup>6, 13, 95</sup> TTCC is expressed in embryonic and adult heart, including SAN, the AVN and the Purkinje fiber network, but not in other working cardiomyocytes.<sup>95, 120-128</sup> Comparison of the expression of  $\text{Ca}_v3.1$  protein in human SAN, paranodal area and right atrium shows a significant higher expression of  $\text{Ca}_v3.1$  in SAN and paranodal area than in right atrium (Figure 5).<sup>88</sup> Comparison of  $I_{\text{Ca,T}}$  density in SAN between species indicates a reverse dependence upon the body size, i.e.  $I_{\text{Ca,T}}$  density is larger in small animals and become smaller as the body size increases.<sup>129</sup> The  $I_{\text{Ca,T}}$  density sequence for different species is mouse>guinea pig>rabbit>pig, while it is substantial in mouse SAN cells and almost absent in porcine SAN cells.<sup>129</sup>

In contrast to LTCC, TTCC displays slower activation, faster voltage dependent inactivation and lower channel conductance.<sup>96, 130</sup> Besides, unlike LTCC, TTCC is insensitive to dihydropyridines, but sensitive to micromolar  $\text{Ni}^{2+}$  ions. Application of  $\text{Ni}^{2+}$  to SAN cells slows pacemaking.<sup>95, 100, 131</sup> However, the mechanism under the contribution of TTCC to SAN automaticity is not fully understood. The low activation voltage may indicate its involvement in initiation of diastolic depolarization and SAN automaticity. Moreover, a research suggested that  $I_{\text{Ca,T}}$  triggers  $\text{Ca}^{2+}$  sparks from the SR, which in turn stimulate NCX activation and depolarize the pacemaker potential to threshold in cat SAN cells.<sup>131, 132</sup> Although, one study found  $\text{Ni}^{2+}$  only

slightly decreased cycle length, and did not decrease the number of  $\text{Ca}^{2+}$  sparks in rabbit SAN cells, while a species dependent role of TTCC may exist.<sup>133</sup> Notably,  $\text{Ni}^{2+}$  is also used as an inhibitor of NCX.

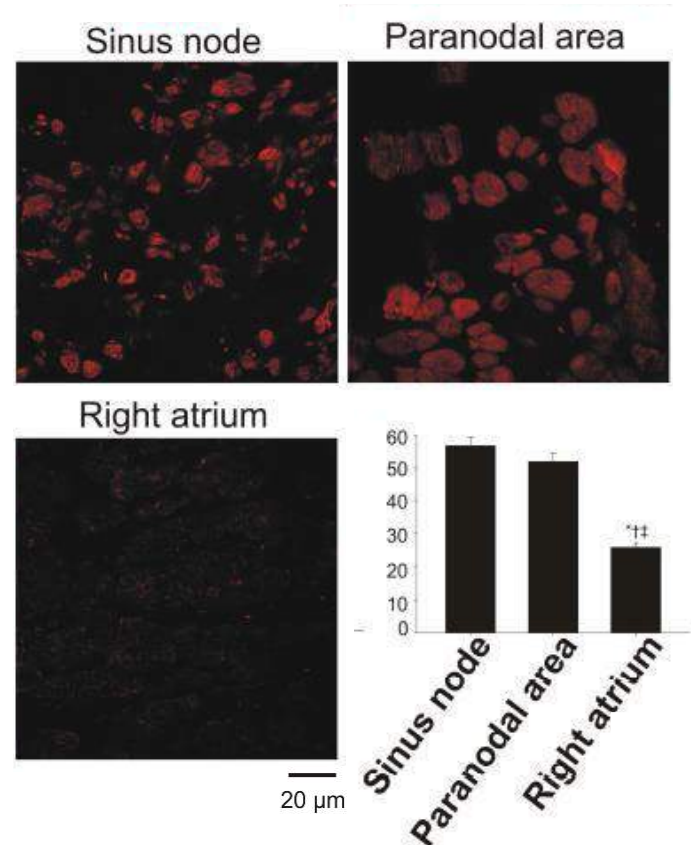


Figure 5. Expression of  $\text{Ca}_v3.1$  protein in human SAN, paranodal area and right atrium. The three high power images show the immunolabelled  $\text{Ca}_v3.1$  (red signal) in the SAN, paranodal area and right atrium. The bar graph indicates the intensity of  $\text{Ca}_v3.1$  protein labeling in the three areas. Means+SEM (n=4) is shown. \* and † represent significantly different ( $P<0.05$ ) from SN (\*) or PN (†) (one-way ANOVA); ‡ indicates significantly different ( $P<0.05$ ) from PN (paired t-test). (Adapted from Chandler et al., 2009<sup>88</sup>)

TTCC is structurally homologous to LTCC. Three  $\alpha_1$  subunits have been cloned for TTCC, termed  $\text{Ca}_v3.1$ ,  $\text{Ca}_v3.2$  and  $\text{Ca}_v3.3$  corresponding to  $\alpha_{1G}$ ,  $\alpha_{1H}$ ,  $\alpha_{1I}$ .<sup>108</sup>  $\text{Ca}_v3.1$  is expressed in cardiac muscle, skeletal muscle and neurons, while  $\text{Ca}_v3.2$  is expressed in cardiac muscle and neurons, and  $\text{Ca}_v3.3$  is only expressed in neurons.<sup>80, 108, 123, 124</sup> The transcription level of  $\text{Ca}_v3.1$  is higher than  $\text{Ca}_v3.2$  in SAN.<sup>134</sup> Genetically modified mice have been used to understand the roles of TTCC isoforms.

Genetic inactivation of  $\text{Ca}_v3.1$  TTCC in mice causes bradycardia, delays atrioventricular conduction, and prolongs the SAN recovery time.<sup>123</sup> Isolated SAN cells present slower pacemaker activity by 37% and a related reduction of the slope of the diastolic depolarization, and isolated AVN cells also show slower pacemaker activity.<sup>119, 123</sup> Le Quang et al. used radiofrequency AVN

ablation to produce atrioventricular block in  $Ca_v3.1$  deficient mice and discovered that loss of T-type  $Ca^{2+}$  channels worsens bradycardia-related mortality, increases bradycardia-associated adverse remodeling, and enhances the risk of malignant ventricular tachyarrhythmias complicating AV block.<sup>135</sup> Thereby, TTCC plays an important role in SAN spontaneous beating generation and infranodal escape automaticity.  $Ca_v3.1$  inactivation completely abolished  $I_{Ca,T}$  suggesting  $Ca_v3.1$  is the major component of  $I_{Ca,T}$  in adult mouse SAN cells.<sup>123</sup>

In contrast, no cardiac arrhythmias are observed in  $Ca_v3.2$  deficient mice, and ECG waveform morphologies are normal, which indicates the insignificant contribution of  $Ca_v3.2$  mediated T-type  $Ca^{2+}$  current to impulse initiation and conduction.<sup>136</sup> However, a research shows a higher expression of  $Ca_v3.2$  compared to  $Ca_v3.1$  in embryonic myocardium, suggesting the functional role of  $Ca_v3.2$  in embryonic murine heart.<sup>137</sup> The adult heart expresses more  $Ca_v3.1$ , switching transcription from  $Ca_v3.2$  to  $Ca_v3.1$  in the perinatal period.<sup>137</sup>

#### **1.2.1.1 4 Sodium channel**

The upstroke of SAN AP is relatively slower than in ventricle, as it is driven by  $Ca^{2+}$  channels rather than  $Na^+$  channels attributed to the lack of  $Na^+$  channels in SAN cells. Recent evidences showed the existence of  $Na^+$  channels in SAN, although, with heterogeneous distribution.

Two sodium currents have been identified in SAN brought out by two kinds of sodium channels: the TTX-resistant cardiac isoform ( $Na_v1.5$ ) inhibited by nanomolar concentration of tetrodotoxin (TTX), and the TTX-sensitive neuronal isoforms ( $Na_v1.1$  in rat,  $Na_v1.1$  and  $Na_v1.3$  in mouse) inhibited by micromolar TTX.<sup>6, 138, 139</sup>

It was shown in different studies that  $Na_v1.5$  is absent in SAN center, but present in the periphery.<sup>138-140</sup> The distribution of  $Na_v1.5$  in periphery indicates its potential contribution in electric impulse propagation.<sup>140</sup>

The distribution of TTX-sensitive sodium channel is controversial. Honjo et al. showed that TTX-sensitive sodium current is absent in small cells from the SAN center, but present in the periphery.<sup>141</sup> In support of this view, Kodama et al. found that blockade of  $Na^+$  current by tetrodotoxin has no effect on SAN center tissue, but slows spontaneous activity in periphery tissue.<sup>101</sup> However, more recent studies showed the  $Na_v1.1$  is present throughout the SAN, while blockage of TTX-sensitive sodium currents results in significant reduction of spontaneous pacemaking.<sup>138, 139</sup> It has also been reported that the TTX-sensitive sodium current accounts for spontaneous activity in the SAN cells from newborn rabbits.<sup>142-144</sup>

#### **1.2.1.1.5 Potassium channels**

There are several types of  $K^+$  channels reported in SAN, such as voltage dependent  $K^+$  channel ( $I_{to}$ ,  $I_{sus}$ ,  $I_{Kr}$ ,  $I_{Ks}$ ), inward rectifier  $K^+$  channel ( $I_{K1}$ ), ATP dependent  $K^+$  channel ( $I_{KATP}$ ), acetylcholine-activated  $K^+$  channel ( $I_{KACH}$ ), calcium-activated  $K^+$  channel ( $I_{KCa}$ ), etc.<sup>6, 16</sup>

$I_{Kr}$  and  $I_{Ks}$  are voltage-gated, and they are also delay rectifier currents which are characterized by an increased positive slope at more positive membrane potential and slow deactivation kinetics.<sup>6, 7</sup> For instance,  $I_{Kr}$  reaches full activation at membrane potential of -10mV and displays strong inward rectification.<sup>145</sup> The activation of  $I_{Kr}$  is counterbalanced by inactivation at positive voltage, and causing the negative slope conductance.<sup>145</sup> When the membrane potential reaches back to negative,  $I_{Kr}$  de-activates slowly and generates tail currents.<sup>145</sup>  $I_{Kr}$  is a “rapidly activating” delay rectifier  $K^+$  current, activated by depolarized membrane potentials from -50mV.<sup>146</sup> Compared with  $I_{Kr}$ ,  $I_{Ks}$  has slower activation and faster deactivation kinetics.<sup>147</sup>  $I_{Kr}$  and  $I_{Ks}$  are encoded by ERG1 gene and KCNQ1 gene, respectively.  $I_{Kr}$  is sensitive to class III methanesulfonanilide compounds, such as E-4031 at micromolar concentration, while  $I_{Ks}$  is not sensitive to these agents.<sup>6, 148</sup> Species dependent differences in  $I_{Kr}$  and  $I_{Ks}$  distribution exist. In porcine SAN cells, E4031 hardly affected  $I_K$ , while blockage of  $I_{Ks}$  inhibited  $I_K$ , indicating  $I_{Ks}$  is the predominant component of  $I_K$  in pig.<sup>149</sup> Satoh et al. supported this view and suggested the only  $I_{Ks}$  current (without  $I_{Kr}$ ) contributes to the porcine SAN.<sup>43</sup> Only  $I_{Kr}$  is recorded in mouse SAN, while both  $I_{Kr}$  and  $I_{Ks}$  account for the rabbit and guinea pig SAN.<sup>6, 43, 149</sup> Besides, blockage of  $I_{Kr}$  by micromolar E-4031 causes a cession of SAN pacemaking in isolated SAN cells of rabbit and guinea pig.<sup>150, 151</sup> E-4031 can also slow pacemaker activity in isolated mouse hearts and in rabbit right atrial preparations.<sup>145, 152</sup> Thus, the presence of  $I_{Ks}$  rather than  $I_{Kr}$  in pig can be a form of adaption to slower heart rate in large mammals than in rodents.<sup>6, 43, 149</sup> Lei et al. also suggested that in rabbit SAN, the contribution of  $I_{Ks}$  to beating rate is small under control condition, but significant during  $\beta$ -adrenergic stimulation.<sup>153</sup>

The transient outward current ( $I_{to}$ ) is characterized by rapid activation and inactivation kinetics, and sensitivity to 4-AP.<sup>154, 155</sup>  $K_V1.4$  ( $I_{to,fast}$ ),  $K_V4.3$  and  $K_V4.2$  ( $I_{to,slow}$ ) conduct the fast and slow components of the outward  $K^+$  current. The sustained outward  $K^+$  current ( $I_{sus}$ ) is the sustained part of initially discovered  $I_{to}$  or  $I_{4-AP}$ .<sup>154</sup>

Inward rectifier current ( $I_{K1}$ ) presents in ventricle and is responsible for the maintenance of resting membrane potential. However, the density of  $I_{K1}$  is generally low in pacemaker cells. It has been reported that  $I_{K1}$  is absent in guinea pig, rabbit and pig SAN, but present in mouse, rat and monkey SAN.<sup>43</sup> Consistent with that, a much lower density of  $I_{K1}$  was found in mouse and rat SAN than in ventricle.<sup>44, 156</sup>

The acetylcholine-activated  $K^+$  current ( $I_{KACH}$ ) has been described in SAN, atria and AVN.<sup>157-159</sup> Two genes Kir3.1 and 3.4 are responsible for  $I_{KACH}$  in the heart.<sup>160</sup>  $I_{KACH}$  is activated by muscarinic



and adenosine receptors via binding of G protein  $\beta\gamma$  subunits to the channel.<sup>6, 11, 160, 161</sup> A recent study showed that genetic or pharmacological inhibition of  $I_{KACH}$  abolishes sick sinus syndrome in CaV1.3 knock-out mice, via allowing net inward current to flow during the DD during cholinergic activation.<sup>162</sup> Thus,  $I_{KACH}$  could be a potential therapeutic target for treatment of sick sinus syndrome. Interestingly, acetylcholine slows the cardiac pacemaking not only through activation of  $I_{KACH}$ , and also through negative regulation of cAMP and concomitant activity of  $I_f$ . Furthermore, low concentration (nanomolar) of acetylcholine is sufficient to inhibit  $I_f$ , whereas higher concentration (micromolar) is required to activate  $I_{KACH}$ .<sup>157</sup> This view is supported by Yamada who found that heart rate reduction induced by low ACh doses (<100 nM) was insensitive to  $I_{KACH}$  inhibition.<sup>163</sup> These data indicate the existence of multiple effects by ACh stimulation, and the less important role of  $I_{KACH}$  in response to nanomolar ACh. The ATP-dependent  $K^+$  current ( $I_{KATP}$ ) is identified in rabbit and rat SAN.<sup>164, 165</sup> It is activated by stretch or by low levels of intracellular ATP.<sup>164, 165</sup> Activation of  $I_{KATP}$  in rabbit SAN cells hyperpolarizes the membrane, and slows or abolishes the pacemaker activity.<sup>165</sup>

The calcium-activated  $K^+$  channels are activated by elevation of cytosolic calcium and accounts for the membrane hyperpolarization.<sup>11, 166</sup> According to the channel conductance, calcium-activated  $K^+$  channels is divided into three subfamilies: BK, SK and IK, which exhibit “big”, “small” and “intermediate” conductance, respectively.<sup>11, 166</sup> Big conductance calcium-activated potassium (BK,  $K_{Ca1.1}$ ) channels are expressed in central nervous system, smooth muscle, and the SAN.<sup>11, 167, 168</sup> It has been recently demonstrated that the BK channels are involved in the regulation of cardiac automaticity. Pharmacological inhibition of BK channels significantly reduces the automaticity of conscious mice heart and isolated rat heart in a dose-dependent manner.<sup>169</sup> Besides, the automaticity of SAN cells is reduced by application of BK channel inhibitors, and isolated SAN cells from mice with genetic deletion of BK exhibit slower firing rate, both associated with the lengthening of the diastolic depolarization phase of SAN cell action potential.<sup>170</sup> Small conductance calcium-activated potassium (SK1-4) channels also play a fundamental role in heart.<sup>11</sup> SK channels in mitochondrial inner membrane of guinea pig ventricular myocytes contribute to mitochondrial  $K^+$  uptake and protect hearts against infarction.<sup>171</sup> SK1 ( $K_{Ca2.1}$ ), SK2 ( $K_{Ca2.2}$ ) and SK3 ( $K_{Ca2.3}$ ) are identified in human and mouse atria and ventricles.<sup>172, 173</sup> Genetic knock-out of SK2 channels results in prolongation of action potential duration especially in repolarization in atrial myocytes, and inducible atrial fibrillation in null mutant mice.<sup>174</sup> Qi et al. further confirmed the participation of SK2 in atrial fibrillation maintenance.<sup>175</sup> SK4 ( $K_{Ca3.1}$ ) channel also play an important role in cardiac pacemaker derived from human embryonic stem cells.<sup>176</sup>

#### **1.2.1.1.6 Other channels**

The sustained inward current ( $I_{st}$ ) was identified in SAN of mouse, rabbit, rat, guinea pig, and also in rabbit AVN, but absent in quiescent cells.<sup>6, 44, 156, 177-180</sup> It is activated at membrane potential of about -70mV, reaches the peak at about -50mV, and shows little inactivation during depolarization.<sup>177, 180</sup> The distinct expression pattern and activation of  $I_{st}$  indicate its role for the membrane depolarization and SAN automaticity generation.<sup>180</sup> This current is carried mainly by  $Na^+$ , but it is distinct from  $I_{Na}$ , as this current is TTX-insensitive, can be blocked by DHP antagonists, facilitated by BAY K 8644 and inhibited by divalent cations.<sup>6, 177</sup> These characteristics of  $I_{st}$  also suggest that  $I_{st}$  might be mediated by a novel subtype of LTCC.<sup>177</sup>

Two kinds of transient receptor potential (TRP) channels were found in SAN, TRPC (C stands for canonical) and TRPM (M stands for melastatin). TRPC channels are nonselective cation channels that regulate ion homeostasis and intracellular  $Ca^{2+}$  signaling in numerous cell types, as well as store-operated calcium entry (SOCE).<sup>181</sup> The TRPC subfamily contains seven isoforms (TRPC1-7), which could be divided into three groups based on the sequence alignments and functional comparisons: TRPC1/4/5, TRPC3/6/7 and TRPC2. TRPC2 is not expressed in human.<sup>182</sup> TRPC3/6/7 are activated by diacylglycerol (DAG), produced by PLC-mediated hydrolysis of phosphatidylinositol 4, 5-bisphosphate (PIP2). TRPC1, 4 and 5 are activated by SR  $Ca^{2+}$  depletion or by stretch.<sup>183, 184</sup> The stromal interaction molecule 1 (STIM1) is located in the SR acting as a  $Ca^{2+}$  sensor and oligomerized when SR  $Ca^{2+}$  is depleted, which in turn activates Orai1 and TRPC1/4/5 via directly binding.<sup>185, 186</sup> STIM1 also indirectly activate TRPC3/6, but not TRPC7.<sup>187</sup> Besides, it has also been suggested that Orai and TRPC form complexes that participate in SOCE.<sup>187</sup> And in support of that, Pani et al. observed that TRPCs are colocalized with STIM1 and Orai in lipid raft domains.<sup>188</sup> However, other investigators have not observed a role for TRPC channels in the Orai/STIM1 complex.<sup>189, 190</sup> Activation of TRPCs promotes cardiac hypertrophy by  $Ca^{2+}$  influx and subsequent calcineurin activation.<sup>191-194</sup> In SAN, TRPC1-4, 6 and 7 are detected, but not TRPC5.<sup>195, 196</sup> TRPCs related SOCE is probably involved in modulation of heart rate rhythm.<sup>196-199</sup> Mice lacking the TRPC3 gene demonstrated the involvement of TRPC3 in sinoatrial arrhythmias.<sup>197, 198</sup> Orai1 is also expressed in SAN and plays a potentially important role in SOCE in SAN pacemaking.<sup>200, 201</sup> Certainly, STIM1 also influences SAN function by reducing SR  $Ca^{2+}$  content and regulating ionic fluxes in SAN cells.<sup>200</sup>

TRPM4 and TRPM7 were detected in SAN, and both of them participate in SAN automaticity generation. TRPM4 is a  $Ca^{2+}$ -activated nonselective cation channel driving sodium and potassium inward current.<sup>202-204</sup> Pharmacological inhibition of TRPM4 reduces the automaticity associated with a reduction in diastolic depolarization slope in mouse or rat heart.<sup>203</sup> TRPM7 is a divalent-permeant channel.<sup>205</sup> Mice with global or SAN restricted TRPM7 deletion show sinus pauses and

AVN block with slower diastolic depolarization and reduced HCN4 mRNA, indicating TRPM7 influences SAN automaticity via regulation of HCN4 expression.<sup>205</sup>

Other electrogenic molecules (such as Na<sup>+</sup>- K<sup>+</sup> pump, etc) also exist on sarcolemmal membrane of SAN cells and influence the maintenance of the ionic homeostasis and the normal SAN automaticity.<sup>6</sup> The Na<sup>+</sup>- K<sup>+</sup> pump excludes three Na<sup>+</sup> for two K<sup>+</sup> uptake resulting in the generation of an outward current, which also influences the pacemaker activity of SAN cells.<sup>6, 206</sup>

### **1.2.1.2 Membrane clock**

The ensemble of sarcolemmal electrogenic molecules forms a voltage membrane oscillator, known as voltage clock or membrane clock. According to membrane clock, the SAN action potential is predominantly generated by the funny current (I<sub>f</sub>), which is activated by membrane hyperpolarization. It depolarizes the membrane, and then activates multiple voltage-gated ion channels, such as TTCC, LTCC, etc.<sup>207, 208</sup> The multiple ion channels lead to diastolic depolarization as well as upstroke of the action potential via LTCC. Then, the membrane potential is repolarized to the maximum diastolic potential by K<sup>+</sup> channel.

### **1.2.2 Ca<sup>2+</sup> clock theory**

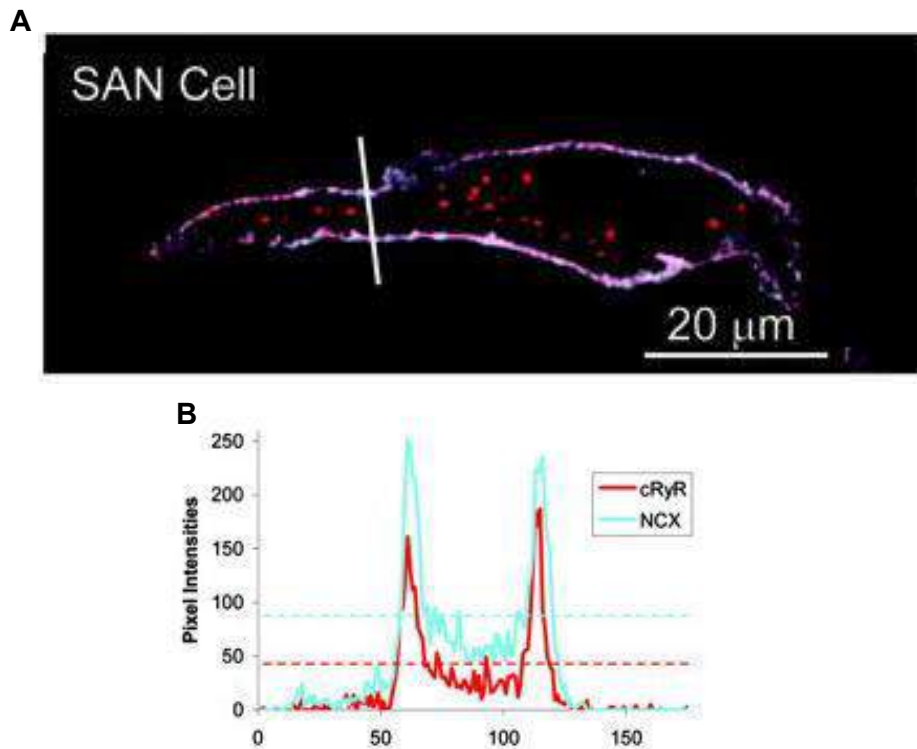
#### **1.2.2.1 Sodium-calcium exchanger (NCX)**

Sodium-calcium exchanger (NCX) is a high-capacity, voltage-dependent, Ca<sup>2+</sup>-dependent and time-independent electrogenic protein. It is located on the sarcolemmal membrane, and colocalized with cardiac RyR (Figure 6).<sup>209</sup> It is one of the major electrogenic molecules that maintain Ca<sup>2+</sup> homeostasis in SAN cells, and also contributes to diastolic depolarization in SAN cells.<sup>16</sup> NCX activity is enhanced by the localized SR Ca<sup>2+</sup> release during diastolic depolarization.<sup>131, 210</sup> It extrudes Ca<sup>2+</sup> from the cell and brings in Na<sup>+</sup>. As one Ca<sup>2+</sup> ion is extruded for exchanging of three Na<sup>+</sup> ions, NCX produces an inward current (I<sub>NCX</sub>) and further depolarizes the membrane (Figure 3).<sup>6, 211</sup> Many studies suggest the RyR-NCX-SERCA crosstalk ensure the SAN cell function (coupled clock).<sup>16, 212</sup> Indeed, acute blockade of the NCX via inhibitor (KB-R7943), via rapid substitution of Na<sup>+</sup> by Li<sup>+</sup>, application of ryanodine (RyR<sub>2</sub> inhibitor), or chelation of intracellular [Ca<sup>2+</sup>]<sub>i</sub> abolishes SAN cells beating.<sup>213-215</sup> These data indicate that I<sub>NCX</sub> is attributed to elevated [Ca<sup>2+</sup>]<sub>i</sub>, and via RyR-NCX-SERCA crosstalk contributing to SAN pacemaking.

The NCX protein contains ten helical transmembrane domains, and a large intracellular loop between the fifth and sixth domains.<sup>216-219</sup> The intracellular loop contains two calcium binding domains (CBD1 and CBD2) that are required for intracellular ion sensing and binding, and a XIP domain which confers sodium inactivation properties.<sup>216</sup> Crystal structure shows that NCX from

*Methanococcus jannaschii* has four ion binding sites at the center of the protein, while one of them is specific for  $\text{Ca}^{2+}$  and the other three are likely for  $\text{Na}^{+}$  to perform the ion exchange.<sup>217</sup>

Three NCX isoforms (NCX1-3) have been found to date. NCX1 is expressed widely in mammalian tissues, and considered as cardiac isoform.<sup>220-222</sup> NCX2 is predominantly expressed in smooth muscles and brain, and NCX3 is mainly expressed in skeletal muscle.<sup>220, 221</sup> Their levels vary considerably during postnatal development.<sup>221</sup>



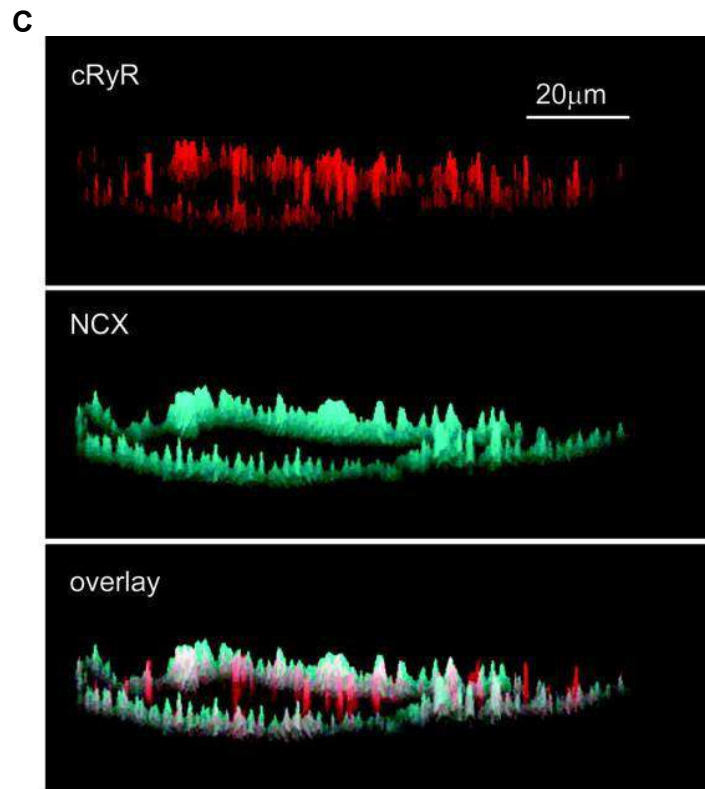


Figure 6 The distribution of NCX and RyR in rabbit SAN cells. A. Confocal image of SAN cell immunolabeled for both NCX and RyR. B. Pixel-by-pixel fluorescence intensities of labeling along the arbitrary line in panel A. And the horizontal dashed lines report the average pixel intensity. C. Topographical profiles of the pixel intensity levels of each antibody labeling and overlay of the small SAN cells in panel A. The maximum height represents the brightest possible pixel in the source image (using an 8-bit image intensity scale). Less bright pixels are accordingly scaled to a smaller height. (Adapted from Lyashkov et al., 2007<sup>209</sup>)

Genetically modified mice are used to understand the contribution of NCX1 to SAN automaticity. A total suppression of NCX1 results in lack of spontaneously beating heart and embryonic lethality.<sup>223</sup> To overcome this problem, Gao et al. generated incomplete NCX1 knockout mice and suggested that NCX1 is critical for fight or flight reaction of SAN, but is not required for resting heart rate.<sup>224</sup> However, this mice model was challenged by Maltsev et al. (2013), who indicated that the lower expression of NCX1 could be compensated by the local cross-talk between  $\text{Ca}^{2+}$  cycling proteins and NCX, i.e. lower NCX1 expression encourages CICR and in turn stabilize the density of  $I_{\text{NCX}}$ . Therefore, they suggested that NCX1 is critical for both SAN “fight or flight” reaction and maintenance of basal automaticity. Indeed, mice, selectively lacking NCX1 in cardiac pacemaking and conduction system, show slower heart rate accompanied by severe arrhythmias.<sup>225</sup> Furthermore, complete atrial-specific NCX knockout mice lack P waves, and the isolated SAN cells are quiescent with consequently impaired  $\text{Ca}^{2+}$  efflux.<sup>226, 227</sup>

### 1.2.2.2 RyR<sub>2</sub> in $\text{Ca}^{2+}$ clock

The involvement of RyR<sub>2</sub> Ca<sup>2+</sup> release in SAN automaticity was first carried out by the observation that application of ryanodine slowed pacemaker activity in cat right atrium.<sup>228</sup> Later studies further illustrated that both ryanodine (RyR blocker) and cyclopiazonic acid (SERCA blocker) reduced pacemaker activity in guinea-pig SAN tissue.<sup>229, 230</sup> A concentration of 30μM of ryanodine abolish activity in 83% of isolated-rabbit SAN cells, although in another study the same concentration of ryanodine only inhibited rabbit SAN cell firing rate by ~20%.<sup>209, 231</sup> Inducible, cardiac-specific knockout of RyR<sub>2</sub> with acute ~50% loss of RyR<sub>2</sub> protein was sufficient to cause bradycardia and arrhythmias.<sup>232</sup> These studies point to the idea that the SR Ca<sup>2+</sup> release through RyR<sub>2</sub> plays an important role in pacemaking.

### 1.2.2.3 Ca<sup>2+</sup> clock

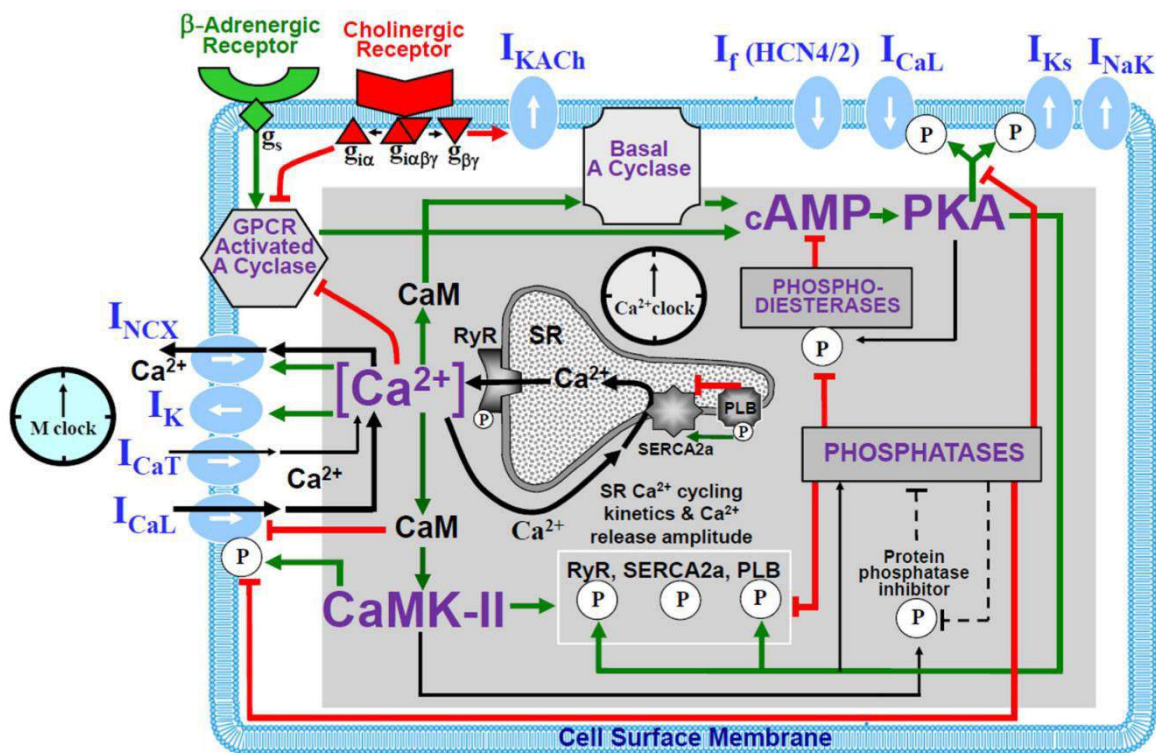


Figure 7: Schematic illustration of interactions of key molecules comprising the system. The common regulatory factors are lettered in purple, which govern the function of both the Ca<sup>2+</sup>-clock (gray intracellular area) and the M-clock (light-blue cell membrane area with blue labels depicting electrogenic proteins). The green arrows illustrate signaling driving action potential (AP) firing, while the red lines suppress the AP firing and balance the system. G protein-coupled receptors (green and red shapes within the membrane) modulate both the Ca<sup>2+</sup>-clock and M-clock function via those same crucial signaling nodes of the system. (Adapted from Maltsev et al., 2014<sup>16</sup>)

According to the Ca<sup>2+</sup> clock, the SR generates rhythmic Ca<sup>2+</sup> release (local Ca<sup>2+</sup> release, LCR) via RyR<sub>2</sub>. The LCRs activate NCX, which generates depolarizing current and causes the slow increase in membrane potential toward an excitation threshold for action potential firing, resulting in pacemaking (Figure 3).<sup>14, 16, 233</sup> The cytosolic Ca<sup>2+</sup> is extruded by NCX, or pumped back into SR

by SERCA (sarcoplasmic/endoplasmic reticulum  $\text{Ca}^{2+}$ -ATPase) to complete the  $\text{Ca}^{2+}$  cycle. The  $\text{Ca}^{2+}$  extruded by NCX should quantitatively match the  $\text{Ca}^{2+}$  entry through sarcolemmal, and the  $\text{Ca}^{2+}$  transferred by SERCA needs to match the  $\text{Ca}^{2+}$  released by  $\text{RyR}_2$ .<sup>6</sup> The involvement of  $\text{Ca}^{2+}$  release from  $\text{RyR}_2$  in SAN pacemaker activity was introduced previously. Subsequent work showed the involvement of following NCX current in pacemaking, and in response to  $\beta$ -adrenergic stimulation.<sup>131, 210, 213-215</sup> Besides, calcium sparks were found during the depolarization under normal  $\text{Ca}^{2+}$  condition, in absence of  $\text{Ca}^{2+}$  overload (Figure 3).<sup>131, 214</sup> It is likely that the LCRs depolarize the cell through activation of NCX that initiate the pacemaking.<sup>131, 214</sup> Moreover, in support of  $\text{Ca}^{2+}$  clock theory, Vinogradova et al. found periodic  $\text{Ca}^{2+}$  oscillations during voltage clamp or in detergent-permeabilized SAN cells in the absence of sarcolemmal function, and independent of diastolic membrane depolarization.<sup>234, 235</sup> For instance, in Figure 8, when the voltage clamp at potentials that prevent SAN cells from  $\text{Ca}^{2+}$  loss via NCX, the SR  $\text{Ca}^{2+}$  clock becomes 'free running' in spite of surface membrane.<sup>83</sup> Furthermore, in physiologic intracellular  $[\text{Ca}^{2+}]_i$  (150 nM), the free running  $\text{Ca}^{2+}$  clock generates roughly periodic LCRs with frequency 2-4 Hz.<sup>83</sup> Similarly, in detergent-permeabilized SAN cells, the LCRs were observed in 100nM bathing  $[\text{Ca}^{2+}]$ .<sup>234</sup> As shown in Figure 8 (right) rhythmic LCRs generate rhythmic current fluctuations in voltage-clamped SAN cell, and the frequency of current fluctuation is as the same as the frequency of LCRs.<sup>83</sup> These evidences indicate existence of LCRs and the independent  $\text{Ca}^{2+}$  clock.

### 1.2.3 Coupled clock theory

Some studies suggested that membrane clock is not the only mechanism of SAN automaticity, as the membrane clock failed to understand some experimental results, such as the reduction or cessation of SAN automaticity produced by specific inhibition of  $\text{Ca}^{2+}$  cycling, and CaMKII or PKA-dependent phosphorylation.<sup>209, 228, 229, 235</sup> Thus, the coupled clock was proposed, which suggests the SAN pacemaker activity is generated by two coupled oscillators, membrane clock and  $\text{Ca}^{2+}$  clock.<sup>233</sup>

In the coupled clock, the membrane clock and  $\text{Ca}^{2+}$  clock are coupled via NCX, which generates an inward current and depolarizes the membrane to reach the threshold of activation of other ion channels, e.g. LTCC, and further regulate the  $\text{Ca}^{2+}$  clock. The  $\text{Ca}^{2+}$  clock is implicated directly by LTCC, NCX, etc, and also indirectly by  $\text{K}^+$  channels, HCN channels, etc, via respective membrane potential changes and regulating  $\text{Ca}^{2+}$  fluxes. For instance,  $\text{K}^+$  channels repolarize the membrane and activate HCN and other channels, while HCN limits the hyperpolarization. The accumulation of cytosolic  $\text{Ca}^{2+}$  in turn implicates membrane clock. The two clocks work together through numerous interactions modulated directly by membrane voltage, subsarcolemmal  $\text{Ca}^{2+}$ , and indirectly by PKA and CaMKII-dependent protein phosphorylation (Figure 7).<sup>14, 16, 233</sup> The cytosolic  $\text{Ca}^{2+}$  binds to calmodulin, and CaMKII and to  $\text{Ca}^{2+}$  dependent adenylyl cyclase (AC) resulting in



the production of high basal cAMP (Figure 7). The contributions of the interactions are discussed below. Based on the mutual entrainment of the interactions, the two clocks form a robust, stable, coupled-clock system that ensure the normal SAN automaticity.<sup>14, 16, 233</sup>

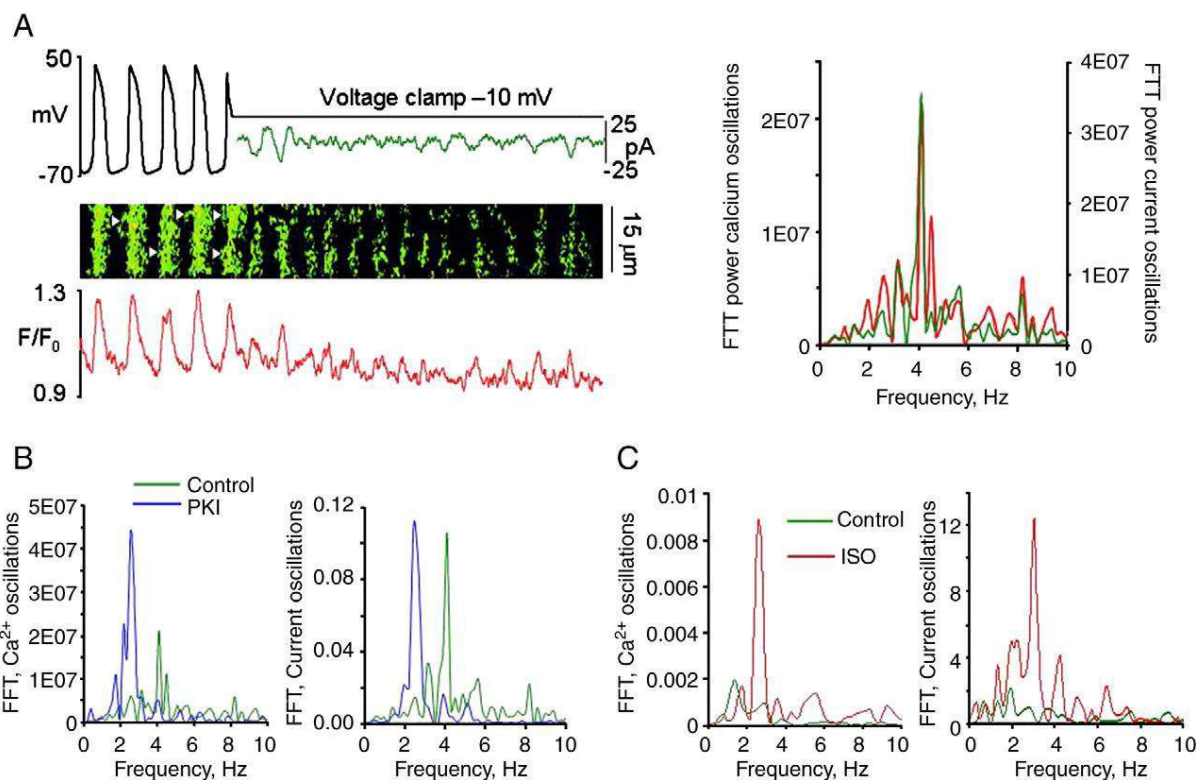


Figure 8 LCRs and current fluctuations in SAN cell during voltage clamp. The left part of panel A shows simultaneous recordings of membrane potential or current (top), confocal line-scan image (middle), and normalized fluo-3 fluorescence (bottom) averaged over the line-scan image, in a representative spontaneously beating rabbit SAN cell; and the right part shows Fast Fourier transform (FFT) of Ca (red) and membrane current fluctuations (green). B. PKA inhibition with PKI shifts FFT of both  $\text{Ca}^{2+}$  and membrane current fluctuations to lower frequencies during voltage clamp. And  $\beta$ -adrenergic receptor stimulation (panel C) with isoproterenol shifts FFT of both Ca and membrane current fluctuations to higher frequencies during voltage clamp. (Adapted from Vinogradova and Lakatta, 2009<sup>83</sup>)

Neutral theories also exist. For instance, Capel and Terrar claimed that the “ $\text{Ca}^{2+}$  clock” plays a modulatory rather than essential role that cooperates with membrane clock, and this is also referred as “coupled clock”.<sup>236</sup> However, more studies are needed in this area.

#### 1.2.4 Autonomic regulation of cardiac automaticity

Autonomic nervous system is the major extracardiac determinant of the heart rate. The cardiac sympathovagal is a complex phenomenon, containing multiple interactions between sympathetic and parasympathetic centers in the central nervous system.<sup>2, 6, 237</sup> In the adult heart, the sympathetic branch of the autonomic nervous system accelerates heart rate, while the parasympathetic branch slows it. It is also worth to note that sympathetic and vagal activations induce shifts in the leading pacemaker site, which could be explained by the regional densities of adrenergic and muscarinic receptors of SAN.<sup>238, 239</sup>



As a terminal part of the cardiac autonomic nervous system, the intrinsic cardiac neuronal plexus (ICNP) plays a pivotal role in regulating heart rate, conduction, myocardial contractile force and coronary blood flow.<sup>240</sup> The canine SAN is densely innervated by nerve fibers of ICNP, which forms ~400 ganglia around the junction between the right atrium and the superior vena cava.<sup>241</sup> The canine atrium, including the SAN, was estimated to be innervated by more than 54,000 intracardiac neurons.<sup>241</sup> A similar organization of SAN innervation by the ICNP was found in human, while the human heart contains on average ~800 epicardial ganglia (ranged from ~700 up to ~1500) and estimated ~43,000 intrinsic neurons (in adult heart, 94,000 in young heart).<sup>242</sup> In rat epicardium, intrinsic nerves clustered into six routes by which they are selectively projected to different atrial and/or ventricular region.<sup>243</sup> For instance, the rat AVN and AV bundle are innervated by a dense network of thin endocardial nerves projecting from a neuronal cluster adjacent to the interatrial septum and the right pulmonary sinus.<sup>243</sup> As seen in human, the number of intrinsic cardiac neurons in rats is also age-dependent, ~6500 in old rats and ~5000 in juvenile rats.<sup>243</sup> In general, small nerves in the SAN contain 5-15 axons, through what the neurotransmitter (such as catecholamine) is released, while gaps between varicosities and nodal cells are 20-100  $\mu\text{m}$  depending on the species.<sup>2</sup> Adrenergic and nonadrenergic release sites are found in close vicinity to each other.<sup>2</sup>

Sympathetic and parasympathetic limbs combine and act as autonomic control regulating the pacemaker activity. However, the ratio between vagal and sympathetic input differs among species.<sup>2, 6</sup> This different ratio of vagal and sympathetic input is one explanation of the different basal heart rates in mammals, which are inversely correlated with the body weight, although the intrinsic properties of pacemaker cells in different species also account.<sup>2, 6</sup> The two branches of the autonomic nervous system interact to generate an adaptable equilibrium, thus SAN automaticity can be under dominance of the sympathetic or parasympathetic limb.<sup>6</sup> In mice, it seems like sympathetic tone is dominant, as the isolated SAN beats significantly slower than the heart rate in vivo, although a vagal tone is nevertheless present.<sup>6</sup> In contrast, dogs and humans show vagal predominance as combined muscarinic plus  $\beta$ -adrenoceptor blockage accelerates the heart rate.<sup>2, 6</sup> When the SAN is under sympathetic tone, the effect of parasympathetic input is greater, and this phenomenon is named “accentuated antagonism”.<sup>237</sup> The ratio between vagal and sympathetic input could also be influenced. For instance, long-term endurance training increases parasympathetic activity and decreases sympathetic activity in human heart at rest, termed cardiovascular adaptation.<sup>244</sup> This enhanced vagal tone could also explain the bradycardia observed in the trained athlete, although the local factors should also be considered, such as downregulation of HCN4 channel.<sup>245, 246</sup>

Besides the autonomic balance, cardiac automaticity is also modulated on a beat-by-beat basis, which results in quickly adapted pacemaking to physiological state of the organism.<sup>6</sup> Thus the high-frequency and low-frequency spectra of the heart rate variability could be used to evaluate the

dynamic regulation of pacemaking.<sup>6, 247-249</sup> However, intrinsic factors might also involve in the beat-by-beat regulation of heart rate.

#### **1.2.4.1 Sympathetic regulation of cardiac automaticity**

Sympathetic control of pacemaker activity is carried out through  $\beta$ -adrenergic receptor ( $\beta$ -AR) activation by catecholamines (Figure 7).  $\beta$ -ARs belong to the superfamily of G-protein-coupled receptors, of which the conformational change could induce activation of associated G protein and in turn activate ACs and ACs/cAMP pathway (Figure 7).<sup>250</sup> AC5 and AC6 are the major isoforms in heart activated by  $\beta$ -AR stimulation, while AC1 and AC8 are  $\text{Ca}^{2+}$  activated.<sup>250</sup> ACs activation results in a higher level of basal cAMP. Thereby, catecholamines activate  $\beta$ -ARs/ACs/cAMP signaling which regulates SAN automaticity through interaction with both membrane and  $\text{Ca}^{2+}$  clock (Figure 7), and the modification of the coupled-clock causes the positive chronotropic effects. The resultant enhanced  $[\text{Ca}^{2+}]_i$  contributes a negative feedback effect that inhibits AC5 and AC6, but a positive feedback effect on  $\text{Ca}^{2+}$ -activated ACs (AC1 and AC8).<sup>251</sup>

#### **AC1- and AC8- induced cAMP-PKA pathway in basal pacemaker activity**

Basal cAMP and cAMP-mediated PKA-dependent phosphorylation forms an essential role in basal SAN pacemaker activity via both  $\text{Ca}^{2+}$  clock and membrane clock. Early studies have demonstrated that superfusion of rabbit SAN with cAMP containing solution increases the spontaneous beating rate, with a marked increase in the DD slope.<sup>252-254</sup> In support of that, addition of adenylyl cyclase (AC, cAMP producer) inhibitors suppressed the spontaneous activity of rabbit SAN, while the effect could be restored after addition of dibutyryl cAMP.<sup>255</sup> The basal cAMP level is ~10-fold higher in rabbit SAN cells than in atrial or ventricular myocytes.<sup>234</sup>

Further researches found a link between  $\text{Ca}^{2+}$  and cAMP (Figure 7), followed by the discovery of  $\text{Ca}^{2+}$ -activated ACs (AC1 and AC8) in SAN.<sup>256, 257</sup> Mammalian ACs consists of nine isoforms.<sup>258</sup> AC5 and AC6 are the major isoforms in the heart activated by  $\beta$ -AR stimulation, while AC5 is predominantly expressed in mature adult ventricle and AC6 is mainly in fetal ventricle.<sup>250</sup> In contrast, AC1 and AC8 are activated by  $\text{Ca}^{2+}/\text{CaM}$ . They are primary found in neuronal tissue and later found in rabbit and guinea-pig SAN within membrane lipid microdomains.<sup>257, 258</sup> The activation of basal AC within physiologic intracellular  $\text{Ca}^{2+}$  range (0.2-1 $\mu\text{M}$ ) is  $\text{Ca}^{2+}$  dependent, indicating that basal  $\text{Ca}^{2+}$  cycling regulates  $\text{Ca}^{2+}$ -activated AC-cAMP pathway resulting in rhythmic LCRs and driving the generation of rhythmic action potential.<sup>257</sup> Besides,  $\beta$ -AR stimulation induced cAMP is not reduced by  $\text{Ca}^{2+}$  chelation, suggesting that this  $\beta$ -AR stimulation related AC activation is distinct from  $\text{Ca}^{2+}$  activated ACs which regulates basal cAMP.<sup>83</sup>

The cAMP also mediates PKA-dependent protein phosphorylation (Figure 7). The high basal cAMP level is attendant with high level of basal PKA-dependent phosphorylation, which is

obligatory for basal pacemaker activity.<sup>235</sup> Gradations in PKA activity, which is represented by targeted PLB phosphorylation and indexed by specific PKA inhibitor peptide (PKI), are highly correlated with gradations in LCR spatiotemporal synchronization and phase, as well as in beating rate (Figure 8).<sup>83, 235</sup> A higher level of PKA inhibition abolishes LCRs and spontaneous beating.<sup>235</sup> It has been shown that PKA phosphorylates many cellular proteins involved in SAN pacemaking, such as LTCC, PLB, RyR<sub>2</sub>, etc.<sup>235, 259</sup> For instance, PKA could phosphorylate PLB (Ser16), and thus the phosphorylated PLB releases the SERCA, which increases SERCA Ca<sup>2+</sup> affinity and enhances the Ca<sup>2+</sup> recovery.<sup>260</sup> However, PLB mutation on PKA target site (S16A) did not affect HR in vivo or firing rate in SAN cells, indicating multiple regulation of PKA on SAN beating activity.<sup>261</sup>

The production of cAMP is balanced by high basal phosphodiesterases (PDE) activity induced hydrolysis, which degrades cAMP into 5'-AMP.<sup>48</sup> This fail safe system controls the basal cAMP level, limits the cAMP-mediated phosphorylation and restricts the spontaneous SAN beating rate. Mammalian PDEs are encoded by 21 genes. They are categorized into 11 families based on sequence homology, enzymatic property and sensitivity to inhibitors. PDE families contain many splice variants that mostly show unique characteristics, such as tissue-expression pattern, enzymatic regulation by phosphorylation and regulatory proteins, subcellular localization, and interaction with association proteins.<sup>262</sup> PDE1, 2, 3, 10 and 11 regulate both cAMP and cGMP, while PDE 4, 7 and 8 regulate cAMP only, and PDE 5, 6 and 9 regulate cGMP only.<sup>262</sup> PDE1-5 and 7 are detected in heart, and PDE3 and PDE4 provide the major cAMP hydrolyzing activity.<sup>262</sup> In human, bovine, dog and rabbit myocardium, the main membrane-bound subtype is PDE3, whereas in mouse and frog ventricle microsomal PDE activity is markedly represented by PDE4.<sup>263</sup> In dog and rabbit ventricular tissue, PDE3 accounts for 70-85% of total cAMP hydrolyzing activity in microsomal fraction and about 30-40% in cytosol.<sup>263</sup> PDE4 represents 13% of the total cAMP hydrolyzing activity in microsomal fraction and 7-8% in cytosole in dog ventricle.<sup>263</sup> However, in murine heart, PDE4 is the dominant PDE subtype accounting for 60% of total cAMP hydrolyzing activity.<sup>263</sup> In rat ventricle, PDE3 and PDE4 activity are in equal level leading to ~90% of the total cAMP hydrolyzing activity.<sup>263</sup> It was also proposed that the localization of PDE3 differs from PDE4. PDE4 targets to sarcolemma in canine and human cardiac microsomal fractions, while PDE3 is mainly associated with T tubule and SR.<sup>263</sup> However, in rat cardiac myocytes, the localizations of PDE3 and PDE4 are mainly associated with sarcolemma.<sup>263</sup> PDE3 and PDE4 equally contribute to cAMP hydrolyzing activity in nuclear fraction of sheep cardiac myocyte in which they are mostly localized within nuclear envelope.<sup>263</sup> In SAN cells, several studies reported that suppression of PDE activity accelerates the spontaneous firing rate, with increased cAMP level and augmented DD slope.<sup>264-266</sup> A recent study inhibited PDE by 100μM IBMX, a broad-spectrum PDE inhibitor, leads

to 9-fold increase in cAMP level and ~55% increase in spontaneous beating rate.<sup>48</sup> Besides, PDE inhibition increased PKA-dependent PLB Ser16 phosphorylation, suggesting that PKA is involved in PDE-dependent regulation of spontaneous SAN firing.<sup>48</sup> Vinogradova et al. also compared the contribution of PDE1-5 to SAN firing rate with specific inhibitors in rabbit SAN,<sup>48</sup> where it was known that PDE3 is the most abundant subtype.<sup>267</sup> PDE3 inhibitor (milrinone) accelerated spontaneous firing (~47%) and increased amplitude of  $I_{Ca,L}$  (~46%), while the effects of other PDE inhibitors are minor, indicating that PDE3 is the major constitutively active PDE in basal state.<sup>48</sup>

RyR<sub>2</sub> function is critical for cAMP/PKA-induced acceleration of SAN spontaneous firing. Gradations in PKA activity affected by specific PKA inhibitor peptide (PKI) are related with gradations in LCRs spatiotemporal synchronization, as well as beating rate.<sup>235</sup> Higher level of PKA inhibition abolishes LCRs, as well as spontaneous beating.<sup>235</sup> Ryanodine limits the increase of SAN beating rate by CPT-cAMP (a membrane-permeable cAMP analog) from ~36% to ~13%.<sup>235</sup> Besides, the PDE inhibition-dependent acceleration also results in increased LCR amplitude and size and decreased LCR period, causing earlier and augmented LCR  $Ca^{2+}$  release, and increased NCX.<sup>48</sup> Addition of ryanodine prevents the IBMX and milrinone induced increase in LCRs,  $I_{NCX}$ , and SAN firing rate, despite the preserved augmentation of  $I_{Ca,L}$  amplitude.<sup>48</sup> These results confirmed that RyR<sub>2</sub> function is critical for cAMP/PKA-induced acceleration of SAN spontaneous firing. Basal constitutive PDE activation provides a powerful mechanism to decrease cAMP, thus via RyR<sub>2</sub> to restrict the spontaneous SAN firing rate.<sup>48</sup> Wu et al. reported that RyR<sub>2</sub> knock-in mutation on PKA target site (S2808A) failed to affect spontaneous firing rate and isoproterenol response in vivo and in SAN cells, indicating multiple PKA targets in SAN cells.<sup>261</sup>

The cAMP has a direct effect on  $I_f$ . DiFrancesco and Tortora showed that cAMP shifted  $I_f$  activation curve to more positive voltages.<sup>268</sup> Besides, several studies demonstrated that PDE inhibition by IBMX or amrinone (PDE3 inhibitor, 0.1 mM) increases  $I_f$  activation by shifting the current activation range to more positive voltage in rabbit SAN cells.<sup>269, 270</sup> This effect was confirmed by Mattick et al., who demonstrated that AC inhibition shifted  $I_f$  activation in the hyperpolarizing direction, as well as  $Ca^{2+}$  chelation, while PDEs inhibition shifted  $I_f$  activation in the depolarizing direction in guinea-pig SAN cells.<sup>256</sup> Although, Vinogradova et al. also showed that in rabbit SAN cells when  $I_f$  is blocked by  $Cs^+$  (2 mM), IBMX (100  $\mu$ M) or milrinone (50  $\mu$ M) still produces a similar increase in spontaneous beating rate as without  $Cs^+$  pretreatment, suggesting  $I_f$  only plays a minor role in PDE inhibition induced acceleration of spontaneous SAN firing.<sup>48</sup> However, this idea is challenged by the limitation of  $Cs^+$ . In particular,  $Cs^+$  does not block  $I_f$  fully, the block is voltage dependent and  $Cs^+$  is also a  $K^+$  channel blocker which could indirectly affect  $I_f$ .<sup>271</sup> Thus, the partially unblocked  $I_f$  by  $Cs^+$  block would still be able to drive the automaticity.<sup>271</sup> HCN4 mutation (HCN4-573X) was observed in a patient with SAN dysfunction, caused by a

heterozygous 1-bp deletion (1631delC) in exon 5 of the human HCN4 gene.<sup>93</sup> HCN4-573X protein had a truncated C-terminus and lacked the cyclic nucleotide-binding domain.<sup>93</sup> COS-7 cells transfected with HCN4-573X cDNA showed that the mutant channel is insensitive to cAMP and exhibits altered deactivation kinetics, providing a likely explanation for the patient's sinus bradycardia and the chronotropic incompetence.<sup>93</sup> Another mutation (S672R) is located near the cAMP-binding site.<sup>272</sup> HEK293 cells expressed this mutant HCN4 channel showed that mutation S672R shifts the channel activation to more negative voltages, which is responsible for the familial bradycardia.<sup>272</sup>

LTCCs are regulated by cAMP/PKA pathway. In ventricular myocytes, addition of membrane-permeable cAMP resulting in several fold increase in  $I_{Ca,L}$ .<sup>273</sup> In addition, inhibition of PDE by IBMX (100  $\mu$ M) increased  $I_{Ca,L}$  by 120% and  $[cAMP]_i$  by 70% in rat ventricular myocytes.<sup>274</sup> Specific inhibitors of PDE1-4 regulate  $I_{Ca,L}$  with rank order of potency PDE4 > PDE3 > PDE2 > PDE1.<sup>274</sup> In rabbit SAN, flash photolysis of caged cAMP (50  $\mu$ M) increased both pacemaking rate and  $I_{Ca,L}$ .<sup>254</sup> PDE3 inhibitor (amrinone, 0.1 mM) increased  $I_{Ca,L}$  by ~25% in rabbit SAN cells.<sup>270</sup> Similar data was got by using another PDE3 inhibitor (milrinone, 50  $\mu$ M), which increased  $I_{Ca,L}$  amplitude by ~46% in rabbit SAN cells.<sup>48</sup> Tanaka et al. also showed Rp-cAMP, a specific competitive antagonist of cAMP-induced activation of PKA, abolished the effect of  $I_{Ca,L}$  by cAMP in rabbit SAN cells.<sup>254</sup> It seems that the cAMP induced increase in  $I_{Ca,L}$  is through the cAMP/PKA-dependent phosphorylation. Indeed, further studies showed both  $\alpha$ 1C subunit (Ser-1928) and  $\beta$ 2 subunit (Ser-478 and Ser-479) of LTCC are PKA substrates, and rapid dephosphorylation of the channel could be provided by the Ser/Thr phosphatases 1 and 2A (PP1 and PP2A).<sup>275-277</sup>

It is demonstrated that cAMP regulate delay rectifier  $K^+$  current ( $I_K$ ) in ventricular myocytes. It increases delay rectifier  $K^+$  current ( $I_K$ ) amplitude, slows  $I_K$  deactivation kinetics, and shifts  $I_K$  activation curve to more negative potentials, mainly via cAMP-mediated PKA-dependent phosphorylation.<sup>278, 279</sup> In rabbit SAN cells, PDE activity also controls the delay rectifier  $K^+$  current ( $I_K$ ), as IBMX (100  $\mu$ M) markedly increases the amplitude of  $I_{K,tail}$  (12%) and shifts  $I_K$  activation to more negative potentials, implicating the effect of cAMP.<sup>48</sup> On the other hand, another PDE3 inhibitor amrinone (0.1 mM) increases delayed rectifier  $K^+$  current ( $I_K$ ) tail by ~22% in rabbit SAN cells.<sup>270</sup>

NCX has been proposed as a substrate for CaMKII or PKA-dependent phosphorylation, as it contains several phosphorylation sites.<sup>83, 280</sup> However, the functional significance of NCX phosphorylation is still a matter of debate.<sup>83, 281, 282</sup>

It has been shown that sex-related difference in SR  $Ca^{2+}$  release exists in ventricular myocytes. Female myocytes had smaller  $[Ca^{2+}]_i$  transients,  $Ca^{2+}$  sparks and EC coupling gain in comparison to

males.<sup>283</sup> Further research found lower cAMP levels in female due, at least in part, to the higher expression of PDE4B, probably resulting in lower phosphorylation levels of Ca<sup>2+</sup> handling proteins and the different Ca<sup>2+</sup> behavior in females than in males.<sup>283</sup> These findings could also explain the sex-related differences in EC coupling, i.e. smaller and slower contraction and underlying [Ca<sup>2+</sup>]<sub>i</sub> transient in females.<sup>284</sup> Whether or not sex steroid hormones are involved in the sex-related differences is not yet understood. However, testosterone has been shown to inhibit PDE activity in the ventricles of male rats, which could explain the higher levels of cAMP in male cells.<sup>285</sup> Thus, testosterone may induce a chronic and sex-related effect on SAN pacemaking, although it has no acute effect on beating rate of isolated rat right atria.<sup>285</sup> Besides, ovariectomy increases PKA activity in female rats, which supports the view that cAMP is suppressed in female.<sup>286</sup> Besides, the lower cAMP level may also limit the positive inotropic responses to β-AR agonists.<sup>283</sup> However, the sex-related effect in SAN cells is not yet investigated.

The basal spontaneous pacemaker activity is controlled by high level of cAMP, produced by Ca<sup>2+</sup>-activated AC and balanced by high level of PDE activity. Moreover, cAMP is also a potential regulator of excitation-transcription coupling (ET coupling).

#### **AC5- and AC6-induced cAMP-PKA pathway under sympathetic regulation**

Under sympathetic regulation, AC5- and AC6-induced cAMP/PKA pathway is accentuated. Besides, kinetics and stoichiometry of increases in PKA activity and protein phosphorylation in rabbit SAN cell are linked with changes in the kinetics and stoichiometry of increases in AP firing rate in response to physiological (β-AR) stimulation or pharmacological (PDE) inhibition.<sup>287</sup>

I<sub>f</sub> has been proposed as an important substrate of heart rate acceleration in response to catecholamines, as the activation of I<sub>f</sub> could be facilitated by direct interaction with cAMP. As mentioned previously, a small cAMP augmentation increases I<sub>f</sub> open probability, and shifts the activation curve positively.<sup>6, 50, 63, 83</sup> It has also being illustrated that low doses of β-AR agonist isoproterenol increase the DD slope without affecting the AP waveform, in respect that changes in DD slope is a common observation of I<sub>f</sub> modulation.<sup>50</sup> In addition, Stieber et al. also shown that cAMP cannot accelerate the heart rate of HCN4<sup>-/-</sup> embryos.<sup>89</sup> All these evidences indicate the contribution of I<sub>f</sub> in sympathetic regulation of pacemaker activity, although this idea is questioned by the observation that the full range of responses to autonomic agonists is possible in the partial absence of I<sub>f</sub> or when I<sub>f</sub> function is deficient.<sup>64, 65</sup>

The involvement of I<sub>Ca,L</sub> in sympathetic regulation of SAN automaticity has also been demonstrated in different species.<sup>6, 83, 95, 133, 210, 288</sup> In isolated hearts from Cav1.3 knock-out mice, the positive chronotropic response to isoproterenol is moderately reduced.<sup>6</sup> In addition, β-AR stimulation still enhanced pacemaking in isolated SAN cells from Cav1.3 knock-out mice, but to a

lesser extent than in WT SAN cells.<sup>112</sup> These results indicate a moderate contribution of Cav1.3 to sympathetic regulation. The  $\beta$ -AR stimulation induced  $I_{Ca,L}$  increase could also be explained by increased cAMP/PKA level. In ventricular myocytes the increased  $I_{Ca,L}$  is linked to PKA-dependent phosphorylation of serine 1928 residue of the C-terminal  $\alpha 1C$  of LTCC.<sup>277</sup>  $\beta$ -AR stimulation increases  $I_{Ca,L}$  by augmenting the channel open time and the open probability in ventricular myocytes.<sup>102</sup> The data in ventricular myocytes implicate the potential effect of  $I_{Ca,L}$  in SAN sympathetic response, suggesting that at least part of the positive chronotropic effect of the  $\beta$ -AR stimulation in SAN automaticity could be explained by the increase of  $I_{Ca,L}$ .

The increased  $I_K$  in SAN by  $\beta$ -AR agonist was first observed in rabbit SAN preparations.<sup>6, 40, 83</sup> This observation was confirmed in isolated SAN cells. The  $\beta$ -AR agonist increased  $I_K$  in rabbit SAN cells, and  $I_{Ks}$  in guinea-pig SAN cells, attributed to the increase in cAMP-mediated, PKA-dependent phosphorylation.<sup>289, 290</sup> Lei et al. also suggested that in rabbit SAN, the contribution of  $I_{Ks}$  to beating rate is small under control conditions, but significant during  $\beta$ -adrenergic stimulation.<sup>153</sup> An additional study demonstrated that this regulation of  $I_{Ks}$  is mediated by a macromolecular signaling complex including the targeting protein AKAP9 (Yotiao) which regulates channel activity by phosphorylation of Ser27 in the N-T of KCNQ1, and of Ser43 in the N-T of Yotiao.<sup>291</sup>

$I_{st}$  is also increased by the  $\beta$ -AR agonist, indicating the potential involvement of  $I_{st}$  in SAN sympathetic response.<sup>83, 177, 179, 292</sup> However, blockage of  $I_{st}$  by 50% produces only ~10% decrease in the isoproterenol induced acceleration in rabbit SAN cells, suggesting that  $I_{st}$  current likely has a minor role in SAN  $\beta$ -AR response.<sup>133</sup>

The cardiac TTX-resistant Scn5A-mediated  $I_{Na}$  is a potential substrate of SAN sympathetic regulation, as it is sensitive to phosphorylation by PKA and PKC.<sup>6, 293, 294</sup> In contrast, the TTX-sensitive  $I_{Na}$  probably contributes more to the DD in basal condition than under adrenergic activation, as in neurons it can be negatively regulated by the sympathetic nervous system.<sup>138</sup> More studies are needed in this area.

$\beta$ -AR stimulation regulates the  $Ca^{2+}$  clock, resulting in an significant contribution to the positive chronotropic response.  $\beta$ -AR stimulation increases the LCRs number, amplitude and size during late DD in rabbit SAN cells.<sup>133</sup> The synchronization is due, at least in part, to the increase in PLB phosphorylation,  $I_{Ca,L}$  and SR  $Ca^{2+}$  content.<sup>48, 133, 235</sup> Besides, the increased  $RyR_2$   $Ca^{2+}$  release reflects the increased  $RyR_2$  phosphorylation, in respect that  $\beta$ -AR stimulation induces cAMP-dependent  $RyR_2$  phosphorylation and concomitant  $Ca^{2+}$  release in ventricular myocytes.<sup>295, 296</sup> Indeed,  $\beta$ -AR stimulation increases the cAMP/PKA dependent  $RyR_2$  phosphorylation.<sup>297</sup> In this sense, mice harboring mutant  $RyR_2$  channels ( $RyR_2$ -S2808A+/+) that cannot be PKA phosphorylated exhibited blunted cardiac contractile response to catecholamines, and similar results

were also found in isolated SAN cells from RyR<sub>2</sub>-S2808A<sup>+/+</sup> mice.<sup>297</sup> In addition, the inhibition of RyR<sub>2</sub> by ryanodine prevented  $\beta$ -adrenergic augmentation of LCRs, DD rate, I<sub>NCX</sub> and SAN cell firing rate, even if the augmented  $\beta$ -adrenergic effect on I<sub>Ca,L</sub> was preserved.<sup>83, 133, 230</sup> Similar effects were found in isolated SAN cells or intact SAN tissue.<sup>235, 298</sup> In contrast, another study suggested that ryanodine (30  $\mu$ M) inhibited basal SAN cell firing rate but failed to block the  $\beta$ -adrenergic rate increase, as the presence of both ryanodine and  $\beta$ -AR agonist still causes ~50% increase in firing rate, although this study did not compare the  $\beta$ -adrenergic effect with and without ryanodine.<sup>231</sup> Besides, it is also noticeable that in contrast to a lower ryanodine concentration, the high concentration used in this study could probably lock the RyR<sub>2</sub> in a close state, preventing the SR Ca<sup>2+</sup> depletion and  $\beta$ -AR stimulation effect.<sup>83, 299</sup> The majority of studies point to the idea that Ca<sup>2+</sup> release through RyR<sub>2</sub> is increased by  $\beta$ -AR stimulation.<sup>133, 230, 235, 298, 300</sup> The augmented and earlier Ca<sup>2+</sup> releases could cause an augmented and earlier activation I<sub>NCX</sub>, leading to increase of membrane DD rate and SAN cell firing rate, considering I<sub>NCX</sub> is dependent to elevated [Ca<sup>2+</sup>]<sub>i</sub> rather than changes in the intrinsic properties.<sup>213, 299</sup> Indeed, Zhou and Lipsius demonstrated that  $\beta$ -AR stimulation induced increase in I<sub>NCX</sub> accounts for the concomitant increase of the DD slope.<sup>210</sup>

It has also been demonstrated that the acceleration of heart rate under  $\beta$ -AR stimulation requires CaMKII activation, considering CaMKII implicates many proteins involved in coupled clock. Indeed, CaMKII inhibited mice showed similar basal heart rate as wild type, but significant slower acceleration of the heart rate during  $\beta$ -AR stimulation.<sup>300</sup> Further investigation showed that CaMKII inhibition prevents  $\beta$ -AR agonist effects on SR Ca<sup>2+</sup> uptake and release, i.e. on CaMKII-dependent PLB phosphorylation (Thr17) and RyR<sub>2</sub> Ca<sup>2+</sup> release, independent of I<sub>f</sub>.<sup>300</sup> Moreover, ryanodine still significantly reduced the firing rate of SAN cells from CaMKII-inhibited mice and the wild type mice, indicating that the positive chronotropic effect of  $\beta$ -AR stimulation requires the RyR<sub>2</sub> Ca<sup>2+</sup> release.<sup>300</sup>

Sex differences in  $\beta$ -adrenergic response have been demonstrated in rabbit hearts in respect of the cardioprotection in female, while the cardioprotection confers a survival benefit in female patients with severe cardiac disease, such as heart failure.<sup>301-303</sup> It was shown that female hearts had a decreased capacity to  $\beta$ -adrenergic response, particularly under conditions of increased demand.<sup>303</sup> The reduced  $\beta$ -adrenergic response was associated with reduced arrhythmic activity.<sup>303</sup> These data is consistent with the lower cAMP level in females.<sup>283</sup>

#### **1.2.4.2 Parasympathetic regulation of cardiac automaticity**

Parasympathetic regulation of cardiac automaticity is achieved by the activation of muscarinic receptors following release of acetylcholine (ACh) from vagal nerve endings. The cholinergic agonists induce a negative chronotropic effect on cardiac automaticity and AV conduction observed



in vivo and in isolated heart preparations.<sup>6, 304, 305</sup> The type 2 muscarinic (M2) receptor is the predominant subtype in the heart. It activates Gi-type G protein in response to ACh, and dissociates  $\alpha_i$  subunit from the  $\beta\gamma$  subunit. The  $\alpha_i$  subunit is negatively coupled to AC activity causing the downregulation of cAMP, while the  $\beta\gamma$  subunit directly opens  $K_{ACh}$  channels, resulting in the negative chronotropic effects on SAN pacemaking. Indeed, numerous studies have reported that vagal stimulation slowed or stopped SAN automaticity. However, the effects were accompanied with a decrease in the DD slope (involvement of  $I_f$ ) or hyperpolarization of maximum diastolic potential, being aware that activation of  $I_{K_{ACh}}$  requires higher concentration (micromolar) of ACh than inhibition of  $I_f$  (nanomolar).<sup>157, 163, 306-309</sup>

As mentioned previously, acetylcholine-activated  $K^+$  current ( $I_{K_{ACh}}$ ) is a substrate of muscarinic agonist. Hutter and Trautwein observed that vagal stimulation increased membrane  $K^+$  conductance in the frog sinus venosus, accounting for the inhibition of spontaneous automaticity.<sup>310, 311</sup> Further investigation found the activation of  $I_{K_{ACh}}$  channel by micromolar concentration of ACh.<sup>157</sup>

$I_f$  is negatively regulated by ACh in respect of the downregulation of cAMP. DiFrancesco et al. observed the negative shift of  $I_f$  activation curve by nanomolar ACh, which slowed pacemaking, but without affecting  $I_{K_{ACh}}$ .<sup>157</sup>  $I_f$  is also more sensitive to ACh than  $I_{Ca,L}$ , as  $I_f$  is inhibited at lower doses of ACh than that required by  $I_{Ca,L}$  inhibition.<sup>312</sup>

$I_{Ca,L}$  is relatively insensitive to muscarinic regulation, as its inhibition requires high doses of ACh.<sup>273, 313</sup> However, Petit-Jacques et al. showed that muscarinic regulation of SAN  $I_{Ca,L}$  is related with the previous  $\beta$ -adrenergic stimulation and cAMP levels.<sup>259</sup> That means if SAN is previously stimulated by  $\beta$ -adrenergic agonists, the moderate doses of ACh can significantly inhibit  $I_{Ca,L}$ .<sup>259</sup> Similarly, accentuated effect of ACh after  $\beta$ -AR activation has also been observed on  $I_f$  in canine Purkinje fibers.<sup>314</sup> The depressing effect of ACh on  $I_{Ca,L}$  was abolished by PKA inhibition or cell dialysis with a nonhydrolyzable cAMP analog.<sup>259</sup>

It has also been illustrated that muscarinic receptor stimulation modulates  $Ca^{2+}$  handling in rabbit SAN cells. When both  $I_f$  and  $I_{K_{ACh}}$  were inhibited, ACh (1  $\mu$ M) was still able to reduce pacemaker frequency by 72%, as ACh also reduced SR  $Ca^{2+}$  content, decreases  $[Ca^{2+}]_i$  transient amplitude, slows  $[Ca^{2+}]_i$  transient rise and decay.<sup>315</sup> These effects are probably mediated by the downregulated cAMP, and the following reduction of PKA and CaMKII. Furthermore, the downregulated cAMP induces the decreased  $[Ca^{2+}]_i$  and concomitantly a negative feedback loop. It is likely that intracellular  $Ca^{2+}$  responds the muscarinic receptor stimulation via cAMP modulation, contributing to the negative chronotropic effect.

Nitric oxide (NO) signaling pathway also underlies muscarinic regulation of SAN automaticity. It is known that muscarinic receptor activation is coupled to NO synthesis, which stimulates

guanylyl cyclase activity and in turn elevates cGMP production.<sup>6</sup> The elevated cGMP production promotes phosphodiesterase (PDE) activity that hydrolyzes cAMP, especially PDE2.<sup>6, 316</sup> Han et al. suggested that NO signaling pathway plays an obligatory role in the muscarinic regulation of rabbit SAN, as blockage of NO synthesis prevents the effects of cholinergic agonists.<sup>317</sup> However, Sasaki et al. showed that NO can partially modulate accentuated antagonism but does not play an essential role in the vagal regulation in canine SAN.<sup>318</sup> The importance of NO signaling pathway in vagal regulation of heart rate is still controversial.<sup>6</sup> The mice lack of endothelial nitric oxide synthase (eNOS) or  $G_{\alpha o}$  protein failed to exhibit the muscarinic response.<sup>316, 319</sup> However, Vandecasteele et al. used another eNOS-deficient mouse line, and observed neither the adrenergic nor muscarinic regulation.<sup>320</sup> In support of that, Mori et al. also reported that NO is not involved in accentuated antagonism in isolated mouse atria.<sup>321</sup>

#### **1.2.4.3 Additional regulator of cardiac automaticity**

##### **Calcium**

Over 40 years ago, Seifen et al. discovered that the increase of extracellular  $[Ca^{2+}]_i$  increases the spontaneous beating rate of SAN, while the intracellular  $[Ca^{2+}]_i$  also increases during the extracellular  $[Ca^{2+}]_i$  increase.<sup>322</sup> Up to date, numerous studies investigated the effect of  $Ca^{2+}$  on pacemaker activity by application of  $Ca^{2+}$  chelators. Zaza et al., who used ruptured patch and buffered the intracellular  $Ca^{2+}$  with EGTA (10 mM), found that spontaneous activity became unstable and ceased in the majority of cells within several minutes after achieving the whole-cell configuration.<sup>323</sup> Application of 10 mM BAPTA from the patch pipette solution causes rapid cessation of spontaneous activity of guinea-pig SAN cells.<sup>324</sup> Some studies exposed the cells to the  $Ca^{2+}$  chelator in acetoxymethyl (AM) ester form. The AM ester renders the  $Ca^{2+}$  chelator cell permeant. Once in the intracellular space, cellular esterases release the chelator. For instance, Sanders et al. applied EGTA-AM and BAPTA-AM to guinea-pig SAN cells, resulting in cessation of spontaneous activity.<sup>215</sup> Even the fluorescent indicator (indo-1 AM), which has inherent buffering capacity, could reduce the firing rate compared to the non-indo loaded guinea-pig SAN cells.<sup>230</sup> The calcium-induced SAN firing rate regulation is, at least partially, produced via direct interaction or indirect act via activation of CaM/CaMKII and AC/cAMP pathways.

It has been reported that  $Ca^{2+}$  regulates of many ion channels, such as  $I_{Ca,L}$ ,  $I_{Ca,T}$ ,  $I_K$ ,  $I_f$ . Calcium regulates both  $I_{Ca,L}$  and  $I_{Ca,T}$ , as an elevation of extracellular  $[Ca^{2+}]_i$  increases in the amplitude of both  $I_{Ca,L}$  and  $I_{Ca,T}$  in rabbit SAN cells.<sup>95</sup> Besides, the inactivation of  $I_{Ca,L}$  is  $Ca^{2+}$ -dependent, to terminate  $Ca^{2+}$  entry. The regulation of delayed rectifier  $K^+$  current ( $I_K$ ) by intracellular  $[Ca^{2+}]_i$  is investigated in ventricular myocytes. The concentration-response curve of  $I_K$  for intracellular  $[Ca^{2+}]_i$  was measured by Tohse in guinea-pig ventricular myocytes.<sup>325</sup> An elevation of  $[Ca^{2+}]_i$  from 10 to

100nM increases  $I_K$  threefold by increased number and open probability of functional  $I_K$  channels.<sup>325</sup> BAPTA-AM markedly suppressed the amplitude of rapid component of  $I_K$  ( $I_{Kr}$ ) in guinea-pig ventricular myocytes.<sup>326</sup> The density of  $I_{Ks}$  was also larger during intracellular dialysis with a higher  $Ca^{2+}$  concentration (100nM) compared with that of a lower  $Ca^{2+}$  concentration (0.1nM).<sup>327</sup> Intracellular  $[Ca^{2+}]$ -induced increase of  $I_f$  and shift of  $I_f$  activation curve were observed in rabbit and rat SAN cells.<sup>328, 329</sup> However, further investigations found out that CaM antagonists (W-7, Calmidazolium and ophiobolin A) causes reduced amplitude of  $I_f$  and shifted voltage-dependent activation to more negative potentials, indicating involvement of CaM in  $I_f$  regulation.<sup>66</sup> These observations could also be explained by the increase of cAMP level on the basis of  $Ca^{2+}$ /CaM activation of AC activity, as cAMP also activates  $I_f$ . It was also reported that the peak of  $I_{st}$  is increased by lowering extracellular  $[Ca^{2+}]$ .<sup>177</sup>  $Ca^{2+}$ -activated  $Cl^-$  current ( $I_{Cl(Ca)}$ ) was identified in one third of rabbit SAN cells, although it only has a limited role in pacemaker activity.<sup>330</sup>

Many  $Ca^{2+}$ -induced effects could control pacemaker activity.<sup>83, 324</sup> For instance, intracellular  $Ca^{2+}$  induces acceleration of AC/cAMP and CaM/CaMKII pathways that further regulates many proteins involved in generation of SAN spontaneous activity.

### **Calmodulin (CaM)**

Calmodulin (CaM) is a ubiquitously expressed, highly conserved, small (17-kDa)  $Ca^{2+}$ -binding protein in eukaryotic cells.<sup>331, 332</sup> It has a dumbbell-shape structure with two globular domains, N-lobe and C-lobe, while each domain contains two EF-hand  $Ca^{2+}$  binding pockets.<sup>331</sup> The N- and C-lobe display different  $Ca^{2+}$  binding affinity. The C-lobe binds  $Ca^{2+}$  with higher affinity but slower association and dissociation rate (slow exchange) than N-lobe (fast exchange).<sup>333</sup> Upon  $Ca^{2+}$  binding, the dumbbell-shaped  $Ca^{2+}$  free calmodulin (Apo-CaM) undergoes a conformational change and forms a compact globular structure of  $Ca^{2+}$ -bound calmodulin (Ca/CaM). Via this conformational changes upon  $Ca^{2+}$  binding, calmodulin translate cytosolic  $Ca^{2+}$  changes to target proteins. CaM interacts with  $RyR_2$  (session 1.4.3), as well as a vast number of proteins and plays a critical role in numerous intracellular processes (Figure 7).

CaM could bind to  $Ca_v1.2$  governing both  $Ca^{2+}$  dependent inactivation (CDI) and  $Ca^{2+}$  dependent facilitation (CDF). The interaction between CaM and  $Ca_v1.2$  is still not fully understood. The C-terminal region of  $Ca_v1.2$  contains an EF hand and three CaM binding sites (A-region, C-region and IQ motif). Apo-CaM binds to the IQ motif of  $Ca_v1.2$  channel via C-lobe.<sup>334</sup> This setting preassociated CaM and serves the optimal position for rapid binding of  $Ca^{2+}$  to the C-lobe of CaM.<sup>335, 336</sup> Upon  $Ca^{2+}$  binding, the dumbbell-shaped  $Ca^{2+}$  free calmodulin (Apo-CaM) undergoes a conformational change and forms a compact globular structure of  $Ca^{2+}$ -bound calmodulin (CaCaM). CaCaM C-lobe interacts with the IQ motif of  $Ca_v1.2$  resulting in CDI, meanwhile the N-lobe has a

role in CDI.<sup>337</sup> Besides IQ motif, CaCaM also interacts with the C-region and A-region via C-lobe. The binding of C-lobe with C-region has a lower affinity ( $K_d \sim 400\text{nM}$ ) than with IQ motif ( $K_d \sim 2.5\text{nM}$ ), and the binding with A-region is even weaker than the CaCaM N-lobe-A-region interaction ( $K_d > 10\mu\text{M}$ ).<sup>9, 338</sup> The binding between ApoCaM and A-C region remains controversial, and may depend on  $\text{Ca}^{2+}$  binding to EF-hand of  $\text{Ca}_v1.2$ .<sup>9, 339, 340</sup> Disruption of CaCaM and C-region interaction has no effect on CDI, but a reduction on CDI.<sup>338</sup> It is proposed that two CaM molecules bind to the C-terminus of  $\text{Ca}_v1.2$  channel.<sup>338, 341</sup> Some mutations on calmodulin are associated with severe disease, such as CPVT, early-onset long-QT syndrome (CQTS), etc. Limpitikul et al. showed that overexpression of mutant CaM (D96V, D130G and F142L) in adult guinea-pig ventricular myocytes induces prolonged action potential duration (APD), enhanced  $[\text{Ca}^{2+}]_i$  transient and proarrhythmic behavior.<sup>342</sup> Further investigation showed deficient CDI of LTCCs, indicating that LTCC is a key contributor of CQTS induced by CaM mutation.<sup>342</sup> However, other proteins interacting with CaM should also be considered.

CaM regulates several types of voltage-gated  $\text{K}^+$  channels, such as  $I_{to}$ ,  $I_{Ks}$ , etc. CaM modulates  $\text{K}_v1.1$  and  $\text{K}_v1.4$  via  $\text{K}_v\beta1.1$  subunits to decelerate the response to the rise in intracellular  $\text{Ca}^{2+}$  concentration, providing a negative feedback to limit neuronal overexcitation, while  $\text{K}_v1.4$  also conduct the  $I_{to,slow}$  in heart.<sup>343</sup> Pharmacological inhibition of  $\text{Ca}^{2+}$ -occupied CaM (with W-7) leads to reduction of  $\text{K}_v4.3$  ( $I_{to,fast}$ ) current.<sup>344</sup>  $I_{Ks}$  could be enhanced by increase in cytosolic  $[\text{Ca}^{2+}]_i$  via allosteric interaction with CaM, rather than phosphorylation.<sup>345, 346</sup> Further investigation confirmed that CaM is responsible for both  $I_{Ks}$  channel assembly and gating.<sup>347</sup> However, a recent research illustrated that CaMKII participates in the enhancement of  $I_{Ks}$  by CaM.<sup>327</sup> CaM regulates  $\text{K}_v10.1$  channel (*ether à go-go* channel, EAG1) via direct binding to the cytosolic N- and C- termini.<sup>348</sup>  $\text{Ca}^{2+}$  activated  $\text{K}^+$  channels (SK1-4) can also be regulated by calmodulin via direct binding.<sup>327, 349-351</sup>

Calmodulin also regulates ion conductance of  $\text{Na}^+$  channel via allosteric interaction at two sites: an IQ motif in the C-terminal domain, and a CaM binding domain (CaMBD) within the DIII-IV linker.<sup>352, 353</sup> At low cytosolic  $\text{Ca}^{2+}$  concentration, apoCaM binds to the IQ motif via C-lobe. However, at higher cytosolic  $\text{Ca}^{2+}$  concentration, the CaCaM C-lobe binds to both the IQ motif and the CaMBD, while the N-lobe also binds to the IQ motif with a greater affinity than the C-lobe.<sup>354</sup> CaM interacts with the DIII-IV linker causing reduced gate inactivation ability, which increases the duration of the  $I_{Na}$ .<sup>9</sup>

CaM is also involved in other protein regulations, such as  $\text{RyR}_2$ ,  $I_f$ . CaM decreases the  $\text{RyR}_2$  opening probability (session 1.4.3). CaM antagonists (W-7, Calmidazolium and ophiobolin A) causes reduced amplitude of  $I_f$  and shifts voltage-dependent activation to more negative potentials, indicating the role of CaM in  $I_f$  regulation.<sup>66</sup> These results could also be explained by the increase of cAMP level on the basis of  $\text{Ca}^{2+}$ /CaM activation of AC activity, as cAMP activates  $I_f$ . Besides

AC/cAMP pathway, CaM also activates CaMKII, and thus regulates numerous proteins via CaMKII phosphorylation.

In ventricular myocytes, CaM is involved in the two signaling pathways of Ca<sup>2+</sup>-dependent excitation-transcription (ET) coupling (Figure 11). Ca/CaM activates calcineurin (Cn), which dephosphorylates NFAT (nuclear factor of activated T cells); NFAT is then imported into nucleus and interacts with hypertrophic transcription factor GATA4 to drive hypertrophic gene transcription.<sup>355-357</sup> GATA transcription factors are characterized by their ability to bind to the DNA sequence 'GATA'. Calcineurin (Cn) has two subunits, CnA and CnB. CnA contains the CaM-binding and phosphatase domains but requires CnB for activity.<sup>358</sup> Cardiac overexpression of activated Cn or NFAT results in massive cardiac hypertrophy and heart failure.<sup>358,359</sup> In contrast, Cn inhibition could prevent hypertrophy, as cardiac expression of dominant negative Cn or CnA $\beta$  knock-out impairs hypertrophic responses to pressure overload, angiotensin II, and isoproterenol infusion.<sup>358-362</sup> Moreover, knock-out of NFATc3, but not NFATc4, induced a significant inhibition in Cn overexpression-, pressure overload- and angiotensin II-induced cardiac hypertrophy.<sup>363</sup> Indeed, transgenic mice overexpressing CaM develop cardiac hypertrophy.<sup>364</sup> However, the CaM effect on ET coupling in SAN is still unclear. The other Ca-dependent ET coupling pathway involves activation of CaMKII by CaM.

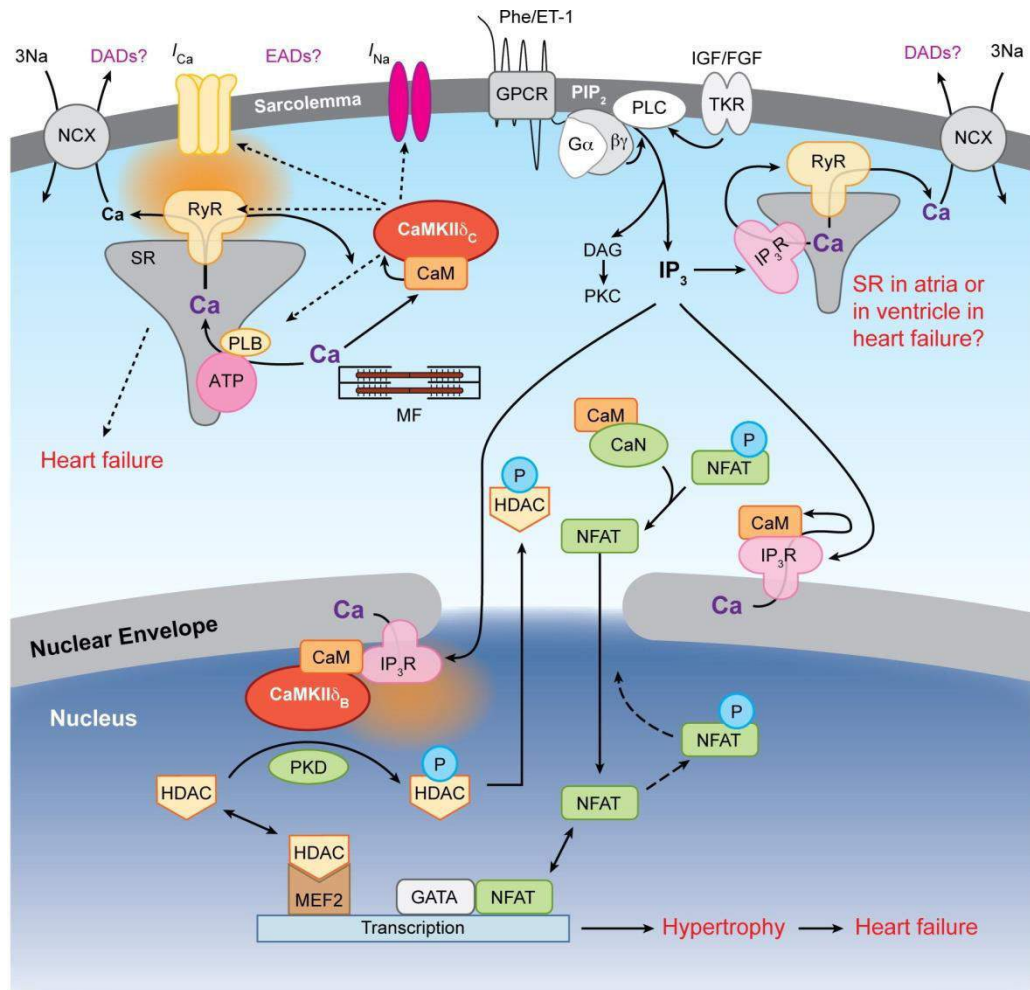


Figure 11  $\text{Ca}^{2+}$ -dependent ET coupling in cardiac myocytes. In addition to the  $\text{Ca}^{2+}$  regulation in EC coupling (top left), and potential role of  $\text{IP}_3\text{R}$  in triggered arrhythmias (top right),  $\text{Ca}^{2+}$ -dependent signaling to the nucleus can modulate transcription. G protein-coupled receptors (GPCR) such as those for endothelin-1 (ET-1) or  $\alpha$ -adrenergic agonists [phenylephrine (Phe)] and tyrosine kinase receptors (TKR) such as those activated by insulin-like growth factor (IGF) and fibroblast growth factor (FGF) can activate phospholipase C (PLC) to produce diacylglycerol (DAG) (which can activate PKC) and InsP3 ( $\text{IP}_3$ ).  $\text{IP}_3\text{R}$  in the nuclear envelope release  $\text{Ca}^{2+}$ , which activates calcium-calmodulin-dependent kinase II $\delta$  (CaMKII $\delta$ ), resulting in histone deacetylase (HDAC) phosphorylation (which also occurs by PKD) and nuclear export. This nuclear export relieves HDAC-dependent suppression of myocyte enhancer factor 2 (MEF2)-driven transcription. On the other side, Calcineurin (CaN) is activated by Ca/CaM and dephosphorylates NFAT (nuclear factor of activated T cells). NFAT is then translocated to the nucleus, where, along with the transcription factor GATA, it can stimulate the transcription of genes contributing to hypertrophy. The orange clouds indicate where local [Ca] elevation is critical for signaling near RyR and InsP3R. P indicates phosphorylation, MF denotes myofibrils, and  $\text{G}\alpha$  and  $\beta\gamma$  are subunits of the G protein Gq. (Adapted from Bers, 2008<sup>358</sup>)

In summary, CaM could not only affect SAN pacemaking via direct or indirect interaction with numerous proteins that are important for pacemaker activity, but also potentially modifying the expression of some proteins involved in SAN pacemaking via ET coupling. Although, the  $\text{Ca}^{2+}$ -dependent ET coupling in SAN has not been proven yet.

### **$\text{Ca}^{2+}$ /CaM activates $\text{Ca}^{2+}$ /calmodulin-dependent protein kinase II (CaMKII)**

CaMKII modulates many proteins that are important in SAN pacemaking within both membrane clock and  $\text{Ca}^{2+}$  clock (Figure 7), such as LTCC,  $\text{K}^+$  channels,  $\text{RyR}_2$  and SERCA (directly and indirectly via phospholamban), etc.<sup>365</sup>

The four main CaMKII isoforms are produced by four different genes ( $\alpha$ ,  $\beta$ ,  $\delta$ , and  $\gamma$ ).<sup>366</sup> The predominant CaMKII isoform in heart is delta (CaMKII $\delta_B$  mainly in nucleus and CaMKII $\delta_c$  mainly in cytosol), while the secondary isoform is gamma (CaMKII $\gamma$ ) and CaMKII $\beta$  is also expressed at a low level.<sup>367-371</sup> The CaMKII monomer consists of three domains: an N-terminal catalytic domain, a regulatory domain and a C-terminal association domain. The regulatory domain is responsible for  $\text{Ca}^{2+}$ /CaM binding and numerous regulations, such as autophosphorylation (Thr287 in CaMKII $\delta$ ), oxidation (Met281/282), O-linked glycosylation (Ser280).<sup>366, 372, 373</sup> The catalytic domain is in charge of the enzymatic activity of CaMKII, and is regulated by the regulatory domain.<sup>366</sup> Figure 12 shows the intracellular distribution of total and autophosphorylated (active) CaMKII in rabbit SA node cells. The autophosphorylated CaMKII is localized beneath the cell membrane, while the total CaMKII is uniformly distributed in the cell.<sup>374</sup>

It was reported that CaMKII could regulate  $I_{\text{Ca,L}}$ , as inhibition of CaMKII (with KN-93) depressed the amplitude of  $I_{\text{Ca,L}}$  without altering the shape of the current-voltage relationship, and depressed SAN firing rate.<sup>374</sup> CaMKII facilitates  $I_{\text{Ca,L}}$  via LTCC phosphorylation, termed slow  $I_{\text{Ca}}$  facilitation, whereas the fast facilitation depends on  $\text{Ca}^{2+}$  released from  $\text{RyR}_2$ .<sup>97, 375-378</sup>  $I_{\text{Ca,L}}$  facilitation drives the possibility to induce pro-arrhythmic consequences.<sup>379</sup> Hudmon et al. suggested that CaMKII phosphorylate the pore-forming  $\alpha_1\text{C}$  subunit of LTCC.<sup>380</sup> Some studies supported this view, and proposed possible phosphorylation sites. Erxleben et al. suggested that Ser439 and Ser1517 are involved in CaMKII phosphorylation in rabbit  $\text{Ca}_{\text{v}1.2}$  channel.<sup>381</sup> Wang et al. demonstrated that CaMKII phosphorylates the Thr1603 residue (Thr1604 in rabbit) in the C-terminal tail of the  $\text{Ca}_{\text{v}1.2}$  channel of guinea-pig, and regulates the CaM binding to the channel.<sup>382</sup> Ser1512 and Ser1517 sites were proposed following experiments in knock-in mice showing decreased voltage-dependent facilitation.<sup>383, 384</sup> Some studies also proposed that CaMKII phosphorylates regulatory  $\beta_2\text{a}$  subunits (Thr498) of LTCC, via Leu493 facilitating the binding.<sup>385-387</sup>

CaMKII regulates several types of  $\text{K}^+$  channels, such as  $I_{\text{to}}$ ,  $I_{\text{K1}}$ ,  $I_{\text{Ks}}$ .<sup>388</sup> CaMKII slows  $I_{\text{to}}$  inactivation in human atrial myocytes.<sup>389</sup> This point was further confirmed in rat ventricular myocytes and showed different CaMKII modulation of  $\text{K}_{\text{V}4.2}$  and  $\text{K}_{\text{V}4.3}$ .<sup>390</sup> CaMKII modulation of  $\text{K}_{\text{V}4.3}$  is through direct effect at S550, thus slowing the inactivation and accelerating the rate of recovery from the inactivation of the channel.<sup>391</sup> It is also reported that CaMKII influences the expression pattern of  $\text{K}^+$  channels, including  $\text{K}_{\text{V}1.4}$  ( $I_{\text{to,slow}}$ ),  $\text{K}_{\text{V}4.2}$  and  $\text{K}_{\text{V}4.3}$  ( $I_{\text{to,fast}}$ ), and Kir2.1 and Kir2.2 ( $I_{\text{K1}}$ ).<sup>392-394</sup>  $I_{\text{Ks}}$  is enhanced by increase in cytosolic  $[\text{Ca}^{2+}]_i$  via allosteric interaction with

CaM rather than phosphorylation.<sup>345</sup> However, a recent research illustrated that CaMKII participates in the enhancement of  $I_{Ks}$  by CaM.<sup>327</sup>

CaMKII regulates cardiac sodium channels by phosphorylation predominantly on I-II linker and to a lesser extent in the C-terminal region.<sup>395</sup> Until now, multiple phosphorylation sites, such as S516, T594, S571 and S516 are proposed.<sup>396-398</sup> S516 phosphorylation is reduced in human heart failure.<sup>398</sup> The general effect of CaMKII phosphorylation seems like increasing  $I_{Na}$ , which leads to a higher cytosolic  $Na^+$  concentration and AP prolongation. Wagner et al. investigated the effect of CaMKII $\delta_C$  overexpression in rabbit ventricular myocytes via adenovirus infection and transgenic CaMKII $\delta_C$  mice.<sup>399</sup> Besides persistent increase in inward  $I_{Na}$  and intracellular  $Na^+$  concentration, they also found that CaMKII $\delta_C$  over-expression shift the voltage dependence of  $Na^+$  channel availability to more negative membrane potential, enhanced intermediate inactivation and slowed recovery from inactivation.<sup>399</sup> In this sense, Ashpole et al. confirmed that CaMKII shifted  $I_{Na}$  activation to a more negative membrane potential.<sup>396</sup> However, another study found that CaMKII shifted the voltage dependence of  $Na^+$  channel availability to more positive membrane potential, hastened recovery from inactivation, as well as increased late current in guinea-pig ventricular myocytes.<sup>395</sup> This work used whole-cell voltage-clamp to investigate  $I_{Na}$  in absence or presence of CaMKII in pipette solution.<sup>395</sup> Thus, regulation of CaMKII to  $Na^+$  channel is important for maintaining  $Na^+$  channel function and membrane excitability under physiological conditions.<sup>397, 400</sup>

CaMKII regulates SERCA via two pathways, direct SERCA phosphorylation and phospholamban (PLB) phosphorylation.<sup>379, 401</sup> SERCA is a 110 kDa, membrane-embedded ATP-driven calcium pump, which pumps  $Ca^{2+}$  back into SR. Dephosphorylated phospholamban (PLB) acts as a reversible inhibitor of SERCA. CaMKII binds to SERCA resulting in collapse of  $Ca^{2+}$  binding sites and stabilization of divalent cation-free conformation of SERCA.<sup>402</sup> When CaMKII phosphorylates PLB, the phosphorylated PLB (Thr17) releases the SERCA, increasing SERCA  $Ca^{2+}$  affinity and enhancing  $Ca^{2+}$  reuptake.<sup>260, 379</sup> Indeed, CaMKII inhibition slows SAN cells responses to isoproterenol associated with decreased SR  $Ca^{2+}$  content, and PLB deficiency rescues SR  $Ca^{2+}$  content and SAN cells isoproterenol responses.<sup>261</sup> These data indicate that normal PLB function and concomitant minimum SR  $Ca^{2+}$  content are essential in CaMKII-related regulation.<sup>261</sup> However, this work also demonstrated that PLB deficiency or PLB mutation on CaMKII target site (T17A) did not affect basal HR in vivo or firing rate in SAN cells.<sup>261</sup>



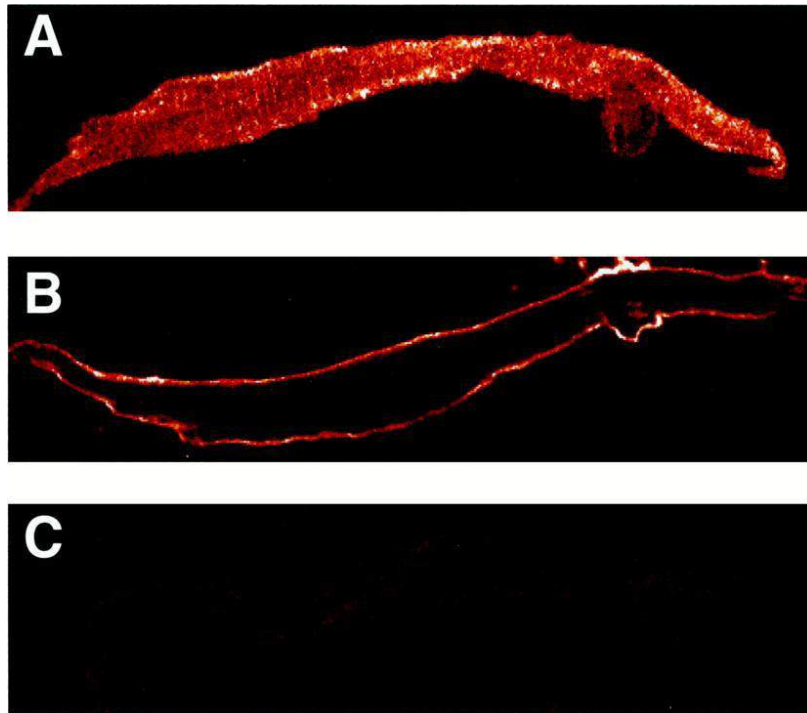


Figure 12. Intracellular distribution of total and autophosphorylated (active) CaMKII in rabbit SA node cells. A, Uniform distribution of the total CaMKII. B, Localization of autophosphorylated (active) CaMKII to the sarcolemmal membrane. C, Negative control, ie, in the absence of the primary antibodies. (Adapted from Vinogradova et al., 2000<sup>374</sup>)

The phosphorylation of RyR<sub>2</sub> by CaMKII is mainly at Ser2808 and Ser2814, while additional phosphorylation sites might also exist, such as Ser2011 (session 1.4.2.8).<sup>403</sup> A significant number of researches illustrated that RyR<sub>2</sub> phosphorylation by CaMKII caused prolonged openings of RyR<sub>2</sub> and excessive SR Ca<sup>2+</sup> leak in ventricular myocytes.<sup>368, 404-406</sup> For instance, Li et al. found that inhibition of CaMKII by KN93 reduces RyR<sub>2</sub> activity (via Ca<sup>2+</sup> spark) in ferret ventricular myocytes,<sup>404</sup> which is confirmed by Currie et al. in rabbit.<sup>405</sup> Guo et al. reported more SR Ca<sup>2+</sup> release (more Ca<sup>2+</sup> sparks in frequency, and longer in duration) after CaMKII activation in mouse ventricular myocytes, and this effect was abolished by CaMKII inhibitor peptides.<sup>406</sup> It has also been reported that CaMKII  $\delta_C$  over-expression in mice increased diastolic SR Ca<sup>2+</sup> leak (via sparks) and reduced SR Ca<sup>2+</sup> load, which contributes to the following heart failure.<sup>368, 407</sup> However, Yang et al. expressed constitutively active CaMKII  $\delta_C$  via adenoviral gene transfer in cultured rat ventricular myocytes and found depressed SR Ca<sup>2+</sup> release, whereas a dominant negative CaMKII enhanced it.<sup>408</sup> Some single channel recordings of RyR<sub>2</sub> channels reconstituted in lipid bilayers also showed CaMKII either increase<sup>409-411</sup> or decrease<sup>412</sup> RyR open probabilities. The controversial results may indicate multiple CaMKII effects on RyR<sub>2</sub>, probably via different target sites on RyR<sub>2</sub> or auxiliary proteins.<sup>388</sup> In general, most works point to an activatory effect of CaMKII on RyR<sub>2</sub>. In SAN, pharmacological inhibition of CaMKII (with KN93 or AIP) reduced LCR number and size in both normal and permeabilized rabbit SAN cells, which decreased the pacemaker activity. However, Wu et al. investigated mice with RyR<sub>2</sub> knock-in mutation that replaced CaMKII target site (S2814) with

alanine and disabled CaMKII phosphorylation at this site.<sup>261</sup> They found that S2814A mutation failed to affect spontaneous firing rate and isoproterenol response in vivo and in SAN cells, indicating multiple CaMKII targets in SAN cells.<sup>261</sup> Further investigations are needed to clarify this issue.

The CaMKII substrates probably lead to a positive feedback via Ca<sup>2+</sup> release, and further enhance CaMKII activity during normal EC coupling and  $\beta$ -adrenergic stimulation.<sup>413</sup> Even though CaMKII targets many proteins within the membrane and Ca<sup>2+</sup> clock in SAN, I<sub>f</sub> is not directly affected.<sup>66</sup>

The contribution of CaMKII in regulating SAN basal pacemaker activity is under debate. Pharmacological inhibition of CaMKII (with KN93 or AIP) decreases the pacemaker activity in rabbit SAN cells.<sup>60, 374</sup> The reduced pacemaker activity by CaMKII inhibition was also confirmed by Rigg et al. in guinea-pig SAN cells.<sup>66</sup> However, these results were questioned because of the documented off-target actions of the inhibitors.<sup>414</sup> Besides, in myocardial targeted transgenic mice with expression of a highly selective CaMKII inhibitory peptide, inhibition of CaMKII did not affect baseline SAN pacemaker activity, but reduced heart rate increases in response to physiological stress associated with decreased SR Ca<sup>2+</sup> content.<sup>261, 300, 414-416</sup> Yet, species dependent differences should be considered.

CaMKII is required for SAN response to  $\beta$ -adrenergic stimulation.<sup>300, 415, 417</sup> Curran et al. found that  $\beta$ -adrenergic receptor agonists increases SR Ca<sup>2+</sup> leak via a CaMKII dependent manner, not PKA dependent.<sup>418</sup> Besides, transgenic mice with CaMKII inhibition have slower heart rates than controls under stress or  $\beta$ -adrenergic stimulation.<sup>300</sup> Isolated SAN cells from CaMKII inhibited mice presented reduced positive chronotropic response to isoprenaline, and related reduced SR Ca<sup>2+</sup> content and Ca<sup>2+</sup> sparks frequency.<sup>300</sup>

In spite of the essential role of CaMKII in coupled clock and  $\beta$ -adrenergic response, CaMKII also regulates SAN bioenergetics.<sup>60</sup> As in contrast with graded reductions in ATP demand by CaMKII inhibition, SAN cells become depleted of ATP, indicating the reduction in mitochondria ATP generation.<sup>60</sup>

Besides, CaMKII is involved in promoting SAN dysfunction. Conditions that favor SAN dysfunction, such as heart failure, hypertension, atrial fibrillation, atrial apoptosis, etc, are associated with elevated ROS and angiotensin II.<sup>414</sup> Interestingly, CaMKII could be activated by pro-oxidant conditions.<sup>372</sup> This redox-dependent CaMKII activation is carried out by oxidative modification of the Met-281/282 site in the regulatory domain, which prevents CaMKII from inactivation after Ca<sup>2+</sup>/CaM removal.<sup>356, 372, 414</sup> Thus, it is reasonable that infusion of angiotensin II in mice increased oxidized CaMKII, and caused SAN cell apoptosis and SAN dysfunction, while

transgenic mice with CaMKII inhibition were protective from angiotensin II induced fibrosis.<sup>419</sup> These results suggest the contribution of CaMKII to SAN and right atrial apoptosis and fibrosis induced by angiotensin II, in respect that activation of CaMKII through oxidation may be involved in SAN dysfunction through any of the channels detailed previously. In addition, increased oxidized CaMKII is also linked with atrial fibrillation and raised mortality in diabetic patients after myocardial infarction.<sup>356, 420, 421</sup>

CaMKII expression and activity are increased in numerous heart diseases, such as hypertrophy, atrial fibrillation, heart failure, etc, making CaMKII as a potential target for clinical therapy.<sup>365, 389, 416, 422-425</sup>

In ventricular myocytes, CaMKII is involved in one of the two signaling pathways of  $Ca^{2+}$ -dependent ET coupling (Figure 11). CaMKII or PKD (protein kinase D) phosphorylates class II histone deacetylases (HDACs, types 4 and 5), relieves HDACs from repression of hypertrophic transcription factor MEF2 (myocyte enhancer factor 2) and increases MEF2 transcription activity.<sup>355, 356, 426, 427</sup> CaMKII binds to a unique docking site of HDAC4 near the key phosphorylation sites, and results in phosphorylation and nuclear export.<sup>426</sup> As a result, CaMKII phosphorylation of HDAC4 could cause hypertrophic growth, which is blocked by a signal-resistant HDAC4 mutant.<sup>426</sup> HDAC5 lacks the CaMKII docking site and a third phosphorylation site. It seems that HDAC5 alone is unresponsive to CaMKII and becomes responsive by oligomerization with HDAC4.<sup>427</sup> Certainly, a parallel Ca-dependent ET coupling pathway involves activation of Cn by  $Ca^{2+}$ /CaM. As the nuclear lumen and SR lumen are continuous but insulated from the cytosol, the CaMKII affect EC coupling and ET coupling by targeting distinct proteins via distinct isoforms (CaMKII $\delta_B$  in nucleus and CaMKII $\delta_c$  in cytosol).<sup>355, 356, 428</sup> However, the  $Ca^{2+}$ -dependent ET coupling in SAN has not been proven yet.

CaMKII directly or indirectly targets proteins accounting for the normal cardiac function and SAN automaticity. Besides, the diverse expression pattern of channels in different region of the heart, including the cardiac disease changed expression pattern of the channels, also makes CaMKII an important regulator for electrical activity in diseased and healthy heart.<sup>388</sup> Moreover, CaMKII level varies in numerous cardiac diseases. All these evidences indicate the critical role of CaMKII in heart function, as well as SAN automaticity.

## Others

The existence of leptin receptors on SAN cells is recently demonstrated. It is known that leptin plays an important role in cardiac contractility, development of hypertrophy and apoptosis.<sup>429-433</sup> Initial studies uncovered that the effects of leptin are indirect via adrenergic receptors stimulation, and later studies indicated the presence of direct interaction via leptin receptors.<sup>434-436</sup> The two

distinct pathways could probably explain the both increased and unchanged/decreased heart rate associated with increased metabolic demands.<sup>437-439</sup> Indeed, a recent research demonstrated the existence of leptin receptor in SAN cells.<sup>440</sup> This study also investigated the effect of low doses (0.1-30 µg/kg) and high doses (150-300 µg/kg) of leptin: low doses of leptin decreased resting heart rate, and high doses of leptin induced a biphasic effect (decrease and then increase) on heart rate. Besides, in the presence of beta-blocker (propranolol), high-dose leptin only reduced heart rate and sometimes caused sinus pauses and ventricular tachycardia. Furthermore, leptin antagonist reversed the leptin-induced inhibition of resting heart rate. These data indicate that in addition to indirect pathway via sympathetic tone, leptin can directly decrease heart rate via its receptor independently of β-adrenergic receptor stimulation.

Cardiac automaticity is also regulated by other factors, such as neuropeptides, adenosine, hormones, mechanical load and atrial stretch, electrolytes and temperature.<sup>6</sup>

### **1.3 CPVT and CPVT related sinus dysfunction**

Catecholaminergic Polymorphic Ventricular Tachycardia (CPVT) is a lethal heritable disease discovered in 1975<sup>441</sup>. It is characterized by exercise/emotion triggered syncope or sudden cardiac death in children or young adults with structurally normal hearts.<sup>442</sup> Recent reports suggest that mutations in genes encoding RyR<sub>2</sub> (sarcoplasmic reticulum Ca<sup>2+</sup> release channel), cardiac calsequestrin (CASQ2), triadin, and calmodulin are related to CPVT.<sup>443-447</sup> Other mutations in gene KCNJ2 (encoding potassium channel) have also been identified with a CPVT-like phenotype, although further and much more research is needed.<sup>448</sup> A large number CPVT families with RyR<sub>2</sub> mutations has been reported in literature, accounted for approximately 60% to 70% of patients.<sup>449-453</sup>

CPVT mutated channels are not only limited to the ventricular myocardium, but also in other regions of the heart (including SAN and atria). Indeed, patients with CPVT are frequently associated with supraventricular arrhythmia and SAN dysfunction, such as sinus bradycardia, which is observed in both RyR<sub>2</sub> and CASQ2 related CPVT patients.<sup>444, 454, 455</sup>

According to Van der Werf et al. sinus bradycardia is observed in 19% of relatives in RyR<sub>2</sub> related CPVT families in their study, while other supraventricular dysrhythmias were present in 16%.<sup>456</sup> Postma et al. investigated heart rate in a series of RyR<sub>2</sub> mutation carriers, and found out heart rate in CPVT patient is significantly lower regardless of the site of the mutation.<sup>454</sup> Domingo et al. also reported a new mutation, RyR<sub>2</sub><sup>R420Q</sup>, found from a Spanish family with several sudden deaths.<sup>457</sup> Electrocardiogram studies, associated with exercise test or epinephrine challenge, confirmed that it is a CPVT related mutation.<sup>457</sup> Besides, this mutation is also associated with sinus dysfunction, such as sinus bradycardia.<sup>457</sup> So far, only one research from our team studied SAN

activity in a RyR<sub>2</sub> linked CPVT model, which carries the Carboxyl-terminal region (C-terminal region) mutation R4496C.<sup>458</sup> The heart rate of RyR<sub>2</sub><sup>R4496C</sup> mice have no difference in basal condition compared to their wild-type littermates, but get significant lower under  $\beta$ -adrenergic stimulation.<sup>458</sup> This impaired  $\beta$ -adrenergic response, which indicates SAN dysfunction, is due to increased activity of mutated RyR<sub>2</sub>.<sup>458</sup>

Sinus dysfunction and inducible atrial tachyarrhythmias were also reported in CASQ2 mutation-induced CPVT patients.<sup>455</sup> SAN dysfunction was further confirmed by CASQ2 null mice.<sup>459</sup> Together with sinus bradycardia, CASQ2 null mice also exhibited enhanced atrial ectopic activity, SAN conduction abnormalities, and slower heart rhythm during  $\beta$ -adrenergic/cholinergic stimulation.

Some studies show gender difference in hearts, such as sex difference in excitation-contraction coupling, or in  $\beta$ -adrenergic responsiveness of action potentials.<sup>283, 284, 303</sup> Cardioprotection in female has also been reported, conferring a survival benefit in female patients with severe cardiac disease, such as heart failure.<sup>301, 302</sup> A study shows sex difference in RyR<sub>2</sub> related CPVT patients: male CPVT patients have a higher risk of cardiac events, while 118 family members including 30 probands were evaluated.<sup>442</sup> Interestingly, there is also a noteworthy difference between genders in heart rates in RyR<sub>2</sub> mutation related CPVT patients. Male patients have a lower heart rate than female patients.<sup>454</sup> But is the severe syndrome in male related with low heart rate? What's their underlying mechanism? What's the difference and mechanism in heart rate between male and female in RyR<sub>2</sub>-CPVT animal model? These questions remain unknown.

### **RyR<sub>2</sub> related CPVT mutations**

CPVT or arrhythmogenic right ventricular dysplasia type 2 (ARVD2) mutations are clustered primarily in three discrete domains of the human RyR<sub>2</sub> polypeptide (Figure 13): the N-terminal (residues 44-466), the central (residues 2246-2534) and the C-terminal domain (residues 3778-4959).<sup>460-463</sup> Mutations on RyR<sub>2</sub> could result in protein gain-of-function or loss-of-function effect that increase or decrease channel activity respectively.

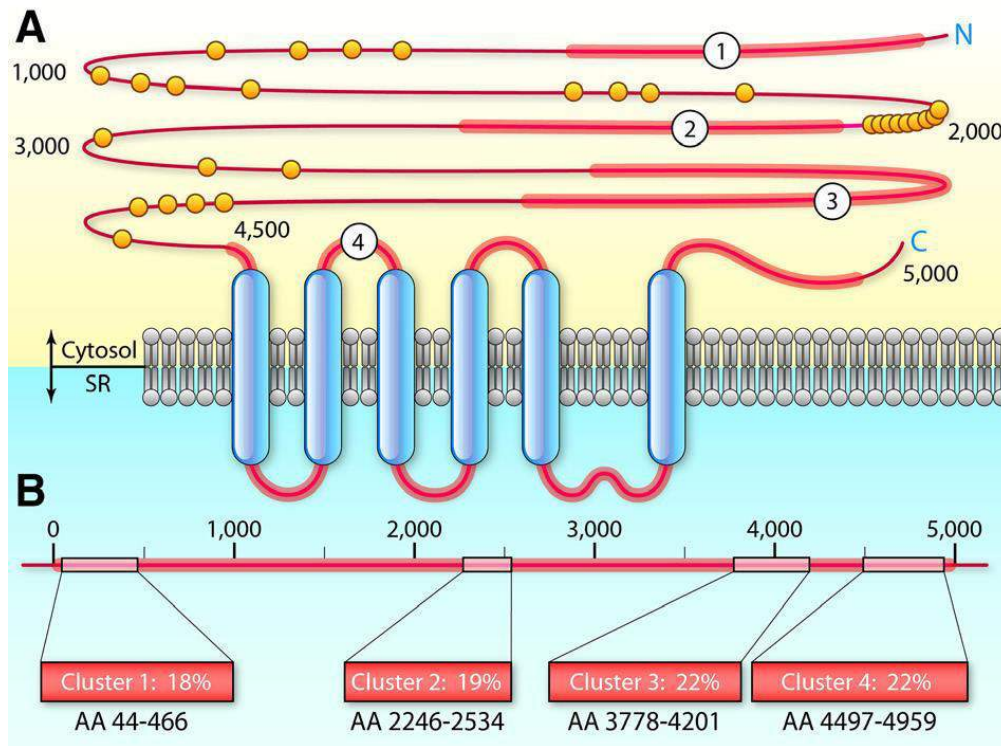


Figure 13 Structure and mutational clusters of RyR<sub>2</sub>. A. Clusters with frequent mutations are depicted with their location along the protein. Clusters are represented by numbered red lines. Individual mutations outside the canonical clusters are depicted as yellow dots. N-terminal region, cluster1. Central domain, cluster2. C-terminal domain, cluster 3 and 4. B. Clusters are represented by boxes, with the amino acid (AA) range of the clusters and the percentage of published mutations for each cluster (AA numbering refers to the human RyR2 protein sequence). The numbers in A correspond to the clusters shown in B. SR indicates sarcoplasmic reticulum. (Adapted from Connie et al., 2015<sup>463</sup>)

Mutations in C-terminus of RyR<sub>2</sub> could induce either gain-of-function or loss-of-function effect. For instance, RyR<sub>2</sub><sup>R4496C</sup> is a gain-of-function mutation, but RyR<sub>2</sub><sup>A4860G</sup> is a loss-of-function mutation. RyR<sub>2</sub><sup>R4496C</sup> mice displayed bidirectional ventricular tachycardia after administration of epinephrine and caffeine, and hearts from RyR<sub>2</sub><sup>A4860G</sup> mice also presented malignant arrhythmias with sympathetic stimulation.<sup>464, 465</sup> Mutation R4496C attributed to the leaky RyR<sub>2</sub> triggering arrhythmogenic disorders in ventricular myocytes.<sup>466</sup> The leaky RyR<sub>2</sub><sup>R4496C</sup> also lowered the SR Ca<sup>2+</sup> content and the threshold for waves, while β-AR stimulation produced Ca<sup>2+</sup> waves via increasing the SR Ca<sup>2+</sup> content.<sup>466</sup> However, isolated ventricular myocytes from RyR<sub>2</sub><sup>A4860G</sup> mouse had decreased the peak of Ca<sup>2+</sup> release during systole, gradually overloading the SR with Ca<sup>2+</sup>.<sup>464</sup> The resultant Ca<sup>2+</sup> overload then randomly caused bursts of prolonged Ca<sup>2+</sup> release, activating electrogenic NCX activity and triggering early afterdepolarizations.<sup>464</sup> Interestingly, RyR<sub>2</sub><sup>R4496C</sup> mice also displayed decreased heart rate after isoproterenol injection, indicating a RyR<sub>2</sub> C-terminal mutation induced SAN dysfunction.<sup>458</sup> Our team investigated the RyR<sub>2</sub><sup>R4496C</sup> behavior in SAN cells and its contribution to SAN automaticity. We found that Ca<sup>2+</sup> spark frequency was increased by 2-fold in RyR<sub>2</sub><sup>R4496C</sup> SAN cells, associated with prolonged cycle length and impaired isoproterenol response.<sup>458</sup> Besides, RyR<sub>2</sub><sup>R4860G</sup> mutant mice also exhibited sinus bradycardia, although the

underlying mechanism remains unknown.<sup>464</sup> Nevertheless, if mutations in N-terminus or central region also attributes to SAN dysfunction, and their mechanisms are unclear.

Central region (zipping domains) interacts with N-terminal region stabilizing the RyR in the closed state. Mutation-resultant reduction in the interaction affinity causes separation of the regions (unzipping), which increases RyR<sub>2</sub> open probability and thereby induces greater Ca<sup>2+</sup> release. For instance, genetic modified mice with CPVT-associated RyR<sub>2</sub> mutation (R2474S) exhibited exercise or drug administration induced ventricular tachycardia. Isolated RyR<sub>2</sub><sup>R2474S</sup> cardiomyocytes have more Ca<sup>2+</sup> spark release both before and after isoproterenol stimulation, associated with decreased threshold of SR Ca<sup>2+</sup> content. Further investigation found defective interaction (unzipping) between N-terminal and central region in mutant RyR<sub>2</sub><sup>R2474S</sup>.

Some N-terminal mutations were also proposed through zipping/unzipping hypothesis modifying RyR<sub>2</sub> Ca<sup>2+</sup> release behavior.<sup>467</sup> Indeed, N-terminal mutation R176Q resulted in gain-of-function. R176Q KI mice exhibited decreased right ventricular end-diastolic volume.<sup>468</sup> Ventricular tachycardia was observed after either caffeine and epinephrine challenge or intracardiac stimulation in R176Q KI mice, but not in WT mice.<sup>468</sup> Isolated cardiomyocytes from R176Q KI mice presented increased Ca<sup>2+</sup> release events, which increase susceptibility to catecholamine-induced VT.<sup>468</sup> However, this mutation was found in patients with ARVD2, which is not pure CPVT. The mechanism underlying RyR<sub>2</sub> N-terminal mutation related CPVT is still unknown. Besides, this mutation is located in A-domain of N-terminus, but mutations in other domains are unclear. Lack of animal model limits the further investigation. When this thesis was studied, no N-terminal C-domain mutation related animal model or N-terminal mutation related CPVT model was reported.

#### **1.4 Ryanodine receptors (RyRs)**

Ryanodine receptors (RyRs) are Ca<sup>2+</sup> release channels located on intracellular calcium storage and release organelle, endoplasmic reticulum (ER)/sarcoplasmic reticulum (SR). In physiological condition, there is a 10<sup>4</sup>-fold Ca<sup>2+</sup> gradient across the SR/ER membrane between the SR matrix (~ 1 mM) and the cytosol (~ 100 nM). A similar gradient also exists between extracellular space and the cytosol. The cytosol [Ca<sup>2+</sup>]<sub>i</sub> is maintained at the low level by plasmalemmal Na<sup>+</sup>/Ca<sup>2+</sup> exchanger (NCX) and Ca<sup>2+</sup>-ATPase (PMCA), the ER/SR Ca<sup>2+</sup>-ATPase (SERCA), by the mitochondrial Ca<sup>2+</sup> uniporter, and by Ca<sup>2+</sup> buffering molecules of differing capacity and kinetics.<sup>469</sup> This low resting cytosolic [Ca<sup>2+</sup>]<sub>i</sub> avoids the toxicity of sustained high [Ca<sup>2+</sup>]<sub>i</sub>, and also bestows on the Ca<sup>2+</sup> signaling system a wide dynamic range and a high signal-to-background ratio.<sup>469</sup> Many Ca<sup>2+</sup> signaling cascades are initiated by rapid mobilization of Ca<sup>2+</sup> among membrane-bound compartments, usually down its electrochemical gradient across the membrane. Ca<sup>2+</sup> enters the cell via diverse Ca<sup>2+</sup>-permeant channels and their gating mechanisms, and NCX acting in the reverse

mode.  $\text{Ca}^{2+}$  release from the ER/SR is mediated by two families of  $\text{Ca}^{2+}$  channels, the RyRs and inositol 1,4,5-triphosphate receptors ( $\text{IP}_3\text{Rs}$ ), and pumped back into SR/ER by SERCA.

Mutations in RyR channel could influence channel function through modification in ion permeation, gating, and sensitivity to regulators and accessory proteins that resulting in the pathogenic consequences. Thus, in this session we are going to introduce RyRs, including their isoforms, tissue distribution, structures, regulation, and accessory proteins. We will focus on the cardiac isoform (ryanodine receptor type 2,  $\text{RyR}_2$ ), which plays an essential role in CICR, SAN automaticity generation, arrhythmia, among others.

#### 1.4.1 RyR isoforms and tissue distribution

RyR are termed like that because they irreversibly bound the alkaloid ryanodine, which blocks the channel in open state.<sup>470</sup> There are two types of major  $\text{Ca}^{2+}$  release channels localized in SR/ER membrane, ryanodine receptors (RyRs) and inositol 1.2.5-triphosphate receptors ( $\text{IP}_3\text{Rs}$ ).<sup>471, 472</sup> RyRs are the largest ion channels to date ( $\sim 2.2\text{MDa}$ ).<sup>473, 474</sup> Each RyR is consisted of four homologous subunits, and each subunit contains approximately 5000 amino acids (a molecular weight of  $\sim 560\text{kDa}$ ).<sup>474, 475</sup> RyRs are crucial for many cellular events, for instance, EC coupling. In skeletal ( $\text{RyR}_1$ ) and cardiac muscle ( $\text{RyR}_2$ ), the membrane (including transverse tubules, t-tubules) depolarization during the action potential activates LTCC inducing SR  $\text{Ca}^{2+}$  release by either mechanical coupling to  $\text{RyR}_1$  in skeletal muscle or by activating the  $\text{RyR}_2$  through  $\text{Ca}^{2+}$  elevation in its vicinity ( $\text{Ca}^{2+}$  induced  $\text{Ca}^{2+}$  release) in cardiac muscle, and the increased cytosolic  $\text{Ca}^{2+}$  initiates cell contraction, termed EC coupling.<sup>211</sup> Depending on species, 70 to 90% of cytosolic  $\text{Ca}^{2+}$  release during EC coupling is from the SR.<sup>476</sup>

In mammals, there are three RyR isoforms ( $\text{RyR}_1$ -3) exhibiting tissue-specific expression patterns.<sup>475, 477</sup>  $\text{RyR}_1$  was the first one to be cloned.<sup>478, 479</sup> It is highly expressed in mammalian skeletal muscle, and also found in cardiac muscle, smooth muscle, kidney, thymus, cerebellum, Purkinje cells, adrenal glands, ovaries, testis, and B-lymphocytes.<sup>477</sup> Because of its high expression in skeletal muscle and ease of purification,  $\text{RyR}_1$  is the most thoroughly examined isoform. The gene encoding  $\text{RyR}_1$  is located on chromosome 19q13.2 and spans 104 exons in human, and on chromosome 7A3 in mice.<sup>480</sup>

$\text{RyR}_2$  is the predominant isoform in cardiac myocytes.<sup>471, 481-483</sup> It is also expressed at high levels in Purkinje cells of cerebellum and cerebral cortex and in low levels in stomach, kidney, adrenal glands, ovaries, thymus, and lungs.<sup>477</sup> Lacking of  $\text{RyR}_2$  is embryonically lethal in mice.<sup>484</sup> The gene encoding  $\text{RyR}_2$  is located on chromosome 1q43 and spans 102 exons in human, and on chromosome 13A2 in mice.<sup>480</sup> It is responsible for EC coupling in cardiac myocytes and spontaneous electrical impulse generation in SAN.



RyR<sub>3</sub> is expressed at low levels in various cell types, including hippocampal neurons, thalamus, Purkinje cells, corpus striatum, skeletal muscles (highest expression in the diaphragm), the smooth muscle cells of the coronary vasculature, lung, kidney, ileum, jejunum, spleen, stomach of mouse and aorta, uterus, ureter, urinary bladder, and esophagus of rabbit.<sup>477, 483</sup> The gene encoding RyR<sub>3</sub> is located on chromosome 15q13.3-14 and spans 103 exons in human, and on chromosome 2E4 in mice.<sup>480</sup>

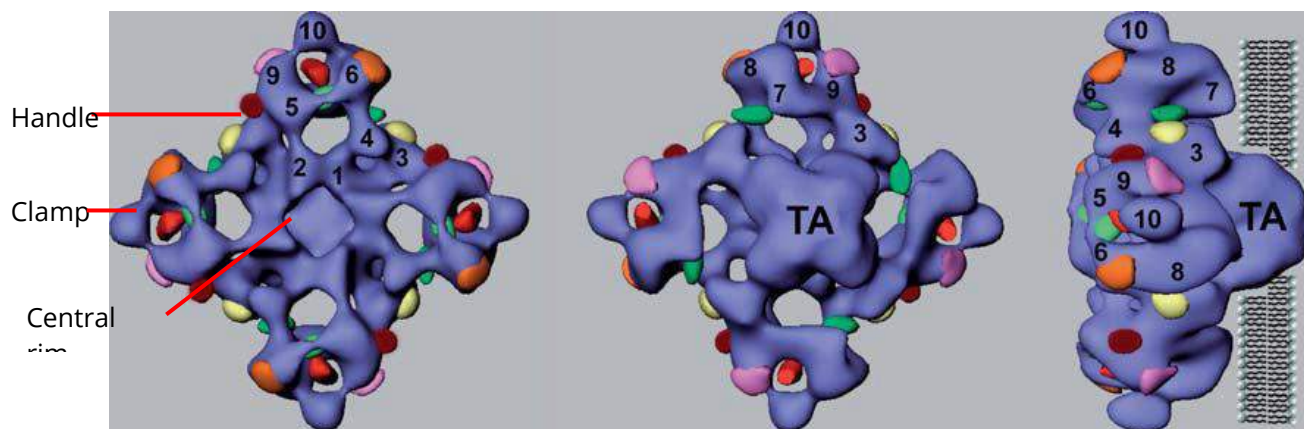


Figure 14. Three-dimensional structure of RyR. The projection view of RyR from the cytosol to sarcoplasmic reticulum (SR) lumen (left panel), from SR lumen to cytosol (middle panel) and side view (right panel). The numerals on the cytosolic cap refer to distinguishable globular domains. TA, transmembrane assembly. The colorful symbols indicate divergent regions D1 (yellow), D2 (orange), D3 (purple), N-terminal regions (red), central domains (light green), FK506-binding protein 12 (FKBP12) (brown) and calmodulin (CaM) (green). Clamp, handle and central rim are shown in right panel. (Modified from Zissimopoulos et al., 2007<sup>331</sup>)

The three mammalian isoforms share 65% sequence identity with three divergent regions, known as D1 (residues 4254-4631 in RyR<sub>1</sub>, residues 4210-4562 in RyR<sub>2</sub>), D2 (residues 1342-1403 in RyR<sub>1</sub>, residues 1353-1397 in RyR<sub>2</sub>), and D3 (residues 1872-1923 in RyR<sub>1</sub>, residues 1852-1890 in RyR<sub>2</sub>) as shown in Figure 14 indicated by yellow, orange and purple symbols respectively.<sup>485</sup> D1 is the largest and most variable region, and D2 is completely absent in RyR<sub>3</sub>.<sup>331</sup> For RyR<sub>1</sub>, mutations in D1 region alter its Ca<sup>2+</sup> and caffeine sensitivity, whereas D2 region contains critical determinants for maintaining interaction with Cav1.1, and D3 region contain Ca<sup>2+</sup> dependent inactivation sites.<sup>486-488</sup>

Non-mammalian vertebrate (birds, amphibians, reptiles and fish) also expresses three RyR isoforms (RyR $\alpha$ , RyR $\beta$  and cardiac type), whereas one single RyR isoform was found in lower organisms, including nematodes, fruit flies and lobster.<sup>331, 475, 477</sup> RyR $\alpha$  and RyR $\beta$  are homologous to mammalian RyR<sub>1</sub> and RyR<sub>3</sub> sequence, respectively.<sup>331</sup>

## 1.4.2 RyR structure

### 1.4.2.1 Overall mammalian RyR structure

Subnanometer-resolution electron cryomicroscopy (Cryo-EM) studies indicate that the overall shapes for all mammalian RyR isoforms are similar.<sup>489-492</sup> Their overall structure can be described as a mushroom shown in Figure 14, with a cap (also called foot) located in the cytosol, and a stalk protruded from cap and crossing the membrane into the SR/ER lumen.<sup>493-496</sup> The transmembrane region is rotated by approximately 40° with respect to cytosolic region.<sup>493, 497</sup> Figure 14 displays RyR architecture as a projection view from the cytosol to sarcoplasmic reticulum (SR) lumen (left panel), from SR lumen to cytosol (middle panel) and side view (right panel). RyR structure has a 4-fold cyclic symmetry around an axis perpendicular to the membrane consistent with the tetrameric nature of the channel.

Each subunit of the RyR homotetramer consists of two main parts: a cytosolic part and a transmembrane part. The cytosolic part contains four-fifths of RyR protein and as an overall square prism shape (dimension of 29nm × 29nm × 12nm, or around 270Å × 270Å × 100Å using cryo-EM at resolution near 10Å).<sup>493-496</sup> It is composed of several portions, named clamps, handles, central rim and columns as seen in Figure 14 and 15, while the left panel of Figure 14 also labels the subdomains in one subunit of RyR<sub>1</sub> with numerals. The clamps, defined by the corners of the cytosolic caps (Figure 14, subdomains 5-10), are connected through the handles (subdomains 3-4) that surround the central cavity (central rim, subdomains 1-2).<sup>475, 477</sup> Each clamp contains seven α-helices and three β-sheets, while one β-sheet is localized on handle region and two more β-sheets are found in central rim (Figure 15).<sup>498</sup> The clamps undergo major conformational changes during the opening and closing of the channel.<sup>495, 498, 499</sup>

The cytosolic part regulates RyR gating via interaction with a variety of intracellular messengers, including FKBP12, calmodulin, ATP, Ca<sup>2+</sup>, and Mg<sup>2+</sup> ions (Figure 14). The four homologous sequences of the tetrameric RyR structure suggest a similar arrangement.

Four columns are between cytosolic cap and transmembrane, holding a height of ~14Å of RyR<sub>1</sub> detected by cryo-EM at resolution around 10Å (Figure 15).<sup>494, 495, 498</sup> Each column consists of one β-sheet (β7 in Figure 15) and eight α-helices, to maintain the connection of cytosolic cap and transmembrane region.<sup>498</sup> Thus, in each RyR<sub>1</sub> subunit cytosolic region, 36 α-helices with various rotations and 7 β-sheets are identified (Figure 15).<sup>498</sup>

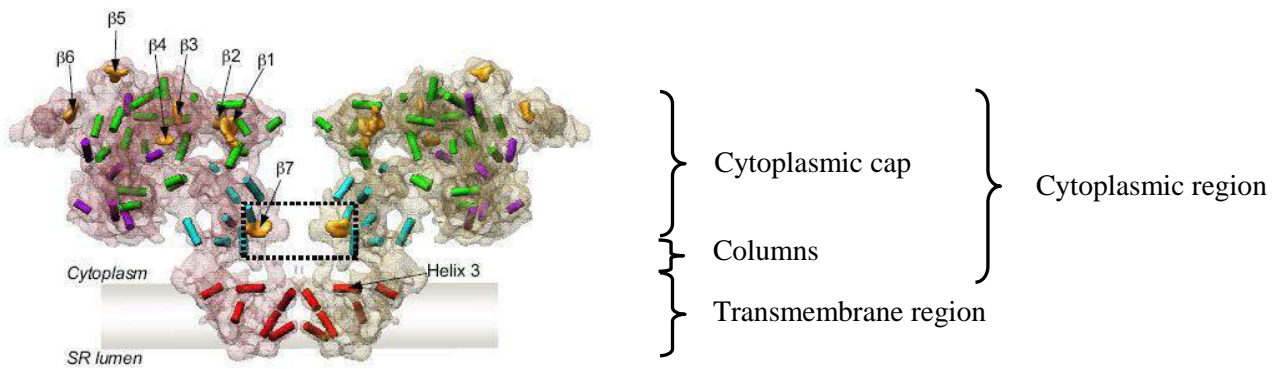


Figure 15 Secondary structure elements of two opposing RyR<sub>1</sub> subunits from the tetramer are shown in a side view.  $\alpha$ -Helices are annotated as cylinders colored according to their locations in the map: red, TM region; green, central part of the CY region; purple, clamps; cyan, column region.  $\beta$ -Sheets are shown as orange symbols. A dashed line indicates  $\beta$ -sheets in the column region. (Adapted from Serysheva et al. 2008<sup>498</sup>).

The transmembrane region/assembly, which contains the other one-fifth of RyR protein, is consisted of membrane spanning and luminal domain (Figure 14, right panel). This square-shaped region has an edge length of 12nm at the attachment side of the cap and approximately 6nm at the luminal side, while 7nm perpendicularly across the ER/SR membrane (RyR<sub>1</sub> dimension of approximately 120Å × 120Å × 60Å using cryo-EM at resolution near 10Å).<sup>493-496</sup> The number of transmembrane helices on each subunit is still under debate. Recent cryo-EM studies at 8-10Å suggest five<sup>496, 498</sup> or six  $\alpha$ -helices<sup>494, 495, 500</sup> with different orientation in the transmembrane region. Two kinds of transmembrane helices, the inner helices and outer helices (the four S5 and S6), together with the pore loops (each contain a pore helix) form the pore-forming region (Figure 15 and 17). The transmembrane part is critical for undergoing large structural changes of RyRs and releasing Ca<sup>2+</sup> during gating.

#### 1.4.2.2 RyR<sub>2</sub> structure

The three-dimensional structure of RyR<sub>2</sub> is detected by cryo-EM at a low resolution of ~30Å and by bioinformatic mapping.<sup>332, 489</sup> The overall shape of RyR<sub>2</sub> structure is similar as RyR<sub>1</sub> in respect of their high degree of sequence conservation.<sup>332, 489, 491</sup> However, some conformational differences are found in the size or shape of certain domains (indicated by arrows in Figure 16). In particular, domains 8, 9, and 10 in the clamp regions of the cytosolic cap are larger, whereas domain 7 is somewhat smaller in RyR<sub>2</sub> relative to RyR<sub>1</sub>. Domains 5 and 6 connected by a bridge in RyR<sub>1</sub> is absent, or weaker, in RyR<sub>2</sub> (left panels of Figure 16, A and B). This bridging density has been found to vary among reconstructions of RyR<sub>1</sub>, and thus the significance of this difference is unclear.<sup>489, 493</sup>

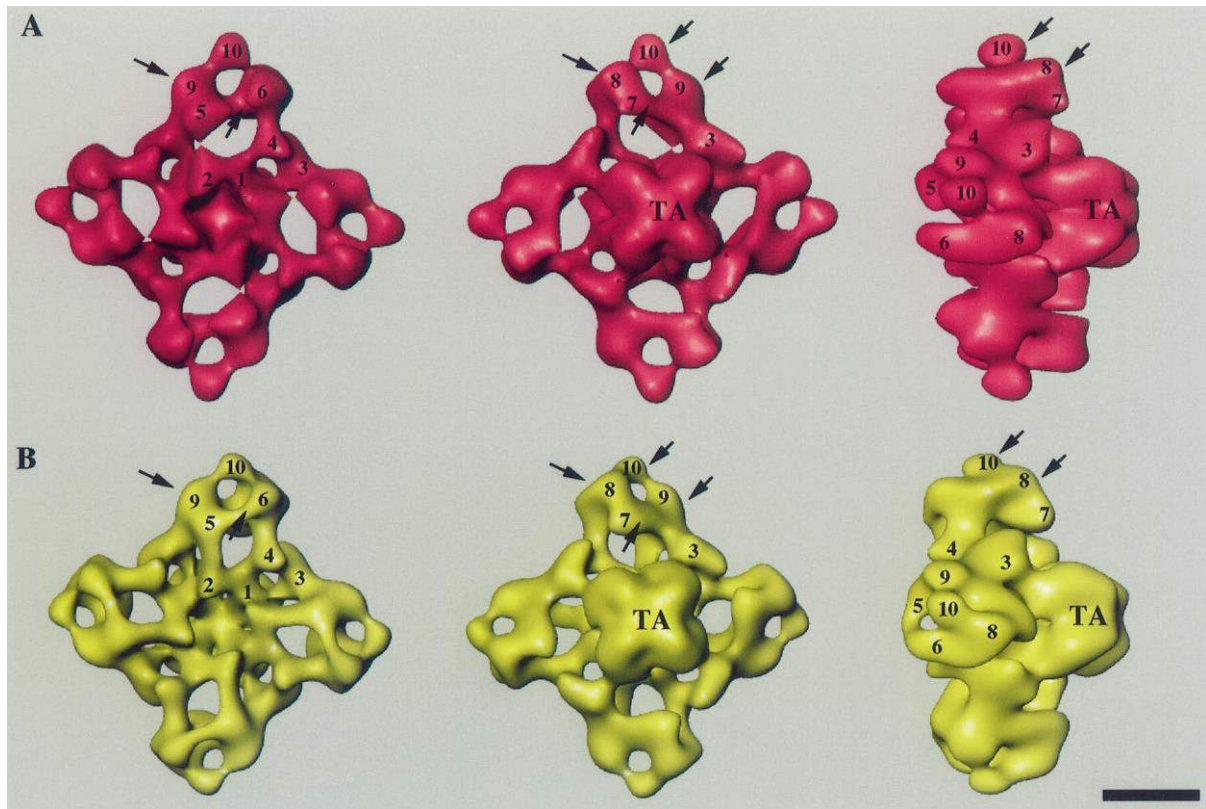


Figure 16. Three-dimensional reconstruction of RyR<sub>2</sub> (A) and RyR<sub>1</sub> (B). Leftmost vertical structures of A and B show the view of RyR<sub>2</sub> and RyR<sub>1</sub> from cytosol. The middle structures show the view from sarcoplasmic reticulum, while the rightmost structures show the side view. Arrows point to obvious differences between RyR<sub>2</sub> and RyR<sub>1</sub>. The putative structural domains are labeled with numerals 1–10 as Figure 14. TA, transmembrane assembly. Scale bar, 100 Å. (Adapted from Sharma et al., 1998<sup>489</sup>)

### 1.4.2.3 Membrane topology and pore region

The number of transmembrane helices is still under debate. Hydrophathy profiles indicate 4 to 12 helices per subunit, while two topology models of 4TM and 10TM segments have been proposed, although four segments of the 4TM model corresponding to M5, M6, M8 and M10 of the 10TM model.<sup>331</sup> Current three-dimensional reconstructions at ~10Å resolution suggest five or six  $\alpha$ -helices are identified.<sup>494-496, 498</sup> A recent advanced cryo-EM study at 4.8 Å resolution further confirm that RyR<sub>1</sub> is a six transmembrane ion channel.<sup>500</sup>

The currently favoured RyR<sub>1</sub> membrane topology is depicted in Figure 17. Each subunit has six transmembrane helices (S1-S6) per subunit surrounding the central pore (Figure 17).<sup>494-496, 500</sup> The transmembrane region could be separated into two domains: the pore domain, formed by two transmembrane helices (S5, S6) and the extended peptide (P-segment); and the interfacing domain formed by S1-S4 that is connected with the pore domain (Figure 17).<sup>500</sup>

The primary sequence of pore forming region is highly conserved (90% identity) among RyR isoforms. The P-segment contains a pore helix, an amino acid motif (GGGIGD) forming the



selectivity filter, and many negatively charged amino acid residues contributing to the high cation conductance.<sup>500, 501</sup>

More recently, cryo-EM study at  $\sim 4.8\text{\AA}$  resolution found that the S6 helix extends  $\sim 30\text{\AA}$  into the cytosol (Figure 17).<sup>500</sup> This study also found that the S6 helix has a  $24^\circ$  kink (centered on G4934) in the middle near the cytosolic face of the membrane, which orients the cytosolic extension of S6 roughly parallel to the channel axis.<sup>500</sup> This glycine residues is conserved in the pore-lining helices of other 6TM ion channels, that may operate as ‘glycine-hinges’ facilitating reorientation of the pore-lining helix and consequent alteration in the cytosolic aperture of the channel.<sup>500, 502</sup> G4934 is also conserved in all RyR isoforms and in a closely related channel, the inositol 1,4,5-trisphosphate receptor. Seven negatively charged residues are also found along the cytosolic extension of S6 and presumably serving the high cation conductance as the ones on P-segment.<sup>500</sup>

The S2-S3 helical bundle lies in close proximity to the putative  $\text{Ca}^{2+}$  binding domain and the Carboxyl-terminal region (Figure 17) suggesting this domain may be involved in transmitting conformational changes in the cytosolic assembly to the pore.<sup>500</sup>

JM1 region form a cytosolic leaflet on the SR membrane (Figure 17),<sup>331</sup> while a recent study further demonstrates that the transmembrane region contains three apparently amphipathic helices (JM1, the first helix of the S2-S3 insertion and the S4-S5 linker helix) that are expected to lie in the plane of the cytosolic surface of the SR membrane.

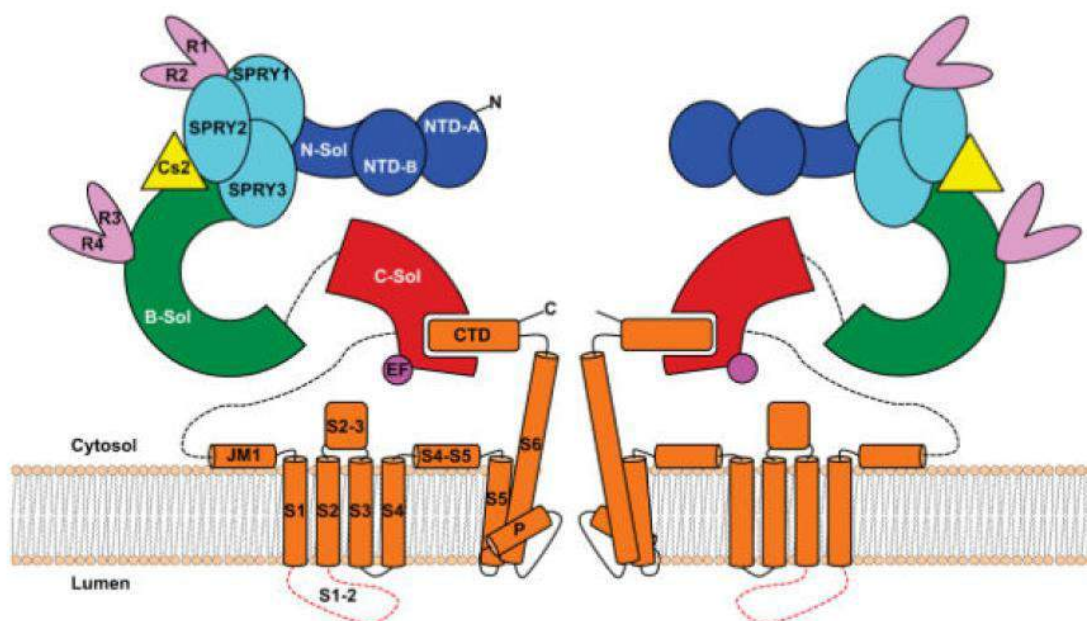


Figure 17 Membrane topology of RyR<sub>1</sub>. Colored as follows: dark blue, N-terminal region, including NTD A and B (N-terminal beta-trefoil domain A and B), and N-Sol (N-terminal solenoid); cyan, SPRY1, SPRY2 and SPRY3 (named from SP1a and the ryanodine receptor); salmon, clamp region (RY12 repeats), and phosphorylation domain (RY34 repeats); yellow, calstabin; green, the bridge solenoid scaffold; red, the core solenoid; and orange, transmembrane and

Carboxyl-terminal domains (CTD); purple, putative  $\text{Ca}^{2+}$  binding domain (EF). Dashed lines represent major disordered segments. (Modified from Zalk et al., 2015<sup>500</sup>)

The negative residues on both sides of the pore forming region are depicted in the study of Welch et al.<sup>501</sup> and Zalk et al.<sup>500</sup> Besides the high conductance, they also contribute to the relative permeabilities of divalent and monovalent cations in RyR. In support of this proposal, neutralization of acidic residues at the luminal entrance to the selectivity filter (ED4832AA) results in non-discrimination between divalent and monovalent cations, and cation conductance is significantly altered.<sup>503</sup> Further more, the regulatory proteins triadin and junctin also interact with the pore forming region through negatively charged residues.<sup>504-506</sup> Junctin binds two different domains of RyR<sub>2</sub>: luminal residues 47-77 of junctin specifically bind to RyR<sub>2</sub> luminal M5-M6 linker (residues 4520-4553), and luminal residues 78-210 bind to the RyR<sub>2</sub> pore loop (residues 4789-4846).<sup>504</sup> However, triadin is more likely to bind single sites: three acidic residues (D4878, D4907 and E4908) are critical for triadin binding to the RyR<sub>1</sub>.<sup>506</sup>

Some studies depicted P-segment as a structurally analogue to the selectivity filter of potassium and sodium channels,<sup>494-496</sup> although a more recent study indicates that it's more similar to the equivalent region of the TRPV1 cation channel.<sup>500</sup> Indeed, the luminal aperture is also comparable to that of the highly  $\text{Ca}^{2+}$ -permeable TRPV1.<sup>500</sup>

#### 1.4.2.4 Ion permeation

The permeation properties of the different RyR channel isoforms are similar, including the ion selectivity and unitary conductance.<sup>507-509</sup>

The physiological role of RyR is to be permeable to  $\text{Ca}^{2+}$  ion to release it from the lumen of the SR to the cytosol. Besides  $\text{Ca}^{2+}$ , RyR channel is also permeable to variously divalent and monovalent cations, but nearly impermeable to anions.<sup>510, 511</sup> The relative permeability of the RyR channel to different monovalent and divalent cations has been defined by single channel recording in planar lipid bilayer.<sup>510, 511</sup> The RyR channel shows very little selectivity among different monovalent cations, or divalent cations. However, the RyR channel is modestly selective between monovalent and divalent cations (permeability ratio  $\text{PCa/PK} \sim 6$ ). In comparison to other  $\text{Ca}^{2+}$  channels like the L-type  $\text{Ca}^{2+}$  channel, which displays a much higher degree of discrimination between monovalent and divalent cations (permeability ratio  $\text{PCa/PK} > 25$ ), RyR channel is not a highly selective  $\text{Ca}^{2+}$  channel.<sup>512-514</sup>

The unitary conductance of the RyR channel with both divalent and monovalent cations is extremely high, approximately 10 times higher than L-type  $\text{Ca}^{2+}$  channel.<sup>331, 510, 511, 514</sup> Channel conductance with divalent (e.g. 135-150 pS for  $\text{Ca}^{2+}$ ) is generally lower than monovalent cations (e.g. 720-800 pS for  $\text{K}^+$ ), in spite of that divalent cations are six to seven times more permeable than

$K^+$ . The conductance sequence of sheep RyR<sub>2</sub> channel for monovalent cations is  $K^+ > Rb^+ = NH_4^+ > Na^+ = Cs^+ > Li^+ \gg Tris^+$  in symmetrical ionic solutions, while for divalent cations is  $Ba^{2+} > Sr^{2+} > Ca^{2+} > Mg^{2+}$ .<sup>508, 510</sup> The high conductance of RyR channel determines less time to perform the steps needed to discriminate between ions. In this respect, the apparent deficiency in  $Ca^{2+}$  selectivity may be related to its high conductance.<sup>512</sup>

Between the cytosol and SR lumen, there is a great free  $[Ca^{2+}]_i$  gradient. The diastolic free  $[Ca^{2+}]_i$  is only ~100 nM in the cytosol but ~1 mM in the SR lumen, while cytosolic concentrations of other ions are much larger (~150 mM  $K^+$ ) or comparable (~1 mM  $Mg^{2+}$ ) on both sides of the SR membrane.<sup>515, 516</sup>  $Ca^{2+}$  is the only cation with this significant concentration gradient across the SR membrane, which makes  $Ca^{2+}$  essentially the only ion released through RyR. The concentration gradient is the major driving force, regardless of the moderate selectivity or lower but still high conductance between divalent and monovalent cations.<sup>331, 513</sup> During the EC coupling, the  $Ca^{2+}$  ions are released from the SR in several milliseconds, accounting for >70% total cytosolic  $Ca^{2+}$  uptake.<sup>476</sup>

#### 1.4.2.5 Gating

During opening, RyR channel performs substantial structural rearrangements while most of the domains appear to move.<sup>337, 475, 496</sup> The main idea of the swiveling movement is to make the 4-fold axis less crowded, to increase the ion gate diameter.<sup>495</sup>

The largest-magnitude conformational change occurs in the cytosolic region.<sup>495, 499</sup> The clamp region (subdomains 9 and 10) together with the structure formed by subdomain 7, 8 and 8a move downwards the ER/SR up to 8 Å (Figure 14 and 18). Concomitantly, the subdomain 2 of central rim move approximately 4 Å upwards and outwards away from the the ER/SR membrane and 4-fold axis, respectively. Subdomain 6 moves approximately 5 Å outwards.<sup>495</sup>

The movement in the cytosolic region is conveyed to the inner branches of columns.<sup>495</sup> The four inner branches are located on the cytosolic side, shaped as thin bent rods.<sup>494, 495, 498</sup> They connected each other and merge into a ring of high density inside the transmembrane assembly above the pore in closed state. In the open state, they rotate 5° and move approximately 6 Å further away from each other, which is directly related to the diameter of the ion gate (Figure 18).<sup>495</sup> By directly linking the cytosolic region, the inner branches are proposed to transmit the conformational changes from the transmembrane region to cytosolic region.<sup>495</sup>

In the transmembrane region, the inner helices form a right-handed helical bundle constricting towards the cytosol in closed state.<sup>494, 495</sup> From closed to open state, changes in angle and the outwards bending of inner helices are seen in a recent research, generating a relaxation of the

helical bundle and the wider ion gate.<sup>495</sup> The pore helices also protrude into the central cavity, and provide a narrow passage.

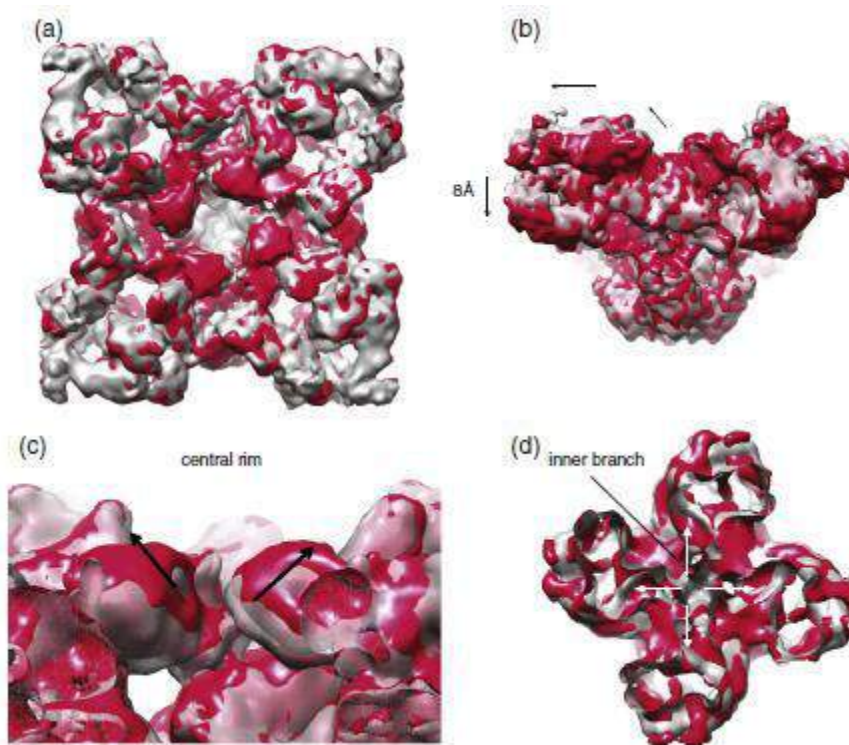


Figure 18 Allosteric changes during opening and closing. (a) View of RyR<sub>1</sub> from cytosol in presumed mass of closed (gray) and open (red) states. The red portion in the central rim indicates that this region moves upward during opening, whereas the gray portions in the clamps indicate that this area moves downward toward the ER/SR membrane. (b) Side view. Arrows indicate relative movements during opening, which can be generally described as a tilting motion. (c) Side view, cut along the center to show movements within the central rim. (d) Top view, cut along the surface plane of inner branches, showing their outward movement. Arrows indicate the relative movement during opening. (Adapted from Van Petegem, 2015<sup>517</sup>)

RyR channel's cytosolic region interacts with proteins or small molecules, such as FKBP12, CaM, L-type Ca<sup>2+</sup> channel, etc (Figure 14).<sup>331, 475</sup> In all cases, the binding sites are situated at least 130 Å away from the ion gate. It is likely that the upward and outwards movement of the cytosolic region pulls the inner branches at the same direction.<sup>495</sup> As the inner branches are directly connected to the ion gate, it is straightforward to see how their being pulled apart and increases the diameter of the ion gate.<sup>495</sup>

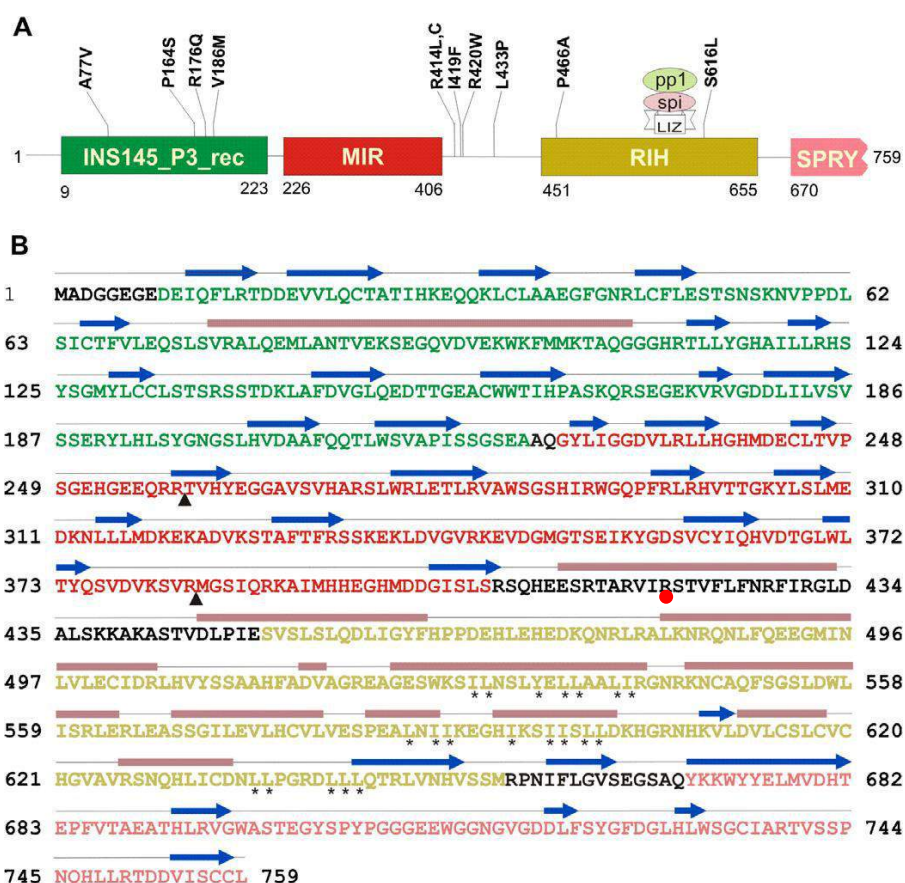
#### 1.4.2.6 N-terminal region and R420 site

As the mutation studied in this thesis (RyR<sub>2</sub><sup>R420Q</sup>) is located on the C-domain of the RyR<sub>2</sub> N-terminus, this session specifically introduces RyR<sub>2</sub> N-terminus mutations. Addition of a peptide corresponding to amino acids 163-195 of RyR<sub>2</sub> markedly increased diastolic calcium release of RyR<sub>2</sub>, which means N-terminal region allosterically regulates channel activity.<sup>518</sup> Indeed,



CPVT/ARVD2 related mutations are found in N-terminal region as shown in Figure 19. All these evidences indicate the importance of N-terminal region to RyR<sub>2</sub> channel function.

The human N-terminal region consists of three domains: A (residues 10–223), B (224–408) and C (409–544) as shown in Figure 19 panel C.<sup>462</sup> Domain A and B correspond to Pfam domain Ins145\_P3\_rec and MIR domain respectively, which are presented in green and red color in panel A of Figure 19 and the amino acids involved are exhibited with the same color in panel B. Domain C contains five  $\alpha$ -helices including the RIH domain (residues 451–655).<sup>332, 462</sup> The first  $\alpha$ -helix of domain C (central helix, residues 410–437) doesn't belong to RIH domain as shown in panel B of Figure 3, where the purple bar between residues 373-434 is labeled. This helix is located in the centre of the structure, forming contacts with all three domains and plays a prominent stabilizing role.<sup>462</sup>



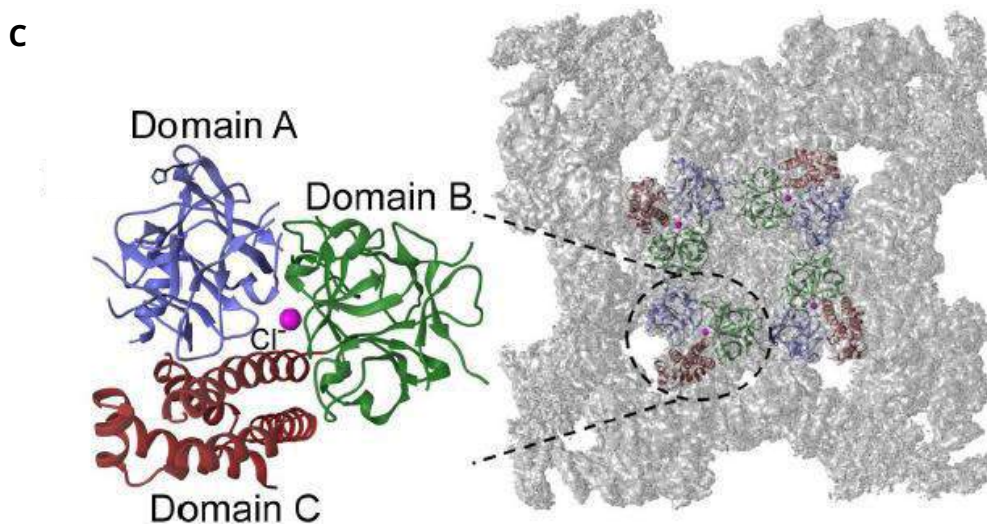


Figure 19 N-terminal fragment (amino acid residues 1-759) of the cardiac human RyR<sub>2</sub> receptor. (A) Schema of domains in the RyR<sub>2</sub> N-terminal fragment. Pfam analysis indicates that it consists of an Ins145\_P3\_rec, MIR, RIH and part of a SPRY domain. Some mutations of specific residues believed to be involved in ARVD2 and CPVT1 are shown. LIZ (residues 554-585) indicates the leucine-isoleucine zipper area, while SPI and PP1 represent spinophilin and protein phosphatase 1, respectively. (B) Alignment of the RyR<sub>2</sub> N-terminal fragment. Amino acids involved in Ins145\_P3\_Rec, MIR, RIH and SPRY domains according Pfam are in green, red, yellow and magenta colors as shown in A. Interdomain amino acids are in black. Purple bars and blue arrows illustrate  $\alpha$ -helices and  $\beta$ -strands, whereas the asterisks represent areas rich in leucines and isoleucines. The trypsin cleavage sites are labeled with black triangles, and residue of R420 is masked with red point. (C) Top view of RyR<sub>2</sub> indicate the structure of N-terminal region and interaction between domain A (blue), domain B (green) and domain C (red). (Panel A and B adapted from Bauerova-Hlinkova et al. 2010,<sup>519</sup> panel C adapted from Xiao et al., 2015<sup>461</sup>)

In RyR<sub>1</sub> N-terminal region, four residues located in all three domains (Asp61, Arg283, Arg 402 and Glu40) form an ionic pair network and stabilize the RyR<sub>1</sub>ABC structure.<sup>520</sup> However, in mice RyR<sub>2</sub>, the ionic pair network is replaced by a chloride ion, which interacts with three residues (Arg420, Arg298 and Arg276) from domain B and C.<sup>520</sup> The human RyR<sub>2</sub> N-terminal structure is substantially different from other N-terminal RyR structures known so far. For instance, the the anion binding site in mice RyR<sub>2</sub> is absent.<sup>462</sup> The domain A, B and C of human RyR<sub>2</sub> are held together by a unique network of interactions, while the central helix (amino acids 410-437) is prominent.<sup>462</sup>

Arg420 is crucial for maintaining a stable A/B/C domain arrangement.<sup>462, 520</sup> It is not conserved between RyRs, but well conserved among RyRs from different organisms.<sup>462</sup> Arg420 is a target for two CPVT mutations, R420Q and R420W. All these evidences indicate the potentially important role of Arg420. R420W mutation structural alteration is well studied. This mutation may cause changes on side chain size, charge and polarity.<sup>462</sup> But it is likely that the tryptophan side chain in the R420W mutation adopts a conformation pointing to the solvent and avoids significant structural changes.<sup>462</sup> This is further conformed by the unchanged thermal stability of R420W with respect to

that of WT and the R420Q mutation.<sup>462, 520</sup> Tang et al. also proposed that R420W mutation contribute to reduced threshold for  $\text{Ca}^{2+}$  release termination and increased fractional release.<sup>521</sup> Recently, some studies suggested that R420Q mutation may induce changes on side chain size and charge, although the thermal stability is not influenced.<sup>462, 520</sup> However, lack of animal model limits the further investigation. When this thesis was studied, no N-terminal C-domain mutation related animal model was reported.

#### 1.4.2.7 RyR<sub>2</sub> $\text{Ca}^{2+}$ release events

$\text{Ca}^{2+}$  signals were first observed in the late 1960s as intracellular  $[\text{Ca}^{2+}]_i$  transients during single twitches in barnacle muscle fibers<sup>522</sup> and first imaged in the late 1970s as  $\text{Ca}^{2+}$  waves in fertilizing Medaka fish eggs.<sup>469, 523, 524</sup> Shortly after,  $[\text{Ca}^{2+}]_i$  transients during cardiac EC coupling were observed in frog cardiac muscle<sup>525</sup> and in canine Purkinje fibers<sup>526</sup>. With the development of  $\text{Ca}^{2+}$  detectors,  $\text{Ca}^{2+}$  sparks, the brief and fast  $\text{Ca}^{2+}$  releases, were visualized in mouse SAN cells from intact tissue (Figure 20).<sup>527</sup>

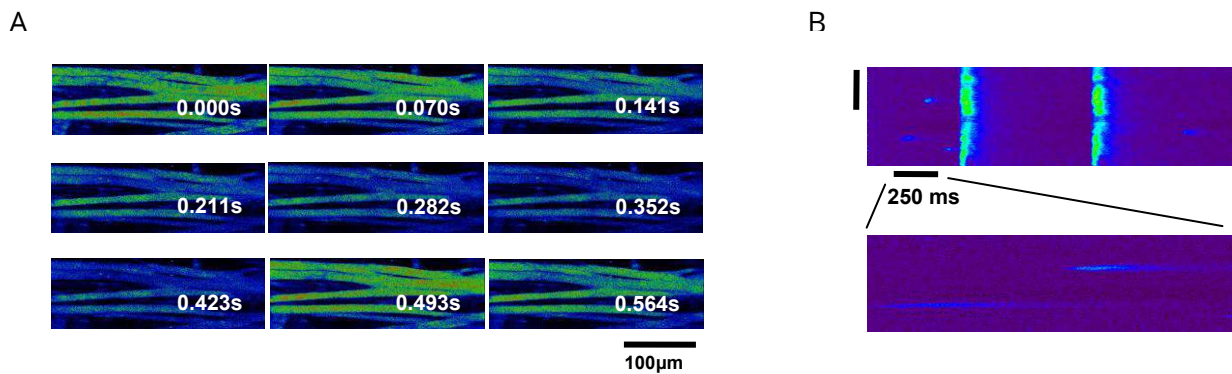


Figure 20  $\text{Ca}^{2+}$  sparks and transients. A. Two-dimensional confocal images of  $[\text{Ca}^{2+}]_i$  transients in mouse SAN cells from intact tissue. B. Line scan confocal images of an action potential (AP)-elicited  $[\text{Ca}^{2+}]_i$  transient (top) and two spontaneous spark (bottom) in one SAN cell, while the bottom image corresponds the 250ms depicting in the upper image. Time and space ordinates are displayed in the horizontal or vertical directions. (Adapted from Cheng and Lederer, 2008<sup>469</sup>)

$\text{Ca}^{2+}$  spark is an intracellular  $\text{Ca}^{2+}$  release event. Its fluorescent recording of  $\text{Ca}^{2+}$  release is from a single  $\text{Ca}^{2+}$  release unit (CRU), which refers to a cluster of  $\text{Ca}^{2+}$  release channels (RyRs) in the SR membrane.<sup>469</sup> In cardiac myocytes,  $\text{Ca}^{2+}$  sparks could occur when the L-type  $\text{Ca}^{2+}$  channels are opened, when local  $[\text{Ca}^{2+}]_i$  is elevated by some other mechanisms, and when RyRs open spontaneously.<sup>106, 469, 528</sup> In rat heart cells, the rate of spontaneous  $\text{Ca}^{2+}$  spark is about 100 per cell per second.  $\text{Ca}^{2+}$  sparks have a variable amplitude ( $\Delta F/F_0$  up to 4), a short duration (half time of decay of ~20-30 ms), and a small diameter (full width at half-maximum of ~2-2.5 $\mu\text{m}$ ).<sup>528</sup> In atrial myocytes, which largely lack T-tubules (TTs) and contain both peripheral junctional and central nonjunctional CRUs, spontaneous  $\text{Ca}^{2+}$  sparks are larger and longer lasting than their ventricular

counterparts (300,000 Ca<sup>2+</sup> in 12 ms versus 100,000 Ca<sup>2+</sup> in 7 ms), with a high prevalence at the periphery.<sup>529-531</sup>

Within a sarcomere, Ca<sup>2+</sup> sparks tend to center on the TTs at the Z-disk of a sarcomere, where discrete CRUs are spreaded on a plane that is perpendicular to the long axis of the cell.<sup>469</sup> In some conditions, Ca<sup>2+</sup> sparks activate nearby CRUs inducing Ca<sup>2+</sup> waves.<sup>469</sup> Ca<sup>2+</sup> sparks also constitute the elementary events of cardiac EC coupling, i.e. a [Ca<sup>2+</sup>]<sub>i</sub> transient is composed of temporal and spatial summation of thousands of Ca<sup>2+</sup> sparks.<sup>469</sup>

#### **1.4.2.8 RyR regulation by endogenous effectors**

RyRs are regulated by endogenous effectors (such as Ca<sup>2+</sup>, Mg<sup>2+</sup> and adenine nucleotides), cellular processes (such as phosphorylation), exogenous compounds (such as ryanodine, tetracaine, caffeine) that can be used for experimental studies. The regulations of the major endogenous effectors are briefly reviewed.

##### **1.4.2.8.1 Cytosolic calcium**

Ca<sup>2+</sup> ion is the most important regulator of RyR activity.<sup>532</sup> Open of all three RyR isoforms can be triggered by Ca<sup>2+</sup>. In cardiac cells RyR<sub>2</sub> are activated by calcium ions that flow into the dyadic space through L-type Ca<sup>2+</sup> channel,<sup>532</sup> while in skeletal muscle, RyR<sub>1</sub> could be activated even without Ca<sup>2+</sup> flow by conformational changes in the L-type Ca<sup>2+</sup> channel when opens.<sup>533, 534</sup>

Steady-state single RyR channel activity is a bell-shaped curve depending on the cytosolic [Ca<sup>2+</sup>].<sup>512, 535-539</sup> The RyR channel is activated by low [Ca<sup>2+</sup>] (1-10 μM) and inhibited by high [Ca<sup>2+</sup>] (1-10 mM).<sup>512</sup> Studies found out RyR<sub>2/3</sub> have some marked differences from RyR<sub>1</sub>. RyR<sub>1</sub> cannot be fully activated by Ca<sup>2+</sup> along, but RyR<sub>2/3</sub> can achieve almost-full/full activation by Ca<sup>2+</sup> along at 100 μM. Furthermore, RyR<sub>2/3</sub> is less sensitive to Ca<sup>2+</sup> inhibition by high [Ca<sup>2+</sup>]. A higher [Ca<sup>2+</sup>] (range from 2 to > 10 mM) is required for half-maximal inhibition for RyR<sub>2/3</sub> (because of the low-affinity of inhibition sites, I1-sites, see below), while 1 mM Ca<sup>2+</sup> is enough to achieve entire inhibition for RyR<sub>1</sub>. The physiological role of this very high Ca<sup>2+</sup> inhibition for RyR<sub>2</sub> is not yet clear, as such high cytosolic [Ca<sup>2+</sup>] is difficult to reach in cells. It is also reported that all RyR<sub>1</sub> don't respond in the same way (functional heterogeneity) with respect to Ca<sup>2+</sup> regulation. But RyR<sub>2/3</sub> responds much more homogeneously, which maybe due to their difference in the redox state.<sup>331, 512</sup>

For RyR<sub>2</sub> channel, both activation and inactivation are rapid, while activation rate is also dependent on [Ca<sup>2+</sup>] but the inactivation is not.<sup>540-542</sup> The rapid activation and inactivation kinetics allow RyRs to respond to physiological calcium signals that last only a few milliseconds.<sup>332</sup> The rapid response and biphasic behavior of RyR<sub>2</sub> reveal that RyR may have several Ca<sup>2+</sup> binding sites.

It has been proposed that there are four  $\text{Ca}^{2+}$  binding sites for  $\text{RyR}_2$ , while three are in cytosol and one in lumen (Figure 21).<sup>543, 544</sup> The three cytosolic sites are: a high-affinity activation site (A-site, 1  $\mu\text{M}$  affinity), a low-affinity inhibition site (I1-site, 10 mM) and a high-affinity inactivation site (I2-site, 1.2  $\mu\text{M}$  affinity).<sup>543</sup> Binding of  $\text{Ca}^{2+}$  at the A-site has a strong positively conformational effect.<sup>545</sup> At diastolic calcium concentrations, almost full of the A-sites are occupied by competitive  $\text{Mg}^{2+}$ .<sup>332, 545</sup> It is generally recognized that the cytosolic  $\text{Ca}^{2+}$  induced activation and inactivation is mediated by A-sites and I1 sites.<sup>543</sup> Concomitantly, because of the high  $[\text{Ca}^{2+}]$  required for I1-sites, the  $[\text{Ca}^{2+}]$  required for  $\text{RyR}_2$  inhibition is very high, even higher than physiological cytosolic  $[\text{Ca}^{2+}]$ . The A site properties are strongly affected by ATP and caffeine, which do not trigger channel open on their own but enhance  $\text{RyR}_2$  response to cytosolic  $\text{Ca}^{2+}$ .<sup>543</sup> Unlike A site, the divalent cation affinity of I1-site is unaffected by ATP or caffeine. I2-site is identified more recently, which causes brief (1 ms) channel closures.<sup>546</sup> The precise locations for these binding sites are still unknown.<sup>544</sup>

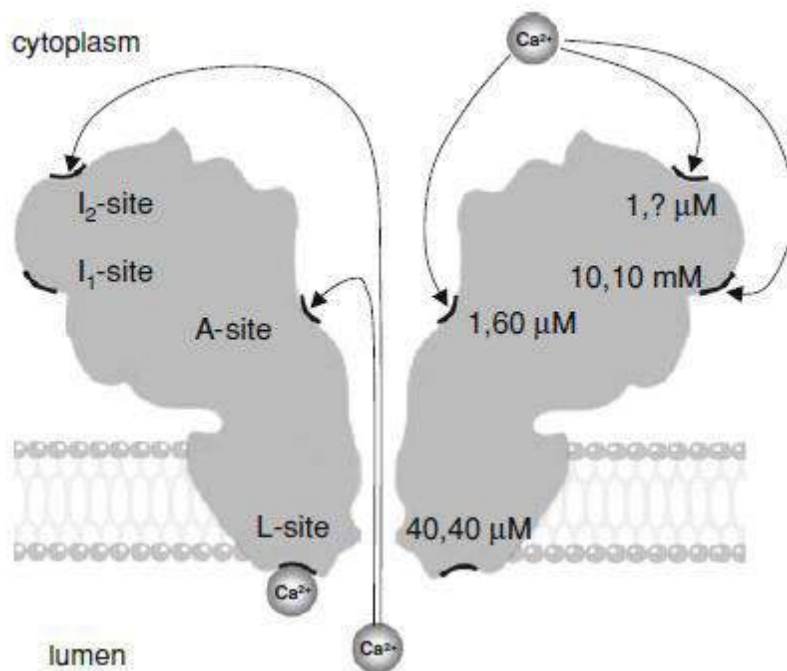


Figure 21  $\text{Ca}^{2+}/\text{Mg}^{2+}$  regulatory sites on the  $\text{RyR}_2$ . The hypothetical locations of four  $\text{Ca}^{2+}/\text{Mg}^{2+}$  sites of  $\text{RyR}_2$  are shown. The names given to these sites are indicated on the left and the corresponding  $\text{Ca}^{2+}/\text{Mg}^{2+}$  affinities of the sites are shown on the right (the  $\text{Mg}^{2+}$  affinity of the I2-site is unknown (?)). The arrows indicate the ability of  $\text{Ca}^{2+}$  on the luminal and cytosolic sides of the membrane to access  $\text{Ca}^{2+}$  sites on the cytosolic domains of the channel (Adapted from Laver, 2009<sup>544</sup>)

A more recently study indicates that a cytosolic  $\text{Ca}^{2+}$  binding site of  $\text{RyR}_1$  is located on the EF-hand pair (Figure 17).<sup>500</sup> It is adjacent to the S2-S3 insertion from a neighboring subunit the C-terminal domain (CTD) of the originating subunit, suggesting a mechanism for  $\text{Ca}^{2+}$  mediated gating. Thereby,  $\text{Ca}^{2+}$ -dependent changes in the conformation of the  $\text{Ca}^{2+}$  binding domain are



transmitted to the pore via contacts with the S2-S3 loop and/or the CTD, inducing a conformational change that alters the cytosolic aperture of the channel.<sup>500</sup>

Diastolic free  $[Ca^{2+}]$  is ~100 nM in the cytosol, and can be changed in pathological conditions, which also change RyR channel activity.<sup>515</sup>

#### 1.4.2.8.2 Luminal calcium

Single RyR<sub>2</sub> channel studies have confirmed the existence of luminal  $Ca^{2+}$  regulation. The luminal  $Ca^{2+}$  could affect RyR<sub>2</sub> activity by binding to the cytosolic  $Ca^{2+}$  binding sites (Figure 21).<sup>543, 544, 547, 548</sup> At low cytosolic  $[Ca^{2+}]$ , when RyR<sub>2</sub> activity is low, the presence of luminal  $Ca^{2+}$  could increase RyR<sub>2</sub> activity by passing through the open channel and binding to the A-site.<sup>547</sup> Cytosolic  $Ca^{2+}$  inactivation site (I2-site) is also involved, which cause brief channel closures.

Luminal  $Ca^{2+}$  also affects RyR<sub>2</sub> activity by binding to luminal binding site, which may be located either on the luminal activation site (L-site, 60  $\mu$ M affinity) or/and on an associated protein (Figure 21).<sup>332, 543, 544, 548</sup> Some studies show that binding of  $Ca^{2+}$  to the L-site triggers brief openings, albeit much weaker than A-site, which produces a 30-fold prolongation of opening.<sup>543</sup> Once the pore is open, luminal  $Ca^{2+}$  again accesses to the A-site and to the I2-site.<sup>543</sup> The negatively charged residues make the L-site possible, while the concomitant  $Ca^{2+}$  binding could alter the channel conformation and increase its open probability.<sup>500, 549</sup> Another possibility is that luminal  $Ca^{2+}$  modulate RyR<sub>2</sub> via associated protein, such as calsequestrin, triadin and junctin.<sup>550-552</sup>

$[Ca^{2+}]$  changes in the SR lumen in the pathological condition (diastolic free  $[Ca^{2+}]_i$  ~1 mM in physiological condition) could also influence RyR channel activity.<sup>516</sup>

#### 1.4.2.8.3 Magnesium

$Mg^{2+}$  is a potent RyR channel inhibitor.<sup>331, 553</sup> The cytosolic free  $[Mg^{2+}]$  in cardiomyocytes is ~1mM.<sup>546, 554</sup> The effect of  $Mg^{2+}$  on RyR<sub>2</sub> is less than RyR<sub>1</sub>.<sup>332, 555</sup>  $Mg^{2+}$  inhibits RyR<sub>2</sub> by competitively binding at the A-site and L-site, but  $Mg^{2+}$  fails to open the channel (Figure 21).<sup>556</sup>

$Mg^{2+}$  competitively binds to A-site (60  $\mu$ M affinity), but unlike  $Ca^{2+}$ ,  $Mg^{2+}$  causes a weak negatively conformational effect and closure of RyR<sub>2</sub> (Figure 21).<sup>544, 545</sup> At diastolic  $Ca^{2+}$  concentrations, the cytosolic activation sites are almost fully occupied by  $Mg^{2+}$ .<sup>545</sup> Since  $Mg^{2+}$  dissociation from this site is relatively slow, it limits the response rate of RyR<sub>2</sub> to  $Ca^{2+}$  elevations, which might have an important role in the physiological regulation of RyR<sub>2</sub>.<sup>331, 545, 557</sup>

$Mg^{2+}$  inhibits the luminal effect of  $Ca^{2+}$  at RyR<sub>2</sub> also by competing with it at the luminal activation site.<sup>544</sup>  $Mg^{2+}$  has the same affinity (40  $\mu$ M) as  $Ca^{2+}$  at the L-site, but its binding does not cause channel opening.<sup>544, 556</sup>

I1-site of RyR<sub>2</sub> does not identify My<sup>2+</sup> with Ca<sup>2+</sup>, both of them cause channel closure.<sup>544, 558</sup> Its physiological role is not clear. As for cytosolic Ca<sup>2+</sup>, I1-site inhibition of RyR<sub>2</sub> also requires a higher [Mg<sup>2+</sup>] than the physiological intracellular [Mg<sup>2+</sup>].<sup>543</sup> Mg<sup>2+</sup> effect at the I2-site is still unclear.<sup>556</sup>

Luminal and cytosolic Mg<sup>2+</sup> inhibitions are alleviated by increasing luminal [Ca<sup>2+</sup>] or cytosolic [Ca<sup>2+</sup>].<sup>556</sup>

#### 1.4.2.8.4 Adenine nucleotides

Adenine nucleotides ATP, ADP, AMP, cyclic-AMP, adenosine and adenine are RyRs activators, while ATP is the most effective one.<sup>331, 332, 477</sup>

The effect of ATP on RyR<sub>2</sub> is more modest than on RyR<sub>1</sub>.<sup>331, 332, 559</sup> Besides, ATP can trigger RyR<sub>1</sub> in the absence of Ca<sup>2+</sup>, although Ca<sup>2+</sup> is needed to reach the maximal activation.<sup>560, 561</sup> But RyR<sub>2</sub> cannot be activated by ATP only, it only increases the sensitivity of the channel to cytosolic Ca<sup>2+</sup> activation, and concomitantly increases open probability of the channel (EC<sub>50</sub> = ~100 μM).<sup>562-564</sup> Most ATP in the cell exist as Mg·ATP complex, although the activating species seems to be free ATP<sup>2-</sup>.<sup>332, 553</sup>

The other adenine nucleotides also activate RyR channel activity, but are much less effective than ATP.<sup>332</sup> Chan et al. suggested ATP is more effective than other adenine nucleotides because it can convert the greatest amount of binding energy into conformational changes and stabilize the open channel state.<sup>565</sup> ADP is a partial agonist with a lower affinity (EC<sub>50</sub> = ~1 mM).<sup>563</sup> Adenosine and adenine also have low effects, while CTP, GTP, ITP and UTP do not activate the channel at all.<sup>566, 567</sup>

Thereby intracellular adenine nucleotides level changes (e.g., heart failure) affect not only energy source, but also RyR channel activity.<sup>568, 569</sup>

In the extracellular milieu, ATP also plays critical roles as neurotransmitter, such as inhibitory neurotransmitter released from enteric nerves and cotransmitter coreleased from postganglionic sympathetic or parasympathetic nerves.<sup>570</sup> Both ATP and adenosine could activate sarcolemmal adenosine A<sub>1</sub> receptor in rat right atria, and cause cardiac arrest.<sup>571</sup>

#### 1.4.2.8.5 Phosphorylation status

RyR contains several conserved phosphorylation/dephosphorylation sites, which can be phosphorylated by serine/threonine protein kinases (e.g. cAMP-dependent protein kinase, PKA; Ca<sup>2+</sup>/calmodulin-dependent protein kinase II, CaMKII; cGMP-dependent protein kinase, PKG; etc) or dephosphorylated by protein phosphatases 1 (PP1) and 2A (PP2A).<sup>331, 332, 572, 573</sup>

The first discovered RyR<sub>2</sub> phosphorylation site was S2808 (S2843 on RyR<sub>1</sub>) in human and rodents (S2809 in rabbit).<sup>409, 573</sup> It is phosphorylated by CaMKII, while later studies shown that PKA and PKG also phosphorylate this site.<sup>574, 575</sup> The second CaMKII phosphorylation site, S2814 (S2815 in rabbit), was found later only for RyR<sub>2</sub>. Addition to S2808, S2030 (S2031 in rabbit) is recently identified as a second and specific PKA phosphorylation site on RyR<sub>2</sub>.<sup>576, 577</sup>

Contradictory results have been reported for the effect of RyR<sub>2</sub> S2808 site phosphorylation. It has been reported that in heart failure patients, S2808 is hyperphosphorylated and in turn enhanced the activity of RyR<sub>2</sub> channel.<sup>296, 573, 575, 578</sup> But the fact that S2808 is already substantially phosphorylated (~50-75%) in normal hearts raising the doubts of the effect of S2808 phosphorylation.<sup>573, 574, 576, 578, 579</sup> Indeed, some studies reveal that mice with genetic ablation of the S2808 phosphorylation site (RyR<sub>2</sub>-S2808A) have normal  $\beta$ -adrenergic response, have unchanged cardiomyocyte function, and lack of protection against heart failure.<sup>580-582</sup> Nevertheless, it has been also suggested that S2808 phosphorylation lead to dissociation of FKBP 12.6, which concomitantly destabilized the closed state of the channel and increased RyR<sub>2</sub> Ca<sup>2+</sup> release.<sup>296, 297, 577</sup> However, the other studies found no effect of RyR<sub>2</sub> phosphorylation in its affinity to FKBP12.6, and some studies even reported FKBP12.6 does not affect RyR<sub>2</sub> activity at all.<sup>403, 583-587</sup>

Unlike S2808, S2814 is barely phosphorylated in quiescent cardiomyocytes.<sup>573</sup> To investigate the contribution of S2814 to inotropic effects induced by  $\beta$ -adrenergic stimulation, mice with genetic ablation (S2814A) or constitutively activation (S2814D) are tested. RyR<sub>2</sub>-S2814A mice were protected from pacing-induced tachyarrhythmias after TAC (transverse aortic constriction) surgery.<sup>423</sup> Consist with that, Respress et al. also reported that S2814A mice are protected from heart failure following TAC surgery, although the protective effects are not observed from MI- (myocardial infarction) induced heart failure.<sup>588</sup> Several researches indicated the protective role of inhibition of S2814 phosphorylation with this same mouse line, which averts the functional and structural damage to the heart induced by heart failure, atrial fibrillation, and other insults.<sup>420, 572, 589, 590</sup> Further more, RyR<sub>2</sub>-S2814D increased RyR<sub>2</sub> channel open probability, while RyR<sub>2</sub>-S2814D mice develop sustained ventricular tachycardia and sudden cardiac death upon catecholaminergic provocation by caffeine/epinephrine or programmed electrical stimulation.<sup>423</sup> However, it is also notable that 2814D mice still have structurally and functionally normal hearts without arrhythmias.<sup>423</sup>

S2030 is highly conserved PKA phosphorylation site in RyR<sub>2</sub>.<sup>576</sup> Xiao et al. reported that the phosphorylation of Ser-2030 responded to isoproterenol stimulation in rat cardiac myocytes in a concentration- and time dependent manner, but not in unstimulated cells.<sup>575, 576</sup> In addition, the extent of the increase in S2030 phosphorylation after isoproterenol stimulation was much more than that for S2808 in both normal and failing hearts.<sup>576</sup> Isoproterenol induced phosphorylation of



S2030, not of S2808, is markedly inhibited by PKI, which is a specific inhibitor of PKA.<sup>575</sup> In summary, it is likely that S2030 is the major PKA activation site responding to acute  $\beta$ -adrenergic stimulation in both normal and failing hearts, but nearly unphosphorylated in normal or failing hearts.<sup>573, 575, 576, 591</sup>

S2811 is another serine residue between S2808 and S2814, and proposed to be phosphorylated by both PKA and CaMKII *in vitro*, but its contribution is still unclear.<sup>403, 572</sup>

In spite of RyRs, CaMKII and PKA can also phosphorylate other proteins (such as L-type  $\text{Ca}^{2+}$  channel, phospholamban, etc) and thus influence RyR  $\text{Ca}^{2+}$  release.<sup>592-594</sup>

In SAN, Wu et al. used the mice with RyR<sub>2</sub> knock-in mutation that replaced CaMKII target site (S2814) or PKA target site (S2808) with alanine and disabled the phosphorylation at these sites.<sup>261</sup> They found that unique S2814A or S2808A mutation failed to affect spontaneous firing rate and isoproterenol response *in vivo* and in SAN cells.<sup>261</sup> However, multiple target sites were not investigated, as both CaMKII and PKA have multiple phosphorylation sites, which could explain the unchanged responses. PKA and CaMKII could also regulate SAN activity via interactions with numerous  $\text{Ca}^{2+}$  handling proteins or other pacemaking-related proteins.<sup>83, 327, 365, 414</sup> More information about CaMKII phosphorylation on RyR<sub>2</sub> and other proteins are given in point 1.2.3.3.

### **1.4.3 RyR accessory proteins**

RyRs interact with endogenous proteins which together ensure RyRs to sense the environment changes and properly regulate  $\text{Ca}^{2+}$  release, such as FKBP (FK506-binding proteins), calmodulin (CaM), and calsequestrin (CASQ). In this session, we will briefly review the accessory proteins.

#### **1.4.3.1 FK506-binding proteins (FKBP)**

FKBP (FK506-binding proteins) is named according to their molecular mass, FKBP12 and 12.6.<sup>477</sup> It belongs to the immunophilins, which are a family of highly conserved proteins that bind immunosuppressive drugs such as FK506 and rapamycin.<sup>331, 332</sup> FKBP12 and FKBP12.6 are 108 amino-acid proteins that share approximately 85% sequence homology. Both FKBP isoforms physically interact with RyR<sub>1</sub> and RyR<sub>2</sub>, but have different expression levels and binding affinities in different tissues.<sup>477, 595, 596</sup> RyR<sub>1</sub> has similar affinities with both FKBP12.6 and FKBP12, but the much higher tissue expression level of FKBP12 makes it the predominant isoform bounding to RyR<sub>1</sub>. However, FKBP12.6 is the predominant isoform for RyR<sub>2</sub> in cardiac tissue because of the higher binding affinity, in spite of the higher expression level of FKBP12 than FKBP12.6.<sup>587, 595</sup>

Each RyR tetramer contains four FKBP binding sites, one for each subunit (Figure 14).<sup>332</sup> The binding site is localized on the amino-terminus (residues 307–1855) or the carboxyl-terminus (residues 3788–4967).<sup>331, 597, 598</sup>

Some studies reported that the interaction of FKBP with RyR stabilizes the closed state of the channel. Removal of FKBP12.6, by application of FK506 or rapamycin or by genetic FKBP12/12.6 deficiency in mice, leads to greater open probability of the RyR<sub>2</sub> and longer open duration.<sup>599-601</sup> Li et al. demonstrated that FKBP12.6 null mice exhibit spontaneous atrial tachyarrhythmia.<sup>602</sup> Our team overexpressed FKBP12.6 in rat cardiac myocytes and found decreased spontaneous Ca<sup>2+</sup> sparks but increased [Ca<sup>2+</sup>]<sub>i</sub> transients, in relation with enhanced SR Ca<sup>2+</sup> load, therefore improving excitation-contraction coupling.<sup>603</sup> Conditional FKBP12.6 overexpression mouse model further indicated that increased FKBP12.6 binding to RyR<sub>2</sub> prevent triggered VT in normal hearts in stress conditions, probably by reducing diastolic SR Ca<sup>2+</sup> leak.<sup>604</sup> However, some studies found that removal or addition of FKBP12.6 does not alter RyR<sub>2</sub> channel behavior or only has modest effects.<sup>585, 587, 600, 605</sup> FKBP12 was also reported to play a critical role in mammalian cardiac development and heart rhythm via trans-sarcolemmal ionic currents (predominately I<sub>Na</sub>) regulation.<sup>599, 606</sup>

#### 1.4.3.2 Calmodulin (CaM)

As mentioned in session 1.2.4, CaM is an intracellular Ca<sup>2+</sup> sensor in eukaryotic cells. It interacts with a vast number of proteins, including RyR<sub>2</sub>, and plays a critical role in numerous intracellular processes.

CaM binds all three mammalian RyRs in both Ca<sup>2+</sup>-free (apoCaM) and Ca<sup>2+</sup>-bound (CaCaM) states, although the effects are different.<sup>539, 607-609</sup> Apo-CaM (at nanomolar Ca<sup>2+</sup> concentration) is an agonist of RyR<sub>1</sub> and RyR<sub>3</sub>, but has no effect on RyR<sub>2</sub>.<sup>539, 609, 610</sup> However, CaCaM (at micromolar Ca<sup>2+</sup> concentration) inhibits all RyR isoforms. Each RyR subunit contains one CaM binding site (four per tetramer, amino acids 3583–3603 in RyR<sub>2</sub>, Figure 14), which are conserved in all RyR isoforms.<sup>331, 611</sup>

In cardiac muscle, CaM negatively shifts the Ca<sup>2+</sup>-dependent RyR<sub>2</sub> activity curve while a higher Ca<sup>2+</sup> concentration is needed to maintain the same RyR<sub>2</sub> activity, and therefore decreases the RyR<sub>2</sub> opening probability.<sup>477, 607</sup> It is also reported that Calmodulin mutations can cause severe cardiac disease, such as CPVT, sudden cardiac death, etc.<sup>447</sup> For instance, heterozygous CaM mutations (N53I, N97S) are linked to CPVT.<sup>447</sup> Further investigation found that these two mutations confer opposite changes on CaM N- and C-lobes.<sup>612</sup> CaM mutation F90L is related to idiopathic ventricular fibrillation manifested in childhood and adolescence.<sup>613</sup> Søndergaard et al. expressed CaM mutations (N53I, D95V, D129G, N97S) in HEK293 cells, and found that mutations increased RyR<sub>2</sub> sensitivity to SR Ca<sup>2+</sup> content and thus increased Ca<sup>2+</sup> release.<sup>614</sup> Thereby, they proposed that aberrant regulation of RyR<sub>2</sub> is a mechanism underlying CPVT and LQTS (long QT syndrome) caused by CaM mutations. On the other hand, mutations on RyR<sub>2</sub> are associated with interaction of

CaM. Fukuda et al. demonstrated that ventricular myocytes from knock-in mice with RyR<sub>2</sub> mutation (R2474) exhibit increased spontaneous Ca<sup>2+</sup> leak, delayed after depolarization, triggered activity, and Ca<sup>2+</sup> spark frequency, which can be explained by the decreased affinity of CaM binding and could be corrected by increased CaM binding affinity.<sup>615</sup>

CaM could also impact RyR<sub>2</sub> activity by acting on other proteins including the L-type Ca<sup>2+</sup> channel. When bound to Ca<sup>2+</sup>, it activates both CaMKII and calcineurin (Cn), a CaM-activated protein phosphatase, etc.<sup>331, 616</sup>

In SAN, CaM influences SAN automaticity via direct and/or indirect interaction with numerous proteins (LTCC, RyR<sub>2</sub>, I<sub>f</sub>, etc) involved in pacemaking in both Ca<sup>2+</sup> clock and membrane clock.

### 1.4.3.3 Calsequestrin (CASQ)

Calsequestrin (CASQ) is the major Ca<sup>2+</sup> binding protein in the SR with a molecular mass of ~40kDa.<sup>331, 617</sup> It is a low-affinity and high-capacity Ca<sup>2+</sup> buffering protein (~ 40 Ca<sup>2+</sup> per protein).<sup>331, 618</sup> It maintains the free [Ca<sup>2+</sup>] in SR at ~1mM while the total [Ca<sup>2+</sup>] could reach up to 20mM.<sup>617</sup> CASQ is rich in negative residues (~30%), most of which are involved in Ca<sup>2+</sup> binding, while Ca<sup>2+</sup> binding also induces CASQ conformational changes: it polymerises when Ca<sup>2+</sup> concentrations approach 1mM.<sup>617, 618</sup> These conformational changes concomitantly resulted in the high Ca<sup>2+</sup> binding capacity, as the condensed CASQ has a higher Ca<sup>2+</sup> binding capacity, at least twice the CASQ monomer.<sup>618</sup>

In addition to Ca<sup>2+</sup> buffering effect, it also modulates the activity of RyR channel in a Ca<sup>2+</sup> dependent manner. It has been reported that CASQ polymer can be anchored to RyR either by binding directly to the RyR or via triadin and junctin, which are two RyR anchoring proteins embedded in the SR membrane.<sup>332, 617</sup> The interactions between CASQ, junctin, triadin, and RyR are important for Ca<sup>2+</sup> release from the SR, contraction and Ca<sup>2+</sup> homeostasis.<sup>617</sup>

There are two CASQ isoforms (CASQ1 and CASQ2), sharing 86% identity homology and exhibiting tissue-specific expression patterns.<sup>331</sup> CASQ1 expresses in skeletal muscle, while CASQ2 expresses in cardiac and at low level also in slow-twitch skeletal muscle.<sup>477</sup> Functionally, CASQ1 reduces RyR<sub>1</sub> activity, but CASQ2 increase RyR<sub>1</sub> and RyR<sub>2</sub> open probability.<sup>619</sup>

CASQ2 mutations are associated with autosomal recessive CPVT and accounts for 3-5% of the CPVT patients.<sup>453</sup> Some of the human mutation carriers of a single CASQ2 mutation are healthy, while some patients carry one or two CASQ2 mutation(s) produce severe forms of CPVT.<sup>444, 620</sup>

CASQ2 mutant mouse models have been used to further investigate human CASQ2 mutations.<sup>621-624</sup> CASQ2-null mice display polymorphic ventricular arrhythmias after exercise challenge, and isolated ventricular myocytes exhibit decreased Ca<sup>2+</sup> content and increased SR Ca<sup>2+</sup>

leak.<sup>622</sup> Likewise, human homozygous CASQ2 mutations, which cause a complete absence of CASQ2, also show CPVT.<sup>444</sup> Compensatory responses were also seen in homozygous CASQ2-null mice, like increased SR volume and near absence of CASQ2-binding proteins triadin-1 and junctin,<sup>622</sup> but not seen in heterozygous CASQ2-null mice.<sup>621</sup> It may explain why heterozygous carriers of CASQ2 mutations are either asymptomatic or significantly less symptomatic compared to homozygous patients.<sup>444, 625</sup> Heterozygous CASQ2-null mice only had a modest reduction (~25%) in functional protein, but still resulted in increased arrhythmia risk and more SR Ca<sup>2+</sup> leak with similar SR Ca<sup>2+</sup> load in isolated ventricular myocytes, which also suggest that the CASQ2 acts not only as a buffer but also as a direct regulator of Ca<sup>2+</sup> release process.<sup>621, 626</sup> Other CASQ2 knock-in mutations also lead to either a severe reduction or complete loss of CASQ2 protein.<sup>623, 624</sup>

SAN dysfunction was seen in both CASQ2 mutations induced CPVT patients and CASQ2 null mice.<sup>444, 455, 459</sup> CASQ2-related CPVT patients frequently have sinus dysfunction and inducible atrial tachyarrhythmias, while CASQ2 null mice also exhibit enhanced atrial ectopic activity, SAN conduction abnormalities, and slower heart rhythm during  $\beta$ -adrenergic/cholinergic stimulation.<sup>444, 455, 459</sup>

#### **1.4.4 Clinical characterization of RyR2<sup>R420Q</sup> mutation**

RyR2 mutation R420Q was found from a CPVT family. This CPVT family was noticed after a sudden death, which is the fourth sudden death in this family (Figure 22).<sup>457</sup> The proband (Figure 22, III: 8), a 14-year-old male with previous history of unexplained exertion syncope, suffered a sports-related sudden death with an unremarkable postmortem. The other three relatives had also died suddenly and young. But unfortunately, no autopsy was performed in these three cases.

Then, clinical and genetic evaluations were performed in this family, following a protocol conforming to the Declaration of Helsinki and previously approved by the local research ethics committee. Informed consent was obtained from each individual. The clinical evaluation was first performed in individual III: 10, including electrocardiogram, echocardiography and maximal exercise testing (Bruce protocol). The CPVT phenotype was unmasked during exercise testing. Then the relatives were tested who are offspring of an affected individual. CPVT phenotype was diagnosed in this family (Figure 22), which presents sudden cardiac death, polymorphic ventricular arrhythmias or frequent premature ventricular contractions (> 10/min) during exercise testing. Sinus, atrial, junctional, and ventricular arrhythmia were evaluated in CPVT phenotype carriers in both resting and exercise electrocardiograms. Sinus bradycardia was defined as a heart rate < 60 bpm over 14 years of age or lower than percentile 2 adjusted to age in younger children.

Meanwhile, the genetic evaluation was also running, firstly on individual III: 10. Gene RyR2, and gene KCNJ2 which is also related with polymorphic exercise-induced ventricular arrhythmias,

are considered and analyzed with ABI Prism 3100 sequencer (Applied Biosystems). In RyR2 gene, exons 3, 8, 14, 15, 37, 44-50, 83, 87-105, and adjacent intronic regions (GenBank accession number NM\_001035) are tested. Later, RyR2 mutation (1259 G>A, R420Q) was identified in exon 14 in individual III: 10. No KCNJ2 mutations were found. Then exon 14 was tested in the relatives, and the ones carrying mutation R420Q were uncovered as Figure 22. DNA was obtained from whole blood (relatives) or from paraffin-embedded myocardium (proband).

Eventually, 25 proband relatives were evaluated, and 11 mutation carriers were found including the proband (III: 8). Among these 11 genotype carriers, 10 were CPVT phenotype carriers (including the proband), only one two-year-old girl (IV: 4) was an unknown phenotype.

Notably, a higher incidence of sinus bradycardia was observed in genotype-positive patients when compared with genotype-negative individuals (78% vs. 25%,  $P = 0.030$ ). Atrial and/or junctional tachyarrhythmias were detected in 7/9 genotype carriers, but none of the non-genotype carriers. These results indicate that RyR2<sup>R420Q</sup> mutation may induce sinoatrial node (SAN) dysfunction.

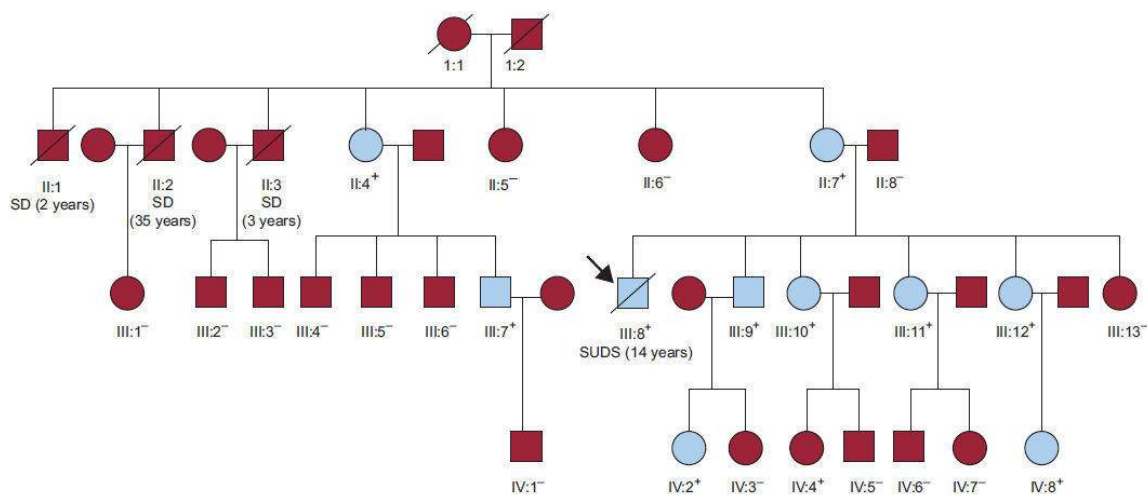


Figure 22 Family pedigree. Square: male. Circle: female. Crossed symbol: deceased individual. Blue symbol: CPVT phenotype carrier (with sudden cardiac death or ventricular effort-related arrhythmias). Plus sign (+): genotype carrier. The arrow points to the proband. Plus and minus signs depict mutation-positive and mutation-negative individuals, respectively. SCD: sudden cardiac death with postmortem without structural heart disease; SD: sudden death, no autopsy. (Adapted from Domingo et al., 2015<sup>457</sup>)

HEK293 cells expressing mutant RyR2<sup>R420Q</sup> showed decreased amplitude of caffeine induced  $Ca^{2+}$  release, and released more  $Ca^{2+}$  at diastolic cytosolic  $Ca^{2+}$  concentration.<sup>457</sup> Additionally, sinus bradycardia, atrial and junctional arrhythmias, and/or post-effort U-waves were also identified, which was the first time that supraventricular arrhythmia and SAN dysfunction were reported in RyR2 N-terminal mutation. Further researches are needed to understand the functional and vivo

contribution, but lack of animal model limits the investigation. Hence, our team generated RyR<sub>2</sub><sup>R420Q</sup> mice model. In this article, we are going to investigate the mechanism of SAN dysfunction of RyR<sub>2</sub><sup>R420Q</sup> mice found in CPVT-related patients.

### **1.5 Objectives**

SAN is the physiological pacemaker in mammalian heart, and is predominantly responsible for spontaneous heart rhythm generation. Ca<sup>2+</sup> release via RyR<sub>2</sub> plays a critical role in maintenance of normal SAN automaticity. That is why SAN dysfunction is commonly observed in RyR<sub>2</sub> mutation induced CPVT patients in respect that mutant RyR<sub>2</sub> is expressed in the entire heart. Our collaborators identified a mutation located in the N-terminus of RyR<sub>2</sub> (R420Q) in a Spanish family with severe CPVT and SAN dysfunction.<sup>457</sup> It is known that N-terminal residue Arg420 (R420) plays an important role in RyR<sub>2</sub> conformation.<sup>462, 520</sup> But the mechanisms about RyR<sub>2</sub> N-terminal mutation related SAN dysfunction is never investigated before. Based of these knowledge and the background presented in the introduction, this thesis seeks to improve the knowledge of the cellular alterations that lead to the SAN dysfunction. In particular, we investigated the mechanism underlying the RyR<sub>2</sub> mutation R420Q contributed SAN dysfunction.

## Chapter 2 Materials and methods

### 2.1 Generation of RyR2 (R420Q) mutation mice (Performed by Institut Clinique de la Souris) and ethics statement

In order to determine the mechanisms involved in this CPVT mutation, we ordered the generation of RyR2<sup>R420Q</sup> KI mice.

Based on C57bl/6 mice line, RyR2<sup>R420Q</sup> mice strain was generated by homologous recombination. It included genetic modification of embryonic stem cells genome, Cre/loxP system, and various strategies. Firstly, targeting vector was constructed. Targeting vector is usually a plasmid or virus, which transfers a specific gene into a target cell and allows the cell to synthesize the protein encoded by the specific gene. For the construction of targeting vector, a genomic sequence containing the mutant exon 14 of RyR2 gene was cloned. Then the genomic region was recombined into a plasmid backbone, flanked by LoxP-NeoR-LoxP cassette (Figure 23 and 24). The NeoR (neomycin resistant gene) is a drug resistant gene used to screen the homologous recombinants, while the LoxP-NeoR-LoxP cassette is a typical floxing and deleting gene-targeting strategy. Secondly, the targeting vectors were electroporated into embryonic stem (ES) cells. After isolation of the drug resistant ES cell clones, the homologous recombinants were further screened by PCR analysis. The homologous recombinant ES clones were then established. After, the homologous recombinant ES cell clones were used to produce the germline-transmitted chimeric mice. The chimeric mice with highest contribution of ES cells were identified, and mated with wild-type mice to produce the heterozygous mice (L2, Figure 24). Finally, after in vivo Cre deletion, the mutant mouse line was established (Figure 24).

As a consequence of gene modification, the DNA sequence in mutant mice was longer than in wild-type. For the primer designed in this article, the PCR detected sequences were 300 bp (wild-type RyR) and 400 bp (knock-in RyR) (see session 2.2.1 for genotyping).

In this thesis, both male and female heterozygous mice were used, and compared to their wild-type littermates (age 4-6 months).

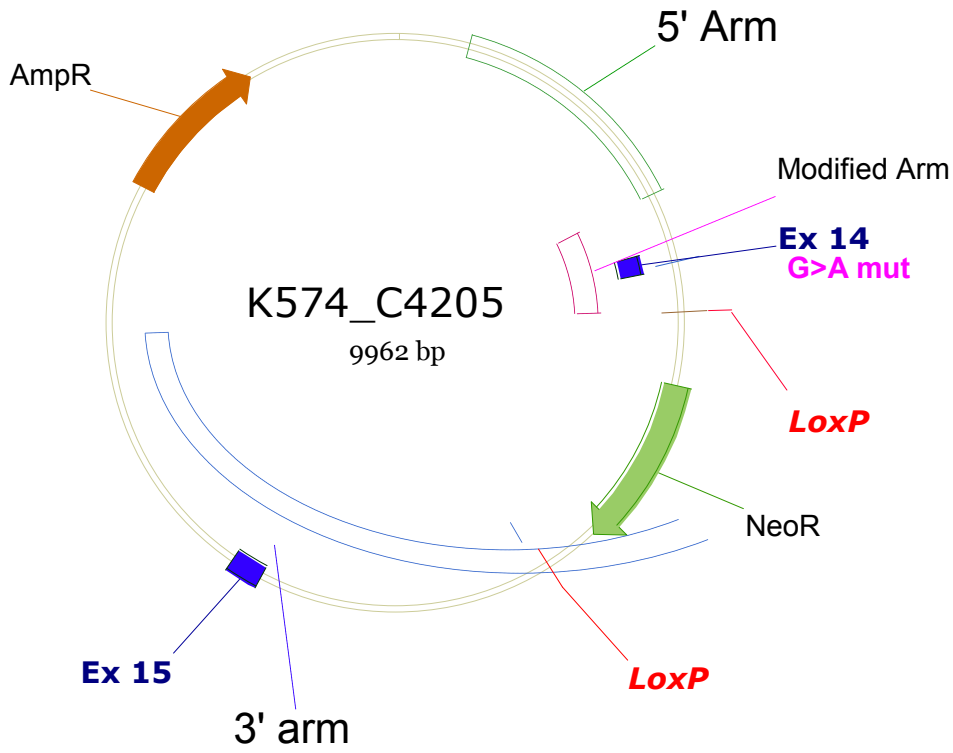


Figure 23 Map of targeting vector plasmid. Ex14: exon 14. Ex15: exon 15. Neomycin resistant gene: NeoR. The mutation is shown in purple.

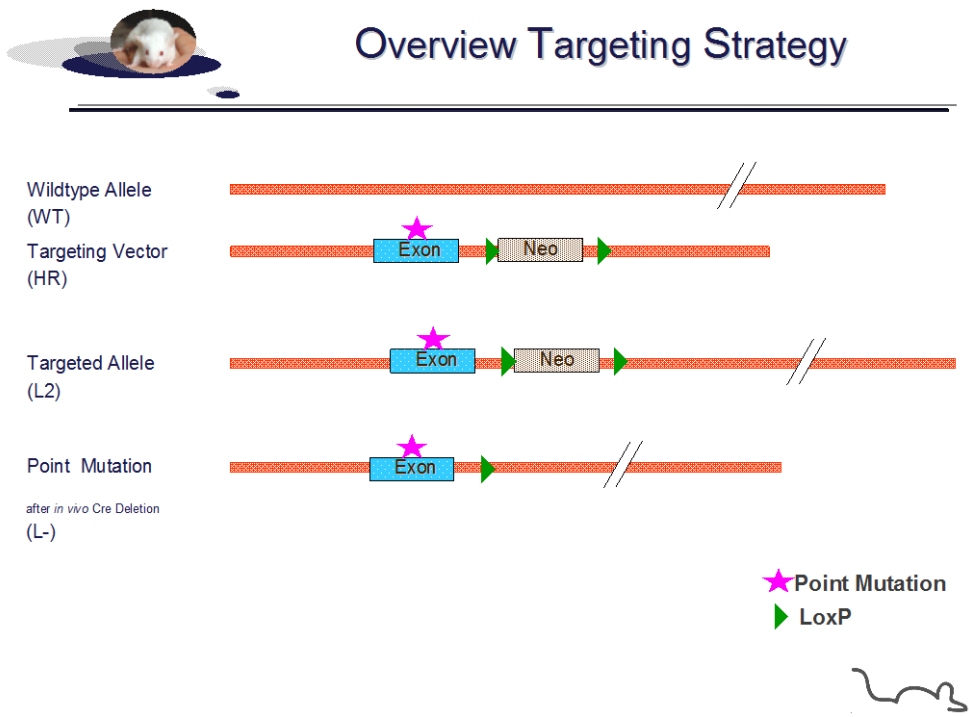


Figure 24 Overview targeting strategy.

**Ethics statement**



All animal experiments are in accordance to the European Community guiding principles, the local ethics committee guide lines, and the French decree in the care and use of animals. Authorizations manipulated according to the decree obtained from the French Ministry of Agriculture, Fisheries and Food.

## **2.2 Genotyping**

The animals were genotyped using tail tips that were collected on weaning. The first step was to extract DNA, and then the specific DNA sequence was replicated by PCR, which was followed by electrophoresis for identification. The principles and specific techniques are explained below.

To extract DNA, we used heating to lyse the tissue, and sodium chloride (NaOH) solution to dissolve DNA. Each tissue sample (about 0.5cm tail tips) was heated at 95°C for 45 min with 300 µl 50 mM NaOH (in water). After, the samples were transferred on ice for 10 min. Then, TRIS HCl (25 µl for each sample, 1M pH 8) was added into it to stop the reaction. The mixtures were centrifuged at 14000 rpm and 4°C for 15 min. Then, DNA was extracted to the supernatant. The DNA samples can be used immediately for PCR or stored at 4°C for later measurements.

To replicate the specific DNA sequence, we used polymerase chain reaction (PCR) technology. It is a technique to produce copies of a specific DNA sequence, i.e. generate a large amount of copies from a small amount of initial sample. PCR is based on thermal cycle, and the fact that DNA can be denatured. The DNA double helix is composed of two linear strands (DNA sequence) stabilized by hydrogen bonds between adenine·guanine (A·T) and thymine·cytosine (G·C) base pairs, which can be disrupted by heating (85-95 °C). This step is named denaturation. At a lower temperature (50-65 °C) the primers, which are short nucleic acid sequences that could precisely recognize the specific DNA sequence, specifically hybridize with the strand. Then a bit higher temperature (75-80 °C) allows DNA polymerase to synthesize a new DNA strand complementary to the DNA template strand along the primers. With more than 20 cycles, the specific DNA sequence is replicated exponentially.

To perform the PCR, each DNA sample (1 µl for each sample) was mixed with PCR buffer (2 µl), Taq polymerase (0.2 µl), dNTPs (0.4 µl), forward primer (0.4 µl), reverse primer (0.4 µl) and H<sub>2</sub>O (15.6 µl). Taq polymerase (Thermo Scientific) was used to synthesize the new DNA strand. Deoxynucleoside triphosphates (dNTPs, Thermo Scientific) were substrates for DNA polymerase to synthesize the new DNA strand. The PCR buffer (contains Tris-HCl, BSA, Tween-20) was used to maintain a suitable chemical environment for optimum activity and stability of the DNA polymerase. The PCR buffer used in this work (DreamTaq Green Buffer, Thermo Scientific) also contains 20mM magnesium ions to optimize the activity of DAN polymerase, and two tracking dyes (a blue dye migrates with 3 to 5 kb DNA fragments and a yellow dye migrates faster than 10

bp DNA fragments in 1% agarose gel) to visually track the DNA during electrophoresis. The two primers were complementary to the 3' end of each strand of the DNA target. The primers are normally 15-30bp, can not be complementary, and each primer can not contain complementary sequences or secondary structure. To avoid unspecific binding, the primers can not share more than 70% homology with unspecific region. In this case, the forward primer was ACGCTTTGCTAGGCTCACAGAATAGAA (Ef, Figure 2.1) and the reverse primer was GATGGCTCAGGGGTTAAGAAGAACATT (Er, Figure 2.1).

PCR consists of 6 steps (initialization step, denaturation step, annealing step, extension step, final elongation and final hold). It begins with an initialization step, followed by a series of 20-40 repeated cycles (including denaturation step, annealing step and extension step), and ends with a final elongation and a final hold step. It repetitively amplifies the specific DNA sequence exponentially. In our case, the cycle was repeated 34 times. The basic steps are explained below:

1) Initialization step. This step is required for activation of DNA polymerase. Normally it is 94-96 °C for 1-9 minutes. The temperature and duration depend on the DNA polymerase used. In our case, the mixtures were heated at 95°C for 240s to activate DNA polymerases.

2) Denaturation step (Figure 25). This is the first step in each cycle. It separates DNA double helix into two DNA strands. The temperature in this step lies in a range of 85-95 °C. It depends on the proportion of G·C base pairs. As each G·C base pair has three hydrogen bonds, it is more stable than an A·T base pair, which has only two hydrogen bonds. As a result, the more G·C base pair the DAN contains, the greater energy it needs to be separated into two strands. When the G·C content increases 1%, the reaction temperature increases ~0.4 °C. In our case, mixtures were heated at 94°C for 40s to melt the DNA.

3) Annealing step (Figure 25). This step decreases the reaction temperature to 50-65 °C, allowing the hybridization of the primer and the DNA strand. The temperature affects the binding. If it's too low, the possibility of unspecific binding is increased. If it's too high, the primer may not bind. In our case, the mixtures were heated at 64°C for 30s to let the primer and the strand hybridize.

4) Extension step (Figure 25). This step allows DNA polymerase to synthesize the new DAN strand according to the DAN template strand, using dNTPs. It is the last step of each cycle. Its reaction temperature is in a range of 75-80 °C, and depends on the DNA polymerase used. In our case, the mixtures were heated at 72°C for 40s to let let polymerase extend the strand.

5) Final elongation. This step is to ensure all the new DNA strands are fully extended, and all the single strands renature to double helix based on complementarity. It is performed at 70-74 °C. In our case, a 420s, 72°C incubation was used.

6) Final hold. This is the last step of PCR, normally at 5-15 °C for an indefinite time. It is seen as a short-term storage. In our case, the reactions were short-term stored at 7°C.

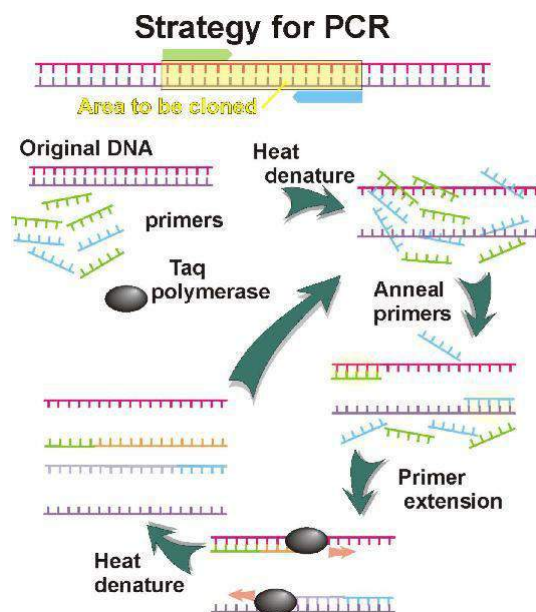


Figure 25 PCR reaction. The cycle of denaturation step, annealing step and extension step is shown. (Adapted from: [www.asst.net/Forensic/DNATestingpdf.pdf](http://www.asst.net/Forensic/DNATestingpdf.pdf) )

After PCR, samples were used immediately for DNA electrophoresis to separate DNA sequences by size. As DNA sequence is formed by nucleotides, and the nucleotide consists of nucleoside and phosphate, this sugar-phosphate backbone determines the negative charge of DNA. With an electric field, DNA migrates toward the anode. The size and charge of DNA sequence determine its mobility. The longer the DNA sequence has the bigger resistance, and the slower it migrates. Therefore the smaller DNA fragments travel faster. The DNA sequences are visualized by fluorescent DNA stain, such as ethidium bromide (EB), GelRed, GelGreen, etc. GelRed and GelGreen belong to a newer generation designed to replace the highly toxic EB. In this work, we used GelRed (Biotium).

Two common types of gel for DNA electrophoresis are agarose (for longer DNA sequence) and polyacrylamide (for shorter DNA sequence) gels. Agarose gel is formed of helical agarose molecules, which are aggregated into a sieving three-dimensional matrix for electrophoresis. It separate molecules based on molecular weight, as small molecules are more easily fit and pass through the pores in the gel. Therefore, smaller molecules pass at faster speed and migrate further than larger molecules. As the pores are too big for protein, it is not suitable for protein electrophoresis, or only for very large proteins. Agarose is conditioned as powder, and is melted in water (or electrophoretic buffer, see next paragraph) at high temperature (>50°C depending on the type of agarose) and then gelled when temperature decreases (<40°C depending on the type of agarose). Different agarose percentages have relatively different size of pores, and are used for

separation of molecules with different sizes. A higher agarose percentage has smaller pore size, hence enhances resolution of smaller bands. Polyacrylamide gel is introduced in session 2.5.

Electrophoretic buffers are used to reduce pH changes induced by the electric field, and provide electrical conductivity. The most common electrophoretic buffers for DNA electrophoresis are TAE and TBE. TAE buffer (Euromedex) was used in this work as running buffer, and also for agarose gel preparation. In agarose gel, TAE buffer allows the DNA run smoothly through the gel by optimizing the pH and ion concentration of the gel. TAE buffer contains Tris base, acetic acid and EDTA, at pH 8.0. The Tris-acetate is used to maintain a consistent pH. The EDTA chelates divalent cations (mainly  $Mg^{2+}$ ), as  $Mg^{2+}$  can activate nucleases for DNA degradation and binds DNA resulting in precipitation. TBE buffer uses boric acid in place of acetic acid. DNA sequences move faster in TBE buffer, but it can be easily exhausted.

In this case, we used 1.5 % agarose (Euromedex) gel with 1× GelRed, and melted with 1× TAE buffer. The mixture was heated up with microwave oven until the solution was transparent (agarose was melted), and then cooled down to around 50°C. Then the mixture was poured into the gel casting apparatus (with combs) kept in flat position, without bubbles. After 10-15 minutes when the gel solidifies, the combs and the end-pieces were removed. The gel was then placed into the electrophoresis bath chamber and submerged in 1× TAE buffer. The PCR samples were loaded into the gel, including at least one 100bp DNA ladder (Thermo Scientific) for the wells on the same plane. The electrophoresis was run at 160V for 1-1:30 hours. In the end, the bands were visualized by UV transmission on a reader. The band at ~300 bp is the wild-type RyR, and at ~400 bp is knock-in RyR. If there are 2 bands, the mouse has both alleles and is heterozygote.

## **2.3 Telemetry**

In order to analyze the basal electrocardiogram (ECG) and arrhythmia we used a telemetry method, which allows us to record ECG in awake animals and avoids the effects of anesthesia.

### **2.3.1 ECG and telemetry**

The electrocardiogram (ECG) is a graphical, accurate and composite record of the electrical activity generated by the heart (see Introduction), recorded through the electrodes on the body surface. ECG is used to depict the electrical function of the heart.

While it is possible to measure ECG in humans in awake conditions, for animal recordings, mostly rodents, it needs anesthesia to immobilize the animal. This may perturb the ECG. Thus we have used a telemetry system, which implant the transmitter (7 ETA-F10) subcutaneously in the animal during surgery. After one week recovery, the ECG can be recorded in awake animals. As it transmits the data to receiving equipment without contact, the data can be continuous monitored in

the cage when mice are placed over the receiver. The telemetry monitoring system normally has 3 electrodes or 5 electrodes, including one electrical ground. Even through the 2 electrodes telemetry like in our case, all the leads still can be positioned by the positive electrode and the negative electrode.

Before the surgery, sterilization of ECG transmitters was needed. The transmitters were soaked by Actril® cold sterilant for a minimum of 5.5 hours at room temperature. They were thoroughly rinsed in sterile saline at least 3 times until no residues left, detected by detector strips provided by Actril manufacturer. The sterile transmitters were then soaked in sterile saline for minimum of 5.5 hours up to 48 hours. If the transmitters will not be reused after 48 hours, it should be air dried at room temperature and stored at dry place. After dry storage, re-sterilization might be necessary.

During the subcutaneous implantation of ECG transmitter, the mouse (4 to 9 month old) was placed in an isoflurane (2.5%) inhalation apparatus for anesthesia induction. Then, the animal was placed on a warm pad fitted with a device to provide a continuous flow of 1.5% isoflurane in 0.5 L/min oxygen for maintenance during surgery.

On the abdomen (Figure 26) or on the dorsum of the mouse, a midline incision was made in the skin to free a subcutaneous pocket for placing the transmitter. The ECG electrodes were positioned as the lead II configuration (Figure 26). The electrode with white sheath was placed on the upper right chest, and the one with red sheath was placed on the left side of the abdomen below the diaphragm. If the transmitter was placed on the abdomen, a blunt scissor was used to detach the skin from the muscle from the incision until the final electrode sites. Then, the electrodes were anchored to the underlying muscle/peritoneal tissue by suture to make a good electrical contact. When the transmitter was placed on the dorsum, two incisions on the position where the electrodes should be placed were cut, and two tunnels from the dorsal incision until each electrode incision were made. And then, the electrodes were pulled through the tunnels and anchored. The incision was closed by suture. During the surgery, tissue was maintained wet by the sterile saline.

Betadine was applied to the wound. Post-operative analgesia was provided in the drinking water (0.5 ml of Ibuprofene syrup for 100 ml of water) for 24 hours.

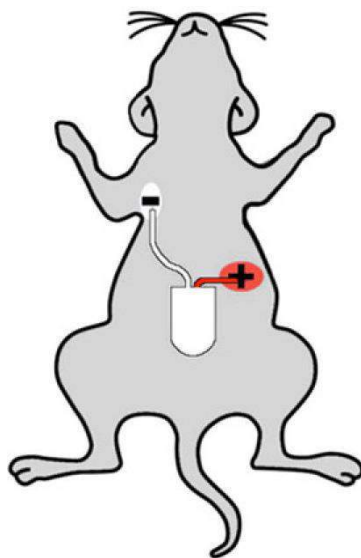


Figure 26 Telemetry implantation on the abdomen of the mouse with proper positive and negative electrode sites. (Adpated from McCauley and Wehrens, 2010)

At least one week after surgery, basal and challenged ECGs were recorded. Basal ECGs were recorded during day and night time. The animals were kept in a cycle of 12 hours light (from 8 to 20h) and 12 hours dark. We analyzed separately day time (rest time for mice, because they are nocturnal) and night time (activity period). The first hour of each light change was discarded.

In order to see if our  $RyR2^{R420Q}$  mice carry the CPVT phenotype, animals were injected with epinephrine (2mg/kg) plus caffeine (120mg/kg), which is the typical CPVT test for mice, as this species is resistant to arrhythmia.<sup>465</sup> ECGs were recorded from 5 minutes after i.p. injection (for letting even body distribution), until at least two hours after injection for full response.

We also analyzed ECG response to sympathetic and parasympathetic stimulation. For sympathetic challenge we injected isoprenaline (ISO, Sigma, 1 mg/kg i.p., in sterilized saline solution, freshly prepared). For parasympathetic challenge, we injected carbachol (CCH, Sigma, 0.25 mg/kg i.p., in sterilized saline solution, freshly prepared), which is a cholinergic receptor agonist, more stable than acetylcholine. Before ISO/CCH injection, a ten to thirty minutes recording was necessary as baseline before ISO/CCH injection. The ECGs were recorded at least two hours after injection for full response.

At the end of the experiments, mice were sacrificed and the ECG transmitters were extracted for reuse. Upon extraction, all possible attached tissue and sutures were gently removed. Then, the transmitters were rinsed with water. Attached tissues rests were dissolved in a 1% (w/v) solution of Terg-A-Zyne® for a minimum of 4 and maximum of 72 hours at room temperature. After thorough rinse, the transmitters were air dried at room temperature and stored in a dry place.

### 2.3.2 ECG analysis

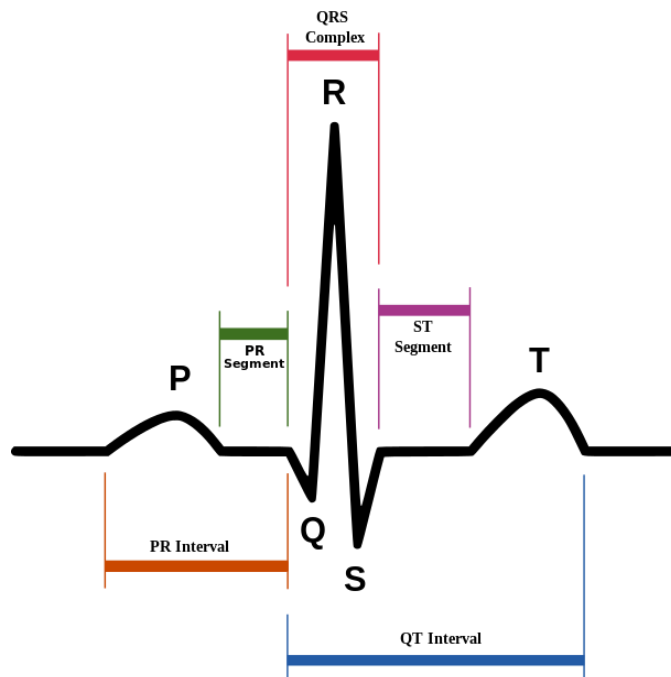


Figure 27 A normal human ECG waveform. The PR interval goes from the beginning of the P wave to the beginning of the QRS complex, while the QT interval is from the beginning of QRS complex until the end of T wave. The PR segment goes from the end of P wave until the beginning of Q wave, and the ST segment is between the end of S wave and the beginning of T wave. (Adapted from <http://en.wikipedia.org/wiki/Electrocardiography>)

The ECG waveform is shown in Figure 27. The electrical activity is initiated from SAN as mentioned previously. It spreads across both right and left atrium, and induces the atria depolarization. This process corresponds to P wave on ECG (Figure 27). Then the impulse goes through the AV node, which corresponds to PR segment, a flat line following the P wave (Figure 27). The PR interval represents the duration from the beginning of atrial depolarization until ventricular depolarization. After that, the impulse travels to His bundle, bundle branches and Purkinje fibers, inducing ventricular depolarization. On the ECG, it is represented by QRS complex (Figure 27). Meanwhile, the atrial repolarization occurs, although it's buried in QRS complex. The Q wave depicts the septum depolarization, from left to right. When the depolarization travels throughout the ventricles, the R wave and S wave show up. Then another flat line, ST segment (Figure 27), indicates no large electrical vector, while ventricle is contracting. The ventricle repolarization represented by T wave (Figure 27). As the epicardial cells repolarize before the endocardial cells, the T wave reflects positively.

For ECG analysis, all the recordings were analyzed firstly with ECGauto (version 3.3.0.5). Heart rate (RR, duration of adjacent R waves), PP (duration of adjacent P waves), PR interval and QT interval (Figure 27) were quantified. The preliminary data was further statistically analyzed by Origin (9.0). QTc (QT interval corrected to heart rate) and heart rate variability (HRV), including SDNN, RMSSD and pNN6, were also evaluated.<sup>627-630</sup> SDNN stands for standard deviation of all consecutive normal R wave intervals.<sup>628-630</sup> RMSSD is the square root of the mean of the sum of the

squares of differences between adjacent normal R wave intervals.<sup>628-630</sup> PNN6 is the percentage of normal consecutive R-R intervals differing by greater than 6 ms (%).<sup>629</sup> QTc, SDNN and RMSSD are shown in the following formulas.

$$QTc = QT / [(RR/100)^{1/2}]$$

$$SDNN = \sqrt{\frac{1}{N-1} \sum_{n=2}^N [I(n) - \bar{I}]^2},$$

$$RMSSD = \sqrt{\frac{1}{N-2} \sum_{n=3}^N [I(n) - I(n-1)]^2}.$$

## 2.4 Ca<sup>2+</sup> handling recording by confocal microscopy

To evaluate Ca<sup>2+</sup> ions dynamics, the SAN tissue was dissected, loaded with fluorescent Ca<sup>2+</sup> dye and recorded by confocal microscope. Their principles and protocols are introduced below.

### 2.4.1 SAN dissection

The mice were anaesthetized by i.p. injection of around 100 mg/kg Na pentobarbital (Ceva Sante Animale) with 50U heparin (Sigma) to avoid blood coagulation. When the mouse lost consciousness and failed to respond to leg pinch, we opened its chest extracted the heart into oxygenated Tyrode solution (Table 2). Tyrode solution is widely used as a physiological bathing medium to reproduce the extracellular environment in vivo. It mimics the ionic composition and pH of blood. Its composition is shown in the following table, and the pH is buffered with Hepes. For SAN dissection, heparin (50 U/ml) was also added into tyrode solution as anticoagulant.

Table 2 Tyrode solution.

| Product                              | Concentration (mM) |
|--------------------------------------|--------------------|
| NaCl                                 | 140                |
| KCl                                  | 5.4                |
| CaCl <sub>2</sub> ·2H <sub>2</sub> O | 1.8                |
| MgCl <sub>2</sub> ·6H <sub>2</sub> O | 1                  |
| Hepes                                | 5                  |
| D-glucose                            | 5.5                |
| pH                                   | 7.4 with NaOH      |



The heart was fixed onto a homemade silicon dish in posterior position under binocular lenses. Ventricles were discarded and the right atrium was fixed, and SAN was exposed between superior vena cava and inferior vena cava. Then the tissue was moved and fixed to the bottom of the homemade dish for confocal microscope recording as shown in Figure 28. It was irrigated with 37°C tyrode solution during all the procedures.

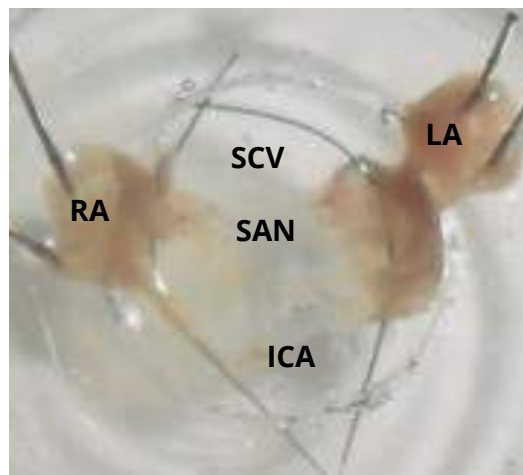


Figure 28 Photograph of typical preparation and SAN location on a homemade dish. SAN, sinoatrial node; SCV, superior vena cava; RA, right atrium; ICA, inferior vena cava; LA, left atrium.

#### 2.4.2 $\text{Ca}^{2+}$ handling recording by confocal microscopy

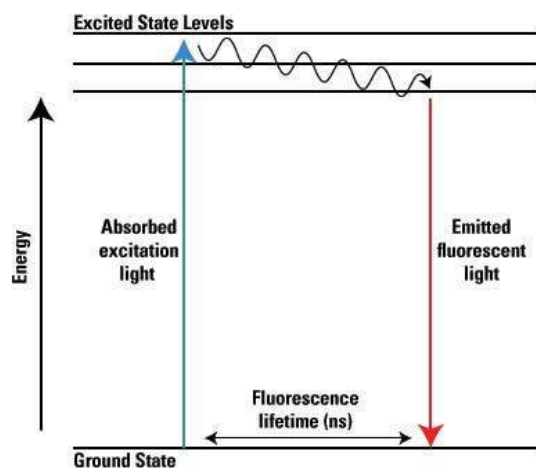


Figure 29 Jablonski energy diagram of fluorescence. (Adapted from <https://www.thermofisher.com>)

To visualize the  $\text{Ca}^{2+}$  dynamics in SAN cells, the SAN was loaded with fluorescence  $\text{Ca}^{2+}$  dye Fluo-4. Fluorescence is the emission of light produced by some molecules which have the property to absorb energy and emit energy in the form of photons. During the excitation, the electron of the molecule goes into an excited electronic state (Figure 29). It firstly dissipates a bit of energy due to molecular vibrations, and then loses the remaining energy and returns to the ground state by emitting light (fluorescence, Figure 29). Thereby the emitted light has lower energy than the

absorbed energy, and concomitantly longer wavelength. Thus, the emitted fluorescence can be distinguished from the excitation light. The excitation and emission of molecule is cyclical, which means it can be excited repeatedly until irreversibly damaged.

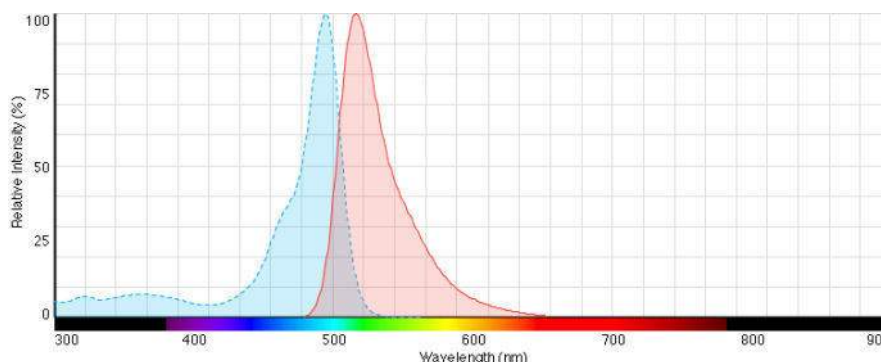


Figure 30 Fluorescent excitation (blue) and emission (red) spectra of Fluo-4. (Adapted from <https://www.thermofisher.com/order/catalog/product/F14201> )

Fluo-4 AM is a calcium indicator used to analyze the spatial dynamics of  $\text{Ca}^{2+}$  ions. It displays high sensitivity to  $\text{Ca}^{2+}$  and large fluorescence increase upon excitation (Figure 30). Fluo-4 is excited at peak 488 nm (Figure 30), and the fluorescence is emitted between 500 and 650nm. The Fluo-4 AM (acetomethyl ester) is a cell permeable form. The AM ester helps the Fluo-4 pass through the lipid membrane and enter the cell. Once inside the cell, esterases in the cytosol cleave the AM residue and release the active Fluo-4. Fluo-4 is only fluorescence when bound to  $\text{Ca}^{2+}$ .

In this work, we dissolved Fluo-4 AM in DMSO with 20% Pluronic acid.<sup>458</sup> Pluronic acid was used to prevent aggregation of Fluo-4 AM and help uptake by the cell. Fluo-4 AM was loaded to the fixed SAN tissue at concentration of 30 $\mu\text{M}$  (diluted by Tyrode solution) for 1h at 37°C on a shaking device. After Fluo-4 AM incubation, the SAN tissue was loaded with Tyrode solution contained Blebbistatin (2.5 $\mu\text{M}$  or 5 $\mu\text{M}$ , Sigma) or cytochalasin D (50 $\mu\text{M}$ ) at least 10 mins before recording to avoid contraction artifacts. Blebbistatin (2.5 $\mu\text{M}$  or 5 $\mu\text{M}$ ) or cytochalasin D (50 $\mu\text{M}$ ) were used to inhibit contraction by inhibition of myosin and actin, respectively.

To evaluate  $\text{Ca}^{2+}$  dynamics in SAN cells, the SAN tissue was detected under confocal microscopy after Fluo-4 AM loading. Confocal microscopy is one of the fluorescence microscopies with a pinhole to eliminate out-of-focus light away from the focal plane, which provides possibility for high-quality images recording of fixed or living cells and tissues.

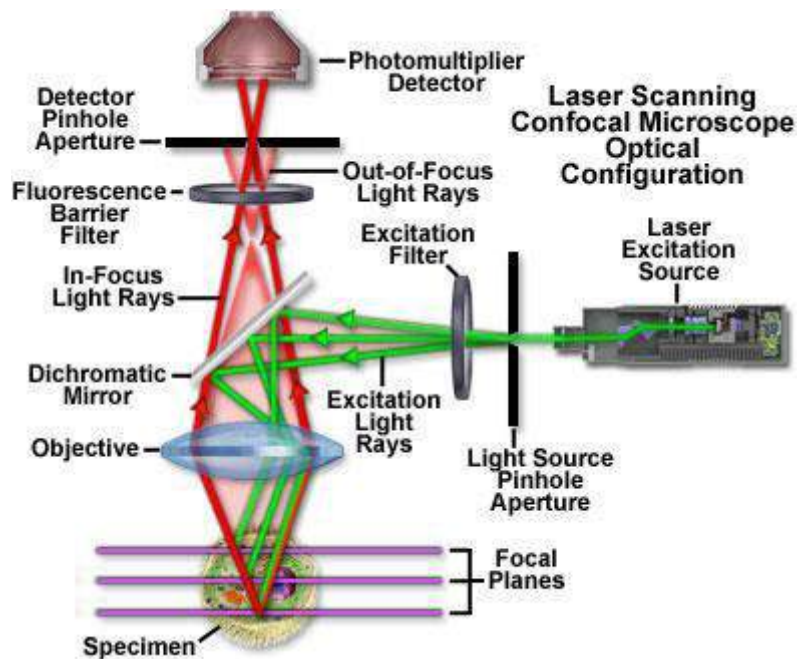


Figure 31 The diagram of a confocal microscopy. (Adapted from <http://www.olympusconfocal.com/theory/> )

A confocal microscope contains laser for excitation source, the beam splitter, the detector pinhole with variable aperture, and the detector (Figure 31). The laser emitted by the laser excitation source passes through the excitation filter, and it is reflected by the beam splitter mirror with a scanning head to scan across the specimen. It directs to a point of fluorophore-labeled specimen, and scans across the specimen in a defined focal plane. The labeled specimen then emits fluorescence, which passes back through the beam splitter mirror and toward the pinhole aperture (termed detector pinhole aperture in Figure 31). The mirror is chosen to match the spectral excitation and emission characteristics of the fluorophore. The pinhole aperture is positioned in front of the detector to select the emitted fluorescence from the focal plane of the specimen, and excludes lights emitted from the above and below planes (termed out-of-focus light rays, Figure 31). Thus the emitted fluorescence becomes confocal through this pinhole aperture, and then detected by the detector. Only a small fraction of the out-of-focus fluorescence emission is delivered through the pinhole aperture, most of this extraneous light is not detected and does not contribute to the resulting image. The confocal microscope equipped with a resonant scanning mirror can generate the necessary speed of 8000 Hz for ultrafast time imaging.

In this work, SAN cells were recorded under a resonant scanning confocal microscope (Leica SP5) equipped a white laser that we tuned to 500 nm, and from different regions of the SAN as basal condition. To visualize the response of each compound, SAN perfused with the compound (such as ISO 20nM, CCH 500nM, etc) for around 10 min. Then the same SAN cells recorded in the basal condition were recorded again. Both line-scan images and 2D images are captured, at a

scanning speed of 8000 Hz. In order to get better signal to noise, 2 line average were used, thus the final speed was 0.25 ms per line. A small window of only one cell was used in the 2 D images to optimize the time between 2 consecutives images. All the recordings are performed at 37°C. The fluorescent emission is collected between 500 and 700nm.

### 2.4.3 Confocal microscope recording analysis

Line-scan images were quantified by IDL (8.2) with homemade programs, and statistically analyzed by Origin (9.0). Characteristics of  $[Ca^{2+}]_i$  transients, including time to peak (ms), amplitude (maximum value of  $F/F_0$ , where  $F$  is the fluorescence signal and  $F_0$  the fluorescence on diastolic period) and decay time constant ( $\tau$ , time constant obtained by fitting the descending portion of the fluorescence trace to a single exponential function, in ms), were quantified. Characteristics of  $[Ca^{2+}]_i$  sparks during diastolic periods were also quantified (Figure 32), including spark frequency (number of sparks/s/100 $\mu$ m), width at half maximum ( $W_{50}$ ,  $\mu$ m), time to peak (ms), duration at half maximum ( $D_{50}$ , ms) and peak amplitude ( $F/F_0$ ).

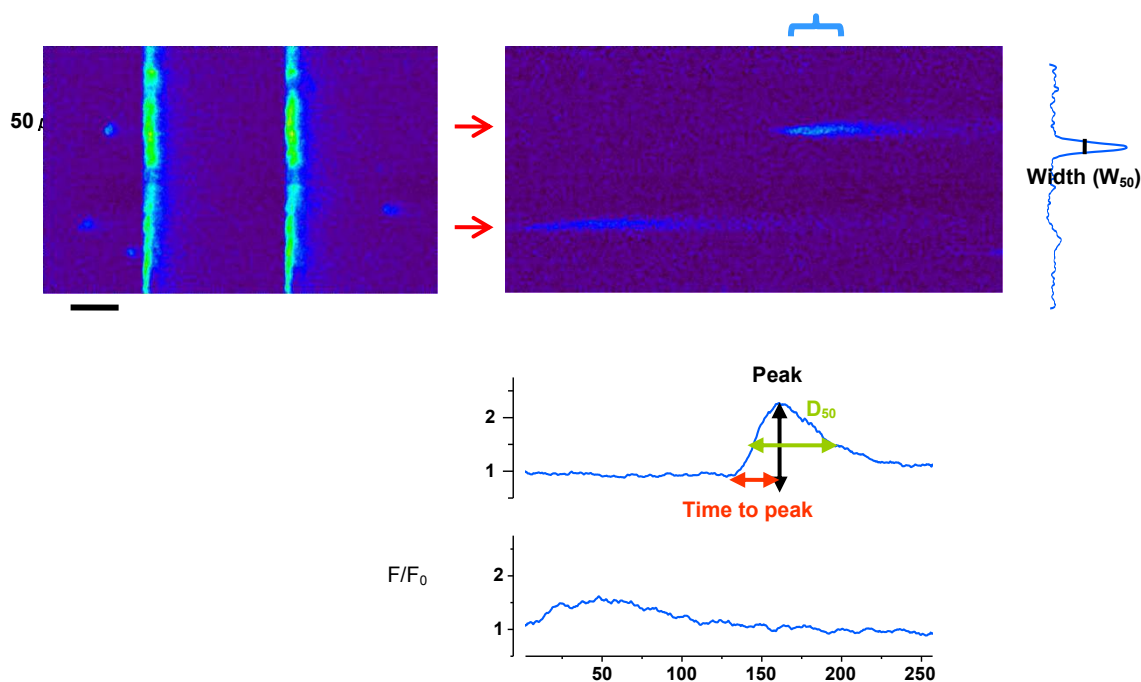


Figure 32  $Ca^{2+}$  spark characteristics. The up-left image shows a line-scan image recorded by confocal microscope. The up-right image corresponds the 250ms depicting in the up-left image, while the linear trace on its right shows the spatial profile in the blue bracket indicating the  $W_{50}$  of the spark. The down-right image presents the time profile of two sparks, and the peak (black arrow),  $D_{50}$  (green arrow) and time to peak (red arrow) of the upper spark.

Global calcium transients of 2D images were quantified using a Region of Interest (ROI) covering the whole cell and further analyzed by Origin (9.0), while the mean cycle length (duration between the peaks of two transients) was measured.

## 2.5 Protein measurement

To measure the channel expression, we extracted protein from SAN and performed western blot.

Protein extraction is the sample preparation step for western blot. In this step, the protein is brought into solution by breaking the tissue or cells, such as homogenization. Lysis and extraction buffer is also used to efficiently lyse cells or tissue, increase protein solubilization, and avoid protein degradation. In this work, we used RIPA buffer. RIPA buffer (radioimmunoprecipitation assay buffer) is a lysis buffer, commonly used for whole cell extracts and membrane-bound proteins. RIPA buffer contains Tris HCl pH 8, NaCl, phosphatase inhibitor, protease inhibitor, Triton X100, DOC (sodium deoxycholate acid), SDS (Table 3). Tris HCl acts as buffer providing an ionic environment similar to that of the cell in vivo and maintaining the protein stability. NaCl maintains or increases the strength of the ionic medium and detergents, to dissolve the cell membranes and concomitantly facilitates the release of proteins. Phosphatase inhibitor and protease inhibitor are used to avoid the protein degradation. DOC, SDS and Triton X-100 are detergents, which are used to lyse cells, solubilize proteins and lipids, etc. DOC and SDS could denature and solubilize the protein, and Triton X100 facilitates lysis.

Table 3 RIPA buffer:

|                                | [stock]  | [final] | 10 ml       | 5 ml        |
|--------------------------------|--|---------|-------------|-------------|
| Tris HCl pH 8                  | 1 M  | 50 mM   | 500 $\mu$ l | 250 $\mu$ l |
| NaCl                           | 3 M  | 150 mM  | 500 $\mu$ l | 250 $\mu$ l |
| Phosphatase inhibitor          | Tablet PhosSTOP, Roche (1 for 5 ml)            |         |             |             |
| Protease inhibitor             | Tablet Complete, EDTA free, Roche (1 for 5 ml) |         |             |             |
| Triton X100                    | 100%   | 1%      | 100 $\mu$ l | 50 $\mu$ l  |
| DOC (sodium deoxycholate acid) | 10%  | 0.5%    | 50 $\mu$ l  | 25 $\mu$ l  |
| SDS                            | 10%  | 0.1%    | 100 $\mu$ l | 50 $\mu$ l  |
| H <sub>2</sub> O               |  |         | 8.75 ml     | 4.375 ml    |

The hearts were dissected on ice, and SAN tissues were cut out. The tissues can be used immediately or stored at -80°C for later use. To extract protein, the tissue samples were placed into Bertin tubes with beads and RIPA buffer (50-75 $\mu$ l for each sample), and homogenized Bertin homogenizer (program: 6500rpm x 10sec, 2 cycles). Then the samples were centrifuged at 4°C 3000 rpm for 1 minute. The lysates can be used immediately, or frozen at -80°C for later use.

The concentration of cell/tissue lysate protein could be measured by many methods, such as BCA assay, Lowry protein assay, etc. In this work, we used BCA assay. BCA assay is a high-precision method, which detects the color change of the sample solution from green to purple in proportion to protein concentration, and compares to protein standards. The peptide bonds of protein reduce the cupric ions ( $\text{Cu}^{2+}$ ) to cuprous ions ( $\text{Cu}^+$ ) in an alkaline environment at a higher temperature (37 to 60°C). Then two BCA molecules chelate one  $\text{Cu}^+$  forming an intense purple complex, which has a strong linear absorbance at 562nm with the increase of protein concentration. The protein concentration of the sample is determined by comparing this absorbance with a standard curve of absorbance from varying bovine serum albumin (BSA).

In this work, we used 96-well flat-bottom plate to perform the BCA. Different BSA concentrations were used to make absorbance curve (30, 25, 20, 15, 10, 5, 2.5, 1.25  $\mu\text{g}$ ). Each sample (2  $\mu\text{l}$ ) was mixed with 98  $\mu\text{l}$   $\text{H}_2\text{O}$  and 100  $\mu\text{l}$  smart BCA solution (contains 98  $\mu\text{l}$  solution A and 2  $\mu\text{l}$  solution B, iNtRON Biotechnology). Samples were performed in triplicate. The plate was then wrapped with aluminum, incubated at 60°C for 20-30 min, and read by TECAN instrument. The protein concentration was calculated by comparing the absorbance with the standard curve, and 20 to 40 $\mu\text{g}$  of total protein was used for western blot.

To detect and quantify specific proteins, we used western blot. Western blot uses gel electrophoresis to separate proteins by their molecular weight, and then transfers the proteins to a membrane, where the specific protein could be stained by targeting antibody.

Before running the gel, the lysate protein was loaded with loading buffer. Loading buffer contains anionic denaturing detergent SDS to denature proteins and make them negatively charged. SDS removes the secondary and tertiary structure, which facilitates the protein separation by molecular weight and the following binding with antibody. Meanwhile, the proteins are negatively charged via attachment to the SDS, with equal charge-densities per unit length as SDS binds to the majority of proteins at a constant ratio of 1.4mg SDS/gm protein.  $\beta$ -mercaptoethanol and dithiothreitol (DTT) are reducing agents used to break disulphide bonds. Glycerol is added to the loading buffer to increase the density of the sample, making the sample easier to load and maintaining at the bottom of the well. A small anionic dye molecule (e.g. Bromophenol blue) is also used to track the migration of protein. Since it is anionic and small, it migrates faster than proteins to provide a migration front and monitor the running progress. Loading buffer also contains Tris HCl pH 6.8, which is the same as stacking gel buffer. In this thesis, we used the loading buffer produced by Sigma. Boiling/heating is also useful to denature the protein. The temperature and heating duration depends on the protein. For NCX, the protein was heated at 37°C for 10 min. For HCN4, the protein was heated at 95 °C for 10 min, and for RyR<sub>2</sub>, the protein was not heated at all.

Then, the anionic protein is fractionated on SDS-PAGE (Sodium Dodecyl Sulfate PolyAcrylamide Gel Electrophoresis) gel. The gel is a sieving electrophoresis matrix formed by three-dimensional networks of long hydrocarbons crosslinked by methylene groups. The gel is made of acrylamide, bis-acrylamide, denaturant (such as SDS), a buffer with adjusted pH, and TEMED and APS to initiate polymerization. During electrophoresis, proteins move through the pores of the gel, and are separated based on the molecular weight. Larger molecules pass through at slower speeds and migrate less than smaller molecules. The pore size of a gel is determined by the percentages of acrylamide and cross-linker (bis-acrylamide). A lower percentage gel provides bigger pore size, and is better for resolving higher molecular weight molecules. Normally, a conventional gel is formed by two sections, the running gel on the bottom and the stacking gel on the top. The stacking gel has a lower acrylamide concentration to ensure the proteins enter the gel. The stacking gel also is prepared with low pH buffer to provide a lower ionic strength, which lines the proteins up at the starting line. The running gel has a higher acrylamide concentration and higher pH to separate the proteins. In this thesis, the conventional gel was chosen according to the size of the targeted protein (Table 4), and prepared as follows: the ingredients of the running gel were mixed and added into the gel apparatus reached to around  $\frac{3}{4}$  of total volume, while the rest of cast was filled with water (creates level, removes bubbles); When the running gel polymerized, the stack gel prepared as Table 4 was added to the cast after removal of water. It can be used ~20 min later after polymerization started. This conventional gel was used for separation of NCX1 (8%).

Gradient and discontinuous gradient running gels are also widely used to separate proteins with broader range of molecular weight. In this work, the homemade discontinuous gradient gel was prepared as follows: every acrylamide solutions were made as Table 5, and added to the gel apparatus from 20% to 4% before polymerization, and the two solutions mixed at the interface as the gradient process. The discontinuous gel was used for RyR2 and HCN4 protein separations.

Table 4 Stacking and running gels:

|                               | Component volumes (in ml) per indicated amount of gel |       |       |       |       |
|-------------------------------|---|-------|-------|-------|-------|
| 6% (very large proteins)      | 10 ml   | 20 ml | 30 ml | 40 ml | 50 ml |
| H <sub>2</sub> O              | 5.3   | 10.6  | 15.9  | 21.2  | 26.5  |
| 30% acrylamide mix            | 2   | 4     | 6     | 8     | 10    |
| 1.5 M Tris (pH 8.8)           | 2.5   | 5     | 7.5   | 10    | 12.5  |
| 10% SDS                       | 0.1   | 0.2   | 0.3   | 0.4   | 0.5   |
| 10% ammonium persulfate (APS) | 0.1   | 0.2   | 0.3   | 0.4   | 0.5   |
| TEMED                         | 0.008   | 0.016 | 0.024 | 0.032 | 0.04  |
| 8% (large proteins)           | 10 ml   | 20 ml | 30 ml | 40 ml | 50 ml |

|                               |       |       |       |       |       |
|-------------------------------|-------|-------|-------|-------|-------|
| H <sub>2</sub> O              | 4.6   | 9.2   | 13.8  | 18.4  | 23    |
| 30% acrylamide mix            | 2.7   | 5.4   | 8.1   | 10.8  | 13.5  |
| 1.5 M Tris (pH 8.8)           | 2.5   | 5     | 7.5   | 10    | 12.5  |
| 10% SDS                       | 0.1   | 0.2   | 0.3   | 0.4   | 0.5   |
| 10% ammonium persulfate (APS) | 0.1   | 0.2   | 0.3   | 0.4   | 0.5   |
| TEMED                         | 0.006 | 0.012 | 0.018 | 0.024 | 0.03  |
| 10% (medium size proteins)    | 10 ml | 20 ml | 30 ml | 40 ml | 50 ml |
| H <sub>2</sub> O              | 4     | 8     | 12    | 16    | 20    |
| 30% acrylamide mix            | 3.3   | 6.6   | 9.9   | 13.2  | 16.5  |
| 1.5 M Tris (pH 8.8)           | 2.5   | 5     | 7.5   | 10    | 12.5  |
| 10% SDS                       | 0.1   | 0.2   | 0.3   | 0.4   | 0.5   |
| 10% ammonium persulfate (APS) | 0.1   | 0.2   | 0.3   | 0.4   | 0.5   |
| TEMED                         | 0.004 | 0.008 | 0.012 | 0.016 | 0.02  |
| 12% (small proteins)          | 10 ml | 20 ml | 30 ml | 40 ml | 50 ml |
| H <sub>2</sub> O              | 3.3   | 6.6   | 9.9   | 13.2  | 16.5  |
| 30% acrylamide mix            | 4     | 8     | 12    | 16    | 20    |
| 1.5 M Tris (pH 8.8)           | 2.5   | 5     | 7.5   | 10    | 12.5  |
| 10% SDS                       | 0.1   | 0.2   | 0.3   | 0.4   | 0.5   |
| 10% ammonium persulfate (APS) | 0.1   | 0.2   | 0.3   | 0.4   | 0.5   |
| TEMED                         | 0.004 | 0.008 | 0.012 | 0.016 | 0.02  |
| 15% (very small proteins)     | 10 ml | 20 ml | 30 ml | 40 ml | 50 ml |
| H <sub>2</sub> O              | 2.3   | 4.6   | 6.9   | 9.2   | 11.5  |
| 30% acrylamide mix            | 5     | 10    | 15    | 20    | 25    |
| 1.5 M Tris (pH 8.8)           | 2.5   | 5     | 7.5   | 10    | 12.5  |
| 10% SDS                       | 0.1   | 0.2   | 0.3   | 0.4   | 0.5   |
| 10% ammonium persulfate (APS) | 0.1   | 0.2   | 0.3   | 0.4   | 0.5   |
| TEMED                         | 0.004 | 0.008 | 0.012 | 0.016 | 0.02  |
| 5% (stacking gel)             | 3 ml  | 6 ml  | 9 ml  | 12 ml | 15 ml |
| H <sub>2</sub> O              | 2.1   | 4.2   | 6.3   | 8.4   | 10.5  |
| 30% acrylamide mix            | 0.5   | 1     | 1.5   | 2     | 2.5   |
| 1 M Tris (pH 6.8)             | 0.38  | 0.76  | 1.14  | 1.52  | 1.9   |



|                               |       |       |       |       |       |
|-------------------------------|-------|-------|-------|-------|-------|
| 10% SDS                       | 0.03  | 0.06  | 0.09  | 0.12  | 0.15  |
| 10% ammonium persulfate (APS) | 0.03  | 0.06  | 0.09  | 0.12  | 0.15  |
| TEMED                         | 0.003 | 0.006 | 0.009 | 0.012 | 0.015 |

Table 5 Discontinuous gradient gel:

|                       | 20%(3ml) | 16%(3ml) | 12%(3ml) | 8%(3ml) | 4%(3ml) |
|-----------------------|----------|----------|----------|---------|---------|
| 40% acrylamide (ml)   | 1.5      | 1.2      | 0.9      | 0.6     | 0.3     |
| 1.5M Tris pH 8.8 (ml) | 0.75     | 0.75     | 0.75     | 0.75    | ----    |
| 1M Tris pH 6.8 (ml)   | ----     | ----     | ----     | ----    | 0.38    |
| 10% APS (ml)          | 0.03     | 0.03     | 0.03     | 0.03    | 0.03    |
| TEMED (ml)            | 0.0012   | 0.0012   | 0.0012   | 0.0012  | 0.003   |
| H <sub>2</sub> O (ml) | 0.7      | 1        | 1.3      | 1.6     | 2.3     |

When the gel was polymerized, it was removed to the gel running apparatus which was filled with running buffer (Table 6). Protein ladder (5  $\mu$ l, Euromedex) and samples were loaded in the wells. The generator was run at 80 V for 30 min, and then at 120 V for 1:30 h.

Table 6 10 $\times$  Running buffer:

|                            |                          |
|----------------------------|--------------------------|
| Tris-Base                  | 150 g                    |
| Glycine                    | 720 g                    |
| SDS                        | 50 g                     |
| H <sub>2</sub> O deionized | to 5 liters final volume |

After running the gel, the proteins were transferred from the gel to a nitrocellulose or polyvinylidene difluoride (PVDF) membrane. This step uses an electric current to pull proteins from the gel into the membrane. When an electric field is applied across the gel, the negative charged proteins migrate from the negative electrode and towards the positive electrode, hence from the gel to the membrane. The proteins bind to the membrane through the non-specific hydrophobic interactions. In this thesis, PVDF membrane was used. The membrane was soaked in methanol for 2 minutes, followed by 5 min wash in deionized water and at least 5 min in transfer buffer (Table 7) at 70 rpm agitation. Whatman (filter) papers were also cut to correct size, 2 pieces per gel. Then in the transfer buffer, the transfer apparatus was assembled (black/white board in this case) as follow: Black board on bottom, sponge, filter paper, gel, membrane (hydrophobic side away from gel), filter paper, sponge and the white board on the top. The transfer apparatus was then inserted into transfer box with ice, and transfer in cold room at 110 V for 1.5 hours. Then, the membrane was took out and cut to separate targeted protein and housekeeping protein according to the ladder, and rinsed separately in TTBS (TBS with 1% Tween, Table 8).

Table 7 10× Transfer buffer:

|               |                          |
|---------------|--------------------------|
| Tris-Base     | 150 g                    |
| Glycine       | 150 g                    |
| H2O deionized | to 5 liters final volume |

Table 8 10× TBS:

|                            |                          |
|----------------------------|--------------------------|
| Tris-Base                  | 121 g                    |
| NaCl                       | 1461 g                   |
| H2O deionized              | to 5 liters final volume |
| Adjust pH to 7.4 with Tris |                          |

Then, to avoid the hydrophobic binding between the membrane and the antibodies, the membrane was blocked by BSA or non-fat dry milk in TBS solution, with a low concentration of detergent (such as Tween 20 or Triton X-100) to prevent unspecific protein-protein interaction. In this work, the membranes were incubated in 5% milk solution (in TTBS), agitated at 35 rpm for 45-50 min.

At last, the membrane was incubated with the primary antibody which binds to the specific protein, and then the labeled secondary antibody which binds to the first antibody. Both antibodies were diluted in 5% milk TTBS solution. Through the second antibody, the specific protein is detected. The second antibody is commonly labeled with horseradish peroxidase (HRP). HRP is an enzyme which oxidizes the chromogenic, fluorogenic, and chemiluminescent substrates that produces colored, fluorimetric or luminescent derivatives, respectively. In this work, the membrane was incubated with the primary antibody overnight at 4°C, 35 rpm. The next morning, the first antibody was collected for reuse (it can be used 3 times) and frozen at -20°C. The membrane was washed with TTBS (at 70 rpm, 3x 10 min), and incubated with the secondary antibody for 1h at 35 rpm, and after, washed in TTBS as previously (at 70 rpm, 3x 10 min).

Antibodies for HCN4 (trial sample from Alomone Labs, APC-052, 200×, anti-rabbit), NCX1 (Swant, R3F1, 1000×, anti-mouse), RyR2 (ThermoFisher Scientific, MA3-916, 1000×, anti-mouse), S2814 phosphorylated RyR2 (Badrilla, A010-31AP, 2000×, anti-rabbit), S2808 phosphorylated RyR2 (Badrilla, A010-30AP, 2000×, anti-rabbit), GAPDH (Abcam, 2000×, anti-rabbit) were prepared with 5% milk in TTBS. The matched secondary antibodies (Santa Cruz Biotechnology) were also diluted from 10000× stock with 5% milk in TTBS.

To visualize the protein, the membrane was placed on the plastic sheet, and loaded with the substrate (Classico, Crescendo, Forte or Femto Luminata Western Substrates, Millipore and Thermo Scientific) depending on the quantity of the proteins. Classico was used for high signals, and femto

was used for the lowest signals. After 5 minutes incubation at room temperature, the substrate was removed by pressing the plastic sheet with paper to clear the substrate. The membrane was exposed and visualized by the chemiluminescence appropriately. After saving the images, the membrane was rinsed and washed with TTBS for around 5 minutes, and sealed to clean plastic sheet. Membranes can be stored at 4°C, and reused for re-blotting of other proteins.

To re-blot the protein, we rinsed the membrane with 1× Re-blot Plus Strong solution (Millipore, 10×, in water), followed by blocking, first/second antibody incubation, and so on.

The western blot images were quantified with Image J, and further statistically analyzed by Origin (9.2).

## **2.6 SAN cell dissociation and patch clamp (Performed by Pietro Mesirca)**

To identify the properties of the action potential, L-type  $\text{Ca}^{2+}$  current, funny current, caffeine-induced current in single cell, SAN cells were dissociated and performed patch clamp.

### **2.6.1 SAN cell dissociation**

In SAN cell dissociation, several solutions are needed. Low  $\text{Ca}^{2+}$  solution is used to prevent cell contraction and destabilize cell-cell adhesion. Enzymatic solution is used to digest the tissue and break down the extracellular matrix. A  $\text{Ca}^{2+}$ -free,  $\text{Na}^+$ -free and high- $\text{K}^+$  solution, Kraftbrühe (K-B) solution, is used to maintain the resting state and wash out the enzyme, and followed by mechanical separation to collapse the tissue. At the end,  $\text{Ca}^{2+}$  should be recovered by progressively increasing the  $\text{Ca}^{2+}$  concentration, while another solution (10  $\mu\text{M}$  NaCl and 1.8  $\mu\text{M}$   $\text{CaCl}_2$  in water) and BSA in Tyrode solution (1mg/mL, Table 2) are used.

### **2.6.2 SAN cell patch clamp (Performed by Pietro Mesirca)**

Patch clamp was developed by Erwin Neher and Bert Sakmann (in 1976) as an electrophysiological technique for single channel study, through a glass pipette with a small opening. The resulting electrical current can be measured through an electronic amplifier connected to the pipette, and another electrode placed in the bath as a ground electrode. Today, technical modifications have enhanced the patch clamp technique, and several common variations of the patch clamp method have been applied (Figure 33), such as cell-attached recording, whole cell recording, inside-out recording, outside-out recording, etc.<sup>631</sup>

Cell-attached patch uses the pipette to tightly contact with the cell membrane. The pipette is sealed onto the membrane after a light suction from the back of the pipette (Figure 33), which ensures that no ions flow through the seal. Via the pipette, the single, or a few, ion channels on the connected patch of the membrane are monitored, i.e. the currents flowing through the channels are

recorded by the electrode in the pipette. This method attaches to the exterior of the cell membrane without influencing the interior, recording the channel behavior under physiological conditions.

In the whole cell recording, the membrane patch within the pipette in the cell attached method is disrupted by a briefly applied strong suction (Figure 33). The pipette is then directly connected with the cell cytoplasm, and records the electrical potentials and the currents through multiple channels over the entire cell membrane. Therefore, whole cell patch could be used to study the electrical behavior of the entire cell.

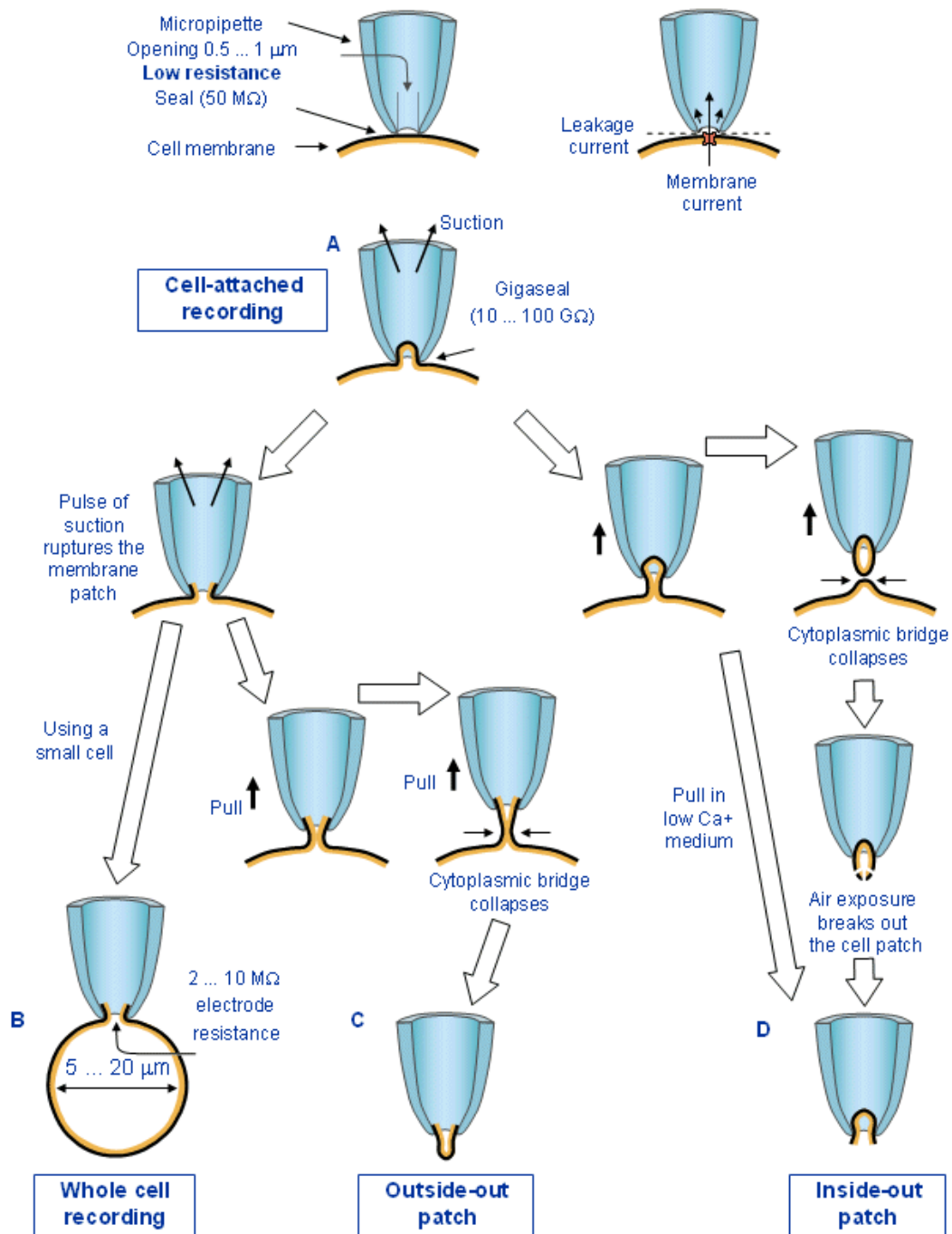


Figure 33 The variations of patch clamp. A shows cell-attached recording, and panel B shows whole cell recording, while C and D show outside-out patch and inside-out patch. (Adapted from <http://www.bem.fi/book/04/04.htm> )

The outside-out patch and the inside-out patch also exist to measure the channel behavior in different extracellular/cytoplasmic medium by changing the bathing solution (Figure 33).

## **2.7 Statistics**

Values were expressed as mean±s.e.m. Student's t-test and ANOVA were used to assess significant differences. A value of  $p < 0.05$  was considered significant.

## **2.8 Materials**

Sodium deoxycholate (DOC), sodium dodecyl sulfate (SDS), DMSO, calcium chloride dihydrate ( $\text{CaCl}_2 \cdot 2\text{H}_2\text{O}$ ), magnesium chloride hexahydrate ( $\text{MgCl}_2 \cdot 6\text{H}_2\text{O}$ ) and hepes were purchased from Sigma. TEMED, acrylamide/bisacrylamide 30%, Tris (hydroxymethyl) aminomethane, sodium chloride (NaCl), potassium chloride (KCl) and D-glucose were from Euromedex. Ammonium Persulfate (APS) was from Carlo Erba.

## Chapter 3 Results

During my Ph.D., I have focused on SAN  $\text{Ca}^{2+}$  regulation in a mice model bearing the  $\text{RyR}_2^{\text{R420Q}}$  mutation found in a CPVT family. The resulting manuscript constitutes the first part of this thesis. Some of the results that I have obtained in this work are not included in the manuscript and they are under “Additional Data”. During the time spend in the laboratory I have also participated in a sutudy of  $\text{Ca}^{2+}$  sparks in a mice model of myocardial infarction. This work has been recently published, but as my participation was partial, I have added de manuscript in the anexe, at the end of the thesis. Because during my thesis work, I was studing  $\text{Ca}^{2+}$  handling in mice SAN and its response to isoproterenol, I did a work on the modulation of SAN  $\text{Ca}^{2+}$  handling by the cAMP effector Epac. This manuscript, that is well advanced, and where I will be first co-author with Anna Llach, still requires few experiments. As this thesis is focused on CPVT, I choosed not to add these data.

### 3.1.1 Manuscript

**Mechanisms of bradycardia in  $\text{RyR}_2^{\text{R420Q}}$  Catecholaminergic Polymorphic Ventricular Tachycardia mutation**

# Mechanisms of bradycardia in RyR<sub>2</sub><sup>R420Q</sup> Catecholaminergic Polymorphic Ventricular Tachycardia mutation

Yue Yi Wang<sup>1</sup>, Pietro Mesirca<sup>2</sup>, Elena Marqués-Sulé<sup>1,4</sup>, Alexandra Zahradnikova Jr<sup>1\*</sup>, Olivier Villejoux<sup>1</sup>, Esther Zorio<sup>3</sup>, Matteo Mangoni<sup>2</sup>, Jean-Pierre Benitah<sup>1</sup>, Ana María Gómez<sup>1</sup>

“The authors have declared that no conflict of interest exists.”

<sup>1</sup>UMR-S 1180, Inserm, Univ. Paris-Sud, Université Paris-Saclay, Châtenay-Malabry, France.

<sup>2</sup>UMR-5203, CNRS, INSERM, U661, Université de Montpellier, Montpellier, France

<sup>3</sup>Hospital Universitario y Politécnico La Fe, Valencia, Spain

<sup>4</sup>Physiotherapy Department, University of Valencia, Valencia, Spain

\*Current address: Institute of Molecular Physiology and Genetics, Slovak Academy of Sciences, Bratislava, Slovakia

Address for correspondence

Ana María Gómez

5 Rue Jean Baptiste Clément,

Faculté de Pharmacie, Université Paris Sud,

Tour D4, 5<sup>ème</sup> étage

Phone : +33 146 83 57 18

e-mail : [ana-maria.gomez@inserm.fr](mailto:ana-maria.gomez@inserm.fr)

Catecholaminergic polymorphic ventricular tachycardia (CPVT) is an inherited disease manifested as syncope or sudden death in children and young adults under stress conditions. CPVT often presents bradycardia and sinoatrial node (SAN) dysfunction. To identify the underlying mechanism, we created a knock-in (KI) mice model carrying a novel CPVT- mutation, RyR<sub>2</sub><sup>R420Q</sup>. ECGs recorded in KI mice showed sustained bidirectional ventricular tachycardia after epinephrine/caffeine challenge, validating the model. KI mice presented slower heart rhythm, and junctional escape beats after  $\beta$ -adrenergic stimulation, denoting alteration in SAN function. Spontaneous  $[Ca^{2+}]_i$  transients rate was slower in KI SAN preparation than in wild type (WT), without any significant alteration in the funny current. L-type  $Ca^{2+}$  current ( $I_{Ca}$ ) was depressed in KI SAN cells, dependent on intracellular  $Ca^{2+}$ .  $[Ca^{2+}]_i$  transients amplitudes were significantly smaller, consistent with reduced sarcoplasmic reticulum (SR)  $Ca^{2+}$  load. This was consistent with higher leak through RyR<sub>2</sub><sup>R420Q</sup>. In fact, the presence of local  $Ca^{2+}$  release was significantly higher in KI SAN cells.  $Ca^{2+}$  sparks frequency between spontaneous beats was slightly increased in KI SAN cells, and their duration was dramatically prolonged. These data showed that RyR<sub>2</sub><sup>R420Q</sup> mutation increases the diastolic  $Ca^{2+}$  leak by producing prolonged  $Ca^{2+}$  sparks, evidencing a new mechanism in CPVT which depresses spontaneous activity.



Catecholaminergic polymorphic ventricular tachycardia (CPVT) is an inherited heart disease manifested as syncope or sudden cardiac death (SCD) in children and young adults under physical or emotional stress<sup>1</sup>. Although CPVT stands for ventricular arrhythmia, it often associates supraventricular (SV) arrhythmias including not only tachyarrhythmias (atrial fibrillation and atrial flutter) but also bradyarrhythmias such as sinus bradycardia caused by sinoatrial (SA) node dysfunction<sup>2-4</sup>. These findings may be of paramount importance in CPVT patients since severe sinus bradycardia may require that implantable cardioverter defibrillator devices (ICD) uses their pacing mode, which consume quicker the ICD battery. Moreover SV tachyarrhythmias may trigger inappropriate ICD discharges stressing the patients and worsening atrial and ventricular arrhythmias which could lead to SCD<sup>3,5</sup>. In not ICD carriers, CPVT patients SV tachyarrhythmias have been also somehow associated to ventricular life-threatening arrhythmias since they have been registered immediately after spontaneous ventricular tachycardia and ventricular fibrillation<sup>5</sup>. Collectively, these data support the idea that non-ventricular arrhythmias are not trivial in CPVT patients.

Thus, CPVT arrhythmic disorders are not limited to the ventricles, as RyR<sub>2</sub> CPVT-related mutations are expressed in the entire heart. Indeed, Postma et al<sup>2</sup> investigated 13 missense mutations in RyR<sub>2</sub> in 12 probands, and reported that the RyR<sub>2</sub>-related CPVT patients exhibit bradycardia regardless of the site of the mutation. In keeping with this observation, van der Werf et al investigated 160 relatives from 15 families, and observed sinus bradycardia in 19% of relatives and other supraventricular dysrhythmias in 16%<sup>6</sup>.

The heart beat is initiated by the automatic electrical firing of the primary pacemaker, located at the sinoatrial node (SAN). SAN cells automatically generate action potentials (AP), which are then conducted to the atria and ventricles assuring the coordinated contraction of the heart. The mechanism of the automatic AP generation involves several ion currents and transporters. While the hyperpolarization activated current, I<sub>f</sub>, plays an important role, intracellular Ca<sup>2+</sup> is also involved<sup>7,8</sup>. Indeed, it has been proposed that rhythmic SR Ca<sup>2+</sup> release via RyR<sub>2</sub> (Ca<sup>2+</sup>-clock), together with the sarcolemmal channels such as I<sub>f</sub> and I<sub>Ca,L</sub> (membrane-clock), control SAN automaticity. The involvement of RyR<sub>2</sub> Ca<sup>2+</sup> release in SAN

automaticity has been demonstrated in numerous studies showing that application of ryanodine slowed SAN pacemaker activity in different species<sup>9-13</sup>. In addition, inducible and cardiac-specific knockout of RyR<sub>2</sub> with acute ~50% loss of RyR<sub>2</sub> protein was sufficient to cause bradycardia and arrhythmias<sup>14</sup>.

Mutations in four genes – RyR<sub>2</sub>, calsequestrin (CASQ2), triadin (TRDN), and calmodulin (CALM1) – are known to cause CPVT or related phenotypes of adrenergically induced life-threatening arrhythmias. Approximately 50 - 65% of CPVT identified mutations are autosomal dominant mutations in RyR<sub>2</sub>. An impaired  $\beta$ -adrenergic SAN response was reported by our group in a RyR<sub>2</sub>-related CPVT mouse model carrying the C-terminal RyR<sub>2</sub><sup>R4496C</sup> mutation, due to an increased Ca<sup>2+</sup> sensitivity<sup>15</sup>. Of note, mutations in other regions of the RyR<sub>2</sub> protein have not been studied with regard to their SV proarrhythmic potential. These CPVT mutations are clustered primarily in three discrete regions of the RyR<sub>2</sub> protein: the N-terminal (residues 77-466), the central (residues 2246-2534) and the C-terminal region (residues 3778-4959)<sup>16</sup>. Thus it is possible that the mechanism underlying arrhythmic disorders differs according to the mutation site within the protein. Besides the intrinsic defect related to the RyR<sub>2</sub> mutation causing SA dysfunction, other mechanisms may account for sinus bradycardia, such as a decreased  $\beta$ -adrenergic receptor density and/or a reduced presynaptic catecholamine recycling. In the past years, an increased G protein coupled receptor kinase type 2 (GRK2) expression in lymphocytes was observed in patients with heart failure mirroring that what happens at the myocardium; its consequences in the failing heart (increased  $\beta$ -adrenergic receptor degradation) directly lead to a loss of  $\beta$ -adrenergic receptor density and cardiac denervation<sup>17</sup>. On the other hand, patients with arrhythmogenic right ventricular cardiomyopathy, right ventricular outflow tract tachycardia and ischemic heart disease have been shown to exhibit left ventricular patchy defects in radionuclide distribution which may identify patients at risk of ventricular arrhythmias and sudden cardiac death<sup>18</sup>. Planar or SPECT imaging with Metaiodobenzylguanidine (MIBG) is considered a pharmaceutical suitable for the assessment of the presynaptic portion of the

cardiac adrenergic innervation<sup>19</sup> although recently, other techniques have also been used, such as PET with <sup>11</sup>C-labeled norepinephrine analog [<sup>11</sup>C]-hydroxyephedrine<sup>18</sup>. Briefly, both  $\beta$ -adrenergic receptor density decrease and heterogeneous sympathetic denervation may create a proarrhythmic substrate to contribute to initiating and sustaining arrhythmias<sup>18</sup>. In this scenario, a given increase in the systemic autonomic tone can trigger a life-threatening arrhythmia in a denervated hypersensitive myocardium, which may accentuate electric heterogeneities of primary arrhythmic conditions<sup>18</sup>.

We have identified a CPVT mutation in the N-terminal portion, RyR<sub>2</sub><sup>R420Q</sup>, in a large Spanish family, which is associated with bradycardia<sup>4</sup>. In the present study, we have created and characterized the SAN activity of the KI mouse model carrying RyR<sub>2</sub> N-terminus mutation (RyR<sub>2</sub><sup>R420Q</sup>). Although CPVT affects both men and women, male CPVT patients have a higher risk of cardiac events and lower heart rate<sup>2, 20</sup>. It is still unclear why the heart rate of CPVT men is lower than that in women, and if the severity of this entity (SCD) is related with low heart rate. Thus we have separately analysed RyR<sub>2</sub><sup>R420Q</sup> males and females mice. Those parameters without differences stratified by gender were pooled together. Other possible mechanisms to explain the presence of sinus bradycardia have been explored in patients with the RyR<sub>2</sub> mutation and non-affected relatives.

In this study, we generated and analyzed a new mouse model of CPVT, carrying out a RyR<sub>2</sub> mutation in the N-terminus (R420Q) which has been described in different CPVT families<sup>4, 21</sup>. Our data show that this N-terminus mutation alters the Ca<sup>2+</sup> homeostasis of SAN cells in KI mice. While gender difference may be due to different autonomic tone, we found that the mutation affected both sexes similarly, manifesting a slowed heart rhythm in KI SAN. Neither a decreased  $\beta$ -receptor density nor a sympathetic denervation could be observed in CPVT patients and, thus, did not account for sinus bradycardia associated to the RyR<sub>2</sub><sup>R420Q</sup> mutation. Slow SAN rhythm was associated with an enhanced Ca<sup>2+</sup> leak during the diastolic period, which unloads the SR of Ca<sup>2+</sup> and inactivates the L-type Ca<sup>2+</sup> channel, thus affecting

both calcium and voltage clocks. The enhanced SR  $\text{Ca}^{2+}$  leak in KI cells is produced by longer  $\text{Ca}^{2+}$  sparks, consisting with abnormally prolonged  $\text{RyR}_2^{\text{R420Q}}$  openings.

## RESULTS

We previously identified the RyR<sub>2</sub><sup>R420Q</sup> mutation in a family of CPVT<sup>4</sup>. Figure 1A shows an ECG presenting burst of bidirectional ventricular tachycardia (BDVT) recorded during recovery of an exercise testing in a 57 year old woman, carrier of the RyR<sub>2</sub><sup>R420Q</sup> mutation. Note a junctional escape beat (JE) and BDVT. In this family, the presence of sinus bradycardia was significantly higher in the RyR<sub>2</sub><sup>R420Q</sup> carriers than those non carriers<sup>4</sup>. Here we analyzed the averaged heart rate in men and women during rest, before any  $\beta$ -blocker therapy. HR was lower in RyR<sub>2</sub><sup>R420Q</sup> carrier females (Fig.1B). To understand the underlying mechanism of the sinoatrial node dysfunction in RyR<sub>2</sub><sup>R420Q</sup> patients, we created a KI mouse model carrying RyR<sub>2</sub><sup>R420Q</sup> mutation. We analyzed ECGs in free moving KI and littermate WT mice by telemetry. After epinephrine/caffeine (2/120 mg/kg) challenge, all KI mice but none of the WT presented sustained bidirectional ventricular tachycardia (VT) (Figure 1C, D), validating the model. Sinus heart rhythm was analyzed in mice by measuring the PP intervals during 24 hours. During night time there were no significant differences between KI and WT mice (Males: 103.70  $\pm$  1.58 ms vs. 102.86  $\pm$  2.40 ms, in 10 WT mice and 11 KI mice; Females: 97.14  $\pm$  2.62 ms in 10 WT vs. 101.64  $\pm$  1.68 ms in 9 KI). During the day time (resting period, where the sympathetic tone is reduced) we found a statistically significant prolongation of the PP interval in females KI compared to WT (Figure 1E). Moreover, we found that WT females have faster heart rate than males (Figure 1E), reminiscent of human data (Figure 1B). We challenged the mice with 2 opposite approaches: either activate the sympathetic system by isoproterenol (ISO) (1 mg/kg) injection or inhibit it with parasympathetic activation (carbachol, CCH, injection, 0.25 mg/kg). As expected, ISO had a positive chronotropic effect (Figure 1F), and CCH had a negative chronotropic effect (Figure 1G) in all mice. Comparison of WT and KI mice showed higher effect of ISO in female KI and of CCH in male KI. Besides this ventricular dysfunction, RyR<sub>2</sub><sup>R420Q</sup> KI mice presented signs of sinus dysfunction after ISO injection, notably evidenced by JEs as shown in the ECG example in Figure 1H, and in the pooled data (Figure 1I). As with the presence of biventricular tachycardia, no difference was observed between males and females, thus data

were pooled together. JEs were also present in RyR<sub>2</sub><sup>R420Q</sup> humans. Figure 1 J shows exercise testing in a 35 year old woman, carrier of the RyR<sub>2</sub><sup>R420Q</sup> mutation with JEs.

We next explored another trigger, emotional stress, by blowing the mice with warm air from a hair-dryer during 15 s followed by 45s rest, and repeated 10 times <sup>22</sup>. In Fig. 2A (top) the RR intervals of a WT mice are shown during this protocol. Each time the air is blown, the heart rate accelerates, and then recovers during the rest periods. With time the animal is getting used to the protocol and the positive chronotropic response weakens and even disappears. In KI mice the response is different (Fig.2A, bottom). At the end of the protocol there is severe sinus dysfunction and a slow ventricular escape rhythm until asystolia is established and the mouse died. Unfortunately, resuscitation maneuvers did not work. Most of the KI mice (5 of 7) died. Because the ECG was continuously recorded after the experiment until next day, we could record some of these deaths. Figure 2B shows the ECG of a KI mouse which died during the recovery phase. Strikingly, although the CPVT mouse, once stressed, developed VT, they were self-terminated and the final arrhythmia underlying the sudden cardiac death one hour later was a severe sinus dysfunction with a progressively slower ventricular escape rhythm ending up with asystolia.

#### *R420Q mutation decreased SAN activity in vitro.*

In order to analyze intrinsic SAN activity, we dissected the SAN and analyzed the frequency of spontaneous [Ca<sup>2+</sup>]<sub>i</sub> transients by confocal microscopy. Figure 3 A shows confocal images of Fluo-4 loaded SAN at different times from a WT (upper images) and KI (lower images) male mice. The cycle length, measured between 2 consecutives automatic [Ca<sup>2+</sup>]<sub>i</sub> transients at their upstroke was significantly longer in KI than in WT, showing a lower rhythm in RyR<sub>2</sub><sup>R420Q</sup> SAN. Both male and female KI SAN cells had longer cycle length than WT, revealing an intrinsic defect in KI SAN (Figure 3B). We didn't pool together all data because of a gender difference in cycle length, but the presence of RyR<sub>2</sub><sup>R420Q</sup> mutation affected similarly both males and females.

Acute ISO treatment decreased the cycle length in all mice, but the response of KI SAN was greater than WT (Figure 3C). On the other hand, CCH prolonged the cycle length equally regardless the sex and genotype (Figure 3D).

#### *Membrane clock*

Several mechanisms account for the automatism of pacemaker cells, including the membrane and calcium clocks. The membrane clock stands for ionic channels in the sarcolemma, and the  $\text{Ca}^{2+}$  clock by the  $\text{Ca}^{2+}$  release channel ( $\text{RyR}_2$ ) and the electrogenic  $\text{Na}^+/\text{Ca}^{2+}$  exchanger ( $\text{NCX}$ )<sup>23</sup>. Although the difference between KI and WT mice is the presence or absence of the  $\text{RyR}_2^{\text{R420Q}}$  mutation, secondary alterations in membrane currents could potentially account for the slowing of SAN cell automatism found in KI. In order to test this possibility, we isolated SAN cells to measure ionic currents by patch-clamp. No differences in current densities in cells isolated from males compared to females were observed, thus all data were pooled together. Figure 4 A shows representative recordings and current - density relationships of  $I_f$ , the main ionic current involved in SAN automatism. As it is shown in the averaged data, no significant differences were found between groups. Likewise, no significant difference was found in  $I_{\text{Ca}}$  between KI and WT (Figure 4B) in presence of a  $\text{Ca}^{2+}$  chelator in the pipette solution (BAPTA). However we observed a reduction in the  $I_{\text{Ca}}$  density was in KI cells compared with WT cells (Figure 4C) in absence of  $\text{Ca}^{2+}$  chelator. These data suggest that intracellular  $\text{Ca}^{2+}$  alteration can induce decrease in  $I_{\text{Ca}}$  in KI mice, which could account for the slowing of SAN pacing rate.

#### *$\text{Ca}^{2+}$ clock*

We recorded fluorescence  $\text{Ca}^{2+}$  images of SAN cells within the tissue in the line-scan mode to gain time resolution. Figure 5A shows such images from one cell of each group. The  $[\text{Ca}^{2+}]_i$  transient amplitude was smaller in KI than in WT cells (Figure 5B). In addition, while the time constant of decay (obtained by fitting the decay fluorescence trace to a single

exponential) was significantly faster in KI animals (Figure 5C), the  $[Ca^{2+}]_i$  transients recorded in KI animals had a longer time to peak (Figure 5D).

The  $Ca^{2+}$  clock has been ascribed as local  $[Ca^{2+}]_i$  transients (which can be seen as a “feet” or “ramp” the before the  $[Ca^{2+}]_i$  transient) precede the global  $[Ca^{2+}]_i$  transient, which corresponds to the late diastolic depolarization. The percentage of cells presenting ramp was higher KI SAN cells than WT (Figure 5E)

#### *SR $Ca^{2+}$ content*

Diastolic  $Ca^{2+}$  release, measured as ramp, instead of activating the  $[Ca^{2+}]_i$  transient could unload the SR, slowing the  $Ca^{2+}$  clock. The caffeine-evoked transient inward current (Figure 6A), which is carried by NCX working in forward mode, was significantly reduced in the KI SAN cells. This was not related to alteration of NCX protein expression (Figure 6B), suggesting that the SR  $Ca^{2+}$  load is reduced. Thus, enhanced diastolic  $Ca^{2+}$  leak causing reduced SR  $Ca^{2+}$  load seems a likely mechanism to explain why the  $Ca^{2+}$  clock slows down in KI SAN.

#### *RyR<sub>2</sub> expression level*

The observed modifications in  $Ca^{2+}$  handling of KI SAN might be due alteration in the RyR<sub>2</sub> expression (happloinsufficiency) and/or its phosphorylation status. We evaluated the total RyR<sub>2</sub> expression level by western blots (examples shown in Figure 6C). Neither the total amount of RyR<sub>2</sub> nor their relative phosphorylation at the 2808 equivalent nor at 2914 equivalent sites was significantly different among groups (Figure 6D-F). These data points to an intrinsic defect of the RyR<sub>2</sub><sup>R420Q</sup> function rather than expression or basal phosphorylation difference.

#### *$Ca^{2+}$ sparks*



Because the presence of the CPVT mutation did not alter neither the expression level nor the phosphorylation status of the protein, we next addressed the function of the channel evaluation. In order to do that, we analysed  $\text{Ca}^{2+}$  sparks that can be registered during the diastolic period. Figure 7 A (left) shows representative examples of confocal images presenting  $\text{Ca}^{2+}$  sparks in WT and KI SAN cells.  $\text{Ca}^{2+}$  sparks frequency, which is an estimate of RyR<sub>2</sub> open probability, was augmented in KI cells (Figure 7A, right). Of note, the increase in  $\text{Ca}^{2+}$  sparks frequency was more modest than that reported in the literature regarding CPVT, including our data of the RyR<sub>2</sub><sup>R4496C</sup> mutation, located at the C-terminal region<sup>15, 24, 25</sup>. We then analyzed  $\text{Ca}^{2+}$  sparks characteristics, in order to estimate the total  $\text{Ca}^{2+}$  leak through  $\text{Ca}^{2+}$  sparks.  $\text{Ca}^{2+}$  sparks in KI male exhibited a markedly higher amplitude (Figure 7B), longer duration at half maximum (Figure 7C), but also a thinner width at half maximum (Figure 7D) than WT mice. Although the narrowing of the  $\text{Ca}^{2+}$  sparks in RyR<sub>2</sub><sup>R420Q</sup> cells was statistically significant, the difference is so small that it may not have functional consequences. Similar alterations were found in female mice, except for the peak amplitude and width that was not significantly altered in KI female (Figure 7B-D). The most striking effect of the RyR<sub>2</sub><sup>R420Q</sup> mutation in  $\text{Ca}^{2+}$  sparks was a marked prolongation of their duration. We then went deeper into the  $\text{Ca}^{2+}$  sparks kinetics by using a resonant scanner confocal microscope, which allows us to get enough points to measure the time to peak. Figure 7E shows that regardless of sex, the RyR<sub>2</sub><sup>R420Q</sup> mice presented  $\text{Ca}^{2+}$  sparks with marked prolongation of the time to peak. Thus, in summary, RyR<sub>2</sub><sup>R420Q</sup> produces some more  $\text{Ca}^{2+}$  sparks of abnormal characteristics than the WT channel.

The altered characteristics of  $\text{Ca}^{2+}$  sparks could modify the total  $\text{Ca}^{2+}$  leak through them. Thus we calculated  $\text{Ca}^{2+}$  spark mass by multiplying  $\text{Ca}^{2+}$  spark characteristics (amplitude x  $D_{50}$  x  $W_{50}$ ) (Figure 7F), and then by frequency, obtaining an indicative of the  $\text{Ca}^{2+}$  released every second through  $\text{Ca}^{2+}$  sparks in each group. Figure 7G shows that SAN cells from both, male and female KI mice present more diastolic  $\text{Ca}^{2+}$  release through  $\text{Ca}^{2+}$  sparks than WT. The KI male presented most dramatic differences, supporting the presence of gender differences.

## Discussion

This manuscript uncovers a new arrhythmogenic mechanism in a CPVT mutation located at the N-terminal portion of the channel, the RyR<sub>2</sub><sup>R420Q</sup>. Besides polymorphic ventricular tachycardia upon stress, the individuals bearing this mutation, as many others CPVT patients, present supraventricular arrhythmias and slow sinus rate at resting conditions. This mutation in the RyR<sub>2</sub> produces prolonged Ca<sup>2+</sup> sparks, which unloads the SR of Ca<sup>2+</sup> at the SAN and also inactivates the L type Ca<sup>2+</sup> channel, slowing the firing rate of the pacemaker cells.

Some studies have shown gender difference in cardiac function, such as in excitation-contraction coupling, or in  $\beta$ -adrenergic responsiveness of action potentials<sup>26, 27</sup>. The sex-dependent difference has also been shown in RyR<sub>2</sub>-related CPVT patients, so that male CPVT patients have a higher risk of cardiac events<sup>20</sup>. In this study, we found some differences in basal heart rate both *in-vivo* and *in-vitro*. In basal conditions, HR is faster in women than in men due to the smaller heart size, and our data in mice are reminiscent of this sex difference. Our data in healthy family members and in WT mice are consistent with these conclusions. However, the autonomic tone has shown some gender differences suggesting higher sympathetic activity in men than in women<sup>28, 29</sup>. In fact, we found that HR response to isoproterenol is higher in female than in male mice the opposite regarding carbachol effect. Moreover, data on dissected SAN support the higher sympathetic tone in males, as the HR is faster (smaller cycle length), as shown in Figure 2. This observation is consistent with the previous hypothesis that cAMP might be higher in male ventricles, due, at least partially, to the lower phosphodiesterase (PDE) PDE4B expression in males<sup>26</sup>. However While the differences between males and females is not the subject of this study, we found that the presence of the RyR<sub>2</sub><sup>R420Q</sup> mutation affects both equally, slowing the spontaneous activity of the SAN.

Bradycardia and sinus dysfunction are common in CPVT patients. However, the mechanisms are not clear. As most CPVT related mutations concern a gain of function, an

acceleration of the calcium clock should be expected. However, the mechanism underlying the gain of function vary in different mutations. We previously analyzed  $\text{Ca}^{2+}$  handling in cardiac myocytes from the  $\text{RyR}_2^{\text{R4496C}}$  mutation, which is located at the C terminal part of the channel. The defect we identified consisted in enhanced  $\text{Ca}^{2+}$  sensitivity of the channel<sup>24</sup>. Other mechanisms have been invoked in mutations located at other hotspots. In myocytes from KI mice harboring CPVT mutations in the central region (such as the  $\text{RyR}_2^{\text{R2474S}}$ ), the functional mechanism underlying the proarrhythmic behavior of the mutation is an altered binding of the mutated  $\text{RyR}_2$  to FKBP12.6 (protein that binds  $\text{RyR}_2$  and stabilizes it in the closed state)<sup>30</sup>. Additionally, the zipping-unzipping mechanism (mediated by the N-terminal and central region interaction) plays a crucial role and has been shown to be disturbed by this  $\text{RyR}_2^{\text{R2474S}}$  mutation, which induces conformational changes and favors the unzipped state. Although most proposed functional alterations caused by the  $\text{RyR}_2$  mutations result in a gain of function, recently a mice model harboring a mutation in the C-terminal portion exhibits loss of function<sup>31</sup>. Here we analyzed cells from a mice model harboring the  $\text{RyR}_2^{\text{R420Q}}$  mutation, which we previously identified in a large Spanish family<sup>4</sup>. Previously, another mutation in the same residue was identified in several CPVT families<sup>32, 33</sup>, and besides our family<sup>4</sup>, two additional reports in the literature connect CPVT with the  $\text{RyR}_2^{\text{R420Q}}$  mutation<sup>21, 34</sup>. Thus the 420 site seems to be important for the  $\text{RyR}_2$  function. In fact, it is a highly conserved residue among species. Structural analyses have shown that this residue plays an important role in the channel conformation<sup>35, 36</sup>. The  $\text{RyR}_2^{\text{R420Q}}$  losses the capacity to bind  $\text{Cl}^-$ , which maintains in place the three regions (A, B, and C) of the N terminal domain<sup>35</sup>, although the functional consequences remain unknown. Here we show that the  $\text{Ca}^{2+}$  sparks in  $\text{RyR}_2^{\text{R420Q}}$  myocytes are abnormally prolonged, mainly due to a longer time to peak. As the time to peak depends on the open time of the  $\text{RyR}_2$ , our data is compatible with long openings of the  $\text{RyR}_2^{\text{R420Q}}$  channel.

Instead of accelerating the calcium clock, the aberrant  $\text{Ca}^{2+}$  leak through  $\text{RyR}_2^{\text{R420Q}}$  channels unloads the SR of  $\text{Ca}^{2+}$ , slowing the calcium clock, and inactivates the neighboring L type  $\text{Ca}^{2+}$  channels, inactivating them and slowing the voltage clock. When the SAN does not fire,

or do it at a smaller pace, there is more probability that ectopic foci are developed, thus augmenting the risk of ventricular tachycardia.

In summary, we have found a new mechanism of bradycardia in a new mice model carrying the RyR<sub>2</sub><sup>R420Q</sup> CPVT mutation. This mutation induces longer channel openings, augmenting the Ca<sup>2+</sup> leak within each Ca<sup>2+</sup> spark, affecting both calcium and voltage clocks.

## Materials and methods

*KI mice.* RyR<sub>2</sub><sup>R420Q</sup> mice were created by the Institute Clinique de la Souris. Mutation converted arginine residue at amino acid 420 to glutamine.

Experiments were performed on male and female mice heterozygous for RyR<sub>2</sub><sup>R420Q</sup> and their wild-type (WT) littermates (aged about 6 months) in accordance with the ethics principles laid down by the French Ministry of Agriculture and ECC directive 86/609/ECC.

*In vivo telemetric ECG recording.* To monitor ECGs in awake free-moving mice, the transmitters (7 ETA-F10) were implanted subcutaneously to the mice. The negative lead was placed on the upper right chest, and the positive lead was placed on the left abdomen below the left diaphragm and below the heart. During the subcutaneous implantation of ECG transmitter the mouse was placed on a warm pad (37°C). Anesthesia was induced with an Isoflurane (2.5%) inhalation apparatus for anesthesia induction. During surgery, the animal was continuously receiving isoflurane (1.5%). At least 7 days after surgery, ECGs were recorded in resting conditions and 5min after epinephrine/caffeine (2/120 mg/kg, i.p.) or iso (1 mg/kg, i.p.) challenge. Data were collected with a signal transmitter receiver (DSI) connected to a data acquisition system, and analyzed with ECG auto software (EMKA Technologies).

*In vitro intact SAN cells recording.* Mice were anesthetized by sodium pentobarbital (50 mg/kg i.p.). The hearts were quickly removed from the animal and placed in Tyrode solution (NaCl 140 mM, KCl 5.4 mM, CaCl<sub>2</sub> 1.8 mM, MgCl<sub>2</sub> 1 mM, HEPES 5 mM, and glucose 5.5 mM, pH 7.4, titrated with NaOH). The solution was oxygenated to saturation and maintained at 37°C. SAN and some surrounding atrial tissue were dissected and pinned down with the endocardial side up in home-made optical chambers bathed with Tyrode solution as previously described<sup>15</sup>. The tissue was loaded with fluo-4 AM (30 μM) during 60 min at 37°C. Images were recorded with a resonant scanning confocal microscope Leica SP5, equipped with a white laser fitted to 500 nm. Excitation was collected at >510nm. 2 D and xt images were recorded from the primary pacemaker region. Experiments and recordings were performed at 37°C. Analysis was made in IDL (Exelis Visual Inc.) by homemade routines.

*Western blot.* SAN samples were lysed by Bertin homogenizer with RIPA lysis buffer, run on 4%-20% discontinuous gradient polyacrylamide gels and transferred to PVDF membranes. PVDF membranes were incubated with blocking buffer of TBS with Tween-20 (1%) and nonfat dry milk (5%). Membranes were then incubated with primary antibodies diluted in 5% milk TBS overnight at 4°C, followed by the secondary antibodies. HCN4 primary antibody was a generous sample from Alomone Labs (APC-052). Antigen complexes were visualized with ChemiDoc and quantified with Image J.

#### *Isolation of Sinoatrial Node Myocytes*

SAN myocytes were isolated from WT and RyR<sub>2</sub><sup>R420Q</sup> KI mice as previously described<sup>37</sup>.

Briefly, mice were anesthetized using 0.01 mg/g xylazine (2% Rompun; Bayer AG) and 0.1 mg/g ketamine (Imalgène; Merial), and beating hearts were quickly removed.

The SAN regions were excised in prewarmed (35 °C) Tyrode's solution containing (in mM/L): 140 NaCl, 5.4 KCl, 1.8 CaCl<sub>2</sub>, 1 MgCl<sub>2</sub>, 5 HEPES-NaOH, and 5.5 D-glucose; adjusted to pH 7.4 with NaOH. SAN tissue strips were then transferred into a "low-Ca<sup>2+</sup>-low-Mg<sup>2+</sup>" solution containing (in mM/L): 140 NaCl, 5.4 KCl, 0.5 MgCl<sub>2</sub>, 0.2 CaCl<sub>2</sub>, 1.2 KH<sub>2</sub>PO<sub>4</sub>, 50 taurine, 5.5 D-glucose, 1 mg/mL BSA, and 5 HEPES-NaOH; adjusted to pH 6.9 with NaOH. Tissue was digested by Liberase TH (229 U/mL; Roche), elastase (1.9 U/mL; Boehringer Mannheim), and 200 μM CaCl<sub>2</sub>. Digestion was carried out for 9–13 min at 35 °C, under manual mechanical agitation. Tissue strips were then washed and transferred into a modified "Kraftbrühe" (KB) medium containing (in mM/L): 70 L-glutamic acid, 20 KCl, 80 KOH, 10 (±)D-β-OH-butyric acid, 10 KH<sub>2</sub>PO<sub>4</sub>, 10 taurine, 1 mg/mL BSA, and 10 HEPES-KOH; adjusted to pH 7.4 with KOH. Single SAN myocytes were then isolated by agitation in KB solution at 35 °C. Cellular automaticity was restored by readapting the cells to a physiological extracellular Ca<sup>2+</sup> concentration by addition of a solution containing (in mM/L): 10 NaCl, 1.8 CaCl<sub>2</sub>, and normal Tyrode's solution containing BSA (1 mg/mL). The final cell storage solution contained (in mM/L): 100 NaCl, 35 KCl, 1.3 CaCl<sub>2</sub>, 0.7 MgCl<sub>2</sub>, 14 L-glutamic acid, 2 (±)D-β-OH-butyric acid, 2 KH<sub>2</sub>PO<sub>4</sub>, 2 taurine, 1 mg/mL BSA (pH 7.4).

*Patch-clamp recordings of SAN myocytes.* The extracellular Tyrode's solution used in all recordings contained (in mM): 140.0 NaCl, 5.4 KCl, 1.8 CaCl<sub>2</sub>, 1.0 MgCl<sub>2</sub>, 5.0 HEPES-NaOH, 5.5 and d-glucose (adjusted to pH 7.4 with NaOH).

I<sub>f</sub> and I<sub>CaL</sub> were recorded under standard whole-cell configuration. Patch-clamp electrodes had a resistance of 4–5MΩ when filled with an intracellular solution containing (mM): K<sup>+</sup>-aspartate 130, NaCl 10.0, ATP-Na<sup>+</sup> salt 2.0, creatine phosphate 6.6, GTP-Mg<sup>2+</sup> 0.1, CaCl<sub>2</sub> 0.04 (pCa 7.0) and HEPES-KOH 10.0 (adjusted to pH 7.2 with KOH). To properly quantify I<sub>f</sub> current densities 2 mM BaCl<sub>2</sub> was added to standard Tyrode to block I<sub>K1</sub>. For I<sub>CaL</sub> recording, 10 mmol/L BAPTA was added when requested by the protocol.

The inward current evoked by rapid application (spritz) of caffeine 10mM was measured at holding potential of -45mV. All currents were recorded using an Axopatch 700B amplifier (Molecular Devices), acquired with Clampex (pClamp9; Molecular Devices), and analyzed with Prism 6 software (GraphPad software). Signals were sampled at 10 kHz and low-pass filtered at 5 kHz. The recording temperature was set to 36°. All chemicals were from SIGMA (St Quentin Fallavier, France).

### **Statistics.**

2-way ANOVA was used for multiple comparisons. An unpaired t test was used to compare 2 independent groups. A paired t test was used to compare measurements made in the same mice or in the same cells under 2 different conditions. A value of P<0.05 was considered significant. Results are expressed as mean±SEM.

### **Study approval**

Animal study was approved by the French Ministry (Ministère de l'Éducation Nationale, de l'Enseignement supérieur et de la recherche) n° B9201901. Written consent was given by the patients prior to the inclusion in this study.

## **AUTHOR CONTRIBUTIONS**

YYW did all the in-vitro confocal experiments and analysis, telemetry implants surgery, genotyping, some of the in-vivo recordings and analysis, and participated with the manuscript preparation. PM did the patch-clamp experiments and analysis, and edited the manuscript. EMS did the ECG arrhythmia analysis, AZJr did the firsts ECGs implants surgery, recording and analysis. OV did some ECG recording and analysis. EZ participated with clinical data, supervised arrhythmia analysis, and edited the manuscript. MM supervised the patch-clamp experiments and edited the manuscript. JPB supervised most of the work, and edited the manuscript. AMG supervised the work, wrote the IDL programs for analyses of confocal images, helped with analyses and wrote the manuscript.

## **ACKNOWLEDGEMENTS**

This work was supported by a collaborative ANR (Agence Nationale de la Recherche) Grant to AMG, MM and EZ (ANR-13-BSV1-0023) and to JPB (ANR-15) and also the Instituto de Salud Carlos III, FEDER “Union Europea, Una forma de hacer Europa” (RD12/0042/0029, PI14/01477), YYW was a recipient of the CSC (Chinese Science Council) doctoral fellowship, and AZJr a post-doctoral fellowship from University Paris-Sud. We want to thank CORDDIM for funding, which helped us to buy the resonant confocal microscope (Equipment 2010) and the telemetry system.

Authors wish to thank the help of the ANIMEX platform for taking care of the mice line, especially Pauline Roberts and Valérie Domergue. We thank also Françoise Boussac for administrative assistance, and Jean-Jacques Mercadier and Bertrand Crozatier for fruitful discussions. UMR-S 1180 is part of the LabEx LERMIT.



## Figures

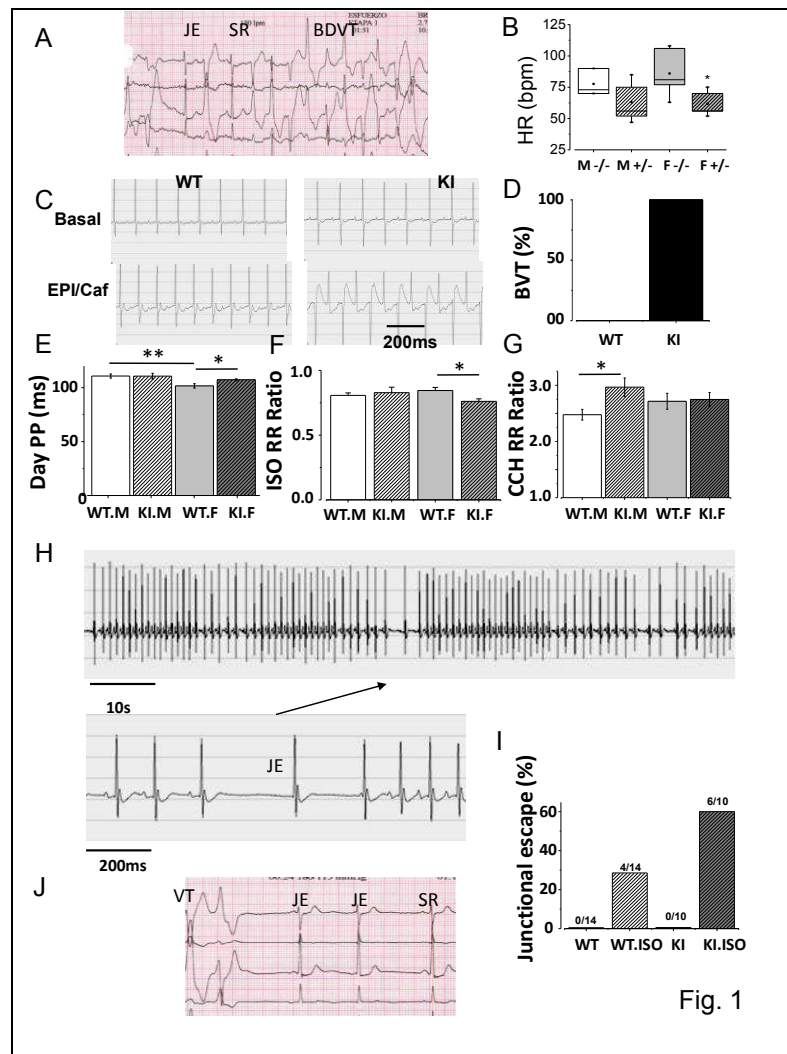


**Figure 1.** KI  $RyR_2^{R420Q}$  mice have CPVT phenotype and sinus dysfunction. **A.** Exercise test in a family member positive for the  $RyR_2^{R420Q}$  mutation. **B.** heart rate (beats per minute, bpm) of the family members without the mutation (-/-) or heterozygous for the  $RyR_2^{R420Q}$  mutation (+/-), male (M) and females (F). Only data before any b-blocker was taken. We did not include two babies (3 and 24 months at the time of the recording) and 4 brothers who were marathon runners. N in data is 3 M-/-, 5M+/-, 6F-/-, and 5 F+/- . 2 way ANOVA revealed a genotype statistical difference at  $p=0.006$ . **C.** Representative examples of ECG recordings obtained before (top panels) and following (bottom panels) epinephrine (2 mg/Kg) + caffeine (120 mg/Kg) injection (i.p.) in a WT mouse (left) and a KI mouse (right). The KI mouse shows BVT after epinephrine/caffeine administration, characteristic of CPVT mice. **D.** After injection, all of the KI mice ( $n=7$ ) show BVT, but none of the WT ( $n=5$ ). **E.** PP intervals recorded during daytime. Female KI mice ( $n=9$ ) beat slower than WT ( $n=10$ ) during daytime. No difference was found for the males (WT  $n=10$  vs. KI  $n=11$ ). **F.** Isoproterenol (ISO, 1 mg/kg) decreased the RR interval in both males ( $n=6$ ) and females ( $n=6$ ), the KI females decreased proportionally more than WT. **G.** Carbachol (CCH, 0.25 mg/kg) increased the RR intervals in both males ( $n=7$ ) and females ( $n=6$ ). **H.** Example of ECG of a KI mice after isoproterenol injection showing a junctional escape beat (JE) marked by the arrow overcoming a transient severe decrease in sinus rate. Scale bar 10s. Below a portion of the same ECG is shown, with scale bar = 200 ms. **I.** Proportion of animals presenting junctional escapes after ISO injection. \* $p<0.05$ ; \*\* $p<0.01$ .

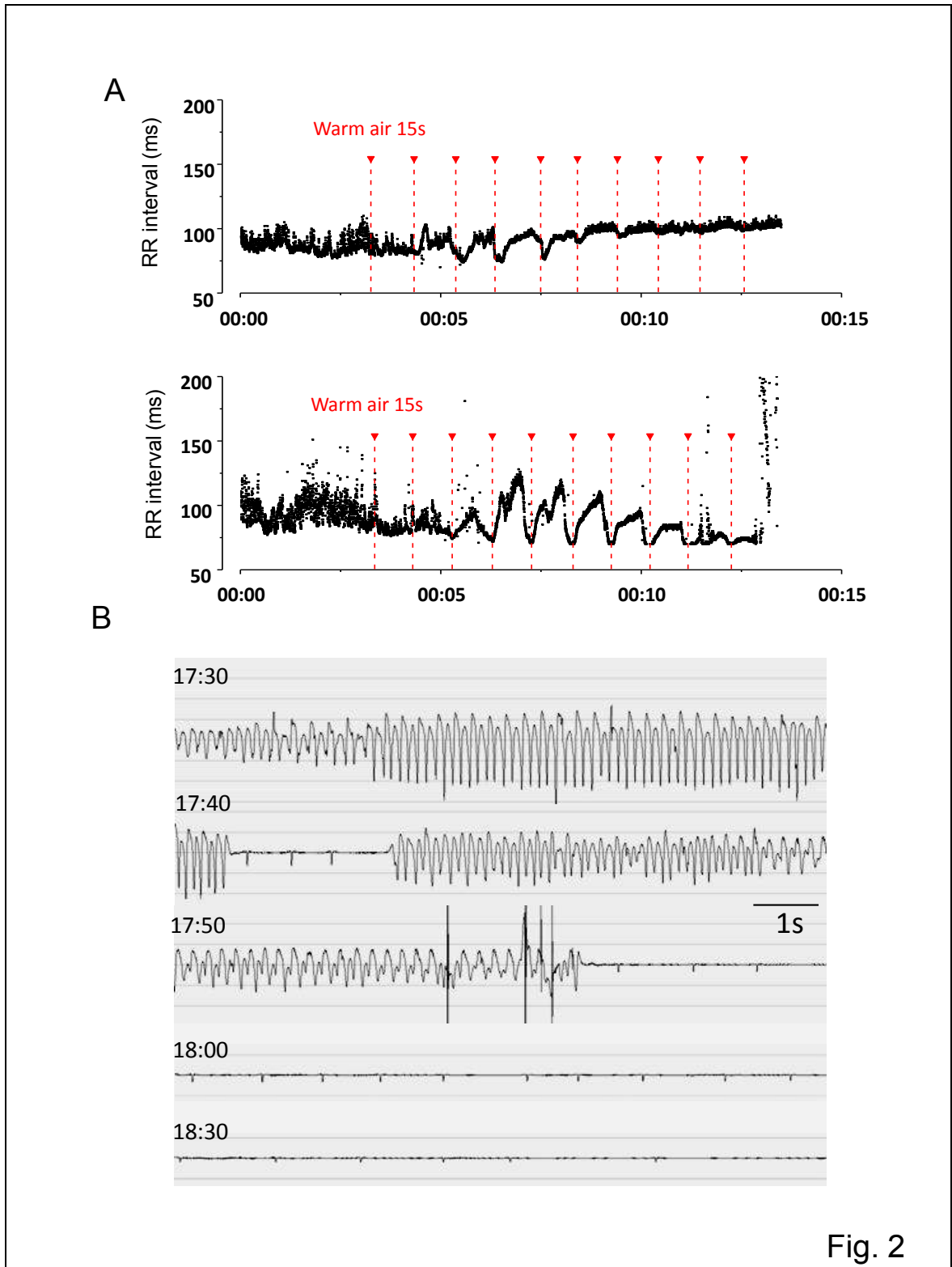


Fig. 2

**Figure 2.** KI mice show sinus dysfunction after emotional stress. **A.** RR intervals during emotional stress protocol in a WT (top) and a KI (bottom) mice. Red dashed line indicates the beginning of the 15s of warm air blowing, 45s rest was allowed before the next air blowing. **B.** An example of ECG recorded from a KI mouse, which died after the blowing stress. On the left, a time reference is provided. Horizontal scale 1s. After ventricular tachycardia and a progressively slower ventricular escape rhythm, the mouse died in asystolia.

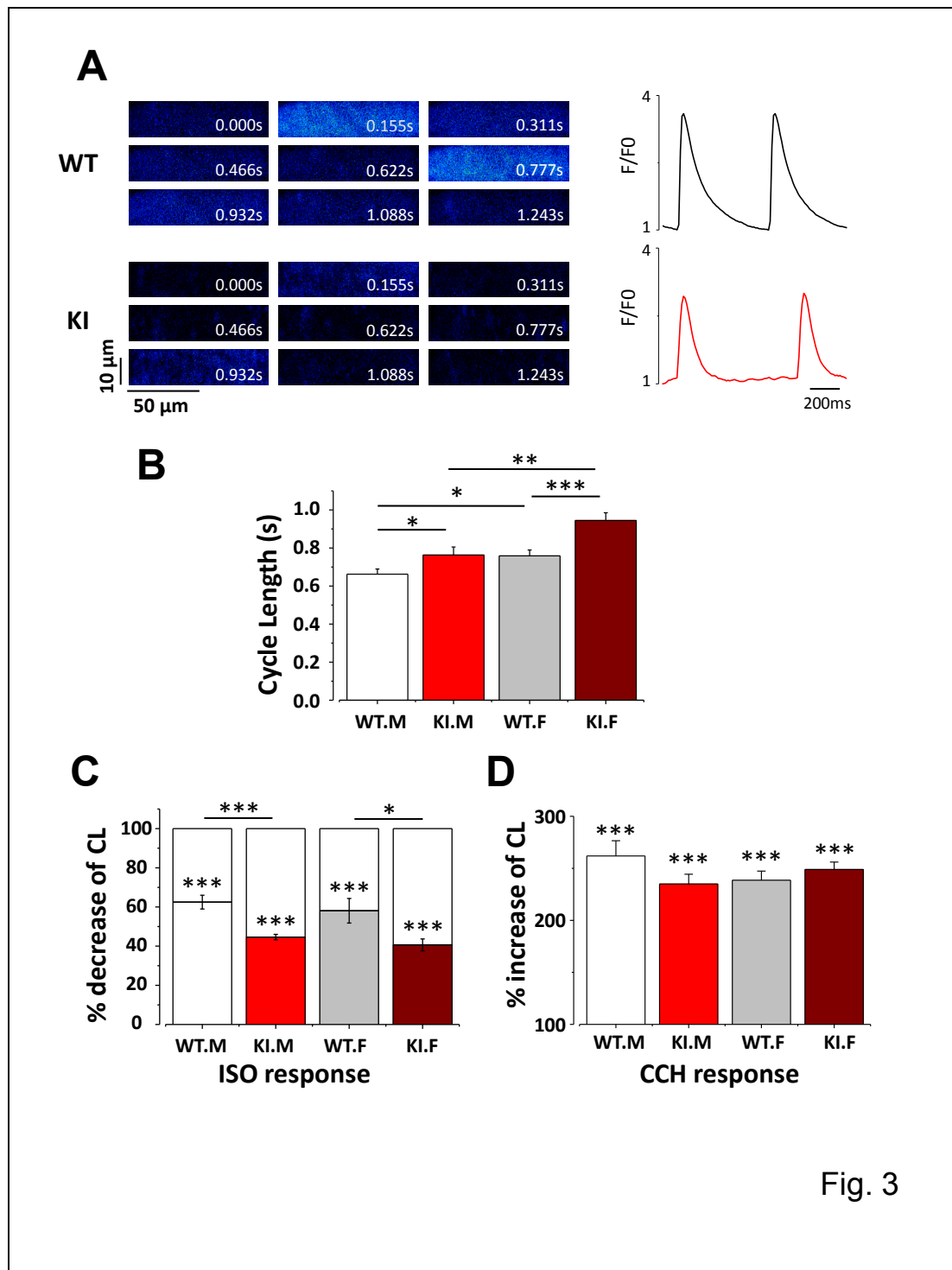
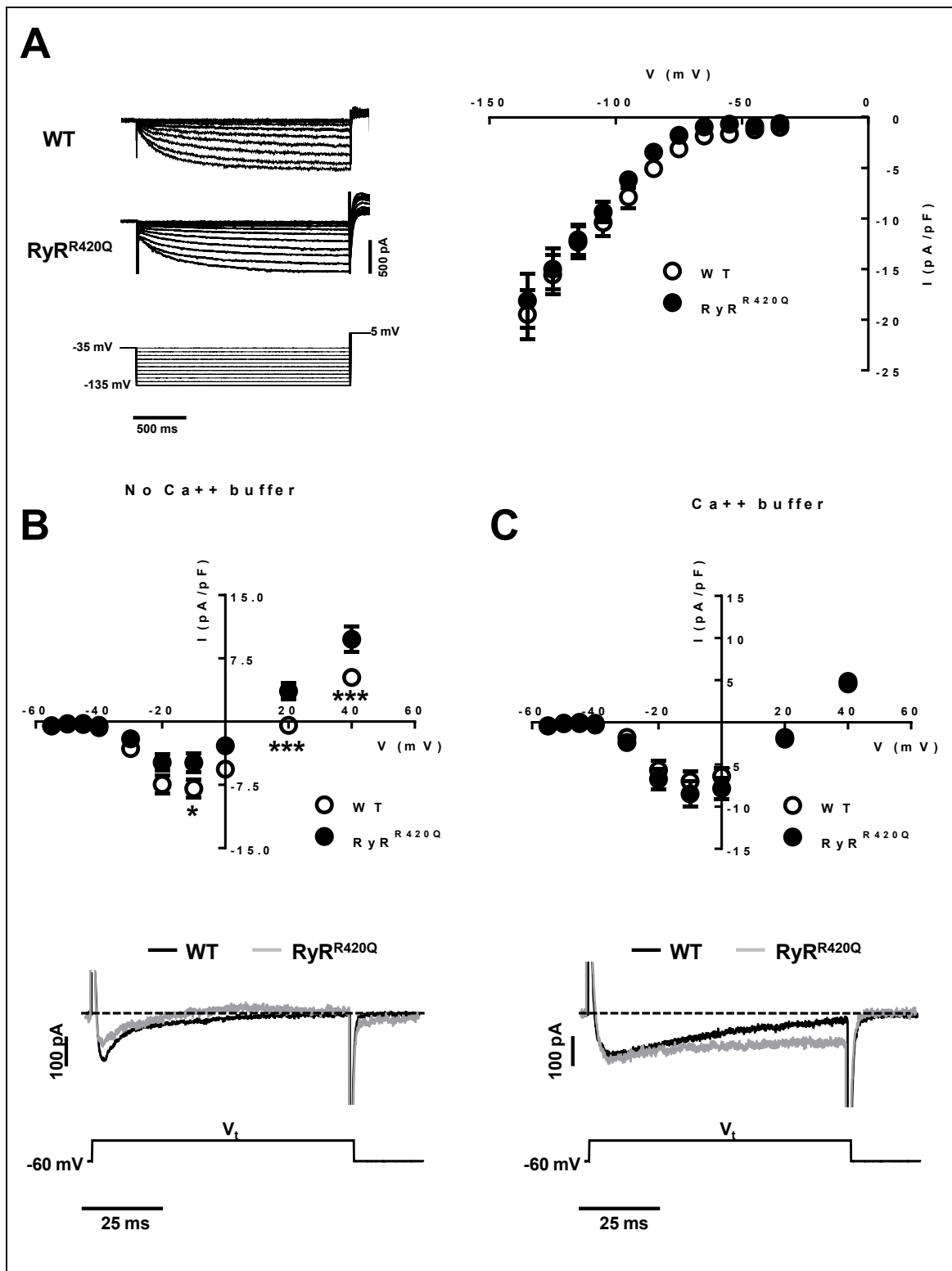


Fig. 3

**Figure 3.** Cycle length (CL) in sinoatrial node (SAN) cells is longer in KI than in WT animals. **A.** Example of 2D confocal images (left) of SAN cells within the intact SAN and the corresponding fluorescence traces (right) in WT (upper) and KI (lower) SAN cell. **B.** The CLs of male WT (n=44 cells from 7 mice) and KI (n=37 cells from 6 mice), and female WT (n=61 cells from 8 mice) and KI mice (n=50 cells from 8 mice). KI mice have markedly longer CL than WT. **C.** ISO decreases CL in all type of SAN, while the response in KI SAN (male: n=18 cells from 3 mice, female: n=22 cells from 3 mice) is larger than in WT (male: n=19 cells from 3 mice, female: n=25 cells from 4 mice). **D.** CCH increases CL in all SAN cells, and no difference between genotype nor sex was observed (WT, male: n=26 cells from 3 mice, female: n=41 cells from 4 mice; KI, male: n=30 cells from 3 mice, female: n=25 cells from 3 mice). \*p<0.05; \*\*p<0.01; \*\*\*p<0.001. Two way ANOVA.



**Figure 4.**  $I_f$  is normal, but  $I_{Ca}$  is depressed in KI SAN cells. **A**, left, family traces of  $I_f$  in a WT (top) and KI (middle) cell. Below is the voltage protocol.  $I_f$  current-voltage relationship in WT cells (open circles) and KI cells (black circles). **B**. Averaged current-voltage curves of  $I_{Ca}$  in isolated SAN cells in unbuffered intrapippete solution. **C**. The same as in C but with \*\*\* mM BAPTA in the intracellular solution. \* $p < 0.05$ ; \*\* $p < 0.01$ ; \*\*\* $p < 0.001$ .

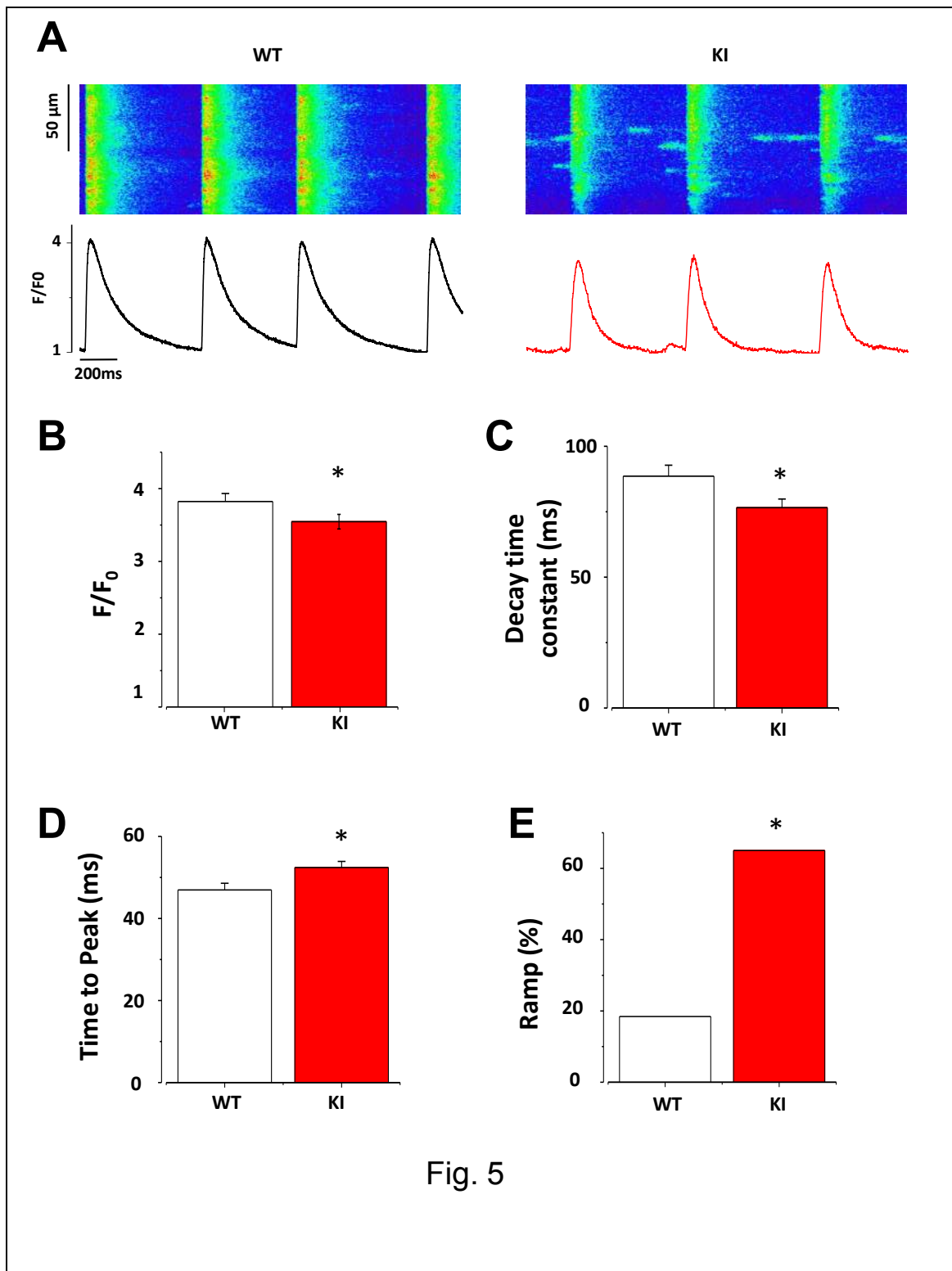


Fig. 5

**Figure 5.** Characteristics of  $[\text{Ca}^{2+}]_i$  transients are altered in SAN cells from KI mice. **A.** Examples of line-scan confocal images showing  $[\text{Ca}^{2+}]_i$  transients from WT (upper) and KI (lower) SAN cells. **B.**  $[\text{Ca}^{2+}]_i$  transient amplitude (measured as peak,  $F/F_0$ , where  $F$  is the fluorescence trace and  $F_0$  the fluorescence during the diastolic period). **C.** KI SAN cells have significant smaller decay time constant (obtained by fitting the decay portion of the fluorescence trace to a single exponential). **D.** Time to peak is longer in KI SAN cells. WT  $n=102$  cells from 15 mice; KI  $n=81$  cells from 14 mice. **E.** Percentage of cells that present a ramp (late diastolic  $\text{Ca}^{2+}$  release). WT, white bars; KI, red bars \* $p<0.05$

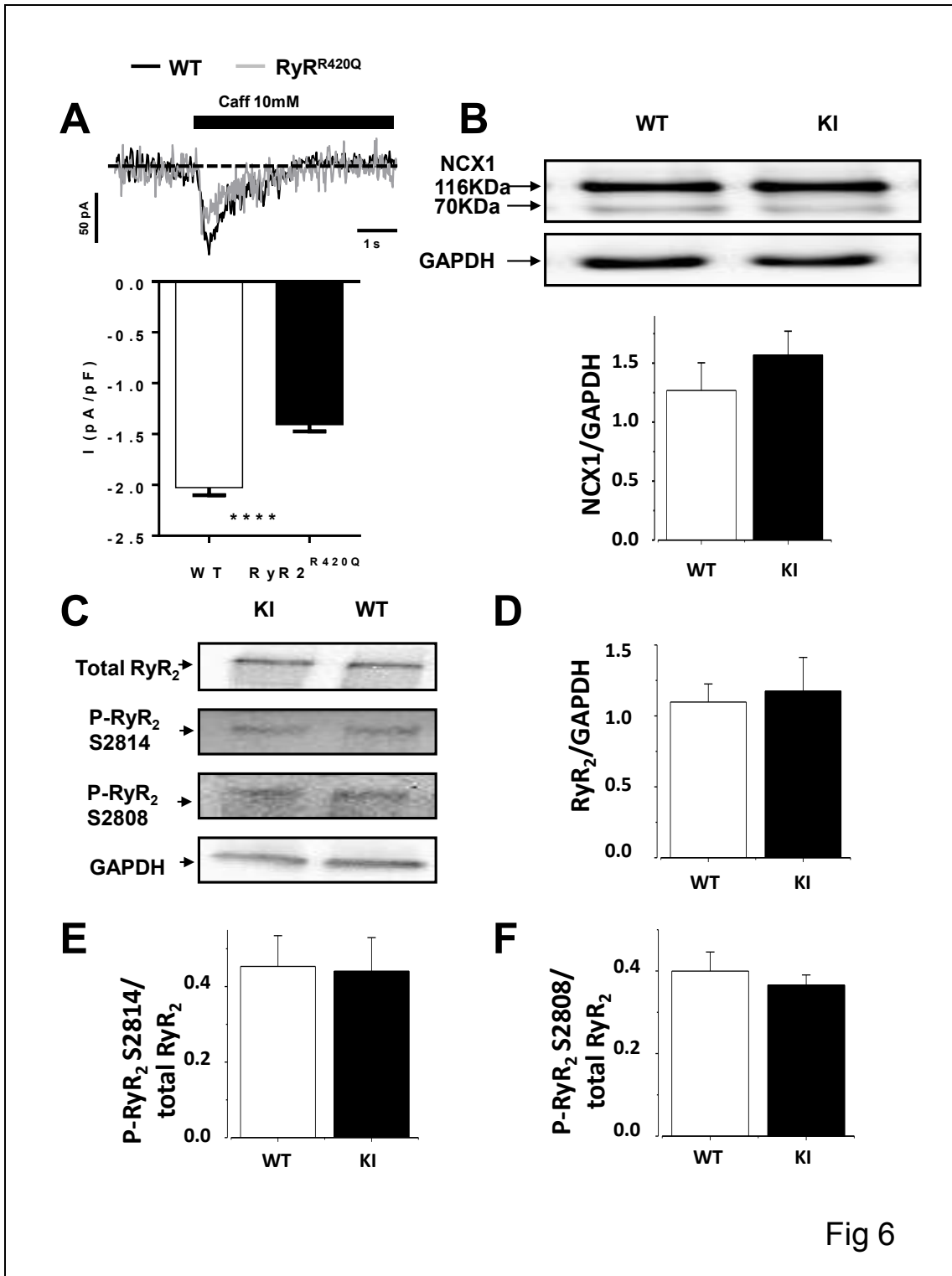
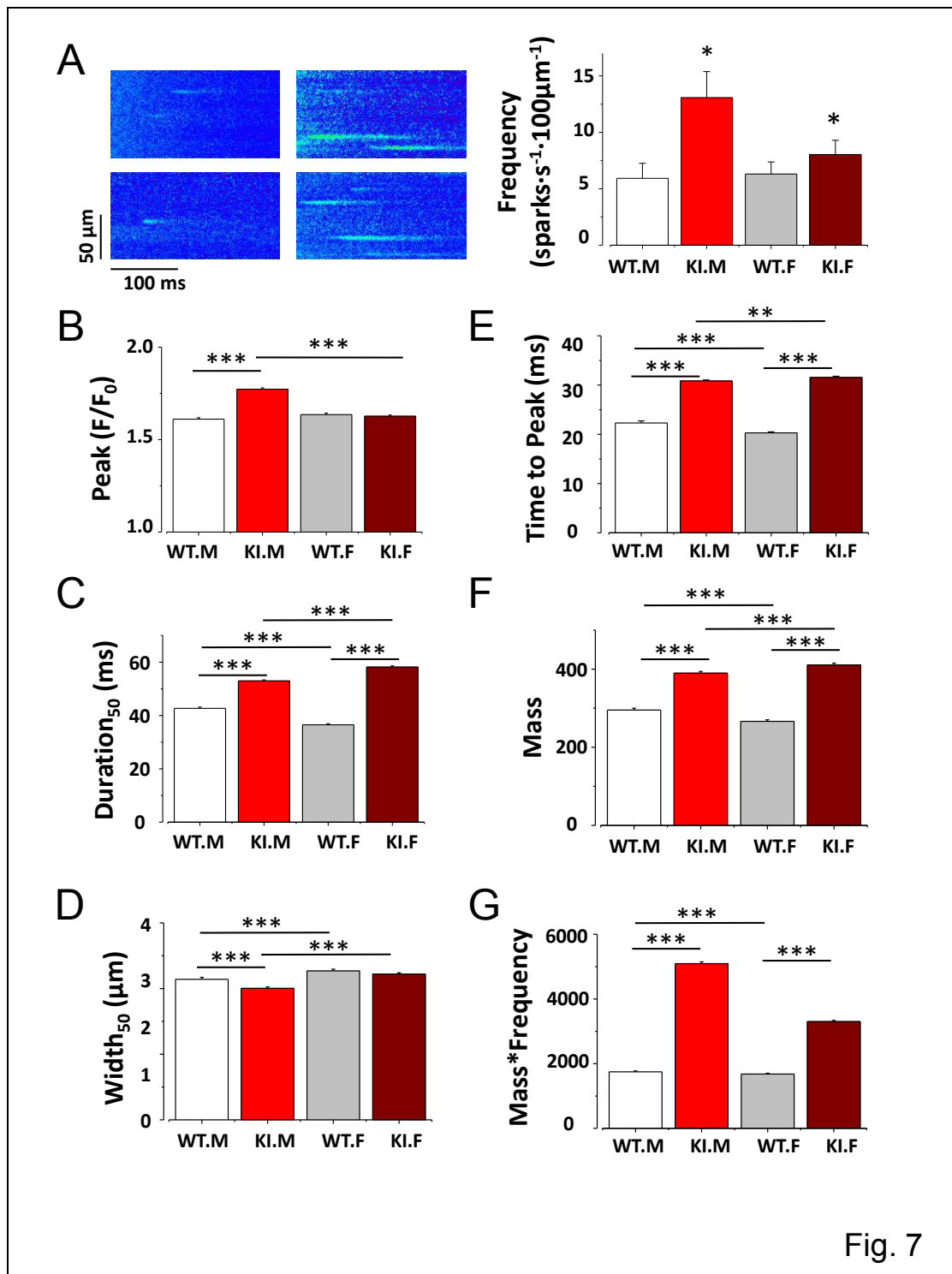


Fig 6

**Figure 6.** Caffeine-evoked inward current was significantly smaller in KI than in WT SAN cells. **A.** Averaged transient inward current evoked by rapid caffeine application to WT SAN cells and KI cells. **B.** NCX expression is unchanged between KI and WT. **C.** Examples of blots obtained for total or phosphorylated RyR<sub>2</sub>. **D-F.** Total RyR<sub>2</sub> expression (C) and phosphorylated (S2814, E and S2808, F) RyR<sub>2</sub> expression are unaltered. N = 4 mice each. White bar, WT, black bar, KI. \*p<0.05



**Figure 7.** KI SAN cells show enhanced Ca<sup>2+</sup> release through Ca<sup>2+</sup> sparks. **A.** Left: Examples of line-scan images of SAN cells within the intact SAN in WT and KI mice (left: WT, right: KI, Top: males, bottom: females). Right: Ca<sup>2+</sup> sparks frequency (number of sparks / s /100 μm) recorded from 38 cells of 7 WT males, 37 cells from 6 KI males, 47 cells from 8 WT females and 44 cells from 8 KI females. **B.** Ca<sup>2+</sup> sparks amplitude (measured as peak F/F<sub>0</sub> as in Fig.5) **C.** Duration at 50% of maximum amplitude, **D.** Width at 50% of maximum amplitude. Females KI mice present Ca<sup>2+</sup> sparks of longer duration (D) than WT. **E.** Time to peak. **F.** Ca<sup>2+</sup> spark mass (amplitude \* width \* duration). **G.** Total Ca<sup>2+</sup> leak through Ca<sup>2+</sup> sparks (Ca<sup>2+</sup> spark mass \* frequency). White bars, male WT; red bars, male KI; gray bars, female WT; dark red bars, female KI. \*p<0.05; \*\*p<0.01; \*\*\*p<0.001.

1. Leenhardt A, Lucet V, Denjoy I, Grau F, Ngoc DD, Coumel P. Catecholaminergic polymorphic ventricular tachycardia in children. A 7-year follow-up of 21 patients. *Circulation*. 1995;91:1512-1519
2. Postma AV, Denjoy I, Kamblock J, Alders M, Lupoglazoff JM, Vaksman G, Dubosq-Bidot L, Sebillon P, Mannens MM, Guicheney P, Wilde AA. Catecholaminergic polymorphic ventricular tachycardia: Ryr2 mutations, bradycardia, and follow up of the patients. *Journal of medical genetics*. 2005;42:863-870
3. Sumitomo N, Sakurada H, Taniguchi K, Matsumura M, Abe O, Miyashita M, Kanamaru H, Karasawa K, Ayusawa M, Fukamizu S, Nagaoka I, Horie M, Harada K, Hiraoka M. Association of atrial arrhythmia and sinus node dysfunction in patients with catecholaminergic polymorphic ventricular tachycardia. *Circ J*. 2007;71:1606-1609
4. Domingo D, Neco P, Fernandez-Pons E, Zissimopoulos S, Molina P, Olague J, Suarez-Mier MP, Lai FA, Gomez AM, Zorio E. Non-ventricular, clinical, and functional features of the ryr2(r420q) mutation causing catecholaminergic polymorphic ventricular tachycardia. *Rev Esp Cardiol (Engl Ed)*. 2015;68:398-407
5. Sy RW GM, Klein GJ, Yee R, Skanes AC, Gula LJ, Leong-Sit P, Gow RM, Green MS, Birnie DH, Krahn AD. Arrhythmia characterization and long-term outcomes in catecholaminergic polymorphic ventricular tachycardia. *Heart Rhythm*. 2011;8:864-871
6. van der Werf C, Kannankeril PJ, Sacher F, Krahn AD, Viskin S, Leenhardt A, Shimizu W, Sumitomo N, Fish FA, Bhuiyan ZA, Willems AR, van der Veen MJ, Watanabe H, Laborderie J, Haissaguerre M, Knollmann BC, Wilde AA. Flecainide therapy reduces exercise-induced ventricular arrhythmias in patients with catecholaminergic polymorphic ventricular tachycardia. *J Am Coll Cardiol*. 2011;57:2244-2254
7. DiFrancesco D. The role of the funny current in pacemaker activity. *Circ Res*. 2010;106:434-446
8. Lakatta EG MV, Vinogradova TM. A coupled system of intracellular ca<sup>2+</sup> clocks and surface membrane voltage clocks controls the timekeeping mechanism of the heart's pacemaker. *Circ Res*. 2010;106:659-673
9. Rubenstein DS, Lipsius SL. Mechanisms of automaticity in subsidiary pacemakers from cat right atrium. *Circ Res*. 1989;64:648-657
10. Rigg L TD. Possible role of calcium release from the sarcoplasmic reticulum in pacemaking in guinea-pig sino-atrial node. *Exp Physiol*. 1996;81:877-880
11. Rigg L, Heath BM, Cui Y, Terrar DA. Localisation and functional significance of ryanodine receptors during beta-adrenoceptor stimulation in the guinea-pig sino-atrial node. *Cardiovasc Res*. 2000;48:254-264
12. Lyashkov AE, Juhaszova M, Dobrzynski H, Vinogradova TM, Maltsev VA, Juhasz O, Spurgeon HA, Sollott SJ, Lakatta EG. Calcium cycling protein density and functional importance to automaticity of isolated sinoatrial nodal cells are independent of cell size. *Circ Res*. 2007;100:1723-1731
13. Maltsev VA, Yaniv Y, Maltsev AV, Stern MD, Lakatta EG. Modern perspectives on numerical modeling of cardiac pacemaker cell. *Journal of pharmacological sciences*. 2014;125:6-38
14. Broun MJ, Asghari P, Wambolt RB, Bohunek L, Smits C, Philit M, Kieffer TJ, Lakatta EG, Boheler KR, Moore ED, Allard MF, Johnson JD. Cardiac ryanodine receptors control heart rate and rhythmicity in adult mice. *Cardiovasc Res*. 2012;96:372-380



15. Neco P, Torrente A, Mesirca P, Zorio E, Liu N, Priori S, Napolitano C, Richard S, Benitah J, Mangoni M, Gómez A. Paradoxical effect of increased diastolic  $Ca^{2+}$  release and decreased sinoatrial node activity in a mouse model of catecholaminergic polymorphic ventricular tachycardia. *Circulation*. 2012;126:392-401
16. Zissimopoulos S, Lai FA. Ryanodine receptor structure, function and pathophysiology. in *Calcium-A matter of life or death*. edited by Joachim Krebs and Marek Michalak. 2007;41:287-342
17. Iaccarino G, Barbato E, Cipolletta E, De Amicis V, Margulies KB, Leosco D, Trimarco B, Koch WJ. Elevated myocardial and lymphocyte grk2 expression and activity in human heart failure. *Eur Heart J*. 2005;26:1752-1758
18. Travin MI, Feng D, Taub CC. Novel imaging approaches for predicting arrhythmic risk. *Circulation. Cardiovascular imaging*. 2015;8:e003019
19. Teresinska A. Metaiodobenzylguanidine scintigraphy of cardiac sympathetic innervation. *Nuclear medicine review. Central & Eastern Europe*. 2012;15:61-70
20. Priori SG, Memmi M, Colombi B, Drago F, Gasparini M, DeSimone L, Coltorti F, Bloise R, Keegan R, Cruz Filho FE, Vignati G, Benatar A, DeLogu A. Clinical and molecular characterization of patients with catecholaminergic polymorphic ventricular tachycardia. *Circulation*. 2002;106:69-74
21. Medeiros-Domingo A, Tester DJ, et al. . The ryr2-encoded ryanodine receptor/calcium release channel in patients diagnosed previously with either catecholaminergic polymorphic ventricular tachycardia or genotype negative, exercise-induced long qt syndrome: A comprehensive open reading frame mutational analysis. *J Am Coll Cardiol*. 2009;54:2065–2074
22. Knollmann BC, Kirchhof P, Sirenko SG, Degen H, Greene AE, Schober T, Mackow JC, Fabritz L, Potter JD, Morad M. Familial hypertrophic cardiomyopathy-linked mutant troponin t causes stress-induced ventricular tachycardia and  $Ca^{2+}$ -dependent action potential remodeling. *Circ Res*. 2003;92:428-436
23. Mangoni ME, Nargeot J. Genesis and regulation of the heart automaticity. *Physiol Rev*. 2008;88:919-982
24. Fernández-Velasco M, Rueda A, Rizzi N, Benitah JP, Colombi B, Napolitano C, Priori SG, Richard S, Gómez AM. Increased  $Ca^{2+}$  sensitivity of the ryanodine receptor mutant ryr2r4496c underlies catecholaminergic polymorphic ventricular tachycardia. *Circ Res*. 2009;104:201-209, 212p following 209
25. Fernández-Velasco M, Ruiz-Hurtado G, Rueda A, Neco P, Mercado-Morales M, Delgado C, Napolitano C, Priori SG, Richard S, Gómez AM, Benitah JP. Ryrca2+ leak limits cardiac  $Ca^{2+}$  window current overcoming the tonic effect of calmodulinin mice. *PLoS One*. 2011;6:e20863
26. Parks RJ, Ray G, Bienvenu LA, Rose RA, Howlett SE. Sex differences in sr  $Ca^{2+}$  release in murine ventricular myocytes are regulated by the camp/pka pathway. *J Mol Cell Cardiol*. 2014;75:162-173
27. Parks RJ, Howlett SE. Sex differences in mechanisms of cardiac excitation-contraction coupling. *Pflugers Arch*. 2013;465:747-763
28. Britton A, Singh-Manoux A, Hnatkova K, Malik M, Marmot MG, Shipley M. The association between heart rate variability and cognitive impairment in middle-aged men and women. The whitehall ii cohort study. *Neuroepidemiology*. 2008;31:115-121
29. Dart AM, Du XJ, Kingwell BA. Gender, sex hormones and autonomic nervous control of the cardiovascular system. *Cardiovasc Res*. 2002;53:678-687
30. Lehnart SE, Mongillo M, Bellinger A, Lindegger N, Chen BX, Hsueh W, Reiken S, Wronska A, Drew LJ, Ward CW, Lederer WJ, Kass RS, Morley G, Marks AR. Leaky

- ca<sup>2+</sup> release channel/ryanodine receptor 2 causes seizures and sudden cardiac death in mice. *J Clin Invest*. 2008;118:2230-2245
31. Zhao YT, Valdivia CR, Gurrola GB, Powers PP, Willis BC, Moss RL, Jalife J, Valdivia HH. Arrhythmogenesis in a catecholaminergic polymorphic ventricular tachycardia mutation that depresses ryanodine receptor function. *Proc Natl Acad Sci U S A*. 2015;112:E1669-1677
  32. Nishio H, Iwata M, Suzuki K. Postmortem molecular screening for cardiac ryanodine receptor type 2 mutations in sudden unexplained death: R420W mutated case with characteristics of status thymico-lymphatics. *Circ J*. 2006;70:1402-1406
  33. Bauce B, Rampazzo A, Basso C, Bagattin A, Daliento L, Tiso N, Turrini P, Thiene G, Danieli GA, Nava A. Screening for ryanodine receptor type 2 mutations in families with effort-induced polymorphic ventricular arrhythmias and sudden death: Early diagnosis of asymptomatic carriers. *J Am Coll Cardiol*. 2002;40:341-349
  34. Itzhaki I, Maizels L, Huber I, Gepstein A, Arbel G, Caspi O, Miller L, Belhassen B, Nof E, Glikson M, Gepstein L. Modeling of catecholaminergic polymorphic ventricular tachycardia with patient-specific human-induced pluripotent stem cells. *J Am Coll Cardiol*. 2012;60:990-1000
  35. Kimlicka L, Tung CC, Carlsson AC, Lobo PA, Yuchi Z, Van Petegem F. The cardiac ryanodine receptor n-terminal region contains an anion binding site that is targeted by disease mutations. *Structure*. 2013;21:1440-1449
  36. Borko L, Bauerova-Hlinkova V, Hostinova E, Gasperik J, Beck K, Lai FA, Zahradnikova A, Sevcik J. Structural insights into the human ryr2 n-terminal region involved in cardiac arrhythmias. *Acta crystallographica. Section D, Biological crystallography*. 2014;70:2897-2912
  37. Mangoni M, Nargeot J. Properties of the hyperpolarization-activated current (i<sub>f</sub>) in isolated mouse sino-atrial cells. *Cardiovasc Res* 2001;52:51-64

### 3.1.2. Additional data on RyR<sub>2</sub><sup>R420Q</sup> SAN.

#### *Sex differences in RyR<sub>2</sub><sup>R420Q</sup> mice.*

As explained in the manuscript, in order to test the CPVT phenotype in RyR<sub>2</sub><sup>R420Q</sup> mice, we injected epi+caff (2mg/Kg+120mg/Kg), and measured ECG starting 5 minutes after injection to have comparable levels in the circulating blood and have them recovered from the handling and injection stress. All RyR<sub>2</sub><sup>R420Q</sup> mice showed bidirectional ventricular tachycardia, characteristic of CPVT in mice. The ECG was continuously recorded over night. We also measured the time in which the animals stayed in tachycardia after the injection. Figure 34 shows that males KI mice stayed in the arrhythmic state for longer time, showing a sex-dependent difference.

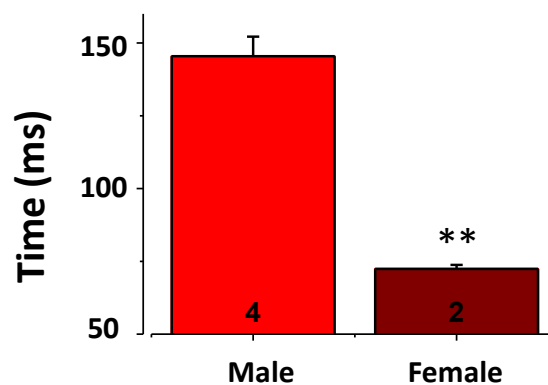


Figure 34. Duration of BVT. Female KI mice (n=2) stayed less time in BVT than males (n=4).

#### *Autonomic modulation of SAN Ca<sup>2+</sup> handling*

When analyzing the effect of ISO and CCH on spontaneous SAN activity, I also analyzed the effect on [Ca<sup>2+</sup>]<sub>i</sub> transients characteristics and Ca<sup>2+</sup> sparks. Fig. 35 shows [Ca<sup>2+</sup>]<sub>i</sub> transient amplitudes in WT and KI cells under basal conditions and during 20nM ISO or 500 nM CCH. Both ISO and CCH had the tendency to decrease [Ca<sup>2+</sup>]<sub>i</sub> transient amplitude in both WT and KI SAN cells. However, ISO had no significant effect, while CCH only significantly decreased [Ca<sup>2+</sup>]<sub>i</sub> transient amplitude in KI mice SAN cells, but not in WT.

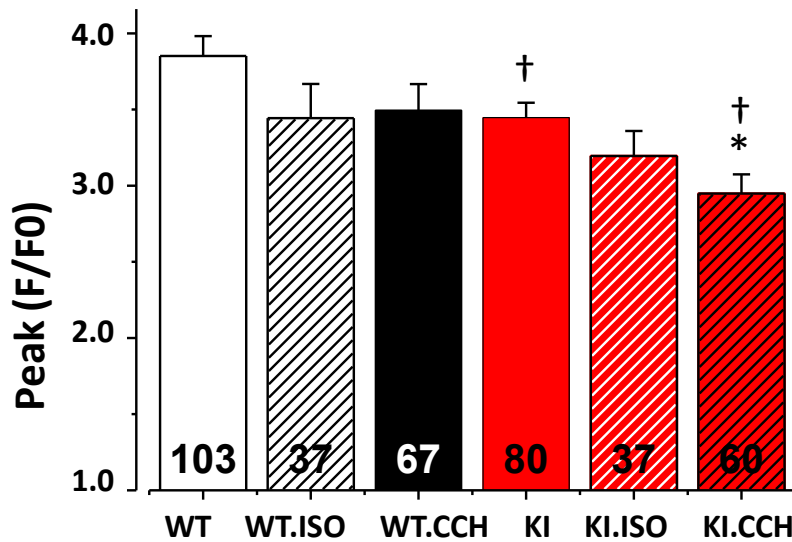


Figure 35. ISO and CCH effects on  $[Ca^{2+}]_i$  transient amplitudes. Bar graph showing peak  $[Ca^{2+}]_i$  transient amplitudes measured as peak F/F0 where F is the fluorescence trace and F0 the basal fluorescence during diastolic period. Numbers in each bar indicate cell number (animals: basal, 15 WT vs. 14 KI; ISO, 7 WT vs. 6KI; CCH, 7 WT vs. 6KI). WT, wildtype SAN. WT.ISO, wildtype SAN during ISO application. WT.CCH, wildtype SAN during carbachol application. KI, knock-in SAN. KI.ISO, knock-in SAN during ISO application. KI.CCH, knock-in SAN during carbachol application. \* $p < 0.05$ , compared before and after ISO/CCH stimulation. † $p < 0.05$ , compared between genotypes.

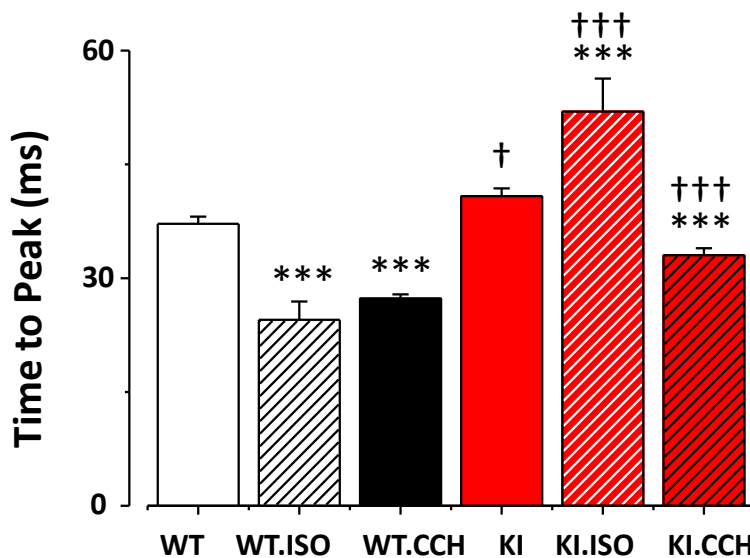


Figure 36. ISO and CCH effect on  $[Ca^{2+}]_i$  transient time to peak. Cell and mice numbers, and labels are as in Fig. 35. \* $p < 0.05$ , \*\* $P < 0.01$ , \*\*\* $P < 0.001$ , compared before and after ISO/CCH stimulation. † $p < 0.05$ , †† $P < 0.01$ , ††† $P < 0.001$ , compared between genotypes.

Next we addressed the analyses of  $[Ca^{2+}]_i$  transient kinetics under sympathetic and parasympathetic stimulation. Figure 36 and 37 show the time to peak and the decay time constant for the  $[Ca^{2+}]_i$  transient. The time to peak was shortened by ISO in WT, but prolonged in KI,

suggesting the defect in ISO response. In contrast, CCH decreased  $[Ca^{2+}]_i$  transient time to peak in both WT and KI SAN cells. Decay time constant was accelerated by ISO in both genotypes, although CCH had no effect.

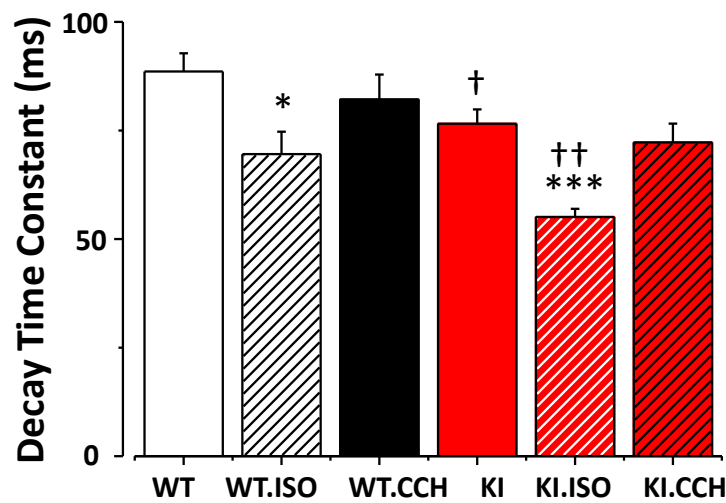


Figure 37. ISO and CCH effect on  $[Ca^{2+}]_i$  transient decay time. Bar graph showing  $[Ca^{2+}]_i$  transient decay time (Tau) obtained by fitting the descending portion of the fluorescence trace to a single exponential. Cell and mice numbers, and labels are as in Fig. 35. \* $p < 0.05$ , \*\*\* $P < 0.001$ , compared before and after ISO/CCH stimulation. † $p < 0.05$ , †† $P < 0.01$ , compared between genotypes.

In SAN tissue, not all cells show the late diastolic  $Ca^{2+}$  release, measured as a ramp. The percentage of cells in which this ramp was recorded is presented in Fig 38A. WT had more ramp occurrence than KI as we discussed previously in basal condition as described in manuscript. ISO significantly enhanced ramp occurrence in both genotypes, while KI had much more than WT. In contrast, CCH did not alter ramp occurrence in WT and KI, but KI still had more than WT. In basal condition, KI has significant weaker ramp peak than WT. ISO increased ramp peak in KI SAN cells reaching the same level as WT, but this effect is not observed in WT (Figure 38B). Ramp peak is decreased significantly by CCH in WT, but not in KI resulting in the relatively greater ramp peak in KI after CCH stimulation. Ramp time to peak was unaltered by ISO regardless WT or KI (Figure 38C). However, CCH causes converse response in WT and KI. WT has significantly decreased ramp time to peak, but KI showed opposite results.

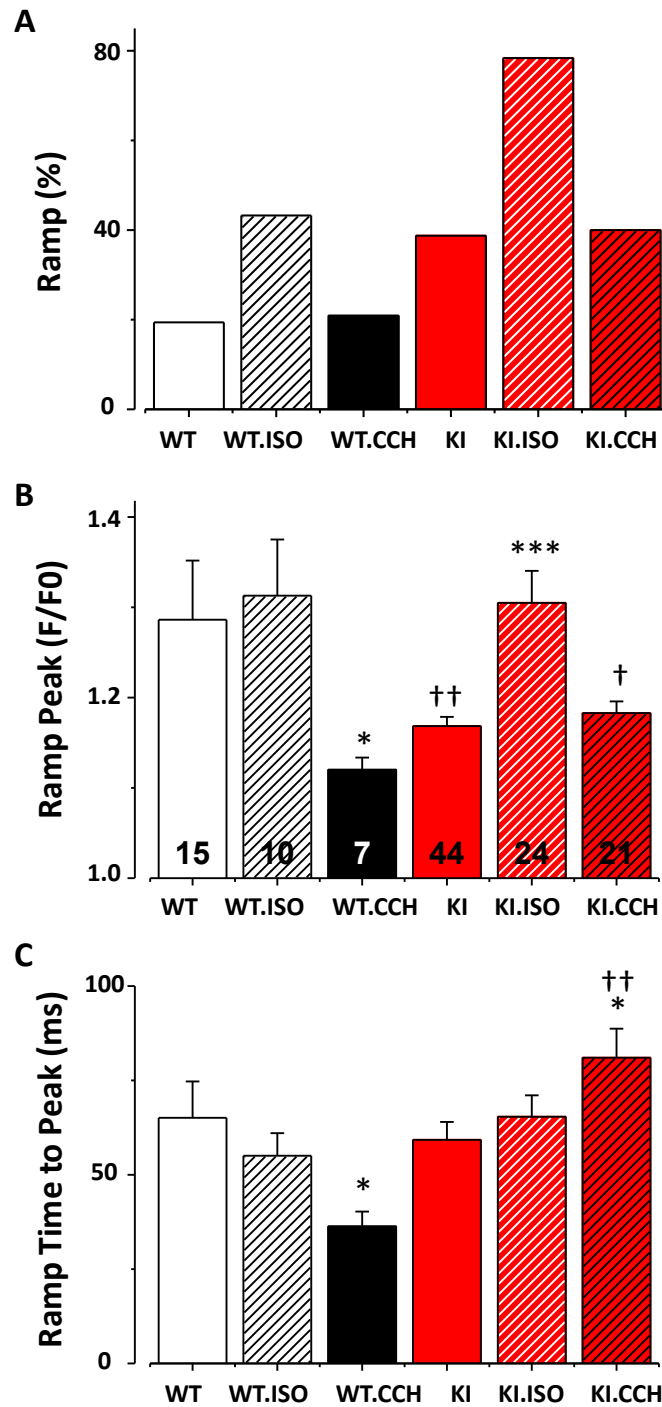


Figure 38. ISO and CCH effect on  $[Ca^{2+}]_i$  transient ramp. A. Percentage of cells where ramp was observed at least once over the 20 s recording period. Total number of cells in each group is the same than in Fig. 35. B. Maximum value of  $Ca^{2+}$  ramp, just before the upstroke of  $[Ca^{2+}]_i$  transient, measured as in Fig. 35. Numbers in each bar indicate number of cells with ramp (from mice: basal, 15 WT vs. 14 KI; ISO, 7 WT vs. 6KI; CCH, 7 WT vs. 6KI). C. Time to peak of ramp, measured from the same Cells as in panel B. \* $p < 0.05$ , \*\*\* $P < 0.001$ , compared before and after ISO/CCH stimulation. † $p < 0.05$ , †† $P < 0.01$ , compared between genotypes. Labels are as in Fig. 35.

Under ISO, the  $[Ca^{2+}]_i$  transient enhanced frequency and the extremely high diastolic  $Ca^{2+}$  release precluded us to accurately measure individual  $Ca^{2+}$  sparks.  $Ca^{2+}$  sparks analysis under CCH application is presented in Fig 39. CCH decreased  $Ca^{2+}$  spark frequency only in KI females, while

the others have no change.  $\text{Ca}^{2+}$  spark amplitude is decreased in WT male and female after CCH stimulation, but increased in KI male and female. Besides,  $\text{Ca}^{2+}$  spark duration is shortened in both WT and KI by CCH, but KI still have longer sparks than WT. Eventually,  $\text{Ca}^{2+}$  release as sparks (per spark, Figure 39 E; per second per 100 $\mu\text{m}$ , Figure 39 F) during DD is significantly higher in KI than in WT cells.

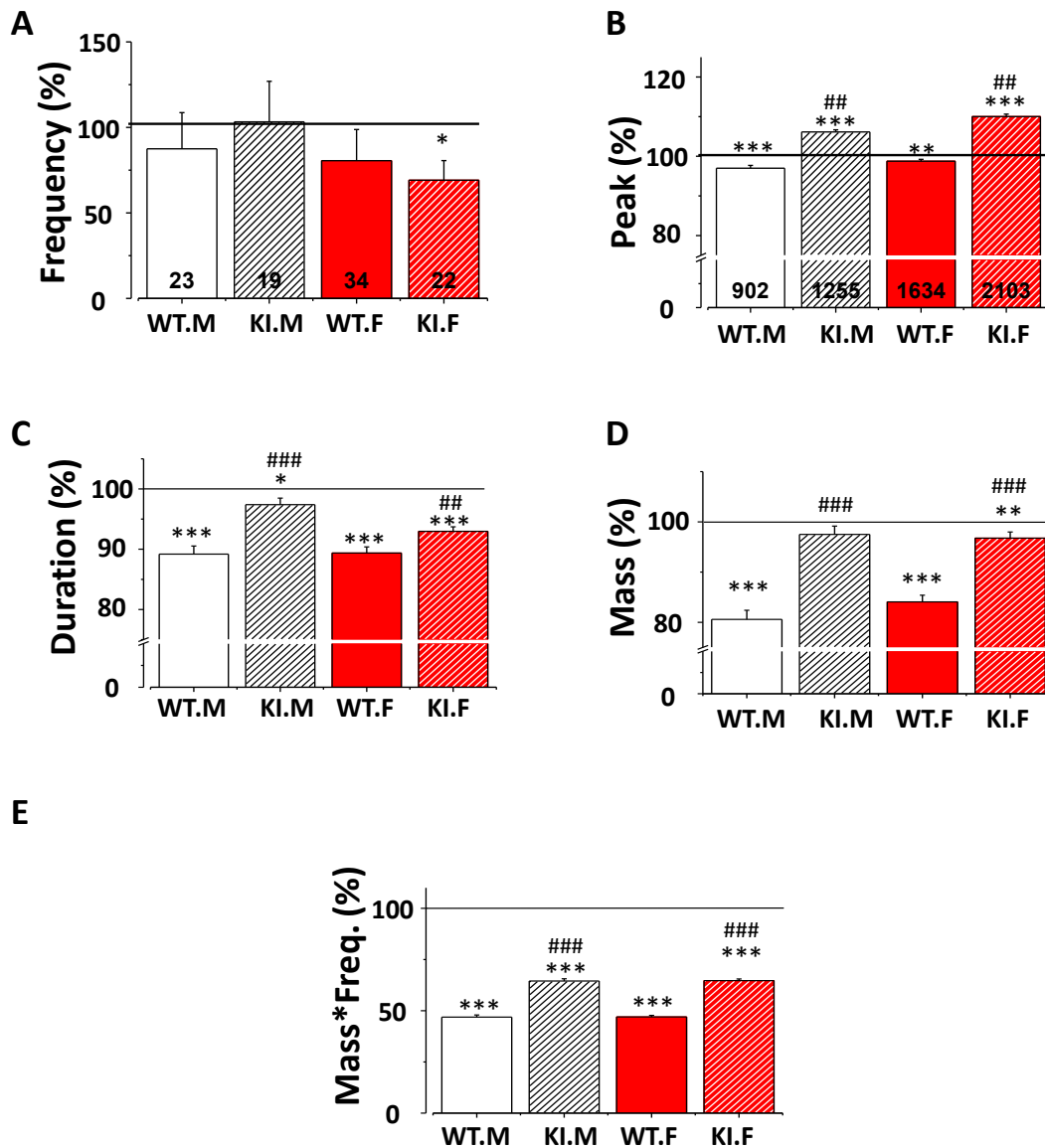


Figure 39. CCH effect on  $\text{Ca}^{2+}$  spark, normalized by the sparks from the same SAN in basal condition. A. Frequency of  $\text{Ca}^{2+}$  sparks expressed as percentage of number of  $\text{Ca}^{2+}$  sparks per second per 100  $\mu\text{m}$  in the presence of charbachol with respect to the same node before charbachol. Numbers in each bar indicate cells (4 WT female and 3 WT male vs. 3 KI female and 3 KI male). B. Percentage of  $\text{Ca}^{2+}$  spark amplitude (measured as peak  $F/F_0$  as in Fig. 35). C. Percentage of  $\text{Ca}^{2+}$  spark duration at 50% of maximum amplitude. D. Percentage of  $\text{Ca}^{2+}$  spark mass (amplitude\*width\*duration). E. Percentage of total  $\text{Ca}^{2+}$  leak through  $\text{Ca}^{2+}$  spark ( $\text{Ca}^{2+}$  spark mass\*frequency). Numbers in each bar of panel B indicated number of  $\text{Ca}^{2+}$  sparks, which are the same for panel C-E. WT.M, wildtype male. WT.F, wildtype female. KI.M, knock-in male. KI.F, knock-in female. \* $p < 0.05$ , \*\* $p < 0.01$ , \*\*\* $p < 0.001$ , compared with basal condition (100%).

†p<0.05, ††P<0.01, †††P<0.001, compared between genotypes.

### ***Mechanism of RyR<sub>2</sub><sup>R420Q</sup> dysfunction***

In order to evaluate the RyR<sub>2</sub><sup>R420Q</sup> dysfunction, we addressed two hypothesis based on other published data in CPVT RyR<sub>2</sub> mutations from us and other authors. We started by analyzing the Ca<sup>2+</sup> sensitivity by analyzing Ca<sup>2+</sup> sparks frequency in permeabilized cardiomyocytes perfused with different [Ca<sup>2+</sup>]<sub>i</sub>. We did this experiment in ventricular cardiomyocytes as they have the same RyR<sub>2</sub><sup>R420Q</sup> and the cell isolation provides more cells. Myocytes were permeabilized by 90 s exposure to saponin (0.01%). Ca<sup>2+</sup> sparks were recorded in intracellular solution with fixed [Ca<sup>2+</sup>]<sub>i</sub> calculated by Max chelator. Figure 40 shows that KI cardiomyocytes were slightly more sensitive to Ca<sup>2+</sup> than WT at 100nM [Ca<sup>2+</sup>]<sub>i</sub>. As the RyR<sub>2</sub><sup>R420Q</sup> might have some enhanced Ca<sup>2+</sup> sensitivity although at most analyzed concentrations the response was similar, it may not be the main mechanism.

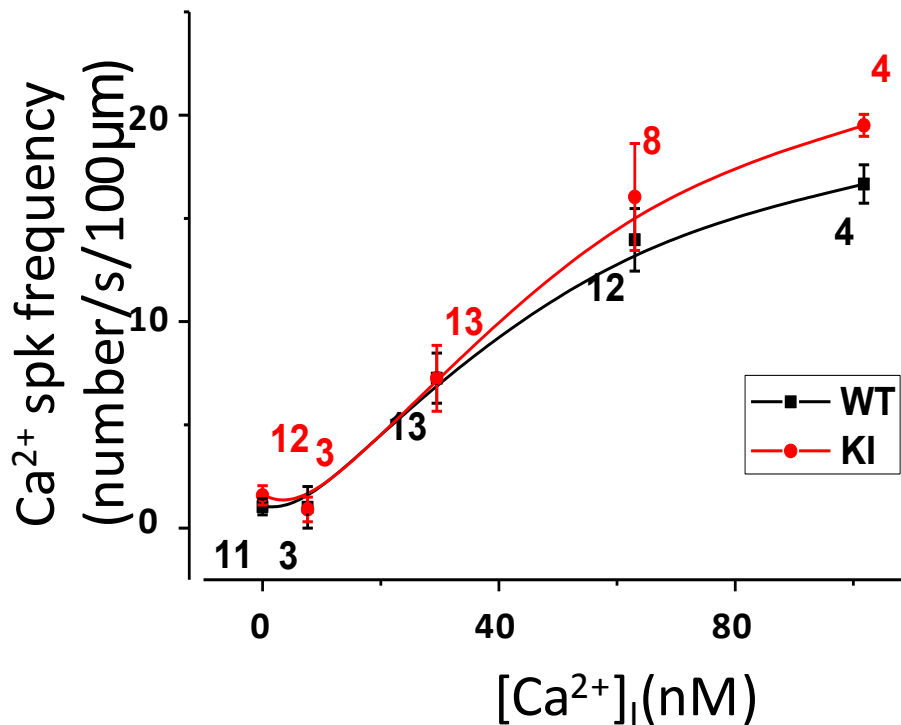


Figure 40. Ca<sup>2+</sup> spark frequency measured as the number of Ca<sup>2+</sup> sparks per second per 100µm at different [Ca<sup>2+</sup>]<sub>i</sub>. Numbers of cells are included close to the data points.



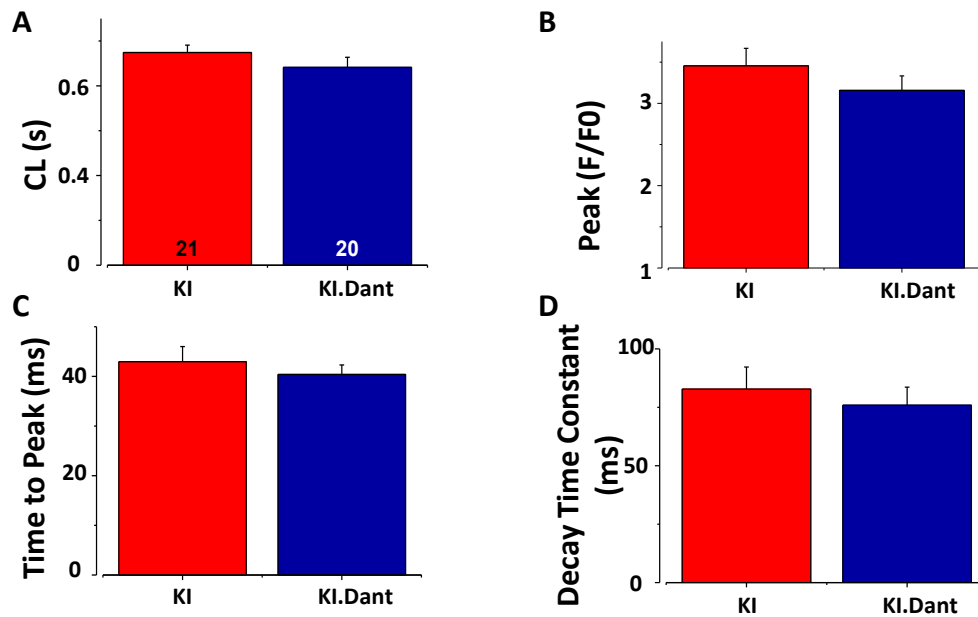


Figure 41. Dantrolene effect on knock-in (KI) SAN cells. A. Averaged duration of two consecutive beatings during 30 s recording (Cycle length, CL). Numbers in the bars indicate cells from 5 SAN before and during dantrolene application. B-D.  $[Ca^{2+}]_i$  transient peak, time to peak and decay time constant, measured as in Fig 35, 36 and 37 respectively and measured from the same cells as panel A. Red bar: knock-in SAN in basal condition. Blue bar: the same knock-in SAN during dantrolene application.

Other proposed mechanism is the alteration of zipping unzipping mechanism. Zipping is interaction between N and central domains which stabilizes the channel in the closed estate. Because  $RyR_2^{R420Q}$  is located at the N-terminal region, it could be a possible mechanism. It has been postulated that dantrolen stabilizes the zypping state. Thus we analyzed dantrolene effects on  $RyR_2^{R420Q}$  SAN. Figure 41 shows the effect in CL and the whole  $[Ca^{2+}]_i$  transients. The spontaneous  $[Ca^{2+}]_i$  transient frequency (Figure 41A) and characteristics (Figure 41B-D) were not significantly different before and during dantrolene application.  $Ca^{2+}$  sparks occurrence was depressed by dantrolene, like the  $Ca^{2+}$  spark duration (Figure 42), but without changes in  $Ca^{2+}$  spark amplitude or width. Thus dantrolene showed some improvement in KI SAN, however the effect was too small to explain zipping unzipping as the mechanism of R420Q dysfunction.

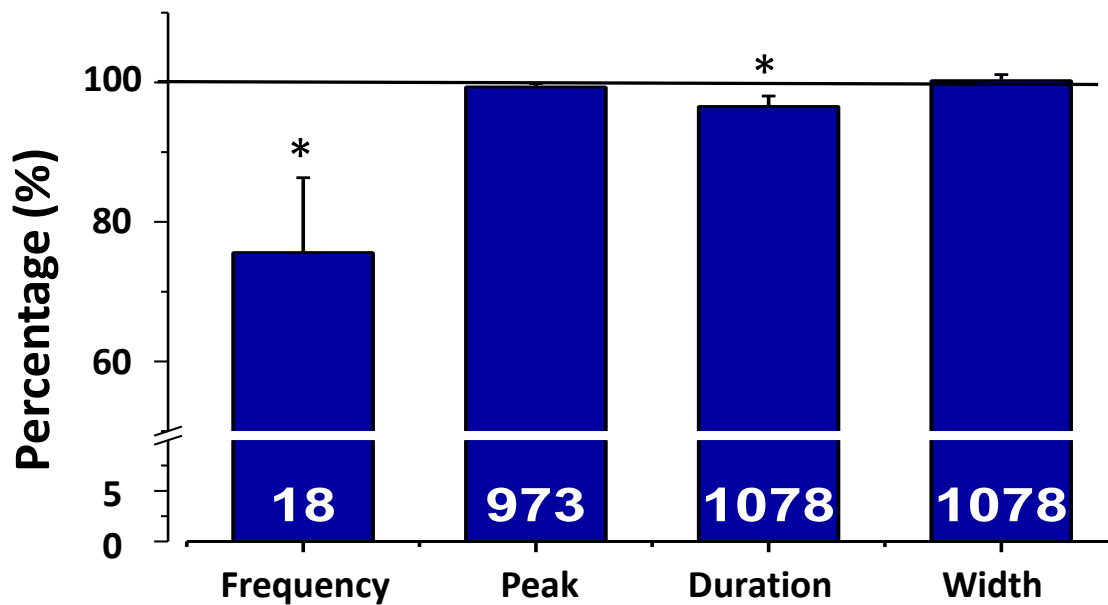


Figure 41. Dantrolene effects on  $\text{Ca}^{2+}$  spark frequency and characteristics, normalized by basal condition in each SAN. Numbers indicated cells (frequency) or  $\text{Ca}^{2+}$  spark number (peak, duration and width) from 5 SAN. \* $p < 0.05$  compared with basal condition (100%).

#### *Discussion of this additional data*

This additional part of results includes the sex-dependent response, ISO and CCH effect on  $[\text{Ca}^{2+}]_i$  transient and  $\text{Ca}^{2+}$  spark,  $\text{Ca}^{2+}$  sensitivity and dantrolene effect, further revealed the arrhythmogenic mechanism of mutation  $\text{RyR}_2^{\text{R420Q}}$ .

The shorter duration of BVT after epinephrine and caffeine injection in KI females than KI males indicates a cardio-protection in female, which was reported in severe cardiac diseases, such as heart failure.<sup>301-303</sup> Besides, this observation is consistent with a previous research suggesting that female patients have a lower risk of cardiac events.<sup>442</sup>

ISO increases cAMP level and protein phosphorylation level which should increase  $[\text{Ca}^{2+}]_i$  transient amplitude. But in SAN, the resultant ISO response also accelerates the pacemaking rhythm and leaves less time for SR to refill, resulting in the similar even a tendency of smaller  $[\text{Ca}^{2+}]_i$  transient amplitude. In contrast, CCH slows pacemaking rhythm associated with depressed protein phosphorylation level ( $\text{I}_{\text{Ca,L}}$ , PLB,  $\text{RyR}_2$ ), cAMP level (depress  $\text{I}_f$ ) and activated  $\text{I}_{\text{KACH}}$ . Thus, the longer SR refill time is balanced with the other responses, causing the tendency of smaller (WT) or significant smaller (KI)  $[\text{Ca}^{2+}]_i$  transient amplitude.

ISO shortened  $[\text{Ca}^{2+}]_i$  transient time to peak in WT SAN cells, corresponding to the enhanced cAMP and phosphorylation level. However, the ones in KI SAN cells were prolonged. This opposite response in  $[\text{Ca}^{2+}]_i$  transient time to peak between WT and KI suggests a defect in KI SAN

and impaired ISO response. In contrast, CCH decreased  $[Ca^{2+}]_i$  transient time to peak in both genotypes, in respect that CCH decreases cAMP level and activates  $I_{KACH}$ .

Decay time constant was accelerated by ISO in both WT and KI SAN cells, as it is expected, by the PKA phosphorylation of phospholamban. In contrast, CCH did not alter decay time in either WT or KI.

ISO also increased ramp occurrence in both genotypes, probably because of the enhanced phosphorylation of RyR<sub>2</sub>. Eventually KI SAN cells had more possibility to have ramp not only in basal condition, also during ISO stimulation, with enhanced ramp amplitude. In contrast, CCH did not alter ramp occurrence in either genotype. The CCH resulted decrease in ramp peak and time to peak in WT were absent in KI, and the ramp time to peak in KI was even significant prolonged, suggesting an impaired coupled-clock. During CCH application, KI (male and female) SAN cells still had more  $Ca^{2+}$  leak as  $Ca^{2+}$  sparks, indicating the defect in RyR<sub>2</sub> channel is maintained under parasympathetic tone.

The slightly enhanced  $Ca^{2+}$  spark frequency in permeabilized ventricular myocytes only at 100nM  $[Ca^{2+}]_i$  revealed that the mutant RyR<sub>2</sub> may behave as with increased  $Ca^{2+}$  sensitivity, but it does not have a shift in the curve, disregarding enhanced  $Ca^{2+}$  sensitivity as the main defect. Dantrolene decreased  $Ca^{2+}$  spark frequency and duration yielding some improvement. However, dantrolene failed to regain the CL and  $[Ca^{2+}]_i$  transient characteristics, which is unlikely to explain zipping unzipping as the mechanism of R420Q dysfunction.

This part of results allows us to further understand R420Q mutation in addition to the manuscript, and also provides insight to clinical therapy.

## Chapter 4 Discussion

SAN is the primary pacemaker of the heart. It spontaneously generates the electrical signal resulting in the contraction of the heart, which further pumps blood throughout the body and sustains life. Many pathological conditions favor SAN dysfunction, such as heart failure, hypertension, atrial fibrillation, etc.<sup>414</sup> Considering that RyR<sub>2</sub> has a critical role in SAN automaticity generation alteration on its function may underlie SAN dysfunction. In particular, CPVT patients presenting RyR<sub>2</sub> mutations frequently show SAN dysfunction, such as bradycardia, and inducible atrial tachyarrhythmias.<sup>454, 455, 632</sup> However, its molecular basis is not fully understood. Our team investigated the SAN dysfunction in a CPVT mouse model bearing RyR<sub>2</sub> C-terminal mutation (R4496C).<sup>458</sup> The mechanism of SAN dysfunction attributed to other RyR<sub>2</sub> mutations has never been published before. In this thesis, we used transgenic animal (RyR<sub>2</sub><sup>R420Q</sup>) to address this important issue, and characterized the molecular basis of the SAN dysfunction in a KI mouse model of CPVT carrying this novel mutation in RyR<sub>2</sub>, located at the N-terminal region.

### **RyR<sub>2</sub> N-terminal mutation R420Q**

Unlike mutation R4496C, mutation R420Q only increases Ca<sup>2+</sup> spark frequency slightly, but meanwhile dramatically causes prolongation of the spark duration in SAN cells, showing distinct modifications and contributions of the two mutations. Indeed, R4496 is located in the C-terminal portion of the channel (cytosolic side), close to the proposed molecular region involved in Ca<sup>2+</sup>-dependent activation (residues 4485 to 4494).<sup>633-636</sup> Thus, it is reasonable that R4496C enhanced RyR<sub>2</sub> open probability by enhancing Ca<sup>2+</sup> sensitivity. However, R420 is located on the top of the cytosolic domain, stabilizing the structure of N-terminal region of mice/human RyR<sub>2</sub>. As mentioned in introduction, Arginine 420 participates to the binding of a Cl<sup>-</sup> which holds the three parts of the N-terminal region in position. RyR<sub>2</sub><sup>R420Q</sup> mutation ablates chloride binding in mice, resulting in reorientations of the first two regions relative to the third one.<sup>520</sup> Based on our data in Ca sparks, these changes likely interfere with channel closing, contributing to the longer sparks. R420 is a highly conserved residue, being common in all species analyzed, including humans.<sup>462</sup>

### **Gain-of-function and loss-of-function mutation**

Mutations on RyR<sub>2</sub> could result in protein gain-of-function or loss-of-function effect that increase or decrease channel activity respectively. In ventricular myocytes, the gain-of-function mutations promote SR Ca<sup>2+</sup> leak during diastole and DADs (delayed afterdepolarizations), triggering arrhythmogenic disorders.<sup>637</sup> In respect of that, Thomas et al. analyzed four SCD-(sudden cardiac death) related CPVT/ARVD2 mutations (L433P, N2386I, R176Q, T2504M), and found that three SCD-related mutations (N2386I, R176Q, T2504M) exhibit a gain-of-function phenotype.<sup>638</sup> However, the SCD-related mutation L433P was less sensitive than the WT, suggesting that loss-of-function mutation could also promote arrhythmias.<sup>637, 638</sup> Moreover, a recent research reported that

CPVT mutation RyR<sub>2</sub><sup>A4860G</sup> is a loss-of-function and also arrhythmogenic mutation, as mentioned in introduction.<sup>464</sup> Thus, both gain-of-function and loss-of-function mutations are capable to induce arrhythmogenic disorders in ventricular myocytes.

The RyR<sub>2</sub> N-terminal mutations are not well studied, while lack of animal model restricts the further investigation. There is one research studied a mouse model carrying N-terminal mutation R176Q.<sup>468</sup> This mutation is a gain-of-function mutation, found together with other mutation (T2504) in a family of arrhythmogenic right ventricular dysplasia (ARVD). However, this mutation is located in domain A. The only mouse model carrying RyR<sub>2</sub> N-terminal C-domain mutation was reported by Okudaira et al. that the homogeneous RyR<sub>2</sub><sup>R420W</sup> mutation caused the abnormal calcium dynamics and arrhythmogenesis in mutated mouse ventricular myocytes. However, this research did not investigate the RyR<sub>2</sub><sup>R420W</sup> behavior, and whether the arrhythmogenesis effect of RyR<sub>2</sub><sup>R420W</sup> was induced by RyR<sub>2</sub> gain-of-function or loss-of-function was not known.<sup>639</sup> Tang et al. studied RyR<sub>2</sub><sup>R420W</sup> behavior in inducible HEK293 cell line.<sup>521</sup> However, R420W mutation adopts a conformation pointing to the solvent and avoids significant structural changes of RyR<sub>2</sub>, which differs from R420Q mutation.<sup>462, 520</sup> In this thesis, we for the first time reported an increased Ca<sup>2+</sup> release effect of an N-terminal C-domain mutant RyR<sub>2</sub> in a mouse model, and demonstrated that R420Q is a gain-of-function mutation, likely not only by a gain in its open probability but also by a loss in its closing capabilities, or an increase in the open time. The biophysical properties of single RyR<sub>2</sub><sup>R420Q</sup> are being analyzed, while the analysis of Ca<sup>2+</sup> sparks shows a marked increase in the time to peak. When a cluster of RyRs opens to produce a Ca<sup>2+</sup> spark, the released Ca<sup>2+</sup> is around it and the Ca<sup>2+</sup> concentration increases during the time there is release. Then the channels close and Ca<sup>2+</sup> decreases mainly by diffusion. Thus the enhanced time to peak is reminiscent of prolonged open times.

It was also reported that loss-of-function mutation A4860G induced sinus bradycardia in heterozygous mutated mice.<sup>464</sup> Besides, inhibition of RyR<sub>2</sub> reduces the SAN pacemaker activity. One may expect that gain of function mutation on RyR<sub>2</sub> could induce accelerated SAN activity, taking into account that increased Ca<sup>2+</sup> release could enhance NCX current and depolarize the membrane. However, the RyR<sub>2</sub>-induced CPVT patients are frequently associated with sinus bradycardia, as well as in gain-of-function mutation R4496C carriers.<sup>458</sup> Our team investigated the RyR<sub>2</sub><sup>R4496C</sup> behavior both in ventricular and in SAN cells. It was found that Ca<sup>2+</sup> spark frequency was increased by 2-fold in RyR<sub>2</sub><sup>R4496C</sup> SAN cells, associated with prolonged cycle length and impaired isoproterenol response.<sup>458</sup> However this mutation is located in C-terminal of the RyR<sub>2</sub>, and this is also the only research that studied the mechanism of the SAN dysfunction induced by the CPVT-related RyR<sub>2</sub> mutation. Thus, this thesis for the first time investigated the SAN function in a mouse model carrying N-terminal RyR<sub>2</sub> mutation. In RyR<sub>2</sub><sup>R420Q</sup> SAN, we found enhanced Ca<sup>2+</sup>

release during diastolic depolarization, indicating a gain-of-function effect in SAN. This gain-of-function mutation resulted in the slower pacemaking activity in female KI mice, in dissected KI mice SAN, as well as R420Q carrying patients.<sup>457</sup>

It seems that both gain-of-function and loss-of-function RyR<sub>2</sub> mutations could induce slower pacemaking activity, but the mechanisms are probably distinct. The enhanced Ca<sup>2+</sup> leak during diastole may have at least 2 mechanisms to reduce automaticity: one is partially unloading the SR of Ca<sup>2+</sup>. In this respect, Satoh showed that high concentrations (over 5 mM) of caffeine that would unload the SR with Ca<sup>2+</sup> induce a negative chronotropic effect in SAN cells.<sup>640, 641</sup> Moreover, the Ca<sup>2+</sup> release inactivates the L-Type Ca<sup>2+</sup> current (I<sub>Ca,L</sub>), which is also involved in AP generation in SAN. In this respect, it has been recently shown that mice with less I<sub>Ca,L</sub> present bradycardia.<sup>112, 464</sup>

### **R420Q induced SAN dysfunction**

Human RyR<sub>2</sub><sup>R420Q</sup> carriers present higher incidence of sinus bradycardia compared with genotype-negative individuals (78% vs. 25%, P = 0.030). These results revealed the SAN dysfunction induced by RyR<sub>2</sub> mutation R420Q.<sup>457</sup>

In genetic modified mice, RyR<sub>2</sub><sup>R420Q</sup> female mice had lower heart rate than WT females during the day, indicating the SAN dysfunction in this mouse model. Consistent with this observation, dissected SAN from both male and female KI mice presented slower pacemaker activity compared with the relevant WT. The slower pacing rate in KI SAN cells was accompanied with more Ca<sup>2+</sup> release during diastolic depolarization. The ISO response of dissected SAN was greater in R420Q KI than in WT, indicating an enhanced sensitivity to β-AR response. The SAN dysfunction in CPVT patients gives risk of sudden death by letting time to ectopic foci to form, probably favors the ventricular disorder. Moreover, it may limit the dose of β-blocker tolerated and impair the efficacy of ICD (implantable cardioverter defibrillator) therapy for CPVT.

### **Correct RyR<sub>2</sub> function is required for normal SAN automaticity**

As inhibition of RyR<sub>2</sub> reduces the SAN pacemaker activity, it is well accepted that RyR<sub>2</sub> is important for generation of SAN automaticity. However, the effect of point mutations on RyR<sub>2</sub> on SAN automaticity is not well studied. Besides, the RyR<sub>2</sub>-induced CPVT patients are frequently associated with sinus bradycardia, which was seen in N-terminal mutation R420Q carriers. Thus, it is necessary to identify the mechanism of SAN dysfunction induced by RyR<sub>2</sub> point mutation.

Supraventricular arrhythmia has been reported in many CPVT families, including sinus bradycardia at rest.<sup>455</sup> In a previous work, our team<sup>458</sup> found that mice carrying the RyR<sub>2</sub><sup>R4496C</sup> mutation presented heart rates similar between the KI RyR<sub>2</sub><sup>R4496C</sup> mice and the WT. However, the KI mice displayed a dramatic increase in the incidence of SAN pauses during sudden reduced sinus rhythm periods after intraperitoneal injection of isoproterenol, which were overcome by atrial and/or junctional escape beats. The dissected RyR<sub>2</sub><sup>R4496C</sup> SAN presented significantly slower

pacemaker activity and impaired chronotropic response to  $\beta$ -adrenergic stimulation, accompanied by the appearance of pauses (in spontaneous  $[Ca^{2+}]_i$  transients and action potentials) in 75% of the cases.  $Ca^{2+}$  spark frequency was increased by 2-fold in  $RyR_2^{R4496C}$  SAN, which is consistent with the finding of leaky  $RyR_2^{R4496C}$  in ventricular myocytes.<sup>466, 634</sup> Isolated  $RyR_2^{R4496C}$  SAN cells showed reduced  $I_{Ca,L}$  density  $\sim 50\%$ , indicating a modified membrane clock. Isoproterenol dramatically increased the frequency of  $Ca^{2+}$  sparks and waves by  $\sim 5$  and  $\sim 10$ -fold, respectively. The SR  $Ca^{2+}$  content was significantly reduced in  $RyR_2^{R4496C}$  SAN cells in the presence of isoproterenol, which may contribute to the SAN pauses by stopping the “ $Ca^{2+}$  clock” rhythm generation. Thus, R4496C mutation decreased SR  $Ca^{2+}$  content via enhanced  $RyR_2$   $Ca^{2+}$  release influencing the  $Ca^{2+}$  clock, and R4496C mutation also induced reduced  $I_{Ca,L}$  density indirectly depressing the membrane clock. Via the effects on both clocks, it is expected that R4496C mutation slowed the SAN pacemaking activity.

In contrast to  $RyR_2^{R4496C}$  mice,  $RyR_2^{R420Q}$  female mice had lower heart rate than WT females during the day. Dissected SAN also presented slower pacemaker activity compared with WT as seen in  $RyR_2^{R4496C}$  SAN, but accompanied with longer sparks with smaller increase in  $Ca^{2+}$  spark frequency. Eventually, the SR  $Ca^{2+}$  content was reduced in both  $RyR_2^{R4496C}$  and  $RyR_2^{R420Q}$  SAN cells. Besides, as seen in the  $RyR_2^{R4496C}$  SAN cells, isolated  $RyR_2^{R420Q}$  SAN cells also showed significant smaller  $I_{Ca,L}$ . The ISO response of dissected SAN to 20 nM ISO was greater in  $RyR_2^{R420Q}$  KI than in WT, and similar response is also seen in female KI mice, different from the impaired response from  $RyR_2^{R4496C}$  SAN cells. As seen from R4496C mutation, R420Q mutation also impact both  $Ca^{2+}$  clock and membrane clock. For the  $Ca^{2+}$  clock it is likely that via increased  $Ca^{2+}$  release, R420Q mutation retards the SR  $Ca^{2+}$  restoration, and prevents the achievement of SR  $Ca^{2+}$  content threshold for  $[Ca^{2+}]_i$  transient initiation.<sup>16</sup> Indeed, the SR  $Ca^{2+}$  content is reduced in  $RyR_2^{R420Q}$  SAN cells, which is consistent with the previous hypothesis. Similar data has been reported by using SERCA blocker (cyclopiazonic acid) which blocks SR  $Ca^{2+}$  recovery and thus reduced SAN pacemaker activity.<sup>229</sup> Besides the reduced  $I_{Ca,L}$ , the increased cytosolic  $[Ca^{2+}]_i$  also inhibited the activation of  $I_{Ca,L}$  disturbing the membrane clock, while pharmacological inhibition or genetic deficiency of LTCC in SAN results in slower pacemaker activity.<sup>112</sup> Thus, R420Q probably affects the pacemaker activity through slowing generation of periodic  $Ca^{2+}$  oscillations (i.e.  $Ca^{2+}$  clock) and interfered membrane clock resulting in the defective coupled-clock, without modification in  $I_f$  density. Thereby, via different mechanisms, both mutation R4496C and R420Q promote SAN dysfunction via distinct  $RyR_2$  behaviors and mechanisms.

Thus, single point mutation on  $RyR_2$  is sufficient to produce sick SAN activity and  $\beta$ -AR response. On the other hand, extremely correct  $RyR_2$  function is required by normal SAN automaticity.

## Ca<sup>2+</sup> regulation by Ca<sup>2+</sup> in SAN

Ca<sup>2+</sup> released from RyR<sub>2</sub> could regulate Ca<sup>2+</sup> behavior and pacemaker activity of SAN cells as mentioned previously in introduction, as application of Ca<sup>2+</sup> (or Ca<sup>2+</sup> chelator) accelerates (or inhibits) SAN automaticity. Ca<sup>2+</sup> directly regulates ion channels involved in membrane clock, meanwhile, promotes PKA-/CaMKII-dependent protein phosphorylation that drive the coupled clock function.

In RyR<sub>2</sub><sup>R4496C</sup> SAN, it is likely that the enhanced Ca<sup>2+</sup> release inhibited the I<sub>Ca,L</sub>, as it is known that LTCC could be inhibited by Ca<sup>2+</sup>, while compensated effects (such as changed protein expression pattern) might also exist. Thus diastolic Ca<sup>2+</sup> release, regulating the Ca<sup>2+</sup> entry via LTCC and Ca<sup>2+</sup> release via modified SR Ca<sup>2+</sup> content, reduces both Ca<sup>2+</sup> and membrane clock resulting in the expected suppressed SAN automaticity.

In RyR<sub>2</sub><sup>R420Q</sup> mice, the increased diastolic Ca<sup>2+</sup> release influenced the SAN automaticity also via changed Ca<sup>2+</sup> homeostasis. As seen in RyR<sub>2</sub><sup>R4496C</sup>, I<sub>Ca,L</sub> was also reduced in RyR<sub>2</sub><sup>R420Q</sup> SAN cells. To exclude the Ca<sup>2+</sup> inactivation of LTCC, we repeated the experiments with a Ca<sup>2+</sup> chelator in the pipette solution, and no significant difference was found in I<sub>Ca,L</sub> between KI and WT. These data suggest that intracellular Ca<sup>2+</sup> alteration can induce decrease in I<sub>Ca,L</sub> in KI mice, which could account for the slowing of SAN pacing rate. Besides, the increased Ca<sup>2+</sup> release retards SR refill and depresses Ca<sup>2+</sup> clock, together with the damaged membrane clock, resulting in the slower SAN automaticity.

In spite of the different mechanisms, R4496C and R420Q are both RyR<sub>2</sub> mutations that through altered Ca<sup>2+</sup> behavior influence SAN automaticity, indicating the critical role of Ca<sup>2+</sup> regulation in SAN automaticity.

### R420Q mutation on mouse and human RyR<sub>2</sub>

RyR<sub>2</sub><sup>R420Q</sup> mouse model presents CPVT phenotype after typical CPVT test (epinephrine plus caffeine injection), indicating that this genetically modified mouse model is effectual to be used as a preclinical model. However, there is still some difference of this mouse model compared to human patients.

From the vivo basal ECG recordings, only RyR<sub>2</sub><sup>R420Q</sup> female displays significant difference compared to WT female, but not RyR<sub>2</sub><sup>R420Q</sup> male. These data differ from the human clinical observation that SAN dysfunction (such as sinus bradycardia) was shown in both male and female CPVT patients. This difference could be due to the different adrenergic tone, which is higher in mice than in human (session 1.5). In support of this hypothesis, both dissected male and female SAN (lacks autonomic innervation, in this case, sympathetic tone particularly) from KI mice had slower basal pacemaker activity.



## SAN automaticity in male and female mice

From previous data, the team found some significant differences between male and females in  $\text{Ca}^{2+}$  sparks.<sup>642, 643</sup> In this study, the *in-vivo* basal PP interval in WT male was longer than WT female during both day and night. However, the *in-vitro* WT male cycle length was shorter than in relevant WT female in dissected SAN cells, and WT male SAN cells have more  $\text{Ca}^{2+}$  release during diastolic depolarization than the WT female. This observation is consistent with a previous hypothesis that cAMP level is higher in male ventricles (session 1.4.3.4), due, at least partially, to the lower PDE4B expression.<sup>283</sup> The contradictory results in genders between *in-vivo* and *in-vitro* indicate multiple and compromised actions. Hypothetically the cAMP level is higher in males,<sup>283</sup> resulting in faster beating rate *in vitro*. However, the heart size is smaller in females, what needs to enhance the heart rate to maintain good ejection fraction *in vivo*. But interestingly, as shown in the *in-vivo* data from KI mice, the difference in PP intervals between KI male and KI female is almost absent (non-significant), because of the relatively longer PP interval in KI females compared to WT females. As the longer cycle length in KI mice *in vitro* persisted *in vivo* KI females but lost between males, it is more likely that KI males have relatively shorter PP intervals, suggesting a more complicated and compensated sympathetic/parasympathetic system in KI males. Hypothetically, in contrast with the KI females, the KI males probably have relatively higher adrenergic tone than WT males *in vivo*, resulting in the similar PP interval as WT males. This hypothesis could also explain the greater CCH response in KI males than WT males *in vivo*, which was not observed *in vitro*, as when the heart rate is increased by sympathetic stimulation the vagal stimulus is considerably greater.<sup>237</sup> However, the WT and KI females were thought to have greater adrenergic tone than males, but their CCH responses were only a bit greater than WT males (not statistically different) and smaller than KI males, probably attributed to the lower cAMP level in females. Although, more complicated and compensated effect may exist.

It was reported that sex-related differences existed in RyR<sub>2</sub>-induced CPVT patients: male patients have a higher risk of cardiac events.<sup>442</sup> The cardio-protection in female conferring survival benefits was also reported in severe cardiac diseases, such as heart failure.<sup>301-303</sup> Consistent with these observations, we found a significant shorter duration of BVT after epinephrine and caffeine injection in KI females than KI males, also indicating a more complicated and severe effect in KI males.

In contrast with the *in-vitro* ISO responses in dissected SAN, which were greater in both male and female KI mice than in WT, the *in-vivo* response was only preserved between KI females and WT females, not between males. ISO shortened RR interval more dramatically in KI female *in vivo* than WT females. However, a different ISO response was not observed in KI males *in vivo*,

probably due to the lower adrenergic tone (compared to females) resulting in an insufficient ISO dosage in males.

### **Sympathetic and parasympathetic stimulation**

It seems like that in dog and human vagal tone is dominant as combined muscarinic plus  $\beta$ -adrenoceptor blockage accelerates the heart rate.<sup>2, 6</sup> In contrast, mice show sympathetic predominance as the isolated SAN beats significantly slower than the heart rate *in vivo*.<sup>6</sup>

In this thesis, *in vivo* sympathetic stimulation (isoproterenol injection) induced significant responses (heart rate increase) in all types of mice, but the response was greater in KI female than in WT female. The *in vivo* parasympathetic stimulation (carbachol injection) also induced significant response (heart rate decrease) in all type of mice, and the response was greater in KI male than in WT male. Consistent with the *in-vivo* observation, the SAN dissected from all types of mice increased pacing rate significantly after ISO stimulation, although the response is significant greater in all KI mice than the relevant WT mice. Carbachol also prolonged the pacing rate in all types of dissected SAN, but no differences between KI and WT mice *in vivo*.

In summary, in this thesis, we investigated the novel RyR<sub>2</sub> N-terminal mutation R420Q. We found that this mutation induced sinus bradycardia and SAN dysfunction in human patient and in mouse model, and further investigation suggests that the mutation interferes RyR<sub>2</sub> channel closing resulting in longer  $[Ca^{2+}]_i$  sparks and SR replenishment, accounting for the sick SAN function and ISO response. The SAN dysfunction may in turn favor the initiation of ectopic foci. Our work for the first time reported the gain-of-function effect resulted by an N-terminal C-domain mutation R420Q, and for the first time investigated the SAN dysfunction induced by RyR<sub>2</sub> N-terminal mutation and found a novel mechanism (defect in channel closing) caused SAN dysfunction. Our work provides a new mechanism to CPVT related SAN dysfunction and insight to CPVT therapy.

However, it is still unknown about the behaviors of other N-terminal mutation related RyR<sub>2</sub>, the resultant SAN function, SAN  $\beta$ -AR response and gender-dependent effect. The contribution of loss-of-function RyR<sub>2</sub> to SAN function is also desirable.

## Reference:

1. GAZTANAGA L, MARCHLINSKI FE, BETENSKY BP. MECHANISMS OF CARDIAC ARRHYTHMIAS. *REV ESP CARDIOL (ENGL ED)*. 2012;65:174-185
2. OPTHOF T. THE NORMAL RANGE AND DETERMINANTS OF THE INTRINSIC HEART RATE IN MAN. *CARDIOVASC RES*. 2000;45:177-184
3. KEITH A, FLACK M. THE FORM AND NATURE OF THE MUSCULAR CONNECTIONS BETWEEN THE PRIMARY DIVISIONS OF THE VERTEBRATE HEART. *JOURNAL OF ANATOMY AND PHYSIOLOGY*. 1907;41:172-189
4. JAMES TN. STRUCTURE AND FUNCTION OF THE SINUS NODE, AV NODE AND HIS BUNDLE OF THE HUMAN HEART: PART II--FUNCTION. *PROGRESS IN CARDIOVASCULAR DISEASES*. 2003;45:327-360
5. DOBRZYNSKI H, ANDERSON RH, ATKINSON A, BORBAS Z, D'SOUZA A, FRASER JF, INADA S, LOGANTHA SJ, MONFREDI O, MORRIS GM, MOORMAN AF, NIKOLAIDOU T, SCHNEIDER H, SZUTS V, TEMPLE IP, YANNI J, BOYETT MR. STRUCTURE, FUNCTION AND CLINICAL RELEVANCE OF THE CARDIAC CONDUCTION SYSTEM, INCLUDING THE ATRIOVENTRICULAR RING AND OUTFLOW TRACT TISSUES. *PHARMACOL THER*. 2013;139:260-288
6. MANGONI ME, NARGEOT J. GENESIS AND REGULATION OF THE HEART AUTOMATICITY. *PHYSIOL REV*. 2008;88:919-982
7. BERS DM. EXCITATION-CONTRACTION COUPLING AND CARDIAC CONTRACTILE FORCE. *KLUWER ACADEMIC PUBLISHERS*. 2001
8. AMIN AS, TAN HL, WILDE AA. CARDIAC ION CHANNELS IN HEALTH AND DISEASE. *HEART RHYTHM*. 2010;7:117-126
9. SORENSEN AB, SONDERGAARD MT, OVERGAARD MT. CALMODULIN IN A HEARTBEAT. *THE FEBS JOURNAL*. 2013;280:5511-5532
10. NERBONNE JM, KASS RS. MOLECULAR PHYSIOLOGY OF CARDIAC REPOLARIZATION. *PHYSIOL REV*. 2005;85:1205-1253
11. WEISBROD D, KHUN SH, BUENO H, PERETZ A, ATTALI B. MECHANISMS UNDERLYING THE CARDIAC PACEMAKER: THE ROLE OF SK4 CALCIUM-ACTIVATED POTASSIUM CHANNELS. *ACTA PHARMACOL SIN*. 2016;37:82-97
12. CHRISTEL CJ, CARDONA N, MESIRCA P, HERRMANN S, HOFMANN F, STRIESSNIG J, LUDWIG A, MANGONI ME, LEE A. DISTINCT LOCALIZATION AND MODULATION OF CAV1.2 AND CAV1.3 L-TYPE CA<sup>2+</sup> CHANNELS IN MOUSE SINOATRIAL NODE. *J PHYSIOL*. 2012;590:6327-6341
13. MESIRCA P, TORRENTE AG, MANGONI ME. FUNCTIONAL ROLE OF VOLTAGE GATED CA(2+) CHANNELS IN HEART AUTOMATICITY. *FRONTIERS IN PHYSIOLOGY*. 2015;6:19
14. MONFREDI O, MALTSEV VA, LAKATTA EG. MODERN CONCEPTS CONCERNING THE ORIGIN OF THE HEARTBEAT. *PHYSIOLOGY*. 2013;28:74-92
15. SCHRAM G, POURRIER M, MELNYK P, NATTEL S. DIFFERENTIAL DISTRIBUTION OF CARDIAC ION CHANNEL EXPRESSION AS A BASIS FOR REGIONAL SPECIALIZATION IN ELECTRICAL FUNCTION. *CIRC RES*. 2002;90:939-950
16. MALTSEV VA, YANIV Y, MALTSEV AV, STERN MD, LAKATTA EG. MODERN PERSPECTIVES ON NUMERICAL MODELING OF CARDIAC PACEMAKER CELL. *JOURNAL OF PHARMACOLOGICAL SCIENCES*. 2014;125:6-38
17. BOGDANOV KY, MALTSEV VA, VINOGRADOVA TM, LYASHKOV AE, SPURGEON HA, STERN MD, LAKATTA EG. MEMBRANE POTENTIAL FLUCTUATIONS RESULTING FROM SUBMEMBRANE CA<sup>2+</sup> RELEASES IN RABBIT SINOATRIAL NODAL CELLS IMPART AN EXPONENTIAL PHASE TO THE LATE DIASTOLIC DEPOLARIZATION THAT CONTROLS THEIR CHRONOTROPIC STATE. *CIRC RES*. 2006;99:979-987
18. GRANT AO. CARDIAC ION CHANNELS. *CIRC ARRHYTHM ELECTROPHYSIOL*. 2009;2:185-194
19. PIAN P, BUCCHI A, ROBINSON RB, SIEGELBAUM SA. REGULATION OF GATING AND RUNDOWN OF HCN HYPERPOLARIZATION-ACTIVATED CHANNELS BY EXOGENOUS AND ENDOGENOUS PIP<sub>2</sub>. *J GEN PHYSIOL*. 2006;128:593-604
20. ZONG X, ECKERT C, YUAN H, WAHL-SCHOTT C, ABICHT H, FANG L, LI R, MISTRİK P, GERSTNER A, MUCH B, BAUMANN L, MICHALAKIS S, ZENG R, CHEN Z, BIEL M. A

- NOVEL MECHANISM OF MODULATION OF HYPERPOLARIZATION-ACTIVATED CYCLIC NUCLEOTIDE-GATED CHANNELS BY SRC KINASE. *J BIOL CHEM*. 2005;280:34224-34232
21. YU H, CHANG F, COHEN IS. PHOSPHATASE INHIBITION BY CALYCUKULIN A INCREASES I(F) IN CANINE PURKINJE FIBERS AND MYOCYTES. *PFLUGERS ARCH*. 1993;422:614-616
  22. ACCILI EA, REDAELLI G, DIFRANCESCO D. DIFFERENTIAL CONTROL OF THE HYPERPOLARIZATION-ACTIVATED CURRENT (I(F)) BY CAMP GATING AND PHOSPHATASE INHIBITION IN RABBIT SINO-ATRIAL NODE MYOCYTES. *J PHYSIOL*. 1997;500 ( PT 3):643-651
  23. DIFRANCESCO D. BLOCK AND ACTIVATION OF THE PACE-MAKER CHANNEL IN CALF PURKINJE FIBRES: EFFECTS OF POTASSIUM, CAESIUM AND RUBIDIUM. *J PHYSIOL*. 1982;329:485-507
  24. DIFRANCESCO D, FERRONI A, MAZZANTI M, TROMBA C. PROPERTIES OF THE HYPERPOLARIZING-ACTIVATED CURRENT (IF) IN CELLS ISOLATED FROM THE RABBIT SINO-ATRIAL NODE. *J PHYSIOL*. 1986;377:61-88
  25. ROBINSON RB, BARUSCOTTI M, DIFRANCESCO D. AUTONOMIC MODULATION OF HEART RATE: PITFALLS OF NONSELECTIVE CHANNEL BLOCKADE. *AM J PHYSIOL HEART CIRC PHYSIOL*. 2003;285:H2865; AUTHOR REPLY H2865
  26. LUDWIG A, ZONG X, JEGLITSCH M, HOFMANN F, BIEL M. A FAMILY OF HYPERPOLARIZATION-ACTIVATED MAMMALIAN CATION CHANNELS. *NATURE*. 1998;393:587-591
  27. LUDWIG A, ZONG X, STIEBER J, HULLIN R, HOFMANN F, BIEL M. TWO PACEMAKER CHANNELS FROM HUMAN HEART WITH PROFOUNDLY DIFFERENT ACTIVATION KINETICS. *EMBO J*. 1999;18:2323-2329
  28. DIFRANCESCO D. A STUDY OF THE IONIC NATURE OF THE PACE-MAKER CURRENT IN CALF PURKINJE FIBRES. *J PHYSIOL*. 1981;314:377-393
  29. YU X, CHEN XW, ZHOU P, YAO L, LIU T, ZHANG B, LI Y, ZHENG H, ZHENG LH, ZHANG CX, BRUCE I, GE JB, WANG SQ, HU ZA, YU HG, ZHOU Z. CALCIUM INFLUX THROUGH IF CHANNELS IN RAT VENTRICULAR MYOCYTES. *AMERICAN JOURNAL OF PHYSIOLOGY. CELL PHYSIOLOGY*. 2007;292:C1147-1155
  30. YU X, DUAN KL, SHANG CF, YU HG, ZHOU Z. CALCIUM INFLUX THROUGH HYPERPOLARIZATION-ACTIVATED CATION CHANNELS (I(H) CHANNELS) CONTRIBUTES TO ACTIVITY-EVOKED NEURONAL SECRETION. *PROC NATL ACAD SCI U S A*. 2004;101:1051-1056
  31. DOYLE DA, MORAIS CABRAL J, PFUETZNER RA, KUO A, GULBIS JM, COHEN SL, CHAIT BT, MACKINNON R. THE STRUCTURE OF THE POTASSIUM CHANNEL: MOLECULAR BASIS OF K+ CONDUCTION AND SELECTIVITY. *SCIENCE*. 1998;280:69-77
  32. ZHOU Y, MORAIS-CABRAL JH, KAUFMAN A, MACKINNON R. CHEMISTRY OF ION COORDINATION AND HYDRATION REVEALED BY A K+ CHANNEL-FAB COMPLEX AT 2.0 Å RESOLUTION. *NATURE*. 2001;414:43-48
  33. ISHII TM, TAKANO M, XIE LH, NOMA A, OHMORI H. MOLECULAR CHARACTERIZATION OF THE HYPERPOLARIZATION-ACTIVATED CATION CHANNEL IN RABBIT HEART SINOATRIAL NODE. *J BIOL CHEM*. 1999;274:12835-12839
  34. D'AVANZO N, PEKHLETSKI R, BACKX PH. P-LOOP RESIDUES CRITICAL FOR SELECTIVITY IN K CHANNELS FAIL TO CONFER SELECTIVITY TO RABBIT HCN4 CHANNELS. *PLOS ONE*. 2009;4:E7712
  35. MACRI V, ANGOLI D, ACCILI EA. ARCHITECTURE OF THE HCN SELECTIVITY FILTER AND CONTROL OF CATION PERMEATION. *SCIENTIFIC REPORTS*. 2012;2:894
  36. WAHL-SCHOTT C, BIEL M. HCN CHANNELS: STRUCTURE, CELLULAR REGULATION AND PHYSIOLOGICAL FUNCTION. *CELLULAR AND MOLECULAR LIFE SCIENCES : CMLS*. 2009;66:470-494
  37. LUDWIG A, ZONG X, HOFMANN F, BIEL M. STRUCTURE AND FUNCTION OF CARDIAC PACEMAKER CHANNELS. *CELL PHYSIOL BIOCHEM*. 1999;9:179-186.
  38. SANTORO B, LIU DT, YAO H, BARTSCH D, KANDEL ER, SIEGELBAUM SA, TIBBS GR. IDENTIFICATION OF A GENE ENCODING A HYPERPOLARIZATION-ACTIVATED PACEMAKER CHANNEL OF BRAIN. *CELL*. 1998;93:717-729
  39. WAHL-SCHOTT C, FENSKE S, BIEL M. HCN CHANNELS: NEW ROLES IN SINOATRIAL NODE FUNCTION. *CURR OPIN PHARMACOL*. 2014;15:83-90

40. BROWN HF DD, NOBLE SJ. . HOW DOES ADRENALINE ACCELERATE THE HEART? *NATURE* 1979;280:235-236.
41. DIFRANCESCO D. THE ROLE OF THE FUNNY CURRENT IN PACEMAKER ACTIVITY. *CIRC RES.* 2010;106:434-446
42. DIFRANCESCO D. FUNNY CHANNEL GENE MUTATIONS ASSOCIATED WITH ARRHYTHMIAS. *J PHYSIOL.* 2013;591:4117-4124
43. SATOH H. SINO-ATRIAL NODAL CELLS OF MAMMALIAN HEARTS: IONIC CURRENTS AND GENE EXPRESSION OF PACEMAKER IONIC CHANNELS. *JOURNAL OF SMOOTH MUSCLE RESEARCH = NIHON HEIKATSUKIN GAKKAI KIKANSHI.* 2003;39:175-193
44. SHINAGAWA Y, SATOH H, NOMA A. THE SUSTAINED INWARD CURRENT AND INWARD RECTIFIER K<sup>+</sup> CURRENT IN PACEMAKER CELLS DISSOCIATED FROM RAT SINOATRIAL NODE. *J PHYSIOL.* 2000;523 PT 3:593-605
45. DENYER JC, BROWN HF. PACEMAKING IN RABBIT ISOLATED SINO-ATRIAL NODE CELLS DURING CS<sup>+</sup> BLOCK OF THE HYPERPOLARIZATION-ACTIVATED CURRENT I<sub>F</sub>. *J PHYSIOL.* 1990;429:401-409
46. THOLLON C, BEDUT S, VILLENEUVE N, COGE F, PIFFARD L, GUILLAUMIN JP, BRUNEL-JACQUEMIN C, CHOMARAT P, BOUTIN JA, PEGLION JL, VILAINE JP. USE-DEPENDENT INHIBITION OF HHCN4 BY IVABRADINE AND RELATIONSHIP WITH REDUCTION IN PACEMAKER ACTIVITY. *BR J PHARMACOL.* 2007;150:37-46
47. VERKERK AO, WILDERS R, VAN BORREN MM, PETERS RJ, BROEKHUIS E, LAM K, CORONEL R, DE BAKKER JM, TAN HL. PACEMAKER CURRENT (I<sub>F</sub>) IN THE HUMAN SINOATRIAL NODE. *EUR HEART J.* 2007;28:2472-2478
48. VINOGRADOVA TM, SIRENKO S, LYASHKOV AE, YOUNES A, LI Y, ZHU W, YANG D, RUKNUDIN AM, SPURGEON H, LAKATTA EG. CONSTITUTIVE PHOSPHODIESTERASE ACTIVITY RESTRICTS SPONTANEOUS BEATING RATE OF CARDIAC PACEMAKER CELLS BY SUPPRESSING LOCAL CA<sup>2+</sup> RELEASES. *CIRC RES.* 2008;102:761-769
49. NOMA A, MORAD M, IRISAWA H. DOES THE "PACEMAKER CURRENT" GENERATE THE DIASTOLIC DEPOLARIZATION IN THE RABBIT SA NODE CELLS? *PFLUGERS ARCH.* 1983;397:190-194
50. BARUSCOTTI M BA, DIFRANCESCO D. . PHYSIOLOGY AND PHARMACOLOGY OF THE CARDIAC PACEMAKER ("FUNNY") CURRENT. . *PHARMACOL THER* 2005;107:59-79
51. BUCCHI A, BARUSCOTTI M, DIFRANCESCO D. CURRENT-DEPENDENT BLOCK OF RABBIT SINO-ATRIAL NODE I<sub>F</sub> CHANNELS BY IVABRADINE. *J GEN PHYSIOL.* 2002;120:1-13
52. GOETHALS M, RAES A, VAN BOGAERT PP. USE-DEPENDENT BLOCK OF THE PACEMAKER CURRENT I<sub>F</sub> IN RABBIT SINOATRIAL NODE CELLS BY ZATEBRADINE (UL-FS 49). ON THE MODE OF ACTION OF SINUS NODE INHIBITORS. *CIRCULATION.* 1993;88:2389-2401
53. VAN BOGAERT PP, GOETHALS M, SIMOENS C. USE- AND FREQUENCY-DEPENDENT BLOCKADE BY UL-FS 49 OF THE I<sub>F</sub> PACEMAKER CURRENT IN SHEEP CARDIAC PURKINJE FIBRES. *EUR J PHARMACOL.* 1990;187:241-256
54. VAN BOGAERT PP, PITTOORS F. USE-DEPENDENT BLOCKADE OF CARDIAC PACEMAKER CURRENT (I<sub>F</sub>) BY CILOBRADINE AND ZATEBRADINE. *EUR J PHARMACOL.* 2003;478:161-171
55. YANIV Y, MALTSEV VA, ZIMAN BD, SPURGEON HA, LAKATTA EG. THE "FUNNY" CURRENT (I<sub>F</sub>) INHIBITION BY IVABRADINE AT MEMBRANE POTENTIALS ENCOMPASSING SPONTANEOUS DEPOLARIZATION IN PACEMAKER CELLS. *MOLECULES.* 2012;17:8241-8254
56. BOIS P, BESCOND J, RENAUDON B, LENFANT J. MODE OF ACTION OF BRADYCARDIC AGENT, S 16257, ON IONIC CURRENTS OF RABBIT SINOATRIAL NODE CELLS. *BR J PHARMACOL.* 1996;118:1051-1057
57. DU XJ, FENG X, GAO XM, TAN TP, KIRIAZIS H, DART AM. I<sub>F</sub> CHANNEL INHIBITOR IVABRADINE LOWERS HEART RATE IN MICE WITH ENHANCED SYMPATHOADRENERGIC ACTIVITIES. *BR J PHARMACOL.* 2004;142:107-112
58. LEONI AL, MARIONNEAU C, DEMOLOMBE S, LE BOUTER S, MANGONI ME, ESCANDE D, CHARPENTIER F. CHRONIC HEART RATE REDUCTION REMODELS ION CHANNEL TRANSCRIPTS IN THE MOUSE SINOATRIAL NODE BUT NOT IN THE VENTRICLE. *PHYSIOL GENOMICS.* 2005;24:4-12

59. SIMON L, GHALEH B, PUYBASSET L, GIUDICELLI JF, BERDEAUX A. CORONARY AND HEMODYNAMIC EFFECTS OF S 16257, A NEW BRADYCARDIC AGENT, IN RESTING AND EXERCISING CONSCIOUS DOGS. *J PHARMACOL EXP THER.* 1995;275:659-666
60. YANIV Y, SIRENKO S, ZIMAN BD, SPURGEON HA, MALTSEV VA, LAKATTA EG. NEW EVIDENCE FOR COUPLED CLOCK REGULATION OF THE NORMAL AUTOMATICITY OF SINOATRIAL NODAL PACEMAKER CELLS: BRADYCARDIC EFFECTS OF IVABRADINE ARE LINKED TO SUPPRESSION OF INTRACELLULAR CA<sub>2</sub>(<sup>2+</sup>) CYCLING. *J MOL CELL CARDIOL.* 2013;62:80-89
61. ZHANG H, VASSALLE M. ROLE OF I(K) AND I(F) IN THE PACEMAKER MECHANISMS OF SINO-ATRIAL NODE MYOCYTES. *CANADIAN JOURNAL OF PHYSIOLOGY AND PHARMACOLOGY.* 2001;79:963-976
62. MALTSEV VA, LAKATTA EG. DYNAMIC INTERACTIONS OF AN INTRACELLULAR CA<sub>2</sub><sup>+</sup> CLOCK AND MEMBRANE ION CHANNEL CLOCK UNDERLIE ROBUST INITIATION AND REGULATION OF CARDIAC PACEMAKER FUNCTION. *CARDIOVASC RES.* 2008;77:274-284
63. DIFRANCESCO D. PACEMAKER MECHANISMS IN CARDIAC TISSUE. *ANNU REV PHYSIOL.* 1993;55:455-472.
64. HERRMANN S, STIEBER J, STOCKL G, HOFMANN F, LUDWIG A. HCN4 PROVIDES A 'DEPOLARIZATION RESERVE' AND IS NOT REQUIRED FOR HEART RATE ACCELERATION IN MICE. *EMBO J.* 2007;26:4423-4432
65. HOESL E, STIEBER J, HERRMANN S, FEIL S, TYBL E, HOFMANN F, FEIL R, LUDWIG A. TAMOXIFEN-INDUCIBLE GENE DELETION IN THE CARDIAC CONDUCTION SYSTEM. *J MOL CELL CARDIOL.* 2008;45:62-69
66. RIGG L, MATTICK PA, HEATH BM, TERRAR DA. MODULATION OF THE HYPERPOLARIZATION-ACTIVATED CURRENT (I(F)) BY CALCIUM AND CALMODULIN IN THE GUINEA-PIG SINO-ATRIAL NODE. *CARDIOVASC RES.* 2003;57:497-504
67. SEIFERT R, SCHOLTEN A, GAUSS R, MINCHEVA A, LICHTER P, KAUPP UB. MOLECULAR CHARACTERIZATION OF A SLOWLY GATING HUMAN HYPERPOLARIZATION-ACTIVATED CHANNEL PREDOMINANTLY EXPRESSED IN THALAMUS, HEART, AND TESTIS. *PROC NATL ACAD SCI U S A.* 1999;96:9391-9396
68. SHAH MM. CORTICAL HCN CHANNELS: FUNCTION, TRAFFICKING AND PLASTICITY. *J PHYSIOL.* 2014;592:2711-2719
69. HERRMANN S, SCHNORR S, LUDWIG A. HCN CHANNELS--MODULATORS OF CARDIAC AND NEURONAL EXCITABILITY. *INTERNATIONAL JOURNAL OF MOLECULAR SCIENCES.* 2015;16:1429-1447
70. ALTOMARE C, TERRAGNI B, BRIOSCHI C, MILANESI R, PAGLIUCA C, VISCOMI C, MORONI A, BARUSCOTTI M, DIFRANCESCO D. HETEROMERIC HCN1-HCN4 CHANNELS: A COMPARISON WITH NATIVE PACEMAKER CHANNELS FROM THE RABBIT SINOATRIAL NODE. *J PHYSIOL.* 2003;549:347-359
71. CHEN S, WANG J, SIEGELBAUM SA. PROPERTIES OF HYPERPOLARIZATION-ACTIVATED PACEMAKER CURRENT DEFINED BY COASSEMBLY OF HCN1 AND HCN2 SUBUNITS AND BASAL MODULATION BY CYCLIC NUCLEOTIDE. *J GEN PHYSIOL.* 2001;117:491-504
72. MUCH B, WAHL-SCHOTT C, ZONG X, SCHNEIDER A, BAUMANN L, MOOSMANG S, LUDWIG A, BIEL M. ROLE OF SUBUNIT HETEROMERIZATION AND N-LINKED GLYCOSYLATION IN THE FORMATION OF FUNCTIONAL HYPERPOLARIZATION-ACTIVATED CYCLIC NUCLEOTIDE-GATED CHANNELS. *J BIOL CHEM.* 2003;278:43781-43786
73. ULENS C, TYTGAT J. FUNCTIONAL HETEROMERIZATION OF HCN1 AND HCN2 PACEMAKER CHANNELS. *J BIOL CHEM.* 2001;276:6069-6072
74. WHITAKER GM, ANGOLI D, NAZZARI H, SHIGEMOTO R, ACCILI EA. HCN2 AND HCN4 ISOFORMS SELF-ASSEMBLE AND CO-ASSEMBLE WITH EQUAL PREFERENCE TO FORM FUNCTIONAL PACEMAKER CHANNELS. *J BIOL CHEM.* 2007;282:22900-22909
75. XUE T, MARBAN E, LI RA. DOMINANT-NEGATIVE SUPPRESSION OF HCN1- AND HCN2- ENCODED PACEMAKER CURRENTS BY AN ENGINEERED HCN1 CONSTRUCT: INSIGHTS INTO STRUCTURE-FUNCTION RELATIONSHIPS AND MULTIMERIZATION. *CIRC RES.* 2002;90:1267-1273
76. KAUPP UB, SEIFERT R. MOLECULAR DIVERSITY OF PACEMAKER ION CHANNELS. *ANNU REV PHYSIOL.* 2001;63:235-257

77. HERRMANN S, LAYH B, LUDWIG A. NOVEL INSIGHTS INTO THE DISTRIBUTION OF CARDIAC HCN CHANNELS: AN EXPRESSION STUDY IN THE MOUSE HEART. *J MOL CELL CARDIOL*. 2011;51:997-1006
78. FENSKE S, MADER R, SCHARR A, PAPANIZOS C, CAO-EHLKER X, MICHALAKIS S, SHALTIEL L, WEIDINGER M, STIEBER J, FEIL S, FEIL R, HOFMANN F, WAHL-SCHOTT C, BIEL M. HCN3 CONTRIBUTES TO THE VENTRICULAR ACTION POTENTIAL WAVEFORM IN THE MURINE HEART. *CIRC RES*. 2011;109:1015-1023
79. SHI W, WYMORE R, YU H, WU J, WYMORE RT, PAN Z, ROBINSON RB, DIXON JE, MCKINNON D, COHEN IS. DISTRIBUTION AND PREVALENCE OF HYPERPOLARIZATION-ACTIVATED CATION CHANNEL (HCN) MRNA EXPRESSION IN CARDIAC TISSUES. *CIRC RES*. 1999;85:E1-6
80. MARIONNEAU C, COUETTE B, LIU J, LI H, MANGONI ME, NARGEOT J, LEI M, ESCANDE D, DEMOLOMBE S. SPECIFIC PATTERN OF IONIC CHANNEL GENE EXPRESSION ASSOCIATED WITH PACEMAKER ACTIVITY IN THE MOUSE HEART. *J PHYSIOL*. 2005;562:223-234
81. MOOSMANG S, STIEBER J, ZONG X, BIEL M, HOFMANN F, LUDWIG A. CELLULAR EXPRESSION AND FUNCTIONAL CHARACTERIZATION OF FOUR HYPERPOLARIZATION-ACTIVATED PACEMAKER CHANNELS IN CARDIAC AND NEURONAL TISSUES. *EUROPEAN JOURNAL OF BIOCHEMISTRY / FEBS*. 2001;268:1646-1652
82. FENSKE S, KRAUSE SC, HASSAN SI, BECIROVIC E, AUER F, BERNARD R, KUPATT C, LANGE P, ZIEGLER T, WOTJAK CT, ZHANG H, HAMMELMANN V, PAPANIZOS C, BIEL M, WAHL-SCHOTT CA. SICK SINUS SYNDROME IN HCN1-DEFICIENT MICE. *CIRCULATION*. 2013;128:2585-2594
83. VINOGRADOVA TM, LAKATTA EG. REGULATION OF BASAL AND RESERVE CARDIAC PACEMAKER FUNCTION BY INTERACTIONS OF CAMP-MEDIATED PKA-DEPENDENT CA<sup>2+</sup> CYCLING WITH SURFACE MEMBRANE CHANNELS. *J MOL CELL CARDIOL*. 2009;47:456-474
84. ROBINSON RB, BRINK PR, COHEN IS, ROSEN MR. I(F) AND THE BIOLOGICAL PACEMAKER. *PHARMACOLOGICAL RESEARCH*. 2006;53:407-415
85. LUDWIG A, BUDDE T, STIEBER J, MOOSMANG S, WAHL C, HOLTHOFF K, LANGE BARTELS A, WOTJAK C, MUNSCH T, ZONG X, FEIL S, FEIL R, LANCEL M, CHIEN KR, KONNERTH A, PAPE HC, BIEL M, HOFMANN F. ABSENCE EPILEPSY AND SINUS DYSRHYTHMIA IN MICE LACKING THE PACEMAKER CHANNEL HCN2. *EMBO J*. 2003;22:216-224
86. STIEBER J, HOFMANN F, LUDWIG A. PACEMAKER CHANNELS AND SINUS NODE ARRHYTHMIA. *TRENDS CARDIOVASC MED*. 2004;14:23-28
87. YANIV Y, TSUTSUI K, LAKATTA EG. POTENTIAL EFFECTS OF INTRINSIC HEART PACEMAKER CELL MECHANISMS ON DYSRHYTHMIC CARDIAC ACTION POTENTIAL FIRING. *FRONTIERS IN PHYSIOLOGY*. 2015;6:47
88. CHANDLER NJ GI, TELLEZ JO, INADA S, MUSA H, MOLENAAR P, DIFRANCESCO D, BARUSCOTTI M, LONGHI R, ANDERSON RH, BILLETTER R, SHARMA V, SIGG DC, BOYETT MR & DOBRZYNSKI H. MOLECULAR ARCHITECTURE OF THE HUMAN SINUS NODE – INSIGHTS INTO THE FUNCTION OF THE CARDIAC PACEMAKER. *CIRCULATION* 2009;119:1562–1575
89. STIEBER J, HERRMANN S, FEIL S, LOSTER J, FEIL R, BIEL M, HOFMANN F, LUDWIG A. THE HYPERPOLARIZATION-ACTIVATED CHANNEL HCN4 IS REQUIRED FOR THE GENERATION OF PACEMAKER ACTION POTENTIALS IN THE EMBRYONIC HEART. *PROC NATL ACAD SCI U S A*. 2003;100:15235-15240
90. BARUSCOTTI M, BUCCHI A, VISCOMI C, MANDELLI G, CONSALEZ G, GNECCHIRUSCONI T, MONTANO N, CASALI KR, MICHELONI S, BARBUTI A, DIFRANCESCO D. DEEP BRADYCARDIA AND HEART BLOCK CAUSED BY INDUCIBLE CARDIAC-SPECIFIC KNOCKOUT OF THE PACEMAKER CHANNEL GENE HCN4. *PROC NATL ACAD SCI U S A*. 2011;108:1705-1710
91. VERKERK AO, WILDERS R. PACEMAKER ACTIVITY OF THE HUMAN SINOATRIAL NODE: EFFECTS OF HCN4 MUTATIONS ON THE HYPERPOLARIZATION-ACTIVATED CURRENT. *EUROPACE*. 2014;16:384-395
92. VERKERK AO, WILDERS R. PACEMAKER ACTIVITY OF THE HUMAN SINOATRIAL

- NODE: AN UPDATE ON THE EFFECTS OF MUTATIONS IN HCN4 ON THE HYPERPOLARIZATION-ACTIVATED CURRENT. *INTERNATIONAL JOURNAL OF MOLECULAR SCIENCES*. 2015;16:3071-3094
93. SCHULZE-BAHR E, NEU A, FRIEDERICH P, KAUPP UB, BREITHARDT G, PONGS O, ISBRANDT D. PACEMAKER CHANNEL DYSFUNCTION IN A PATIENT WITH SINUS NODE DISEASE. *J CLIN INVEST*. 2003;111:1537-1545
  94. ORKAND RK, NIEDERGERKE R. HEART ACTION POTENTIAL: DEPENDENCE ON EXTERNAL CALCIUM AND SODIUM IONS. *SCIENCE*. 1964;146:1176-1177
  95. HAGIWARA N, IRISAWA H, KAMEYAMA M. CONTRIBUTION OF TWO TYPES OF CALCIUM CURRENTS TO THE PACEMAKER POTENTIALS OF RABBIT SINO-ATRIAL NODE CELLS. *J PHYSIOL*. 1988;395:233-253.
  96. PEREZ-REYES E. MOLECULAR PHYSIOLOGY OF LOW-VOLTAGE-ACTIVATED T-TYPE CALCIUM CHANNELS. *PHYSIOL REV*. 2003;83:117-161
  97. TREINYS R, JUREVICIUS J. L-TYPE CA<sup>2+</sup> CHANNELS IN THE HEART: STRUCTURE AND REGULATION. *MEDICINA*. 2008;44:491-499
  98. MANGONI ME, COUETTE B, BOURINET E, PLATZER J, REIMER D, STRIESSING J, NARGEOT J. FUNCTIONAL ROLE OF L-TYPE CAV1.3 CA<sup>2+</sup> CHANNELS IN CARDIAC PACEMAKER ACTIVITY. *PROC NATL ACAD SCI U S A*. 2003;100:5543-5548
  99. VERHEIJCK EE, VAN GINNEKEN AC, WILDERS R, BOUMAN LN. CONTRIBUTION OF L-TYPE CA<sup>2+</sup> CURRENT TO ELECTRICAL ACTIVITY IN SINOATRIAL NODAL MYOCYTES OF RABBITS. *AM J PHYSIOL*. 1999;276:H1064-1077
  100. DOERR T, DINGER R, TRAUTWEIN W. CALCIUM CURRENTS IN SINGLE SA NODAL CELLS OF THE RABBIT HEART STUDIED WITH ACTION POTENTIAL CLAMP. *PFLUGERS ARCH*. 1989;413:599-603
  101. KODAMA I, NIKMARAM MR, BOYETT MR, SUZUKI R, HONJO H, OWEN JM. REGIONAL DIFFERENCES IN THE ROLE OF THE CA<sup>2+</sup> AND NA<sup>+</sup> CURRENTS IN PACEMAKER ACTIVITY IN THE SINOATRIAL NODE. *AM J PHYSIOL*. 1997;272:H2793-2806
  102. VAN DER HEYDEN MA, WIJNHOFEN TJ, OPTHOF T. MOLECULAR ASPECTS OF ADRENERGIC MODULATION OF CARDIAC L-TYPE CA<sup>2+</sup> CHANNELS. *CARDIOVASC RES*. 2005;65:28-39
  103. SPEDDING M, PAOLETTI R. CLASSIFICATION OF CALCIUM CHANNELS AND CALCIUM ANTAGONISTS: PROGRESS REPORT. *CARDIOVASCULAR DRUGS AND THERAPY / SPONSORED BY THE INTERNATIONAL SOCIETY OF CARDIOVASCULAR PHARMACOTHERAPY*. 1992;6:35-39
  104. VERHEIJCK EE, WESSELS A, VAN GINNEKEN AC, BOURIER J, MARKMAN MW, VERMEULEN JL, DE BAKKER JM, LAMERS WH, OPTHOF T, BOUMAN LN. DISTRIBUTION OF ATRIAL AND NODAL CELLS WITHIN THE RABBIT SINOATRIAL NODE: MODELS OF SINOATRIAL TRANSITION. *CIRCULATION*. 1998;97:1623-1631
  105. LANDE G, DEMOLOMBE S, BAMMERT A, MOORMAN A, CHARPENTIER F, ESCANDE D. TRANSGENIC MICE OVEREXPRESSING HUMAN KVLQT1 DOMINANT-NEGATIVE ISOFORM. PART II: PHARMACOLOGICAL PROFILE. *CARDIOVASC RES*. 2001;50:328-334
  106. GOMEZ AM, VALDIVIA HH, CHENG H, LEDERER MR, SANTANA LF, CANNELL MB, MCCUNE SA, ALTSCHULD RA, LEDERER WJ. DEFECTIVE EXCITATION-CONTRACTION COUPLING IN EXPERIMENTAL CARDIAC HYPERTROPHY AND HEART FAILURE. *SCIENCE*. 1997;276:800-806
  107. WAGNER E, LAUTERBACH MA, KOHL T, WESTPHAL V, WILLIAMS GS, STEINBRECHER JH, STREICH JH, KORFF B, TUAN HT, HAGEN B, LUTHER S, HASENFUSS G, PARLITZ U, JAFRI MS, HELL SW, LEDERER WJ, LEHNART SE. STIMULATED EMISSION DEPLETION LIVE-CELL SUPER-RESOLUTION IMAGING SHOWS PROLIFERATIVE REMODELING OF T-TUBULE MEMBRANE STRUCTURES AFTER MYOCARDIAL INFARCTION. *CIRC RES*. 2012;111:402-414
  108. CATTERALL WA, STRIESSNIG J, SNUTCH TP, PEREZ-REYES E, INTERNATIONAL UNION OF P. INTERNATIONAL UNION OF PHARMACOLOGY. XL. COMPENDIUM OF VOLTAGE-GATED ION CHANNELS: CALCIUM CHANNELS. *PHARMACOL REV*. 2003;55:579-581
  109. CATTERALL WA. STRUCTURE AND REGULATION OF VOLTAGE-GATED CA<sup>2+</sup> CHANNELS. *ANNU REV CELL DEV BIOL*. 2000;16:521-555.
  110. MANGONI ME CB, MARGER L, BOURINET E, STRIESSNIG J, J. N. VOLTAGE-DEPENDENT CALCIUM CHANNELS AND CARDIAC PACEMAKER



ACTIVITY: FROM IONIC CURRENTS TO GENES. *PROG BIOPHYS MOL BIOL*. 2006;90:38–63

111. ZHANG Z, HE Y, TUTEJA D, XU D, TIMOFEYEV V, ZHANG Q, GLATTER KA, XU Y, SHIN HS, LOW R, CHIAMVIMONVAT N. FUNCTIONAL ROLES OF CAV1.3(ALPHA1D) CALCIUM CHANNELS IN ATRIA: INSIGHTS GAINED FROM GENE-TARGETED NULL MUTANT MICE. *CIRCULATION*. 2005;112:1936-1944
112. TORRENTE AG, MESIRCA P, NECO P, RIZZETTO R, DUBEL S, BARRERE C, SINEGGER-BRAUNS M, STRIESSNIG J, RICHARD S, NARGEOT J, GOMEZ AM, MANGONI ME. L-TYPE CAV1.3 CHANNELS REGULATE RYANODINE RECEPTOR-DEPENDENT CA<sup>2+</sup> RELEASE DURING SINO-ATRIAL NODE PACEMAKER ACTIVITY. *CARDIOVASC RES*. 2016;109:451-461
113. KOSCHAK A, REIMER D, HUBER I, GRABNER M, GLOSSMANN H, ENGEL J, STRIESSNIG J. ALPHA 1D (CAV1.3) SUBUNITS CAN FORM L-TYPE CA<sup>2+</sup> CHANNELS ACTIVATING AT NEGATIVE VOLTAGES. *J BIOL CHEM*. 2001;276:22100-22106
114. PLATZER J, ENGEL J, SCHROTT-FISCHER A, STEPHAN K, BOVA S, CHEN H, ZHENG H, STRIESSNIG J. CONGENITAL DEAFNESS AND SINOATRIAL NODE DYSFUNCTION IN MICE LACKING CLASS D L-TYPE CA<sup>2+</sup> CHANNELS. *CELL*. 2000;102:89-97
115. MATTHES J, JAGER A, HANDROCK R, GRONER F, MEHLHORN U, SCHWINGER RH, VARADI G, SCHWARTZ A, HERZIG S. CA<sup>2+</sup>-DEPENDENT MODULATION OF SINGLE HUMAN CARDIAC L-TYPE CALCIUM CHANNELS BY THE CALCINEURIN INHIBITOR CYCLOSPORINE. *J MOL CELL CARDIOL*. 2004;36:241-255
116. ZHANG Z, XU Y, SONG H, RODRIGUEZ J, TUTEJA D, NAMKUNG Y, SHIN HS, CHIAMVIMONVAT N. FUNCTIONAL ROLES OF CA(V)1.3 (ALPHA(1D)) CALCIUM CHANNEL IN SINOATRIAL NODES: INSIGHT GAINED USING GENE-TARGETED NULL MUTANT MICE. *CIRC RES*. 2002;90:981-987
117. SINNEGGER-BRAUNS MJ, HETZENAUER A, HUBER IG, RENSTROM E, WIETZORREK G, BERJUKOV S, CAVALLI M, WALTER D, KOSCHAK A, WALDSCHUTZ R, HERING S, BOVA S, RORSMAN P, PONGS O, SINGEWALD N, STRIESSNIG J. ISOFORM-SPECIFIC REGULATION OF MOOD BEHAVIOR AND PANCREATIC BETA CELL AND CARDIOVASCULAR FUNCTION BY L-TYPE CA<sup>2+</sup> CHANNELS. *J CLIN INVEST*. 2004;113:1430-1439
118. ZHANG Q, TIMOFEYEV V, QIU H, LU L, LI N, SINGAPURI A, TORADO CL, SHIN HS, CHIAMVIMONVAT N. EXPRESSION AND ROLES OF CAV1.3 (ALPHA1D) L-TYPE CA(2)+ CHANNEL IN ATRIOVENTRICULAR NODE AUTOMATICITY. *J MOL CELL CARDIOL*. 2011;50:194-202
119. MARGER L, MESIRCA P, ALIG J, TORRENTE A, DUBEL S, ENGELAND B, KANANI S, FONTANAUD P, STRIESSNIG J, SHIN HS, ISBRANDT D, EHMKE H, NARGEOT J, MANGONI ME. FUNCTIONAL ROLES OF CA(V)1.3, CA(V)3.1 AND HCN CHANNELS IN AUTOMATICITY OF MOUSE ATRIOVENTRICULAR CELLS: INSIGHTS INTO THE ATRIOVENTRICULAR PACEMAKER MECHANISM. *CHANNELS (AUSTIN)*. 2011;5:251-261
120. BAKER K, WARREN KS, YELLEN G, FISHMAN MC. DEFECTIVE "PACEMAKER" CURRENT (I<sub>H</sub>) IN A ZEBRAFISH MUTANT WITH A SLOW HEART RATE. *PROC NATL ACAD SCI U S A*. 1997;94:4554-4559
121. CRIBBS LL, MARTIN BL, SCHRODER EA, KELLER BB, DELISLE BP, SATIN J. IDENTIFICATION OF THE T-TYPE CALCIUM CHANNEL (CA(V)3.1D) IN DEVELOPING MOUSE HEART. *CIRC RES*. 2001;88:403-407
122. CRIBBS L. T-TYPE CALCIUM CHANNEL EXPRESSION AND FUNCTION IN THE DISEASED HEART. *CHANNELS (AUSTIN)*. 2010;4:447-452
123. MANGONI ME, TRABOULSIE A, LEONI AL, COUETTE B, MARGER L, LE QUANG K, KUPFER E, COHEN-SOLAL A, VILAR J, SHIN HS, ESCANDE D, CHARPENTIER F, NARGEOT J, LORY P. BRADYCARDIA AND SLOWING OF THE ATRIOVENTRICULAR CONDUCTION IN MICE LACKING CAV3.1/ALPHA1G T-TYPE CALCIUM CHANNELS. *CIRC RES*. 2006;98:1422-1430
124. LEURANGUER V, MONTEIL A, BOURINET E, DAYANITHI G, NARGEOT J. T-TYPE CALCIUM CURRENTS IN RAT CARDIOMYOCYTES DURING POSTNATAL DEVELOPMENT: CONTRIBUTION TO HORMONE SECRETION. *AM J PHYSIOL HEART CIRC PHYSIOL*. 2000;279:H2540-2548.
125. FERMINI B, NATHAN RD. REMOVAL OF SIALIC ACID ALTERS BOTH T- AND L-TYPE CALCIUM CURRENTS IN CARDIAC MYOCYTES. *AM J PHYSIOL*. 1991;260:H735-743

126. EFIMOV IR, NIKOLSKI VP, ROTHENBERG F, GREENER ID, LI J, DOBRZYNSKI H, BOYETT M. STRUCTURE-FUNCTION RELATIONSHIP IN THE AV JUNCTION. *THE ANATOMICAL RECORD. PART A, DISCOVERIES IN MOLECULAR, CELLULAR, AND EVOLUTIONARY BIOLOGY*. 2004;280:952-965
127. HIRANO Y, FOZZARD HA, JANUARY CT. CHARACTERISTICS OF L- AND T-TYPE CA<sup>2+</sup> CURRENTS IN CANINE CARDIAC PURKINJE CELLS. *AM J PHYSIOL*. 1989;256:H1478-1492
128. TSENG GN, BOYDEN PA. MULTIPLE TYPES OF CA<sup>2+</sup> CURRENTS IN SINGLE CANINE PURKINJE CELLS. *CIRC RES*. 1989;65:1735-1750
129. ONO K, IJIMA T. PATHOPHYSIOLOGICAL SIGNIFICANCE OF T-TYPE CA<sup>2+</sup> CHANNELS: PROPERTIES AND FUNCTIONAL ROLES OF T-TYPE CA<sup>2+</sup> CHANNELS IN CARDIAC PACEMAKING. *JOURNAL OF PHARMACOLOGICAL SCIENCES*. 2005;99:197-204
130. CARBONE E, LUX HD. KINETICS AND SELECTIVITY OF A LOW-VOLTAGE-ACTIVATED CALCIUM CURRENT IN CHICK AND RAT SENSORY NEURONES. *J PHYSIOL*. 1987;386:547-570
131. HUSER J, BLATTER LA, LIPSIUS SL. INTRACELLULAR CA<sup>2+</sup> RELEASE CONTRIBUTES TO AUTOMATICITY IN CAT ATRIAL PACEMAKER CELLS. *J PHYSIOL*. 2000;524 PT 2:415-422
132. LIPSIUS SL, HUSER J, BLATTER LA. INTRACELLULAR CA<sup>2+</sup> RELEASE SPARKS ATRIAL PACEMAKER ACTIVITY. *NEWS IN PHYSIOLOGICAL SCIENCES : AN INTERNATIONAL JOURNAL OF PHYSIOLOGY PRODUCED JOINTLY BY THE INTERNATIONAL UNION OF PHYSIOLOGICAL SCIENCES AND THE AMERICAN PHYSIOLOGICAL SOCIETY*. 2001;16:101-106
133. VINOGRADOVA TM BK, LAKATTA EG. . BETA-ADRENERGIC STIMULATION MODULATES RYANODINE RECEPTOR CA(2+) RELEASE DURING DIASTOLIC DEPOLARIZATION TO ACCELERATE PACEMAKER ACTIVITY IN RABBIT SINOATRIAL NODAL CELLS. *CIRC RES*. . 2002;90:73-79
134. MESIRCA P, TORRENTE AG, MANGONI ME. T-TYPE CHANNELS IN THE SINO-ATRIAL AND ATRIOVENTRICULAR PACEMAKER MECHANISM. *PFLUGERS ARCH*. 2014;466:791-799
135. LE QUANG K, BENITO B, NAUD P, QI XY, SHI YF, TARDIF JC, GILLIS MA, DOBREV D, CHARPENTIER F, NATTEL S. T-TYPE CALCIUM CURRENT CONTRIBUTES TO ESCAPE AUTOMATICITY AND GOVERNS THE OCCURRENCE OF LETHAL ARRHYTHMIAS AFTER ATRIOVENTRICULAR BLOCK IN MICE. *CIRC ARRHYTHM ELECTROPHYSIOL*. 2013;6:799-808
136. CHEN CC, LAMPING KG, NUNO DW, BARRESI R, PROUTY SJ, LAVOIE JL, CRIBBS LL, ENGLAND SK, SIGMUND CD, WEISS RM, WILLIAMSON RA, HILL JA, CAMPBELL KP. ABNORMAL CORONARY FUNCTION IN MICE DEFICIENT IN ALPHA1H T-TYPE CA<sup>2+</sup> CHANNELS. *SCIENCE*. 2003;302:1416-1418
137. NIWA N, YASUI K, OPTHOF T, TAKEMURA H, SHIMIZU A, HORIBA M, LEE JK, HONJO H, KAMIYA K, KODAMA I. CAV3.2 SUBUNIT UNDERLIES THE FUNCTIONAL T-TYPE CA<sup>2+</sup> CHANNEL IN MURINE HEARTS DURING THE EMBRYONIC PERIOD. *AM J PHYSIOL HEART CIRC PHYSIOL*. 2004;286:H2257-2263
138. MAIER SK, WESTENBROEK RE, YAMANUSHI TT, DOBRZYNSKI H, BOYETT MR, CATTERALL WA, SCHEUER T. AN UNEXPECTED REQUIREMENT FOR BRAIN-TYPE SODIUM CHANNELS FOR CONTROL OF HEART RATE IN THE MOUSE SINOATRIAL NODE. *PROC NATL ACAD SCI U S A*. 2003;100:3507-3512
139. LEI M JS, LIU J, LANCASTER MK, FUNG SS, DOBRZYNSKI H,, CAMELLITI P MS, NOBLE D, BOYETT MR. . REQUIREMENT OF NEURONAL AND CARDIAC-TYPE SODIUM CHANNELS FOR MURINE SINOATRIAL NODE PACEMAKING. *J PHYSIOL*. . 2004;559:835– 848
140. INADA S, ZHANG H, TELLEZ JO, SHIBATA N, NAKAZAWA K, KAMIYA K, KODAMA I, MITSUI K, DOBRZYNSKI H, BOYETT MR, HONJO H. IMPORTANCE OF GRADIENTS IN MEMBRANE PROPERTIES AND ELECTRICAL COUPLING IN SINOATRIAL NODE PACING. *PLOS ONE*. 2014;9:E94565
141. HONJO H, BOYETT MR, KODAMA I, TOYAMA J. CORRELATION BETWEEN ELECTRICAL ACTIVITY AND THE SIZE OF RABBIT SINO-ATRIAL NODE CELLS. *J PHYSIOL*. 1996;496 ( PT 3):795-808
142. BARUSCOTTI M, DIFRANCESCO D, ROBINSON RB. A TTX-SENSITIVE INWARD SODIUM

- CURRENT CONTRIBUTES TO SPONTANEOUS ACTIVITY IN NEWBORN RABBIT SINO-ATRIAL NODE CELLS. *J PHYSIOL*. 1996;492 ( PT 1):21-30
143. BARUSCOTTI M, WESTENBROEK R, CATTERALL WA, DIFRANCESCO D, ROBINSON RB. THE NEWBORN RABBIT SINO-ATRIAL NODE EXPRESSES A NEURONAL TYPE I-LIKE NA<sup>+</sup> CHANNEL. *J PHYSIOL*. 1997;498 ( PT 3):641-648
  144. BARUSCOTTI M, DIFRANCESCO D, ROBINSON RB. NA(+) CURRENT CONTRIBUTION TO THE DIASTOLIC DEPOLARIZATION IN NEWBORN RABBIT SA NODE CELLS. *AM J PHYSIOL HEART CIRC PHYSIOL*. 2000;279:H2303-2309
  145. CLARK RB, MANGONI ME, LUEGER A, COUETTE B, NARGEOT J, GILES WR. A RAPIDLY ACTIVATING DELAYED RECTIFIER K<sup>+</sup> CURRENT REGULATES PACEMAKER ACTIVITY IN ADULT MOUSE SINOATRIAL NODE CELLS. *AM J PHYSIOL HEART CIRC PHYSIOL*. 2004;286:H1757-1766
  146. ITO H, ONO K. A RAPIDLY ACTIVATING DELAYED RECTIFIER K<sup>+</sup> CHANNEL IN RABBIT SINOATRIAL NODE CELLS. *AM J PHYSIOL*. 1995;269:H443-452
  147. LEI M, BROWN HF. TWO COMPONENTS OF THE DELAYED RECTIFIER POTASSIUM CURRENT, I<sub>K</sub>, IN RABBIT SINO-ATRIAL NODE CELLS. *EXPERIMENTAL PHYSIOLOGY*. 1996;81:725-741
  148. TAMARGO J, CABALLERO R, GOMEZ R, VALENZUELA C, DELPON E. PHARMACOLOGY OF CARDIAC POTASSIUM CHANNELS. *CARDIOVASC RES*. 2004;62:9-33
  149. ONO K, SHIBATA S, IJIMA T. PROPERTIES OF THE DELAYED RECTIFIER POTASSIUM CURRENT IN PORCINE SINO-ATRIAL NODE CELLS. *J PHYSIOL*. 2000;524 PT 1:51-62
  150. ONO K, ITO H. ROLE OF RAPIDLY ACTIVATING DELAYED RECTIFIER K<sup>+</sup> CURRENT IN SINOATRIAL NODE PACEMAKER ACTIVITY. *AM J PHYSIOL*. 1995;269:H453-462
  151. MATSUURA H, EHARA T, DING WG, OMATSU-KANBE M, ISONO T. RAPIDLY AND SLOWLY ACTIVATING COMPONENTS OF DELAYED RECTIFIER K(+) CURRENT IN GUINEA-PIG SINO-ATRIAL NODE PACEMAKER CELLS. *J PHYSIOL*. 2002;540:815-830
  152. VERHEIJCK EE, WILDERS R, BOUMAN LN. ATRIO-SINUS INTERACTION DEMONSTRATED BY BLOCKADE OF THE RAPID DELAYED RECTIFIER CURRENT. *CIRCULATION*. 2002;105:880-885
  153. LEI M, COOPER PJ, CAMELLITI P, KOHL P. ROLE OF THE 293B-SENSITIVE, SLOWLY ACTIVATING DELAYED RECTIFIER POTASSIUM CURRENT, I(K<sub>S</sub>), IN PACEMAKER ACTIVITY OF RABBIT ISOLATED SINO-ATRIAL NODE CELLS. *CARDIOVASC RES*. 2002;53:68-79
  154. HONJO H, LEI M, BOYETT MR, KODAMA I. HETEROGENEITY OF 4-AMINOPYRIDINE-SENSITIVE CURRENT IN RABBIT SINOATRIAL NODE CELLS. *AM J PHYSIOL*. 1999;276:H1295-1304
  155. LEI M, HONJO H, KODAMA I, BOYETT MR. CHARACTERISATION OF THE TRANSIENT OUTWARD K<sup>+</sup> CURRENT IN RABBIT SINOATRIAL NODE CELLS. *CARDIOVASC RES*. 2000;46:433-441
  156. CHO HS, TAKANO M, NOMA A. THE ELECTROPHYSIOLOGICAL PROPERTIES OF SPONTANEOUSLY BEATING PACEMAKER CELLS ISOLATED FROM MOUSE SINOATRIAL NODE. *J PHYSIOL*. 2003;550:169-180
  157. DIFRANCESCO D, DUCOURET P, ROBINSON RB. MUSCARINIC MODULATION OF CARDIAC RATE AT LOW ACETYLCHOLINE CONCENTRATIONS. *SCIENCE*. 1989;243:669-671
  158. GILES W, NOBLE SJ. CHANGES IN MEMBRANE CURRENTS IN BULLFROG ATRIUM PRODUCED BY ACETYLCHOLINE. *J PHYSIOL*. 1976;261:103-123
  159. NOMA A, TRAUTWEIN W. RELAXATION OF THE ACH-INDUCED POTASSIUM CURRENT IN THE RABBIT SINOATRIAL NODE CELL. *PFLUGERS ARCH*. 1978;377:193-200
  160. WICKMAN K, KRAPIVINSKY G, COREY S, KENNEDY M, NEMEC J, MEDINA I, CLAPHAM DE. STRUCTURE, G PROTEIN ACTIVATION, AND FUNCTIONAL RELEVANCE OF THE CARDIAC G PROTEIN-GATED K<sup>+</sup> CHANNEL, I<sub>KACH</sub>. *ANN N Y ACAD SCI*. 1999;868:386-398
  161. REUVENY E, SLESINGER PA, INGLESE J, MORALES JM, INIGUEZ-LLUHI JA, LEFKOWITZ RJ, BOURNE HR, JAN YN, JAN LY. ACTIVATION OF THE CLONED MUSCARINIC POTASSIUM CHANNEL BY G PROTEIN BETA GAMMA SUBUNITS. *NATURE*. 1994;370:143-146
  162. MESIRCA P, BIDAUD I, BRIEC F, EVAÏN S, TORRENTE AG, LE QUANG K, LEONI AL,

- BAUDOT M, MARGER L, CHUNG YOU CHONG A, NARGEOT J, STRIESSNIG J, WICKMAN K, CHARPENTIER F, MANGONI ME. G PROTEIN-GATED IKACH CHANNELS AS THERAPEUTIC TARGETS FOR TREATMENT OF SICK SINUS SYNDROME AND HEART BLOCK. *PROC NATL ACAD SCI U S A*. 2016;113:E932-941
163. YAMADA M. THE ROLE OF MUSCARINIC K(+) CHANNELS IN THE NEGATIVE CHRONOTROPIC EFFECT OF A MUSCARINIC AGONIST. *J PHARMACOL EXP THER*. 2002;300:681-687
164. VAN WAGONER DR. MECHANOSENSITIVE GATING OF ATRIAL ATP-SENSITIVE POTASSIUM CHANNELS. *CIRC RES*. 1993;72:973-983
165. HAN X, LIGHT PE, GILES WR, FRENCH RJ. IDENTIFICATION AND PROPERTIES OF AN ATP-SENSITIVE K+ CURRENT IN RABBIT SINO-ATRIAL NODE PACEMAKER CELLS. *J PHYSIOL*. 1996;490 ( PT 2):337-350
166. VERGARA C, LATORRE R, MARRION NV, ADELMAN JP. CALCIUM-ACTIVATED POTASSIUM CHANNELS. *CURRENT OPINION IN NEUROBIOLOGY*. 1998;8:321-329
167. KNAUS HG, SCHWARZER C, KOCH RO, EBERHART A, KACZOROWSKI GJ, GLOSSMANN H, WUNDER F, PONGS O, GARCIA ML, SPERK G. DISTRIBUTION OF HIGH-CONDUCTANCE CA(2+)-ACTIVATED K+ CHANNELS IN RAT BRAIN: TARGETING TO AXONS AND NERVE TERMINALS. *THE JOURNAL OF NEUROSCIENCE : THE OFFICIAL JOURNAL OF THE SOCIETY FOR NEUROSCIENCE*. 1996;16:955-963
168. NELSON MT, CHENG H, RUBART M, SANTANA LF, BONEV AD, KNOT HJ, LEDERER WJ. RELAXATION OF ARTERIAL SMOOTH MUSCLE BY CALCIUM SPARKS. *SCIENCE*. 1995;270:633-637
169. IMLACH WL, FINCH SC, MILLER JH, MEREDITH AL, DALZIEL JE. A ROLE FOR BK CHANNELS IN HEART RATE REGULATION IN RODENTS. *PLOS ONE*. 2010;5:E8698
170. LAI MH, WU Y, GAO Z, ANDERSON ME, DALZIEL JE, MEREDITH AL. BK CHANNELS REGULATE SINOATRIAL NODE FIRING RATE AND CARDIAC PACING IN VIVO. *AM J PHYSIOL HEART CIRC PHYSIOL*. 2014;307:H1327-1338
171. XU W, LIU Y, WANG S, MCDONALD T, VAN EYK JE, SIDOR A, O'ROURKE B. CYTOPROTECTIVE ROLE OF CA2+- ACTIVATED K+ CHANNELS IN THE CARDIAC INNER MITOCHONDRIAL MEMBRANE. *SCIENCE*. 2002;298:1029-1033
172. XU Y, TUTEJA D, ZHANG Z, XU D, ZHANG Y, RODRIGUEZ J, NIE L, TUXSON HR, YOUNG JN, GLATTER KA, VAZQUEZ AE, YAMOAH EN, CHIAMVIMONVAT N. MOLECULAR IDENTIFICATION AND FUNCTIONAL ROLES OF A CA(2+)-ACTIVATED K+ CHANNEL IN HUMAN AND MOUSE HEARTS. *J BIOL CHEM*. 2003;278:49085-49094
173. TUTEJA D, XU D, TIMOFEYEV V, LU L, SHARMA D, ZHANG Z, XU Y, NIE L, VAZQUEZ AE, YOUNG JN, GLATTER KA, CHIAMVIMONVAT N. DIFFERENTIAL EXPRESSION OF SMALL-CONDUCTANCE CA2+-ACTIVATED K+ CHANNELS SK1, SK2, AND SK3 IN MOUSE ATRIAL AND VENTRICULAR MYOCYTES. *AM J PHYSIOL HEART CIRC PHYSIOL*. 2005;289:H2714-2723
174. LI N, TIMOFEYEV V, TUTEJA D, XU D, LU L, ZHANG Q, ZHANG Z, SINGAPURI A, ALBERT TR, RAJAGOPAL AV, BOND CT, PERIASAMY M, ADELMAN J, CHIAMVIMONVAT N. ABLATION OF A CA2+-ACTIVATED K+ CHANNEL (SK2 CHANNEL) RESULTS IN ACTION POTENTIAL PROLONGATION IN ATRIAL MYOCYTES AND ATRIAL FIBRILLATION. *J PHYSIOL*. 2009;587:1087-1100
175. QI XY, DINESS JG, BRUNDEL BJ, ZHOU XB, NAUD P, WU CT, HUANG H, HARADA M, AFLAKI M, DOBREV D, GRUNNET M, NATTEL S. ROLE OF SMALL-CONDUCTANCE CALCIUM-ACTIVATED POTASSIUM CHANNELS IN ATRIAL ELECTROPHYSIOLOGY AND FIBRILLATION IN THE DOG. *CIRCULATION*. 2014;129:430-440
176. WEISBROD D, PERETZ A, ZISKIND A, MENAKER N, OZ S, BARAD L, ELIYAHU S, ITSKOVITZ-ELDOR J, DASCAL N, KHANANSHVILI D, BINAH O, ATTALI B. SK4 CA2+ ACTIVATED K+ CHANNEL IS A CRITICAL PLAYER IN CARDIAC PACEMAKER DERIVED FROM HUMAN EMBRYONIC STEM CELLS. *PROC NATL ACAD SCI U S A*. 2013;110:E1685-1694
177. GUO J, ONO K, NOMA A. A SUSTAINED INWARD CURRENT ACTIVATED AT THE DIASTOLIC POTENTIAL RANGE IN RABBIT SINO-ATRIAL NODE CELLS. *J PHYSIOL*. 1995;483 ( PT 1):1-13
178. GUO J, NOMA A. EXISTENCE OF A LOW-THRESHOLD AND SUSTAINED INWARD CURRENT IN RABBIT ATRIO-VENTRICULAR NODE CELLS. *THE JAPANESE JOURNAL OF*

- PHYSIOLOGY*. 1997;47:355-359
179. GUO J, MITSUIYE T, NOMA A. THE SUSTAINED INWARD CURRENT IN SINO-ATRIAL NODE CELLS OF GUINEA-PIG HEART. *PFLUGERS ARCH*. 1997;433:390-396
  180. MITSUIYE T, SHINAGAWA Y, NOMA A. SUSTAINED INWARD CURRENT DURING PACEMAKER DEPOLARIZATION IN MAMMALIAN SINOATRIAL NODE CELLS. *CIRC RES*. 2000;87:88-91
  181. VENKATACHALAM K, MONTELL C. TRP CHANNELS. *ANNUAL REVIEW OF BIOCHEMISTRY*. 2007;76:387-417
  182. LOF C, VIITANEN T, SUKUMARAN P, TORNQUIST K. TRPC2: OF MICE BUT NOT MEN. *ADV EXP MED BIOL*. 2011;704:125-134
  183. NILIUS B, OWSIANIK G, VOETS T, PETERS JA. TRANSIENT RECEPTOR POTENTIAL CATION CHANNELS IN DISEASE. *PHYSIOL REV*. 2007;87:165-217
  184. ABRAMOWITZ J, BIRNBAUMER L. PHYSIOLOGY AND PATHOPHYSIOLOGY OF CANONICAL TRANSIENT RECEPTOR POTENTIAL CHANNELS. *FASEB J*. 2009;23:297-328
  185. FRISCHAUF I, SCHINDL R, DERLER I, BERGSMANN J, FAHRNER M, ROMANIN C. THE STIM/ORAI COUPLING MACHINERY. *CHANNELS (AUSTIN)*. 2008;2:261-268
  186. YUAN JP, ZENG W, HUANG GN, WORLEY PF, MUALLEM S. STIM1 HETEROMULTIMERIZES TRPC CHANNELS TO DETERMINE THEIR FUNCTION AS STORE-OPERATED CHANNELS. *NAT CELL BIOL*. 2007;9:636-645
  187. LIAO Y, PLUMMER NW, GEORGE MD, ABRAMOWITZ J, ZHU MX, BIRNBAUMER L. A ROLE FOR ORAI IN TRPC-MEDIATED CA<sup>2+</sup> ENTRY SUGGESTS THAT A TRPC:ORAI COMPLEX MAY MEDIATE STORE AND RECEPTOR OPERATED CA<sup>2+</sup> ENTRY. *PROC NATL ACAD SCI U S A*. 2009;106:3202-3206
  188. PANI B, ONG HL, LIU X, RAUSER K, AMBUDKAR IS, SINGH BB. LIPID RAFTS DETERMINE CLUSTERING OF STIM1 IN ENDOPLASMIC RETICULUM-PLASMA MEMBRANE JUNCTIONS AND REGULATION OF STORE-OPERATED CA<sup>2+</sup> ENTRY (SOCE). *J BIOL CHEM*. 2008;283:17333-17340
  189. DEHAVEN WI, JONES BF, PETRANKA JG, SMYTH JT, TOMITA T, BIRD GS, PUTNEY JW, JR. TRPC CHANNELS FUNCTION INDEPENDENTLY OF STIM1 AND ORAI1. *J PHYSIOL*. 2009;587:2275-2298
  190. DOMINGUEZ-RODRIGUEZ A, RUIZ-HURTADO G, BENITAH JP, GOMEZ AM. THE OTHER SIDE OF CARDIAC CA(2+) SIGNALING: TRANSCRIPTIONAL CONTROL. *FRONTIERS IN PHYSIOLOGY*. 2012;3:452
  191. BUSH EW, HOOD DB, PAPST PJ, CHAPO JA, MINOBE W, BRISTOW MR, OLSON EN, MCKINSEY TA. CANONICAL TRANSIENT RECEPTOR POTENTIAL CHANNELS PROMOTE CARDIOMYOCYTE HYPERTROPHY THROUGH ACTIVATION OF CALCINEURIN SIGNALING. *J BIOL CHEM*. 2006;281:33487-33496
  192. KUWAHARA K, WANG Y, MCANALLY J, RICHARDSON JA, BASSEL-DUBY R, HILL JA, OLSON EN. TRPC6 FULFILLS A CALCINEURIN SIGNALING CIRCUIT DURING PATHOLOGIC CARDIAC REMODELING. *J CLIN INVEST*. 2006;116:3114-3126
  193. NAKAYAMA H, WILKIN BJ, BODI I, MOLKENTIN JD. CALCINEURIN-DEPENDENT CARDIOMYOPATHY IS ACTIVATED BY TRPC IN THE ADULT MOUSE HEART. *FASEB J*. 2006;20:1660-1670
  194. ONOHARA N, NISHIDA M, INOUE R, KOBAYASHI H, SUMIMOTO H, SATO Y, MORI Y, NAGAO T, KUROSE H. TRPC3 AND TRPC6 ARE ESSENTIAL FOR ANGIOTENSIN II-INDUCED CARDIAC HYPERTROPHY. *EMBO J*. 2006;25:5305-5316
  195. JU YK, CHU Y, CHAULET H, LAI D, GERVASIO OL, GRAHAM RM, CANNELL MB, ALLEN DG. STORE-OPERATED CA<sup>2+</sup> INFLUX AND EXPRESSION OF TRPC GENES IN MOUSE SINOATRIAL NODE. *CIRC RES*. 2007;100:1605-1614
  196. JU YK, ALLEN DG. STORE-OPERATED CA<sup>2+</sup> ENTRY AND TRPC EXPRESSION; POSSIBLE ROLES IN CARDIAC PACEMAKER TISSUE. *HEART, LUNG & CIRCULATION*. 2007;16:349-355
  197. JU YK, WOODCOCK EA, ALLEN DG, CANNELL MB. INOSITOL 1,4,5-TRISPHOSPHATE RECEPTORS AND PACEMAKER RHYTHMS. *J MOL CELL CARDIOL*. 2012;53:375-381
  198. JU YK, LEE BH, TRAJANOVSKA S, HAO G, ALLEN DG, LEI M, CANNELL MB. THE INVOLVEMENT OF TRPC3 CHANNELS IN SINOATRIAL ARRHYTHMIAS. *FRONTIERS IN PHYSIOLOGY*. 2015;6:86
  199. SALIDO GM, SAGE SO, ROSADO JA. TRPC CHANNELS AND STORE-OPERATED CA(2+)

- ENTRY. *BIOCHIM BIOPHYS ACTA*. 2009;1793:223-230
200. ZHANG H, SUN AY, KIM JJ, GRAHAM V, FINCH EA, NEPLIOUEV I, ZHAO G, LI T, LEDERER WJ, STIBER JA, PITT GS, BURSAC N, ROSENBERG PB. STIM1-CA<sup>2+</sup> SIGNALING MODULATES AUTOMATICITY OF THE MOUSE SINOATRIAL NODE. *PROC NATL ACAD SCI U S A*. 2015;112:E5618-5627
  201. LIU J, XIN L, BENSON VL, ALLEN DG, JU YK. STORE-OPERATED CALCIUM ENTRY AND THE LOCALIZATION OF STIM1 AND ORA11 PROTEINS IN ISOLATED MOUSE SINOATRIAL NODE CELLS. *FRONTIERS IN PHYSIOLOGY*. 2015;6:69
  202. DEMION M, BOIS P, LAUNAY P, GUINAMARD R. TRPM4, A CA<sup>2+</sup>-ACTIVATED NONSELECTIVE CATION CHANNEL IN MOUSE SINO-ATRIAL NODE CELLS. *CARDIOVASC RES*. 2007;73:531-538
  203. HOF T, SIMARD C, ROUET R, SALLE L, GUINAMARD R. IMPLICATION OF THE TRPM4 NONSELECTIVE CATION CHANNEL IN MAMMALIAN SINUS RHYTHM. *HEART RHYTHM*. 2013;10:1683-1689
  204. LITTLE SC, MOHLER PJ. TRPM4 MODULATES SINUS NODE DIASTOLIC DEPOLARIZATION. *HEART RHYTHM*. 2013;10:1690-1691
  205. SAH R, MESIRCA P, VAN DEN BOOGERT M, ROSEN J, MABLY J, MANGONI ME, CLAPHAM DE. ION CHANNEL-KINASE TRPM7 IS REQUIRED FOR MAINTAINING CARDIAC AUTOMATICITY. *PROC NATL ACAD SCI U S A*. 2013;110:E3037-3046
  206. SAKAI R, HAGIWARA N, MATSUDA N, KASSANUKI H, HOSODA S. SODIUM--POTASSIUM PUMP CURRENT IN RABBIT SINO-ATRIAL NODE CELLS. *J PHYSIOL*. 1996;490 ( PT 1):51-62
  207. DIFRANCESCO D, NOBLE D. THE FUNNY CURRENT HAS A MAJOR PACEMAKING ROLE IN THE SINUS NODE. *HEART RHYTHM*. 2012;9:299-301
  208. CHEN PS, JOUNG B, SHINOHARA T, DAS M, CHEN Z, LIN SF. THE INITIATION OF THE HEART BEAT. *CIRC J*. 2010;74:221-225
  209. LYASHKOV AE, JUHASZOVA M, DOBRZYNSKI H, VINOGRADOVA TM, MALTSEV VA, JUHASZ O, SPURGEON HA, SOLLOTT SJ, LAKATTA EG. CALCIUM CYCLING PROTEIN DENSITY AND FUNCTIONAL IMPORTANCE TO AUTOMATICITY OF ISOLATED SINOATRIAL NODAL CELLS ARE INDEPENDENT OF CELL SIZE. *CIRC RES*. 2007;100:1723-1731
  210. ZHOU Z, LIPSIOUS SL. NA(+)-CA<sup>2+</sup> EXCHANGE CURRENT IN LATENT PACEMAKER CELLS ISOLATED FROM CAT RIGHT ATRIUM. *J PHYSIOL*. 1993;466:263-285
  211. BERS DM. CARDIAC EXCITATION-CONTRACTION COUPLING. *NATURE*. 2002;415:198-205.
  212. MALTSEV AV, YANIV Y, STERN MD, LAKATTA EG, MALTSEV VA. RYR-NCX-SERCA LOCAL CROSS-TALK ENSURES PACEMAKER CELL FUNCTION AT REST AND DURING THE FIGHT-OR-FLIGHT REFLEX. *CIRC RES*. 2013;113:E94-E100
  213. JU YK AD. INTRACELLULAR CALCIUM AND NA<sup>+</sup>-CA<sup>2+</sup> EXCHANGE CURRENT IN ISOLATED TOAD PACEMAKER CELLS. *J PHYSIOL*. 1998;508:153-166
  214. BOGDANOV KY, VINOGRADOVA TM, LAKATTA EG. SINOATRIAL NODAL CELL RYANODINE RECEPTOR AND NA(+)-CA(2+) EXCHANGER: MOLECULAR PARTNERS IN PACEMAKER REGULATION. *CIRC RES*. 2001;88:1254-1258
  215. SANDERS L RS, LOWE M, MATTICK PA, AND A TERRAR DA. . FUNDAMENTAL IMPORTANCE OF NA<sup>+</sup>-CA<sup>2+</sup> EXCHANGE FOR THE PACEMAKING MECHANISM IN GUINEA-PIG SINO-ATRIAL NODE. . *J PHYSIOL*. . 2006;571:639-649
  216. SHARMA V, O'HALLORAN DM. RECENT STRUCTURAL AND FUNCTIONAL INSIGHTS INTO THE FAMILY OF SODIUM CALCIUM EXCHANGERS. *GENESIS*. 2014;52:93-109
  217. LIAO J, LI H, ZENG W, SAUER DB, BELMARES R, JIANG Y. STRUCTURAL INSIGHT INTO THE ION-EXCHANGE MECHANISM OF THE SODIUM/CALCIUM EXCHANGER. *SCIENCE*. 2012;335:686-690
  218. REN X, PHILIPSON KD. THE TOPOLOGY OF THE CARDIAC NA(+)/CA(2)(+) EXCHANGER, NCX1. *J MOL CELL CARDIOL*. 2013;57:68-71
  219. SHATTOCK MJ, OTTOLIA M, BERS DM, BLAUSTEIN MP, BOGUSLAVSKYI A, BOSSUYT J, BRIDGE JH, CHEN-IZU Y, CLANCY CE, EDWARDS A, GOLDBABER J, KAPLAN J, LINGREL JB, PAVLOVIC D, PHILIPSON K, SIPIDO KR, XIE ZJ. NA<sup>+</sup>/CA<sup>2+</sup> EXCHANGE AND NA<sup>+</sup>/K<sup>+</sup>-ATPASE IN THE HEART. *J PHYSIOL*. 2015;593:1361-1382
  220. QUEDNAU BD, NICOLL DA, PHILIPSON KD. TISSUE SPECIFICITY AND ALTERNATIVE

- SPLICING OF THE  $\text{Na}^+/\text{Ca}^{2+}$  EXCHANGER ISOFORMS NCX1, NCX2, AND NCX3 IN RAT. *AM J PHYSIOL*. 1997;272:C1250-1261
221. LEVITSKY DO. THREE TYPES OF MUSCLES EXPRESS THREE SODIUM-CALCIUM EXCHANGER ISOFORMS. *ANN N Y ACAD SCI*. 2007;1099:221-225
  222. LEE SL, YU AS, LYTTON J. TISSUE-SPECIFIC EXPRESSION OF  $\text{Na}^+/\text{Ca}^{2+}$  EXCHANGER ISOFORMS. *J BIOL CHEM*. 1994;269:14849-14852
  223. KOUSHIK SV, WANG J, ROGERS R, MOSKOPHIDIS D, LAMBERT NA, CREAZZO TL, CONWAY SJ. TARGETED INACTIVATION OF THE SODIUM-CALCIUM EXCHANGER (NCX1) RESULTS IN THE LACK OF A HEARTBEAT AND ABNORMAL MYOFIBRILLAR ORGANIZATION. *FASEB J*. 2001;15:1209-1211
  224. GAO Z, RASMUSSEN TP, LI Y, KUTSCHKE W, KOVAL OM, WU Y, WU Y, HALL DD, JOINER ML, WU XQ, SWAMINATHAN PD, PUROHIT A, ZIMMERMAN K, WEISS RM, PHILIPSON KD, SONG LS, HUND TJ, ANDERSON ME. GENETIC INHIBITION OF  $\text{Na}^+/\text{Ca}^{2+}$  EXCHANGER CURRENT DISABLES FIGHT OR FLIGHT SINOATRIAL NODE ACTIVITY WITHOUT AFFECTING RESTING HEART RATE. *CIRC RES*. 2013;112:309-317
  225. HERRMANN S, LIPP P, WIESEN K, STIEBER J, NGUYEN H, KAISER E, LUDWIG A. THE CARDIAC SODIUM-CALCIUM EXCHANGER NCX1 IS A KEY PLAYER IN THE INITIATION AND MAINTENANCE OF A STABLE HEART RHYTHM. *CARDIOVASC RES*. 2013;99:780-788
  226. GROENKE S, LARSON ED, ALBER S, ZHANG R, LAMP ST, REN X, NAKANO H, JORDAN MC, KARAGUEUZIAN HS, ROOS KP, NAKANO A, PROENZA C, PHILIPSON KD, GOLDHABER JI. COMPLETE ATRIAL-SPECIFIC KNOCKOUT OF SODIUM-CALCIUM EXCHANGE ELIMINATES SINOATRIAL NODE PACEMAKER ACTIVITY. *PLOS ONE*. 2013;8:E81633
  227. TORRENTE AG, ZHANG R, ZAINI A, GIANI JF, KANG J, LAMP ST, PHILIPSON KD, GOLDHABER JI. BURST PACEMAKER ACTIVITY OF THE SINOATRIAL NODE IN SODIUM-CALCIUM EXCHANGER KNOCKOUT MICE. *PROC NATL ACAD SCI U S A*. 2015;112:9769-9774
  228. RUBENSTEIN DS, LIPSIUS SL. MECHANISMS OF AUTOMATICITY IN SUBSIDIARY PACEMAKERS FROM CAT RIGHT ATRIUM. *CIRC RES*. 1989;64:648-657
  229. RIGG L TD. POSSIBLE ROLE OF CALCIUM RELEASE FROM THE SARCOPLASMIC RETICULUM IN PACEMAKING IN GUINEA-PIG SINO-ATRIAL NODE. *EXP PHYSIOL*. 1996;81:877-880
  230. RIGG L, HEATH BM, CUI Y, TERRAR DA. LOCALISATION AND FUNCTIONAL SIGNIFICANCE OF RYANODINE RECEPTORS DURING BETA-ADRENOCEPTOR STIMULATION IN THE GUINEA-PIG SINO-ATRIAL NODE. *CARDIOVASC RES*. 2000;48:254-264
  231. HONJO H, INADA S, LANCASTER MK, YAMAMOTO M, NIWA R, JONES SA, SHIBATA N, MITSUI K, HORIUCHI T, KAMIYA K, KODAMA I, BOYETT MR. SARCOPLASMIC RETICULUM  $\text{Ca}^{2+}$  RELEASE IS NOT A DOMINATING FACTOR IN SINOATRIAL NODE PACEMAKER ACTIVITY. *CIRC RES*. 2003;92:E41-44
  232. BROUND MJ, ASGHARI P, WAMBOLT RB, BOHUNEK L, SMITS C, PHILIT M, KIEFFER TJ, LAKATTA EG, BOHELER KR, MOORE ED, ALLARD MF, JOHNSON JD. CARDIAC RYANODINE RECEPTORS CONTROL HEART RATE AND RHYTHMICITY IN ADULT MICE. *CARDIOVASC RES*. 2012;96:372-380
  233. LAKATTA EG MV, VINOGRADOVA TM. A COUPLED SYSTEM OF INTRACELLULAR  $\text{Ca}^{2+}$  CLOCKS AND SURFACE MEMBRANE VOLTAGE CLOCKS CONTROLS THE TIMEKEEPING MECHANISM OF THE HEART'S PACEMAKER. *CIRC RES*. 2010;106:659-673
  234. VINOGRADOVA TM ZY, MALTSEV V, LYASHKOV A, STERN M, LAKATTA EG. RHYTHMIC RYANODINE RECEPTOR  $\text{Ca}^{2+}$  RELEASES DURING DIASTOLIC DEPOLARIZATION OF SINOATRIAL PACEMAKER CELLS DO NOT REQUIRE MEMBRANE DEPOLARIZATION. *CIRC RES*. 2004;94:802-809
  235. VINOGRADOVA TM, LYASHKOV AE, ZHU W, RUKNUDIN AM, SIRENKO S, YANG D, DEO S, BARLOW M, JOHNSON S, CAFFREY JL, ZHOU YY, XIAO RP, CHENG H, STERN MD, MALTSEV VA, LAKATTA EG. HIGH BASAL PROTEIN KINASE A-DEPENDENT PHOSPHORYLATION DRIVES RHYTHMIC INTERNAL  $\text{Ca}^{2+}$  STORE OSCILLATIONS AND SPONTANEOUS BEATING OF CARDIAC PACEMAKER CELLS. *CIRC RES*. 2006;98:505-514

236. CAPEL RA, TERRAR DA. THE IMPORTANCE OF CA(2+)-DEPENDENT MECHANISMS FOR THE INITIATION OF THE HEARTBEAT. *FRONTIERS IN PHYSIOLOGY*. 2015;6:80
237. LEVY MN. SYMPATHETIC-PARASYMPATHETIC INTERACTIONS IN THE HEART. *CIRC RES*. 1971;29:437-445
238. OPTHOF T. THE MAMMALIAN SINOATRIAL NODE. *CARDIOVASCULAR DRUGS AND THERAPY / SPONSORED BY THE INTERNATIONAL SOCIETY OF CARDIOVASCULAR PHARMACOTHERAPY*. 1988;1:573-597
239. BOYETT MR, HONJO H, KODAMA I. THE SINOATRIAL NODE, A HETEROGENEOUS PACEMAKER STRUCTURE. *CARDIOVASC RES*. 2000;47:658-687
240. ARDELL JL. STRUCTURE AND FUNCTION OF MAMMALIAN INTRINSIC CARDIAC NEURONS. *IN NEUROCARDIOLOGY, EDITED BY ARMOUR JA, ARDELL JL, OXFORD UNIVERSITY PRESS*. 1994:95-114
241. PAUZA DH, SKRIPKA V, PAUZIENE N, STROPUS R. ANATOMICAL STUDY OF THE NEURAL GANGLIONATED PLEXUS IN THE CANINE RIGHT ATRIUM: IMPLICATIONS FOR SELECTIVE DENERVATION AND ELECTROPHYSIOLOGY OF THE SINOATRIAL NODE IN DOG. *THE ANATOMICAL RECORD*. 1999;255:271-294
242. PAUZA DH, SKRIPKA V, PAUZIENE N, STROPUS R. MORPHOLOGY, DISTRIBUTION, AND VARIABILITY OF THE EPICARDIAC NEURAL GANGLIONATED SUBPLEXUSES IN THE HUMAN HEART. *THE ANATOMICAL RECORD*. 2000;259:353-382
243. BATULEVICIUS D, PAUZIENE N, PAUZA DH. TOPOGRAPHIC MORPHOLOGY AND AGE-RELATED ANALYSIS OF THE NEURONAL NUMBER OF THE RAT INTRACARDIAC NERVE PLEXUS. *ANNALS OF ANATOMY = ANATOMISCHER ANZEIGER : OFFICIAL ORGAN OF THE ANATOMISCHE GESELLSCHAFT*. 2003;185:449-459
244. CARTER JB, BANISTER EW, BLABER AP. EFFECT OF ENDURANCE EXERCISE ON AUTONOMIC CONTROL OF HEART RATE. *SPORTS MEDICINE*. 2003;33:33-46
245. COOTE JH, WHITE MJ. CROSSTALK PROPOSAL: BRADYCARDIA IN THE TRAINED ATHLETE IS ATTRIBUTABLE TO HIGH VAGAL TONE. *J PHYSIOL*. 2015;593:1745-1747
246. D'SOUZA A, SHARMA S, BOYETT MR. CROSSTALK OPPOSING VIEW: BRADYCARDIA IN THE TRAINED ATHLETE IS ATTRIBUTABLE TO A DOWNREGULATION OF A PACEMAKER CHANNEL IN THE SINUS NODE. *J PHYSIOL*. 2015;593:1749-1751
247. GEHRMANN J, HAMMER PE, MAGUIRE CT, WAKIMOTO H, TRIEDMAN JK, BERUL CI. PHENOTYPIC SCREENING FOR HEART RATE VARIABILITY IN THE MOUSE. *AM J PHYSIOL HEART CIRC PHYSIOL*. 2000;279:H733-740
248. CASADEI B, MOON J, JOHNSTON J, CAIAZZA A, SLEIGHT P. IS RESPIRATORY SINUS ARRHYTHMIA A GOOD INDEX OF CARDIAC VAGAL TONE IN EXERCISE? *J APPL PHYSIOL (1985)*. 1996;81:556-564
249. BERNARDI L, SALVUCCI F, SUARDI R, SOLDA PL, CALCIATI A, PERLINI S, FALCONE C, RICCIARDI L. EVIDENCE FOR AN INTRINSIC MECHANISM REGULATING HEART RATE VARIABILITY IN THE TRANSPLANTED AND THE INTACT HEART DURING SUBMAXIMAL DYNAMIC EXERCISE? *CARDIOVASC RES*. 1990;24:969-981
250. TOBISE K, ISHIKAWA Y, HOLMER SR, IM MJ, NEWELL JB, YOSHIE H, FUJITA M, SUSANNIE EE, HOMCY CJ. CHANGES IN TYPE VI ADENYLYL CYCLASE ISOFORM EXPRESSION CORRELATE WITH A DECREASED CAPACITY FOR CAMP GENERATION IN THE AGING VENTRICLE. *CIRC RES*. 1994;74:596-603
251. HALLS ML, COOPER DM. REGULATION BY CA2+-SIGNALING PATHWAYS OF ADENYLYL CYCLASES. *COLD SPRING HARBOR PERSPECTIVES IN BIOLOGY*. 2011;3:A004143
252. TUGANOWSKI W, KOPEC P. EFFECT OF EXOGENOUS CAMP IN THE RABBIT RIGHT AURICLE. *POLISH JOURNAL OF PHARMACOLOGY AND PHARMACY*. 1978;30:451-454
253. YAMASAKI Y, FUJIWARA M, TODA N. EFFECTS OF INTRACELLULARLY APPLIED CYCLIC 3',5'-ADENOSINE MONOPHOSPHATE AND DIBUTYRYL CYCLIC 3',5'-ADENOSINE MONOPHOSPHATE ON THE ELECTRICAL ACTIVITY OF SINOATRIAL NODAL CELLS OF THE RABBIT. *J PHARMACOL EXP THER*. 1974;190:15-20
254. TANAKA H, CLARK RB, GILES WR. POSITIVE CHRONOTROPIC RESPONSES OF RABBIT SINO-ATRIAL NODE CELLS TO FLASH PHOTOLYSIS OF CAGED ISOPROTERENOL AND CYCLIC AMP. *PROCEEDINGS. BIOLOGICAL SCIENCES / THE ROYAL SOCIETY*. 1996;263:241-248
255. TUGANOWSKI W. THE INFLUENCE OF ADENYLYLATE CYCLASE INHIBITORS ON THE



- SPONTANEOUS ACTIVITY OF THE CARDIAC PACEMAKER. *ARCHIVES INTERNATIONALES DE PHARMACODYNAMIE ET DE THERAPIE*. 1977;225:275-286
256. MATTICK P, PARRINGTON J, ODIA E, SIMPSON A, COLLINS T, TERRAR D. CA<sup>2+</sup>-STIMULATED ADENYLYL CYCLASE ISOFORM AC1 IS PREFERENTIALLY EXPRESSED IN GUINEA-PIG SINO-ATRIAL NODE CELLS AND MODULATES THE I(F) PACEMAKER CURRENT. *J PHYSIOL*. 2007;582:1195-1203
  257. YOUNES A, LYASHKOV AE, GRAHAM D, SHEYDINA A, VOLKOVA MV, MITSAK M, VINOGRADOVA TM, LUKYANENKO YO, LI Y, RUKNUDIN AM, BOHELER KR, VAN EYK J, LAKATTA EG. CA(2+) -STIMULATED BASAL ADENYLYL CYCLASE ACTIVITY LOCALIZATION IN MEMBRANE LIPID MICRODOMAINS OF CARDIAC SINOATRIAL NODAL PACEMAKER CELLS. *J BIOL CHEM*. 2008;283:14461-14468
  258. HANOUNE J, DEFER N. REGULATION AND ROLE OF ADENYLYL CYCLASE ISOFORMS. *ANNU REV PHARMACOL TOXICOL*. 2001;41:145-174
  259. PETIT-JACQUES J, BOIS P, BESCOND J, LENFANT J. MECHANISM OF MUSCARINIC CONTROL OF THE HIGH-THRESHOLD CALCIUM CURRENT IN RABBIT SINO-ATRIAL NODE MYOCYTES. *PFLUGERS ARCH*. 1993;423:21-27
  260. MATTIAZZI A, MUNDINA-WEILENMANN C, GUOXIANG C, VITTONI L, KRANIAS E. ROLE OF PHOSPHOLAMBAN PHOSPHORYLATION ON THR17 IN CARDIAC PHYSIOLOGICAL AND PATHOLOGICAL CONDITIONS. *CARDIOVASC RES*. 2005;68:366-375
  261. WU Y, VALDIVIA HH, WEHRENS XH, ANDERSON ME. A SINGLE PROTEIN KINASE A OR CALMODULIN KINASE II SITE DOES NOT CONTROL THE CARDIAC PACEMAKER CA<sup>2+</sup> CLOCK. *CIRC ARRHYTHM ELECTROPHYSIOL*. 2016;9:E003180
  262. OMORI K, KOTERA J. OVERVIEW OF PDES AND THEIR REGULATION. *CIRC RES*. 2007;100:309-327
  263. OSADCHII OE. CARDIAC HYPERTROPHY INDUCED BY SUSTAINED BETA-ADRENORECEPTOR ACTIVATION: PATHOPHYSIOLOGICAL ASPECTS. *HEART FAIL REV*. 2007;12:66-86
  264. ORITO K, TAKASE H, FUJIKI H, MORI T. EFFECTS OF TOBORINONE (OPC-18790), A NEW POSITIVE INOTROPIC AGENT, ON ACTION POTENTIAL IN GUINEA PIG SINOATRIAL NODE: COMPARED WITH MILRINONE AND E-4031. *JAPANESE JOURNAL OF PHARMACOLOGY*. 1996;72:79-82
  265. KODAMA I, KONDO N, SHIBATA S. EFFECTS OF AMRINONE ON THE TRANSMEMBRANE ACTION POTENTIAL OF RABBIT SINUS NODE PACEMAKER CELLS. *BR J PHARMACOL*. 1983;80:511-517
  266. SHAHID M, RODGER IW. CHRONOTROPIC AND INOTROPIC ACTIONS OF AMRINONE, CARBAZERAN AND ISOBUTYLMETHYL XANTHINE: ROLE OF PHOSPHODIESTERASE INHIBITION. *BR J PHARMACOL*. 1989;98:291-301
  267. SHAKUR Y, FONG M, HENSLEY J, CONE J, MOVSESIAN MA, KAMBAYASHI J, YOSHITAKE M, LIU Y. COMPARISON OF THE EFFECTS OF CILOSTAZOL AND MILRINONE ON CAMP-PDE ACTIVITY, INTRACELLULAR CAMP AND CALCIUM IN THE HEART. *CARDIOVASCULAR DRUGS AND THERAPY / SPONSORED BY THE INTERNATIONAL SOCIETY OF CARDIOVASCULAR PHARMACOTHERAPY*. 2002;16:417-427
  268. DIFRANCESCO D TP. DIRECT ACTIVATION OF CARDIAC PACEMAKER CHANNELS BY INTRACELLULAR CYCLIC AMP. *NATURE*. 1991;351:145-147
  269. DIFRANCESCO D TC. MUSCARINIC CONTROL OF THE HYPERPOLARIZATION-ACTIVATED CURRENT (IF) IN RABBIT SINO-ATRIAL NODE MYOCYTES. *J PHYSIOL* 1988;405:493-510
  270. HATA T, NISHIMURA M, OGINO K, UCHIYAMA H, WATANABE Y. ELECTROPHYSIOLOGICAL EFFECTS OF AMRINONE ON THE AUTOMATICITY AND MEMBRANE CURRENT SYSTEM OF THE RABBIT SINOATRIAL NODE CELLS. *HEART VESSELS*. 1998;13:114-121
  271. ROBINSON RB, SIEGELBAUM SA. HYPERPOLARIZATION-ACTIVATED CATION CURRENTS: FROM MOLECULES TO PHYSIOLOGICAL FUNCTION. *ANNU REV PHYSIOL*. 2003;65:453-480
  272. MILANESI R BM, GNECCHI-RUSCONE T, DIFRANCESCO D. . FAMILIAL SINUS BRADYCARDIA ASSOCIATED WITH A MUTATION IN THE CARDIAC PACEMAKER CHANNEL. *N ENGL J MED*. 2006;354:151-157

273. MCDONALD TF, PELZER S, TRAUTWEIN W, PELZER DJ. REGULATION AND MODULATION OF CALCIUM CHANNELS IN CARDIAC, SKELETAL, AND SMOOTH MUSCLE CELLS. *PHYSIOL REV.* 1994;74:365-507.
274. VERDE I, VANDECASTEELE G, LEZOUALC'H F, FISCHMEISTER R. CHARACTERIZATION OF THE CYCLIC NUCLEOTIDE PHOSPHODIESTERASE SUBTYPES INVOLVED IN THE REGULATION OF THE L-TYPE  $Ca^{2+}$  CURRENT IN RAT VENTRICULAR MYOCYTES. *BR J PHARMACOL.* 1999;127:65-74
275. PERETS T, BLUMENSTEIN Y, SHISTIK E, LOTAN I, DASCAL N. A POTENTIAL SITE OF FUNCTIONAL MODULATION BY PROTEIN KINASE A IN THE CARDIAC  $Ca^{2+}$  CHANNEL ALPHA 1C SUBUNIT. *FEBS LETTERS.* 1996;384:189-192
276. GERHARDSTEIN BL, PURI TS, CHIEN AJ, HOSEY MM. IDENTIFICATION OF THE SITES PHOSPHORYLATED BY CYCLIC AMP-DEPENDENT PROTEIN KINASE ON THE BETA 2 SUBUNIT OF L-TYPE VOLTAGE-DEPENDENT CALCIUM CHANNELS. *BIOCHEMISTRY.* 1999;38:10361-10370
277. KAMP TJ, HELL JW. REGULATION OF CARDIAC L-TYPE CALCIUM CHANNELS BY PROTEIN KINASE A AND PROTEIN KINASE C. *CIRC RES.* 2000;87:1095-1102
278. WALSH KB, KASS RS. REGULATION OF A HEART POTASSIUM CHANNEL BY PROTEIN KINASE A AND C. *SCIENCE.* 1988;242:67-69
279. WALSH KB, KASS RS. DISTINCT VOLTAGE-DEPENDENT REGULATION OF A HEART-DELAYED  $IK$  BY PROTEIN KINASES A AND C. *AM J PHYSIOL.* 1991;261:C1081-1090
280. NICOLL DA, LONGONI S, PHILIPSON KD. MOLECULAR CLONING AND FUNCTIONAL EXPRESSION OF THE CARDIAC SARCOLEMMA  $Na^{+}$ - $Ca^{2+}$  EXCHANGER. *SCIENCE.* 1990;250:562-565
281. SCHULZE DH, MUQHAL M, LEDERER WJ, RUKNUDIN AM. SODIUM/CALCIUM EXCHANGER (NCX1) MACROMOLECULAR COMPLEX. *J BIOL CHEM.* 2003;278:28849-28855
282. GINSBURG KS, BERS DM. ISOPROTERENOL DOES NOT ENHANCE  $Ca$ -DEPENDENT  $Na/Ca$  EXCHANGE CURRENT IN INTACT RABBIT VENTRICULAR MYOCYTES. *J MOL CELL CARDIOL.* 2005;39:972-981
283. PARKS RJ, RAY G, BIENVENU LA, ROSE RA, HOWLETT SE. SEX DIFFERENCES IN SR  $Ca^{2+}$  RELEASE IN MURINE VENTRICULAR MYOCYTES ARE REGULATED BY THE CAMP/PKA PATHWAY. *J MOL CELL CARDIOL.* 2014;75:162-173
284. PARKS RJ, HOWLETT SE. SEX DIFFERENCES IN MECHANISMS OF CARDIAC EXCITATION-CONTRACTION COUPLING. *PFLUGERS ARCH.* 2013;465:747-763
285. BORDALLO J, CANTABRANA B, SUAREZ L, SANCHEZ M. TESTOSTERONE INHIBITS CAMP-PHOSPHODIESTERASES IN HEART EXTRACTS FROM RATS AND INCREASES CAMP LEVELS IN ISOLATED LEFT ATRIA. *PHARMACOLOGY.* 2011;87:155-160
286. KRAVTSOV GM, KAM KW, LIU J, WU S, WONG TM. ALTERED  $Ca^{2+}$  HANDLING BY RYANODINE RECEPTOR AND  $Na^{+}$ - $Ca^{2+}$  EXCHANGE IN THE HEART FROM OVARIECTOMIZED RATS: ROLE OF PROTEIN KINASE A. *AMERICAN JOURNAL OF PHYSIOLOGY. CELL PHYSIOLOGY.* 2007;292:C1625-1635
287. YANIV Y, GANESAN A, YANG D, ZIMAN BD, LYASHKOV AE, LEVCHENKO A, ZHANG J, LAKATTA EG. REAL-TIME RELATIONSHIP BETWEEN PKA BIOCHEMICAL SIGNAL NETWORK DYNAMICS AND INCREASED ACTION POTENTIAL FIRING RATE IN HEART PACEMAKER CELLS: KINETICS OF PKA ACTIVATION IN HEART PACEMAKER CELLS. *J MOL CELL CARDIOL.* 2015;86:168-178
288. KE Y, LEI M, COLLINS TP, RAKOVIC S, MATTICK PA, YAMASAKI M, BRODIE MS, TERRAR DA, SOLARO RJ. REGULATION OF L-TYPE CALCIUM CHANNEL AND DELAYED RECTIFIER POTASSIUM CHANNEL ACTIVITY BY  $P21$ -ACTIVATED KINASE-1 IN GUINEA PIG SINOATRIAL NODE PACEMAKER CELLS. *CIRC RES.* 2007;100:1317-1327
289. DING WG, TOYODA F, MATSUURA H. BLOCKING ACTION OF CHROMANOL 293B ON THE SLOW COMPONENT OF DELAYED RECTIFIER  $K^{+}$  CURRENT IN GUINEA-PIG SINO-ATRIAL NODE CELLS. *BR J PHARMACOL.* 2002;137:253-262
290. LEI M, BROWN HF, TERRAR DA. MODULATION OF DELAYED RECTIFIER POTASSIUM CURRENT,  $IK$ , BY ISOPRENALINE IN RABBIT ISOLATED PACEMAKER CELLS. *EXPERIMENTAL PHYSIOLOGY.* 2000;85:27-35
291. KUROKAWA J, BANKSTON JR, KAIHARA A, CHEN L, FURUKAWA T, KASS RS. KCNE VARIANTS REVEAL A CRITICAL ROLE OF THE BETA SUBUNIT CARBOXYL TERMINUS

- IN PKA-DEPENDENT REGULATION OF THE IKS POTASSIUM CHANNEL. *CHANNELS (AUSTIN)*. 2009;3:16-24
292. TOYODA F, DING WG, MATSUURA H. RESPONSES OF THE SUSTAINED INWARD CURRENT TO AUTONOMIC AGONISTS IN GUINEA-PIG SINO-ATRIAL NODE PACEMAKER CELLS. *BR J PHARMACOL*. 2005;144:660-668
293. LI M, WEST JW, NUMANN R, MURPHY BJ, SCHEUER T, CATTERALL WA. CONVERGENT REGULATION OF SODIUM CHANNELS BY PROTEIN KINASE C AND CAMP-DEPENDENT PROTEIN KINASE. *SCIENCE*. 1993;261:1439-1442
294. QU Y, ROGERS J, TANADA T, SCHEUER T, CATTERALL WA. MODULATION OF CARDIAC NA<sup>+</sup> CHANNELS EXPRESSED IN A MAMMALIAN CELL LINE AND IN VENTRICULAR MYOCYTES BY PROTEIN KINASE C. *PROC NATL ACAD SCI U S A*. 1994;91:3289-3293
295. VALDIVIA HH, KAPLAN JH, ELLIS-DAVIES GC, LEDERER WJ. RAPID ADAPTATION OF CARDIAC RYANODINE RECEPTORS: MODULATION BY MG<sup>2+</sup> AND PHOSPHORYLATION. *SCIENCE*. 1995;267:1997-2000
296. MARX SO, REIKEN S, HISAMATSU Y, JAYARAMAN T, BURKHOFF D, ROSEMBLIT N, MARKS AR. PKA PHOSPHORYLATION DISSOCIATES FKBP12.6 FROM THE CALCIUM RELEASE CHANNEL (RYANODINE RECEPTOR): DEFECTIVE REGULATION IN FAILING HEARTS. *CELL*. 2000;101:365-376
297. SHAN J, BETZENHAUSER MJ, KUSHNIR A, REIKEN S, MELI AC, WRONSKA A, DURA M, CHEN BX, MARKS AR. ROLE OF CHRONIC RYANODINE RECEPTOR PHOSPHORYLATION IN HEART FAILURE AND BETA-ADRENERGIC RECEPTOR BLOCKADE IN MICE. *J CLIN INVEST*. 2010;120:4375-4387
298. JOUNG B, TANG L, MARUYAMA M, HAN S, CHEN Z, STUCKY M, JONES LR, FISHBEIN MC, WEISS JN, CHEN PS, LIN SF. INTRACELLULAR CALCIUM DYNAMICS AND ACCELERATION OF SINUS RHYTHM BY BETA-ADRENERGIC STIMULATION. *CIRCULATION*. 2009;119:788-796
299. JU YK, ALLEN DG. HOW DOES BETA-ADRENERGIC STIMULATION INCREASE THE HEART RATE? THE ROLE OF INTRACELLULAR CA<sup>2+</sup> RELEASE IN AMPHIBIAN PACEMAKER CELLS. *J PHYSIOL*. 1999;516 ( PT 3):793-804
300. WU Y, GAO Z, CHEN B, KOVAL OM, SINGH MV, GUAN X, HUND TJ, KUTSCHKE W, SARMA S, GRUMBACH IM, WEHRENS XH, MOHLER PJ, SONG LS, ANDERSON ME. CALMODULIN KINASE II IS REQUIRED FOR FIGHT OR FLIGHT SINOATRIAL NODE PHYSIOLOGY. *PROC NATL ACAD SCI U S A*. 2009;106:5972-5977
301. ADAMS KF, JR., SUETA CA, GHEORGHIADE M, O'CONNOR CM, SCHWARTZ TA, KOCH GG, URETSKY B, SWEDBERG K, MCKENNA W, SOLER-SOLER J, CALIFF RM. GENDER DIFFERENCES IN SURVIVAL IN ADVANCED HEART FAILURE. INSIGHTS FROM THE FIRST STUDY. *CIRCULATION*. 1999;99:1816-1821
302. KANNEL WB, WILSON PW, D'AGOSTINO RB, COBB J. SUDDEN CORONARY DEATH IN WOMEN. *AM HEART J*. 1998;136:205-212
303. HOEKER GS, HOOD AR, KATRA RP, POELZING S, POGWIZD SM. SEX DIFFERENCES IN BETA-ADRENERGIC RESPONSIVENESS OF ACTION POTENTIALS AND INTRACELLULAR CALCIUM HANDLING IN ISOLATED RABBIT HEARTS. *PLOS ONE*. 2014;9:E111411
304. IRISAWA H, BROWN, H. F. AND GILES, W. . CARDIAC PACEMAKING IN THE SINOATRIAL NODE. *PHYSIOL. REV.* . 1993;73:197-227
305. MEIJLER FL, JANSE MJ. MORPHOLOGY AND ELECTROPHYSIOLOGY OF THE MAMMALIAN ATRIOVENTRICULAR NODE. *PHYSIOL REV*. 1988;68:608-647
306. TODA N, WEST TC. THE INFLUENCE OF OUABAIN ON CHOLINERGIC RESPONSES IN THE SINOATRIAL NODE. *J PHARMACOL EXP THER*. 1966;153:104-113
307. WEST TC, TODA N. RESPONSE OF THE A-V NODE OF THE RABBIT TO STIMULATION OF INTRACARDIAC CHOLINERGIC NERVES. *CIRC RES*. 1967;20:18-31
308. SHIBATA EF, GILES W, POLLACK GH. THRESHOLD EFFECTS OF ACETYLCHOLINE ON PRIMARY PACEMAKER CELLS OF THE RABBIT SINO-ATRIAL NODE. *PROCEEDINGS OF THE ROYAL SOCIETY OF LONDON. SERIES B, BIOLOGICAL SCIENCES*. 1985;223:355-378
309. VINOGRADOVA TM, FEDOROV VV, YUZYUK TN, ZAITSEV AV, ROSENSHTRAUKH LV. LOCAL CHOLINERGIC SUPPRESSION OF PACEMAKER ACTIVITY IN THE RABBIT SINOATRIAL NODE. *J CARDIOVASC PHARMACOL*. 1998;32:413-424

310. HUTTER OF, TRAUTWEIN W. VAGAL AND SYMPATHETIC EFFECTS ON THE PACEMAKER FIBERS IN THE SINUS VENOSUS OF THE HEART. *J GEN PHYSIOL.* 1956;39:715-733
311. HUTTER OF, TRAUTWEIN W. EFFECT OF VAGAL STIMULATION ON THE SINUS VENOSUS OF THE FROG'S HEART. *NATURE.* 1955;176:512-513
312. ZAZA A, ROBINSON RB, DIFRANCESCO D. BASAL RESPONSES OF THE L-TYPE CA<sup>2+</sup> AND HYPERPOLARIZATION-ACTIVATED CURRENTS TO AUTONOMIC AGONISTS IN THE RABBIT SINO-ATRIAL NODE. *J PHYSIOL.* 1996;491 ( PT 2):347-355
313. HARTZELL HC. REGULATION OF CARDIAC ION CHANNELS BY CATECHOLAMINES, ACETYLCHOLINE AND SECOND MESSENGER SYSTEMS. *PROG BIOPHYS MOL BIOL.* 1988;52:165-247
314. CHANG F, GAO J, TROMBA C, COHEN I, DIFRANCESCO D. ACETYLCHOLINE REVERSES EFFECTS OF BETA-AGONISTS ON PACEMAKER CURRENT IN CANINE CARDIAC PURKINJE FIBERS BUT HAS NO DIRECT ACTION. A DIFFERENCE BETWEEN PRIMARY AND SECONDARY PACEMAKERS. *CIRC RES.* 1990;66:633-636
315. VAN BORREN MM, VERKERK AO, WILDERS R, HAJJI N, ZEGERS JG, BOURIER J, TAN HL, VERHEIJCK EE, PETERS SL, ALEWIJNSE AE, RAVESLOOT JH. EFFECTS OF MUSCARINIC RECEPTOR STIMULATION ON CA<sup>2+</sup> TRANSIENT, CAMP PRODUCTION AND PACEMAKER FREQUENCY OF RABBIT SINOATRIAL NODE CELLS. *BASIC RES CARDIOL.* 2010;105:73-87
316. HAN X, KUBOTA I, FERON O, OPEL DJ, ARSTALL MA, ZHAO YY, HUANG P, FISHMAN MC, MICHEL T, KELLY RA. MUSCARINIC CHOLINERGIC REGULATION OF CARDIAC MYOCYTE ICA-L IS ABSENT IN MICE WITH TARGETED DISRUPTION OF ENDOTHELIAL NITRIC OXIDE SYNTHASE. *PROC NATL ACAD SCI U S A.* 1998;95:6510-6515
317. HAN X, SHIMONI Y, GILES WR. AN OBLIGATORY ROLE FOR NITRIC OXIDE IN AUTONOMIC CONTROL OF MAMMALIAN HEART RATE. *J PHYSIOL.* 1994;476:309-314
318. SASAKI S, DAITOKU K, IWASA A, MOTOMURA S. NO IS INVOLVED IN MCH-INDUCED ACCENTUATED ANTAGONISM VIA TYPE II PDE IN THE CANINE BLOOD-PERFUSED SA NODE. *AM J PHYSIOL HEART CIRC PHYSIOL.* 2000;279:H2509-2518
319. VALENZUELA D, HAN X, MENDE U, FANKHAUSER C, MASHIMO H, HUANG P, PFEFFER J, NEER EJ, FISHMAN MC. G ALPHA(O) IS NECESSARY FOR MUSCARINIC REGULATION OF CA<sup>2+</sup> CHANNELS IN MOUSE HEART. *PROC NATL ACAD SCI U S A.* 1997;94:1727-1732
320. VANDECASTEELE G, ESCHENHAGEN T, SCHOLZ H, STEIN B, VERDE I, FISCHMEISTER R. MUSCARINIC AND BETA-ADRENERGIC REGULATION OF HEART RATE, FORCE OF CONTRACTION AND CALCIUM CURRENT IS PRESERVED IN MICE LACKING ENDOTHELIAL NITRIC OXIDE SYNTHASE. *NATURE MEDICINE.* 1999;5:331-334.
321. MORI T, HASHIMOTO A, TAKASE H, KAMBE T. NITRIC OXIDE (NO) IS NOT INVOLVED IN ACCENTUATED ANTAGONISM FOR CHRONOTROPY IN THE ISOLATED MOUSE ATRIUM. *NAUNYN-SCHMIEDEBERG'S ARCHIVES OF PHARMACOLOGY.* 2004;369:363-366
322. SEIFEN E, SCHAEER H, MARSHALL JM. EFFECT OF CALCIUM ON THE MEMBRANE POTENTIALS OF SINGLE PACEMAKER FIBRES AND ATRIAL FIBRES IN ISOLATED RABBITS ATRIA. *NATURE.* 1964;202:1223-1224
323. ZAZA A, MICHELETTI M, BRIOSCHI A, ROCCHETTI M. IONIC CURRENTS DURING SUSTAINED PACEMAKER ACTIVITY IN RABBIT SINO-ATRIAL MYOCYTES. *J PHYSIOL.* 1997;505 ( PT 3):677-688
324. CAPEL RA, TERRAR DA. CYTOSOLIC CALCIUM IONS EXERT A MAJOR INFLUENCE ON THE FIRING RATE AND MAINTENANCE OF PACEMAKER ACTIVITY IN GUINEA-PIG SINUS NODE. *FRONTIERS IN PHYSIOLOGY.* 2015;6:23
325. TOHSE N. CALCIUM-SENSITIVE DELAYED RECTIFIER POTASSIUM CURRENT IN GUINEA PIG VENTRICULAR CELLS. *AM J PHYSIOL.* 1990;258:H1200-1207
326. HEATH BM, TERRAR DA. PROTEIN KINASE C ENHANCES THE RAPIDLY ACTIVATING DELAYED RECTIFIER POTASSIUM CURRENT, IKR, THROUGH A REDUCTION IN C-TYPE INACTIVATION IN GUINEA-PIG VENTRICULAR MYOCYTES. *J PHYSIOL.* 2000;522 PT 3:391-402
327. XIE Y, DING WG, MATSUURA H. CA<sup>2+</sup>/CALMODULIN POTENTIATES I K<sub>S</sub> IN SINOATRIAL NODE CELLS BY ACTIVATING CA<sup>2+</sup>/CALMODULIN-DEPENDENT PROTEIN KINASE II. *PFLUGERS ARCH.* 2015;467:241-251

328. HAGIWARA N, IRISAWA H. MODULATION BY INTRACELLULAR  $Ca^{2+}$  OF THE HYPERPOLARIZATION-ACTIVATED INWARD CURRENT IN RABBIT SINGLE SINO-ATRIAL NODE CELLS. *J PHYSIOL*. 1989;409:121-141
329. SATOH H. ELECTROPHARMACOLOGY OF TAURINE ON THE HYPERPOLARIZATION-ACTIVATED INWARD CURRENT AND THE SUSTAINED INWARD CURRENT IN SPONTANEOUSLY BEATING RAT SINO-ATRIAL NODAL CELLS. *JOURNAL OF PHARMACOLOGICAL SCIENCES*. 2003;91:229-238
330. VERKERK AO, WILDERS R, ZEGERS JG, VAN BORREN MM, RAVESLOOT JH, VERHEIJCK EE.  $Ca^{2+}$ -ACTIVATED  $Cl^{-}$  CURRENT IN RABBIT SINOATRIAL NODE CELLS. *J PHYSIOL*. 2002;540:105-117
331. ZISSIMOPOULOS S, LAI FA. RYANODINE RECEPTOR STRUCTURE, FUNCTION AND PATHOPHYSIOLOGY. IN *CALCIUM-A MATTER OF LIFE OR DEATH*. EDITED BY JOACHIM KREBS AND MAREK MICHALAK. 2007;41:287-342
332. BAUEROVA-HLINKOVA V, BAUER J, HOSTINOVA E, GASPERIK J, BECK K, BORKO L, FALTINOVA A, ZAHRADNIKOVA A, SEVCIK J. BIOINFORMATICS DOMAIN STRUCTURE PREDICTION AND HOMOLGY MODELING OF HUMAN RYANODINE RECEPTOR 2. . IN *BIOINFORMATICS - TRENDS AND METHODOLOGIES, INTECH*, EDITED BY MAHMOOD A. MAHDAVI. 2011:325-352
333. TELEMAN A, DRAKENBERG T, FORSEN S. KINETICS OF  $Ca^{2+}$  BINDING TO CALMODULIN AND ITS TRYPTIC FRAGMENTS STUDIED BY  $^{43}Ca$ -NMR. *BIOCHIM BIOPHYS ACTA*. 1986;873:204-213
334. EVANS TI, HELL JW, SHEA MA. THERMODYNAMIC LINKAGE BETWEEN CALMODULIN DOMAINS BINDING CALCIUM AND CONTIGUOUS SITES IN THE C-TERMINAL TAIL OF  $Ca_v1.2$ . *BIOPHYSICAL CHEMISTRY*. 2011;159:172-187
335. TANG W, HALLING DB, BLACK DJ, PATE P, ZHANG JZ, PEDERSEN S, ALTSCHULD RA, HAMILTON SL. APOCALMODULIN AND  $Ca^{2+}$  CALMODULIN-BINDING SITES ON THE  $Ca_v1.2$  CHANNEL. *BIOPHYS J*. 2003;85:1538-1547
336. ERICKSON MG, LIANG H, MORI MX, YUE DT. FRET TWO-HYBRID MAPPING REVEALS FUNCTION AND LOCATION OF L-TYPE  $Ca^{2+}$  CHANNEL CAM PREASSOCIATION. *NEURON*. 2003;39:97-107
337. VAN PETEGEM F, CHATELAIN FC, MINOR DL, JR. INSIGHTS INTO VOLTAGE-GATED CALCIUM CHANNEL REGULATION FROM THE STRUCTURE OF THE  $Ca_v1.2$  IQ DOMAIN- $Ca^{2+}$ /CALMODULIN COMPLEX. *NATURE STRUCTURAL & MOLECULAR BIOLOGY*. 2005;12:1108-1115
338. KIM EY, RUMPF CH, VAN PETEGEM F, ARANT RJ, FINDEISEN F, COOLEY ES, ISACOFF EY, MINOR DL, JR. MULTIPLE C-TERMINAL TAIL  $Ca^{2+}$ /CAMS REGULATE  $Ca_v1.2$  FUNCTION BUT DO NOT MEDIATE CHANNEL DIMERIZATION. *EMBO J*. 2010;29:3924-3938
339. PITT GS, ZUHLKE RD, HUDMON A, SCHULMAN H, REUTER H, TSIEN RW. MOLECULAR BASIS OF CALMODULIN TETHERING AND  $Ca^{2+}$ -DEPENDENT INACTIVATION OF L-TYPE  $Ca^{2+}$  CHANNELS. *J BIOL CHEM*. 2001;276:30794-30802
340. HALLING DB, ARACENA-PARKS P, HAMILTON SL. REGULATION OF VOLTAGE-GATED  $Ca^{2+}$  CHANNELS BY CALMODULIN. *SCIENCE'S STKE : SIGNAL TRANSDUCTION KNOWLEDGE ENVIRONMENT*. 2005;2005:RE15
341. ASMARA H, MINOBE E, SAUD ZA, KAMEYAMA M. INTERACTIONS OF CALMODULIN WITH THE MULTIPLE BINDING SITES OF  $Ca_v1.2$   $Ca^{2+}$  CHANNELS. *JOURNAL OF PHARMACOLOGICAL SCIENCES*. 2010;112:397-404
342. LIMPITIKUL WB, DICK IE, JOSHI-MUKHERJEE R, OVERGAARD MT, GEORGE AL, JR., YUE DT. CALMODULIN MUTATIONS ASSOCIATED WITH LONG QT SYNDROME PREVENT INACTIVATION OF CARDIAC L-TYPE  $Ca^{2+}$  CURRENTS AND PROMOTE PROARRHYTHMIC BEHAVIOR IN VENTRICULAR MYOCYTES. *J MOL CELL CARDIOL*. 2014;74:115-124
343. SWAIN SM, SAHOO N, DENNHARDT S, SCHONHERR R, HEINEMANN SH.  $Ca^{2+}$ /CALMODULIN REGULATES  $K_v\beta 1.1$ -MEDIATED INACTIVATION OF VOLTAGE-GATED  $K^{+}$  CHANNELS. *SCIENTIFIC REPORTS*. 2015;5:15509
344. QU YJ, BONDARENKO VE, XIE C, WANG S, AWAYDA MS, STRAUSS HC, MORALES MJ. W-7 MODULATES  $K_v4.3$ : PORE BLOCK AND  $Ca^{2+}$ -CALMODULIN INHIBITION. *AM J PHYSIOL HEART CIRC PHYSIOL*. 2007;292:H2364-2377

345. NITTA J, FURUKAWA T, MARUMO F, SAWANOBORI T, HIRAOKA M. SUBCELLULAR MECHANISM FOR CA(2+)-DEPENDENT ENHANCEMENT OF DELAYED RECTIFIER K+ CURRENT IN ISOLATED MEMBRANE PATCHES OF GUINEA PIG VENTRICULAR MYOCYTES. *CIRC RES*. 1994;74:96-104
346. YUS-NAJERA E, SANTANA-CASTRO I, VILLARROEL A. THE IDENTIFICATION AND CHARACTERIZATION OF A NONCONTINUOUS CALMODULIN-BINDING SITE IN NONINACTIVATING VOLTAGE-DEPENDENT KCNQ POTASSIUM CHANNELS. *J BIOL CHEM*. 2002;277:28545-28553
347. GHOSH S, NUNZIATO DA, PITT GS. KCNQ1 ASSEMBLY AND FUNCTION IS BLOCKED BY LONG-QT SYNDROME MUTATIONS THAT DISRUPT INTERACTION WITH CALMODULIN. *CIRC RES*. 2006;98:1048-1054
348. SCHONHERR R, LOBER K, HEINEMANN SH. INHIBITION OF HUMAN ETHER A GO-GO POTASSIUM CHANNELS BY CA(2+)/CALMODULIN. *EMBO J*. 2000;19:3263-3271
349. SCHUMACHER MA, RIVARD AF, BACHINGER HP, ADELMAN JP. STRUCTURE OF THE GATING DOMAIN OF A CA2+-ACTIVATED K+ CHANNEL COMPLEXED WITH CA2+/CALMODULIN. *NATURE*. 2001;410:1120-1124
350. FANGER CM, GHANSHANI S, LOGSDON NJ, RAUER H, KALMAN K, ZHOU J, BECKINGHAM K, CHANDY KG, CAHALAN MD, AIYAR J. CALMODULIN MEDIATES CALCIUM-DEPENDENT ACTIVATION OF THE INTERMEDIATE CONDUCTANCE KCA CHANNEL, IKCA1. *J BIOL CHEM*. 1999;274:5746-5754
351. KHANNA R, CHANG MC, JOINER WJ, KACZMAREK LK, SCHLICHTER LC. HSK4/HIK1, A CALMODULIN-BINDING KCA CHANNEL IN HUMAN T LYMPHOCYTES. ROLES IN PROLIFERATION AND VOLUME REGULATION. *J BIOL CHEM*. 1999;274:14838-14849
352. TAN HL, KUPERSHMITD S, ZHANG R, STEPANOVIC S, RODEN DM, WILDE AA, ANDERSON ME, BALSER JR. A CALCIUM SENSOR IN THE SODIUM CHANNEL MODULATES CARDIAC EXCITABILITY. *NATURE*. 2002;415:442-447
353. SARHAN MF, VAN PETEGEM F, AHERN CA. A DOUBLE TYROSINE MOTIF IN THE CARDIAC SODIUM CHANNEL DOMAIN III-IV LINKER COUPLES CALCIUM-DEPENDENT CALMODULIN BINDING TO INACTIVATION GATING. *J BIOL CHEM*. 2009;284:33265-33274
354. SARHAN MF, TUNG CC, VAN PETEGEM F, AHERN CA. CRYSTALLOGRAPHIC BASIS FOR CALCIUM REGULATION OF SODIUM CHANNELS. *PROC NATL ACAD SCI U S A*. 2012;109:3558-3563
355. BERS DM. CA(2+)-CALMODULIN-DEPENDENT PROTEIN KINASE II REGULATION OF CARDIAC EXCITATION-TRANSCRIPTION COUPLING. *HEART RHYTHM*. 2011;8:1101-1104
356. ERICKSON JR, HE BJ, GRUMBACH IM, ANDERSON ME. CAMKII IN THE CARDIOVASCULAR SYSTEM: SENSING REDOX STATES. *PHYSIOL REV*. 2011;91:889-915
357. SHIBASAKI F, PRICE ER, MILAN D, MCKEON F. ROLE OF KINASES AND THE PHOSPHATASE CALCINEURIN IN THE NUCLEAR SHUTTLE OF TRANSCRIPTION FACTOR NF-AT4. *NATURE*. 1996;382:370-373
358. BERS DM. CALCIUM CYCLING AND SIGNALING IN CARDIAC MYOCYTES. *ANNU REV PHYSIOL*. 2008;70:23-49
359. MOLKENTIN JD. CALCINEURIN AND BEYOND: CARDIAC HYPERTROPHIC SIGNALING. *CIRC RES*. 2000;87:731-738.
360. MOLKENTIN JD, LU JR, ANTOS CL, MARKHAM B, RICHARDSON J, ROBBINS J, GRANT SR, OLSON EN. A CALCINEURIN-DEPENDENT TRANSCRIPTIONAL PATHWAY FOR CARDIAC HYPERTROPHY. *CELL*. 1998;93:215-228
361. ZOU Y, HIROI Y, UOZUMI H, TAKIMOTO E, TOKO H, ZHU W, KUDOH S, MIZUKAMI M, SHIMOYAMA M, SHIBASAKI F, NAGAI R, YAZAKI Y, KOMURO I. CALCINEURIN PLAYS A CRITICAL ROLE IN THE DEVELOPMENT OF PRESSURE OVERLOAD-INDUCED CARDIAC HYPERTROPHY. *CIRCULATION*. 2001;104:97-101
362. BUENO OF, WILKINS BJ, TYMITZ KM, GLASCOCK BJ, KIMBALL TF, LORENZ JN, MOLKENTIN JD. IMPAIRED CARDIAC HYPERTROPHIC RESPONSE IN CALCINEURIN ABETA -DEFICIENT MICE. *PROC NATL ACAD SCI U S A*. 2002;99:4586-4591
363. WILKINS BJ, DE WINDT LJ, BUENO OF, BRAZ JC, GLASCOCK BJ, KIMBALL TF, MOLKENTIN JD. TARGETED DISRUPTION OF NFATC3, BUT NOT NFATC4, REVEALS AN INTRINSIC DEFECT IN CALCINEURIN-MEDIATED CARDIAC HYPERTROPHIC GROWTH. *MOL CELL BIOL*. 2002;22:7603-7613

364. GRUVER CL, DEMAYO F, GOLDSTEIN MA, MEANS AR. TARGETED DEVELOPMENTAL OVEREXPRESSION OF CALMODULIN INDUCES PROLIFERATIVE AND HYPERTROPHIC GROWTH OF CARDIOMYOCYTES IN TRANSGENIC MICE. *ENDOCRINOLOGY*. 1993;133:376-388
365. YANIV Y, MALTSEV VA. NUMERICAL MODELING CALCIUM AND CAMKII EFFECTS IN THE SA NODE. *FRONTIERS IN PHARMACOLOGY*. 2014;5:58
366. HUND TJ, MOHLER PJ. ROLE OF CAMKII IN CARDIAC ARRHYTHMIAS. *TRENDS CARDIOVASC MED*. 2015;25:392-397
367. ZHANG T, JOHNSON EN, GU Y, MORISSETTE MR, SAH VP, GIGENA MS, BELKE DD, DILLMANN WH, ROGERS TB, SCHULMAN H, ROSS J, JR., BROWN JH. THE CARDIAC-SPECIFIC NUCLEAR DELTA(B) ISOFORM OF CA<sup>2+</sup>/CALMODULIN-DEPENDENT PROTEIN KINASE II INDUCES HYPERTROPHY AND DILATED CARDIOMYOPATHY ASSOCIATED WITH INCREASED PROTEIN PHOSPHATASE 2A ACTIVITY. *J BIOL CHEM*. 2002;277:1261-1267
368. ZHANG T, MAIER LS, DALTON ND, MIYAMOTO S, ROSS J, JR., BERS DM, BROWN JH. THE DELTAC ISOFORM OF CAMKII IS ACTIVATED IN CARDIAC HYPERTROPHY AND INDUCES DILATED CARDIOMYOPATHY AND HEART FAILURE. *CIRC RES*. 2003;92:912-919
369. ZHANG T, KOHLHAAS M, BACKS J, MISHRA S, PHILLIPS W, DYBKOVA N, CHANG S, LING H, BERS DM, MAIER LS, OLSON EN, BROWN JH. CAMKIIDELTA ISOFORMS DIFFERENTIALLY AFFECT CALCIUM HANDLING BUT SIMILARLY REGULATE HDAC/MEF2 TRANSCRIPTIONAL RESPONSES. *J BIOL CHEM*. 2007;282:35078-35087
370. MISHRA S, GRAY CB, MIYAMOTO S, BERS DM, BROWN JH. LOCATION MATTERS: CLARIFYING THE CONCEPT OF NUCLEAR AND CYTOSOLIC CAMKII SUBTYPES. *CIRC RES*. 2011;109:1354-1362
371. BAYER KU, DE KONINCK P, SCHULMAN H. ALTERNATIVE SPLICING MODULATES THE FREQUENCY-DEPENDENT RESPONSE OF CAMKII TO CA(2+) OSCILLATIONS. *EMBO J*. 2002;21:3590-3597
372. ERICKSON JR, JOINER ML, GUAN X, KUTSCHKE W, YANG J, ODDIS CV, BARTLETT RK, LOWE JS, O'DONNELL SE, AYKIN-BURNS N, ZIMMERMAN MC, ZIMMERMAN K, HAM AJ, WEISS RM, SPITZ DR, SHEA MA, COLBRAN RJ, MOHLER PJ, ANDERSON ME. A DYNAMIC PATHWAY FOR CALCIUM-INDEPENDENT ACTIVATION OF CAMKII BY METHIONINE OXIDATION. *CELL*. 2008;133:462-474
373. ERICKSON JR, PEREIRA L, WANG L, HAN G, FERGUSON A, DAO K, COPELAND RJ, DESPA F, HART GW, RIPPLINGER CM, BERS DM. DIABETIC HYPERGLYCAEMIA ACTIVATES CAMKII AND ARRHYTHMIAS BY O-LINKED GLYCOSYLATION. *NATURE*. 2013;502:372-376
374. VINOGRADOVA TM, ZHOU YY, BOGDANOV KY, YANG D, KUSCHEL M, CHENG H, XIAO RP. SINOATRIAL NODE PACEMAKER ACTIVITY REQUIRES CA(2+)/CALMODULIN-DEPENDENT PROTEIN KINASE II ACTIVATION. *CIRC RES*. 2000;87:760-767
375. ANDERSON ME, BRAUN AP, SCHULMAN H, PREMACK BA. MULTIFUNCTIONAL CA<sup>2+</sup>/CALMODULIN-DEPENDENT PROTEIN KINASE MEDIATES CA(2+)-INDUCED ENHANCEMENT OF THE L-TYPE CA<sup>2+</sup> CURRENT IN RABBIT VENTRICULAR MYOCYTES. *CIRC RES*. 1994;75:854-861
376. XIAO RP, CHENG H, LEDERER WJ, SUZUKI T, LAKATTA EG. DUAL REGULATION OF CA<sup>2+</sup>/CALMODULIN-DEPENDENT KINASE II ACTIVITY BY MEMBRANE VOLTAGE AND BY CALCIUM INFLUX. *PROC NATL ACAD SCI U S A*. 1994;91:9659-9663
377. YUAN W, BERS DM. CA-DEPENDENT FACILITATION OF CARDIAC CA CURRENT IS DUE TO CA-CALMODULIN-DEPENDENT PROTEIN KINASE. *AM J PHYSIOL*. 1994;267:H982-993
378. DELGADO C, ARTILES A, GÓMEZ AM, VASSORT G. FREQUENCY-DEPENDENT INCREASE IN CARDIAC CA(2+)CURRENT IS DUE TO REDUCED CA(2+)RELEASE BY THE SARCOPLASMIC RETICULUM. *J MOL CELL CARDIOL*. 1999;31:1783-1793
379. BERS DM, MOROTTI S. CA(2+) CURRENT FACILITATION IS CAMKII-DEPENDENT AND HAS ARRHYTHMOGENIC CONSEQUENCES. *FRONTIERS IN PHARMACOLOGY*. 2014;5:144
380. HUDMON A, SCHULMAN H, KIM J, MALTEZ JM, TSIEN RW, PITT GS. CAMKII TETHERS TO L-TYPE CA<sup>2+</sup> CHANNELS, ESTABLISHING A LOCAL AND DEDICATED INTEGRATOR OF CA<sup>2+</sup> SIGNALS FOR FACILITATION. *J CELL BIOL*. 2005;171:537-547

381. ERXLEBEN C, LIAO Y, GENTILE S, CHIN D, GOMEZ-ALEGRIA C, MORI Y, BIRNBAUMER L, ARMSTRONG DL. CYCLOSPORIN AND TIMOTHY SYNDROME INCREASE MODE 2 GATING OF CAV1.2 CALCIUM CHANNELS THROUGH ABERRANT PHOSPHORYLATION OF S6 HELICES. *PROC NATL ACAD SCI U S A*. 2006;103:3932-3937
382. WANG WY, HAO LY, MINOBE E, SAUD ZA, HAN DY, KAMEYAMA M. CAMKII PHOSPHORYLATES A THREONINE RESIDUE IN THE C-TERMINAL TAIL OF CAV1.2 CA(2+) CHANNEL AND MODULATES THE INTERACTION OF THE CHANNEL WITH CALMODULIN. *THE JOURNAL OF PHYSIOLOGICAL SCIENCES : JPS*. 2009;59:283-290
383. LEE TS, KARL R, MOOSMANG S, LENHARDT P, KLUGBAUER N, HOFMANN F, KLEPPISCH T, WELLING A. CALMODULIN KINASE II IS INVOLVED IN VOLTAGE-DEPENDENT FACILITATION OF THE L-TYPE CAV1.2 CALCIUM CHANNEL: IDENTIFICATION OF THE PHOSPHORYLATION SITES. *J BIOL CHEM*. 2006;281:25560-25567
384. BLAICH A, WELLING A, FISCHER S, WEGENER JW, KOSTNER K, HOFMANN F, MOOSMANG S. FACILITATION OF MURINE CARDIAC L-TYPE CA(V)1.2 CHANNEL IS MODULATED BY CALMODULIN KINASE II-DEPENDENT PHOSPHORYLATION OF S1512 AND S1570. *PROC NATL ACAD SCI U S A*. 2010;107:10285-10289
385. KOVAL OM, GUAN X, WU Y, JOINER ML, GAO Z, CHEN B, GRUMBACH IM, LUCZAK ED, COLBRAN RJ, SONG LS, HUND TJ, MOHLER PJ, ANDERSON ME. CAV1.2 BETA-SUBUNIT COORDINATES CAMKII-TRIGGERED CARDIOMYOCYTE DEATH AND AFTERDEPOLARIZATIONS. *PROC NATL ACAD SCI U S A*. 2010;107:4996-5000
386. GRUETER CE, ABIRIA SA, WU Y, ANDERSON ME, COLBRAN RJ. DIFFERENTIAL REGULATED INTERACTIONS OF CALCIUM/CALMODULIN-DEPENDENT PROTEIN KINASE II WITH ISOFORMS OF VOLTAGE-GATED CALCIUM CHANNEL BETA SUBUNITS. *BIOCHEMISTRY*. 2008;47:1760-1767
387. ABIRIA SA, COLBRAN RJ. CAMKII ASSOCIATES WITH CAV1.2 L-TYPE CALCIUM CHANNELS VIA SELECTED BETA SUBUNITS TO ENHANCE REGULATORY PHOSPHORYLATION. *JOURNAL OF NEUROCHEMISTRY*. 2010;112:150-161
388. BERS DM, GRANDI E. CALCIUM/CALMODULIN-DEPENDENT KINASE II REGULATION OF CARDIAC ION CHANNELS. *J CARDIOVASC PHARMACOL*. 2009;54:180-187
389. TESSIER S, KARCZEWSKI P, KRAUSE EG, PANSARD Y, ACAR C, LANG-LAZDUNSKI M, MERCADIER JJ, HATEM SN. REGULATION OF THE TRANSIENT OUTWARD K(+) CURRENT BY CA(2+)/CALMODULIN-DEPENDENT PROTEIN KINASES II IN HUMAN ATRIAL MYOCYTES. *CIRC RES*. 1999;85:810-819
390. COLINAS O, GALLEGO M, SETIEN R, LOPEZ-LOPEZ JR, PEREZ-GARCIA MT, CASIS O. DIFFERENTIAL MODULATION OF KV4.2 AND KV4.3 CHANNELS BY CALMODULIN-DEPENDENT PROTEIN KINASE II IN RAT CARDIAC MYOCYTES. *AM J PHYSIOL HEART CIRC PHYSIOL*. 2006;291:H1978-1987
391. SERGEANT GP, OHYA S, REIHILL JA, PERRINO BA, AMBERG GC, IMAIZUMI Y, HOROWITZ B, SANDERS KM, KOH SD. REGULATION OF KV4.3 CURRENTS BY CA2+/CALMODULIN-DEPENDENT PROTEIN KINASE II. *AMERICAN JOURNAL OF PHYSIOLOGY. CELL PHYSIOLOGY*. 2005;288:C304-313
392. XIAO L, COUTU P, VILLENEUVE LR, TADEVOSYAN A, MAGUY A, LE BOUTER S, ALLEN BG, NATTEL S. MECHANISMS UNDERLYING RATE-DEPENDENT REMODELING OF TRANSIENT OUTWARD POTASSIUM CURRENT IN CANINE VENTRICULAR MYOCYTES. *CIRC RES*. 2008;103:733-742
393. LI J, MARIONNEAU C, ZHANG R, SHAH V, HELL JW, NERBONNE JM, ANDERSON ME. CALMODULIN KINASE II INHIBITION SHORTENS ACTION POTENTIAL DURATION BY UPREGULATION OF K+ CURRENTS. *CIRC RES*. 2006;99:1092-1099
394. WAGNER S, HACKER E, GRANDI E, WEBER SL, DYBKOVA N, SOSSALLA S, SOWA T, FABRITZ L, KIRCHHOF P, BERS DM, MAIER LS. CA/CALMODULIN KINASE II DIFFERENTIALLY MODULATES POTASSIUM CURRENTS. *CIRC ARRHYTHM ELECTROPHYSIOL*. 2009;2:285-294
395. AIBA T, HESKETH GG, LIU T, CARLISLE R, VILLA-ABRILLE MC, O'ROURKE B, AKAR FG, TOMASELLI GF. NA+ CHANNEL REGULATION BY CA2+/CALMODULIN AND CA2+/CALMODULIN-DEPENDENT PROTEIN KINASE II IN GUINEA-PIG VENTRICULAR MYOCYTES. *CARDIOVASC RES*. 2010;85:454-463
396. ASHPOLE NM, HERREN AW, GINSBURG KS, BROGAN JD, JOHNSON DE, CUMMINS TR,



- BERS DM, HUDMON A. CA<sup>2+</sup>/CALMODULIN-DEPENDENT PROTEIN KINASE II (CAMKII) REGULATES CARDIAC SODIUM CHANNEL NAV1.5 GATING BY MULTIPLE PHOSPHORYLATION SITES. *J BIOL CHEM*. 2012;287:19856-19869
397. HUND TJ, KOVAL OM, LI J, WRIGHT PJ, QIAN L, SNYDER JS, GUDMUNDSSON H, KLINE CF, DAVIDSON NP, CARDONA N, RASBAND MN, ANDERSON ME, MOHLER PJ. A BETA(IV)-SPECTRIN/CAMKII SIGNALING COMPLEX IS ESSENTIAL FOR MEMBRANE EXCITABILITY IN MICE. *J CLIN INVEST*. 2010;120:3508-3519
398. HERREN AW, WEBER DM, RIGOR RR, MARGULIES KB, PHINNEY BS, BERS DM. CAMKII PHOSPHORYLATION OF NA(V)1.5: NOVEL IN VITRO SITES IDENTIFIED BY MASS SPECTROMETRY AND REDUCED S516 PHOSPHORYLATION IN HUMAN HEART FAILURE. *JOURNAL OF PROTEOME RESEARCH*. 2015;14:2298-2311
399. WAGNER S, DYBKOVA N, RASENACK EC, JACOBSHAGEN C, FABRITZ L, KIRCHHOF P, MAIER SK, ZHANG T, HASENFUSS G, BROWN JH, BERS DM, MAIER LS. CA<sup>2+</sup>/CALMODULIN-DEPENDENT PROTEIN KINASE II REGULATES CARDIAC NA<sup>+</sup> CHANNELS. *J CLIN INVEST*. 2006;116:3127-3138
400. YOON JY, HO WK, KIM ST, CHO H. CONSTITUTIVE CAMKII ACTIVITY REGULATES NA<sup>+</sup> CHANNEL IN RAT VENTRICULAR MYOCYTES. *J MOL CELL CARDIOL*. 2009;47:475-484
401. TOYOFUKU T, CUROTTO KURZYDLOWSKI K, NARAYANAN N, MACLENNAN DH. IDENTIFICATION OF SER38 AS THE SITE IN CARDIAC SARCOPLASMIC RETICULUM CA(2+)-ATPASE THAT IS PHOSPHORYLATED BY CA<sup>2+</sup>/CALMODULIN-DEPENDENT PROTEIN KINASE. *J BIOL CHEM*. 1994;269:26492-26496
402. AKIN BL, HURLEY TD, CHEN Z, JONES LR. THE STRUCTURAL BASIS FOR PHOSPHOLAMBAN INHIBITION OF THE CALCIUM PUMP IN SARCOPLASMIC RETICULUM. *J BIOL CHEM*. 2013;288:30181-30191
403. YUCHI Z, LAU K, VAN PETEGEM F. DISEASE MUTATIONS IN THE RYANODINE RECEPTOR CENTRAL REGION: CRYSTAL STRUCTURES OF A PHOSPHORYLATION HOT SPOT DOMAIN. *STRUCTURE*. 2012;20:1201-1211
404. LI L, SATOH H, GINSBURG KS, BERS DM. THE EFFECT OF CA(2+)-CALMODULIN-DEPENDENT PROTEIN KINASE II ON CARDIAC EXCITATION-CONTRACTION COUPLING IN FERRET VENTRICULAR MYOCYTES. *J PHYSIOL (LOND)*. 1997;501:17-31
405. CURRIE S, LOUGHREY CM, CRAIG MA, SMITH GL. CALCIUM/CALMODULIN-DEPENDENT PROTEIN KINASE II DELTA ASSOCIATES WITH THE RYANODINE RECEPTOR COMPLEX AND REGULATES CHANNEL FUNCTION IN RABBIT HEART. *BIOCHEM J*. 2004;377:357-366
406. GUO T, ZHANG T, MESTRIL R, BERS DM. CA<sup>2+</sup>/CALMODULIN-DEPENDENT PROTEIN KINASE II PHOSPHORYLATION OF RYANODINE RECEPTOR DOES AFFECT CALCIUM SPARKS IN MOUSE VENTRICULAR MYOCYTES. *CIRC RES*. 2006;99:398-406
407. MAIER LS, ZHANG T, CHEN L, DESANTIAGO J, BROWN JH, BERS DM. TRANSGENIC CAMKIIDELTA OVEREXPRESSION UNIQUELY ALTERS CARDIAC MYOCYTE CA<sup>2+</sup> HANDLING: REDUCED SR CA<sup>2+</sup> LOAD AND ACTIVATED SR CA<sup>2+</sup> RELEASE. *CIRC RES*. 2003;92:904-911
408. YANG D, ZHU WZ, XIAO B, BROCHET DX, CHEN SR, LAKATTA EG, XIAO RP, CHENG H. CA<sup>2+</sup>/CALMODULIN KINASE II-DEPENDENT PHOSPHORYLATION OF RYANODINE RECEPTORS SUPPRESSES CA<sup>2+</sup> SPARKS AND CA<sup>2+</sup> WAVES IN CARDIAC MYOCYTES. *CIRC RES*. 2007;100:399-407
409. WITCHER DR, KOVACS RJ, SCHULMAN H, CEFALI DC, JONES LR. UNIQUE PHOSPHORYLATION SITE ON THE CARDIAC RYANODINE RECEPTOR REGULATES CALCIUM CHANNEL ACTIVITY. *J BIOL CHEM*. 1991;266:11144-11152
410. WEHRENS XH, LEHNART SE, REIKEN SR, MARKS AR. CA<sup>2+</sup>/CALMODULIN-DEPENDENT PROTEIN KINASE II PHOSPHORYLATION REGULATES THE CARDIAC RYANODINE RECEPTOR. *CIRC RES*. 2004;94:E61-70
411. HAIN J, ONOUE H, MAYRLEITNER M, FLEISCHER S, SCHINDLER H. PHOSPHORYLATION MODULATES THE FUNCTION OF THE CALCIUM RELEASE CHANNEL OF SARCOPLASMIC RETICULUM FROM CARDIAC MUSCLE. *J BIOL CHEM*. 1995;270:2074-2081
412. LOKUTA AJ, ROGERS TB, LEDERER WJ, VALDIVIA HH. MODULATION OF CARDIAC RYANODINE RECEPTORS OF SWINE AND RABBIT BY A PHOSPHORYLATION-DEPHOSPHORYLATION MECHANISM. *J PHYSIOL (LOND)*. 1995;487:609-622

413. SOLTIS AR, SAUCERMAN JJ. SYNERGY BETWEEN CAMKII SUBSTRATES AND BETA-ADRENERGIC SIGNALING IN REGULATION OF CARDIAC MYOCYTE CA(2+) HANDLING. *BIOPHYS J*. 2010;99:2038-2047
414. WU Y, ANDERSON ME. CAMKII IN SINOATRIAL NODE PHYSIOLOGY AND DYSFUNCTION. *FRONTIERS IN PHARMACOLOGY*. 2014;5:48
415. ZHANG R, KHOO MS, WU Y, YANG Y, GRUETER CE, NI G, PRICE EE, JR., THIEL W, GUATIMOSIM S, SONG LS, MADU EC, SHAH AN, VISHNIVETSKAYA TA, ATKINSON JB, GUREVICH VV, SALAMA G, LEDERER WJ, COLBRAN RJ, ANDERSON ME. CALMODULIN KINASE II INHIBITION PROTECTS AGAINST STRUCTURAL HEART DISEASE. *NATURE MEDICINE*. 2005;11:409-417
416. ANDERSON ME, BROWN JH, BERS DM. CAMKII IN MYOCARDIAL HYPERTROPHY AND HEART FAILURE. *J MOL CELL CARDIOL*. 2011;51:468-473
417. GAO Z, SINGH MV, HALL DD, KOVAL OM, LUCZAK ED, JOINER ML, CHEN B, WU Y, CHAUDHARY AK, MARTINS JB, HUND TJ, MOHLER PJ, SONG LS, ANDERSON ME. CATECHOLAMINE-INDEPENDENT HEART RATE INCREASES REQUIRE CA2+/CALMODULIN-DEPENDENT PROTEIN KINASE II. *CIRC ARRHYTHM ELECTROPHYSIOL*. 2011;4:379-387
418. CURRAN J, HINTON MJ, RIOS E, BERS DM, SHANNON TR. BETA-ADRENERGIC ENHANCEMENT OF SARCOPLASMIC RETICULUM CALCIUM LEAK IN CARDIAC MYOCYTES IS MEDIATED BY CALCIUM/CALMODULIN-DEPENDENT PROTEIN KINASE. *CIRC RES*. 2007;100:391-398
419. SWAMINATHAN PD, PUROHIT A, SONI S, VOIGT N, SINGH MV, GLUKHOV AV, GAO Z, HE BJ, LUCZAK ED, JOINER ML, KUTSCHKE W, YANG J, DONAHUE JK, WEISS RM, GRUMBACH IM, OGAWA M, CHEN PS, EFIMOV I, DOBREV D, MOHLER PJ, HUND TJ, ANDERSON ME. OXIDIZED CAMKII CAUSES CARDIAC SINUS NODE DYSFUNCTION IN MICE. *J CLIN INVEST*. 2011;121:3277-3288
420. PUROHIT A, ROKITA AG, GUAN X, CHEN B, KOVAL OM, VOIGT N, NEEF S, SOWA T, GAO Z, LUCZAK ED, STEFANSDOTTIR H, BEHUNIN AC, LI N, EL-ACCAOUI RN, YANG B, SWAMINATHAN PD, WEISS RM, WEHRENS XH, SONG LS, DOBREV D, MAIER LS, ANDERSON ME. OXIDIZED CA(2+)/CALMODULIN-DEPENDENT PROTEIN KINASE II TRIGGERS ATRIAL FIBRILLATION. *CIRCULATION*. 2013;128:1748-1757
421. LUO M, GUAN X, LUCZAK ED, LANG D, KUTSCHKE W, GAO Z, YANG J, GLYNN P, SOSSALLA S, SWAMINATHAN PD, WEISS RM, YANG B, ROKITA AG, MAIER LS, EFIMOV IR, HUND TJ, ANDERSON ME. DIABETES INCREASES MORTALITY AFTER MYOCARDIAL INFARCTION BY OXIDIZING CAMKII. *J CLIN INVEST*. 2013;123:1262-1274
422. WU Y, TEMPLE J, ZHANG R, DZHURA I, ZHANG W, TRIMBLE R, RODEN DM, PASSIER R, OLSON EN, COLBRAN RJ, ANDERSON ME. CALMODULIN KINASE II AND ARRHYTHMIAS IN A MOUSE MODEL OF CARDIAC HYPERTROPHY. *CIRCULATION*. 2002;106:1288-1293
423. VAN OORT RJ, MCCAULEY MD, DIXIT SS, PEREIRA L, YANG Y, RESPRESS JL, WANG Q, DE ALMEIDA AC, SKAPURA DG, ANDERSON ME, BERS DM, WEHRENS XH. RYANODINE RECEPTOR PHOSPHORYLATION BY CALCIUM/CALMODULIN-DEPENDENT PROTEIN KINASE II PROMOTES LIFE-THREATENING VENTRICULAR ARRHYTHMIAS IN MICE WITH HEART FAILURE. *CIRCULATION*. 2010;122:2669-2679
424. CHELU MG, SARMA S, SOOD S, WANG S, VAN OORT RJ, SKAPURA DG, LI N, SANTONASTASI M, MULLER FU, SCHMITZ W, SCHOTTEN U, ANDERSON ME, VALDERRABANO M, DOBREV D, WEHRENS XH. CALMODULIN KINASE II-MEDIATED SARCOPLASMIC RETICULUM CA2+ LEAK PROMOTES ATRIAL FIBRILLATION IN MICE. *J CLIN INVEST*. 2009;119:1940-1951
425. SWAMINATHAN PD, PUROHIT A, HUND TJ, ANDERSON ME. CALMODULIN-DEPENDENT PROTEIN KINASE II: LINKING HEART FAILURE AND ARRHYTHMIAS. *CIRC RES*. 2012;110:1661-1677
426. BACKS J, SONG K, BEZPROZVANNAYA S, CHANG S, OLSON EN. CAM KINASE II SELECTIVELY SIGNALS TO HISTONE DEACETYLASE 4 DURING CARDIOMYOCYTE HYPERTROPHY. *J CLIN INVEST*. 2006;116:1853-1864
427. BACKS J, BACKS T, BEZPROZVANNAYA S, MCKINSEY TA, OLSON EN. HISTONE DEACETYLASE 5 ACQUIRES CALCIUM/CALMODULIN-DEPENDENT KINASE II RESPONSIVENESS BY OLIGOMERIZATION WITH HISTONE DEACETYLASE 4. *MOL CELL*

- BIOL.* 2008;28:3437-3445
428. WU X, BERS DM. SARCOPLASMIC RETICULUM AND NUCLEAR ENVELOPE ARE ONE HIGHLY INTERCONNECTED CA<sup>2+</sup> STORE THROUGHOUT CARDIAC MYOCYTE. *CIRC RES.* 2006;99:283-291
429. HOU N, LUO MS, LIU SM, ZHANG HN, XIAO Q, SUN P, ZHANG GS, LUO JD, CHEN MS. LEPTIN INDUCES HYPERTROPHY THROUGH ACTIVATING THE PEROXISOME PROLIFERATOR-ACTIVATED RECEPTOR ALPHA PATHWAY IN CULTURED NEONATAL RAT CARDIOMYOCYTES. *CLIN EXP PHARMACOL PHYSIOL.* 2010;37:1087-1095
430. MCGAFFIN KR, MORAVEC CS, MCTIERNAN CF. LEPTIN SIGNALING IN THE FAILING AND MECHANICALLY UNLOADED HUMAN HEART. *CIRCULATION. HEART FAILURE.* 2009;2:676-683
431. MCGAFFIN KR, ZOU B, MCTIERNAN CF, O'DONNELL CP. LEPTIN ATTENUATES CARDIAC APOPTOSIS AFTER CHRONIC ISCHAEMIC INJURY. *CARDIOVASC RES.* 2009;83:313-324
432. YANG R, BAROUCH LA. LEPTIN SIGNALING AND OBESITY: CARDIOVASCULAR CONSEQUENCES. *CIRC RES.* 2007;101:545-559
433. ZEIDAN A, JAVADOV S, CHAKRABARTI S, KARMAZYN M. LEPTIN-INDUCED CARDIOMYOCYTE HYPERTROPHY INVOLVES SELECTIVE CAVEOLAE AND RHOA/ROCK-DEPENDENT P38 MAPK TRANSLOCATION TO NUCLEI. *CARDIOVASC RES.* 2008;77:64-72
434. CARLYLE M, JONES OB, KUO JJ, HALL JE. CHRONIC CARDIOVASCULAR AND RENAL ACTIONS OF LEPTIN: ROLE OF ADRENERGIC ACTIVITY. *HYPERTENSION.* 2002;39:496-501
435. HAYNES WG. INTERACTION BETWEEN LEPTIN AND SYMPATHETIC NERVOUS SYSTEM IN HYPERTENSION. *CURRENT HYPERTENSION REPORTS.* 2000;2:311-318
436. PEREGO L, PIZZOCRI P, CORRADI D, MAISANO F, PAGANELLI M, FIORINA P, BARBIERI M, MORABITO A, PAOLISSO G, FOLLI F, PONTIROLI AE. CIRCULATING LEPTIN CORRELATES WITH LEFT VENTRICULAR MASS IN MORBID (GRADE III) OBESITY BEFORE AND AFTER WEIGHT LOSS INDUCED BY BARIATRIC SURGERY: A POTENTIAL ROLE FOR LEPTIN IN MEDIATING HUMAN LEFT VENTRICULAR HYPERTROPHY. *THE JOURNAL OF CLINICAL ENDOCRINOLOGY AND METABOLISM.* 2005;90:4087-4093
437. POIRIER P, GILES TD, BRAY GA, HONG Y, STERN JS, PI-SUNYER FX, ECKEL RH, AMERICAN HEART A, OBESITY COMMITTEE OF THE COUNCIL ON NUTRITION PA, METABOLISM. OBESITY AND CARDIOVASCULAR DISEASE: PATHOPHYSIOLOGY, EVALUATION, AND EFFECT OF WEIGHT LOSS: AN UPDATE OF THE 1997 AMERICAN HEART ASSOCIATION SCIENTIFIC STATEMENT ON OBESITY AND HEART DISEASE FROM THE OBESITY COMMITTEE OF THE COUNCIL ON NUTRITION, PHYSICAL ACTIVITY, AND METABOLISM. *CIRCULATION.* 2006;113:898-918
438. ANDALIB A, BRUGADA R, NATTEL S. ATRIAL FIBRILLATION: EVIDENCE FOR GENETICALLY DETERMINED DISEASE. *CURRENT OPINION IN CARDIOLOGY.* 2008;23:176-183
439. FRALEY MA, BIRCHEM JA, SENKOTTAIYAN N, ALPERT MA. OBESITY AND THE ELECTROCARDIOGRAM. *OBESITY REVIEWS : AN OFFICIAL JOURNAL OF THE INTERNATIONAL ASSOCIATION FOR THE STUDY OF OBESITY.* 2005;6:275-281
440. LIN YC, HUANG J, HILEMAN S, MARTIN KH, HULL R, DAVIS M, YU HG. LEPTIN DECREASES HEART RATE ASSOCIATED WITH INCREASED VENTRICULAR REPOLARIZATION VIA ITS RECEPTOR. *AM J PHYSIOL HEART CIRC PHYSIOL.* 2015;309:H1731-1739
441. REID DS, TYNAN M, BRAIDWOOD L, FITZGERALD GR. BIDIRECTIONAL TACHYCARDIA IN A CHILD. A STUDY USING HIS BUNDLE ELECTROGRAPHY. *BR HEART J.* 1975;37:339-344
442. PRIORI SG NC, MEMMI M, COLOMBI B, DRAGO F, GASPARINI M, DESIMONE L, COLTORTI F, BLOISE R, KEEGAN R, CRUZ FILHO FE, VIGNATI G, BENATAR A, DELOGU A. CLINICAL AND MOLECULAR CHARACTERIZATION OF PATIENTS WITH CATECHOLAMINERGIC POLYMORPHIC VENTRICULAR TACHYCARDIA. *CIRCULATION.* 2002;106:69-74
443. PRIORI SG NC, TISO N, MEMMI M, VIGNATI G, BLOISE R, SORRENTINO V, DANIELI GA. MUTATIONS IN THE CARDIAC RYANODINE RECEPTOR GENE (HRYR2) UNDERLIE

- CATECHOLAMINERGIC POLYMORPHIC VENTRICULAR TACHYCARDIA. *CIRCULATION*. 2001;103:196-200
444. POSTMA AV, DENJOY I, HOORNTJE TM, LUPOGLAZOFF JM, DA COSTA A, SEBILLON P, MANNENS MM, WILDE AA, GUICHENEY P. ABSENCE OF CALSEQUESTRIN 2 CAUSES SEVERE FORMS OF CATECHOLAMINERGIC POLYMORPHIC VENTRICULAR TACHYCARDIA. *CIRC RES*. 2002;91:E21-26
445. CHOPRA N, KNOLLMANN BC. TRIADIN REGULATES CARDIAC MUSCLE COUPLON STRUCTURE AND MICRODOMAIN CA(2+) SIGNALLING: A PATH TOWARDS VENTRICULAR ARRHYTHMIAS. *CARDIOVASC RES*. 2013;98:187-191
446. ROUX-BUISSON N, CACHEUX M, FOUREST-LIEUVIN A, FAUCONNIER J, BROCARD J, DENJOY I, DURAND P, GUICHENEY P, KYNDT F, LEENHARDT A, LE MAREC H, LUCET V, MABO P, PROBST V, MONNIER N, RAY PF, SANTONI E, TREMEAUX P, LACAMPAGNE A, FAURE J, LUNARDI J, MARTY I. ABSENCE OF TRIADIN, A PROTEIN OF THE CALCIUM RELEASE COMPLEX, IS RESPONSIBLE FOR CARDIAC ARRHYTHMIA WITH SUDDEN DEATH IN HUMAN. *HUM MOL GENET*. 2012;21:2759-2767
447. NYEGAARD M, OVERGAARD MT, SONDERGAARD MT, VRANAS M, BEHR ER, HILDEBRANDT LL, LUND J, HEDLEY PL, CAMM AJ, WETTRELL G, FOSDAL I, CHRISTIANSEN M, BORGLUM AD. MUTATIONS IN CALMODULIN CAUSE VENTRICULAR TACHYCARDIA AND SUDDEN CARDIAC DEATH. *AM J HUM GENET*. 2012;91:703-712
448. VEGA AL, TESTER DJ, ACKERMAN MJ, MAKIELSKI JC. PROTEIN KINASE A-DEPENDENT BIOPHYSICAL PHENOTYPE FOR V227F-KCNJ2 MUTATION IN CATECHOLAMINERGIC POLYMORPHIC VENTRICULAR TACHYCARDIA. *CIRC ARRHYTHM ELECTROPHYSIOL*. 2009;2:540-547
449. MEDEIROS-DOMINGO A BZ, TESTER DJ, ET AL. . THE RYR2-ENCODED RYANODINE RECEPTOR/CALCIUM RELEASE CHANNEL IN PATIENTS DIAGNOSED PREVIOUSLY WITH EITHER CATECHOLAMINERGIC POLYMORPHIC VENTRICULAR TACHYCARDIA OR GENOTYPE NEGATIVE, EXERCISE-INDUCED LONG QT SYNDROME: A COMPREHENSIVE OPEN READING FRAME MUTATIONAL ANALYSIS. . *J AM COLL CARDIOL*. 2009;54:2065–2074
450. BAI R, NAPOLITANO C, BLOISE R, MONTEFORTE N, PRIORI SG. YIELD OF GENETIC SCREENING IN INHERITED CARDIAC CHANNELOPATHIES: HOW TO PRIORITIZE ACCESS TO GENETIC TESTING. *CIRC ARRHYTHM ELECTROPHYSIOL*. 2009;2:6-15
451. HAYASHI M, DENJOY I, EXTRAMIANA F, MALTRET A, BUISSON NR, LUPOGLAZOFF JM, KLUG D, TAKATSUKI S, VILLAIN E, KAMBLOCK J, MESSALI A, GUICHENEY P, LUNARDI J, LEENHARDT A. INCIDENCE AND RISK FACTORS OF ARRHYTHMIC EVENTS IN CATECHOLAMINERGIC POLYMORPHIC VENTRICULAR TACHYCARDIA. *CIRCULATION*. 2009;119:2426-2434
452. KAWAMURA M, OHNO S, NAIKI N, NAGAOKA I, DOCHI K, WANG Q, HASEGAWA K, KIMURA H, MIYAMOTO A, MIZUSAWA Y, ITOH H, MAKIYAMA T, SUMITOMO N, USHINOHAMA H, OYAMA K, MURAKOSHI N, AONUMA K, HORIGOME H, HONDA T, YOSHINAGA M, ITO M, HORIE M. GENETIC BACKGROUND OF CATECHOLAMINERGIC POLYMORPHIC VENTRICULAR TACHYCARDIA IN JAPAN. *CIRC J*. 2013;77:1705-1713
453. ACKERMAN MJ, PRIORI SG, WILLEMS S, BERUL C, BRUGADA R, CALKINS H, CAMM AJ, ELLINOR PT, GOLLOB M, HAMILTON R, HERSHBERGER RE, JUDGE DP, LE MAREC H, MCKENNA WJ, SCHULZE-BAHR E, SEMSARIAN C, TOWBIN JA, WATKINS H, WILDE A, WOLPERT C, ZIPES DP. HRS/EHRA EXPERT CONSENSUS STATEMENT ON THE STATE OF GENETIC TESTING FOR THE CHANNELOPATHIES AND CARDIOMYOPATHIES THIS DOCUMENT WAS DEVELOPED AS A PARTNERSHIP BETWEEN THE HEART RHYTHM SOCIETY (HRS) AND THE EUROPEAN HEART RHYTHM ASSOCIATION (EHRA). *HEART RHYTHM*. 2011;8:1308-1339
454. POSTMA AV, DENJOY I, KAMBLOCK J, ALDERS M, LUPOGLAZOFF JM, VAKSMANN G, DUBOSQ-BIDOT L, SEBILLON P, MANNENS MM, GUICHENEY P, WILDE AA. CATECHOLAMINERGIC POLYMORPHIC VENTRICULAR TACHYCARDIA: RYR2 MUTATIONS, BRADYCARDIA, AND FOLLOW UP OF THE PATIENTS. *JOURNAL OF MEDICAL GENETICS*. 2005;42:863-870
455. SUMITOMO N, SAKURADA H, TANIGUCHI K, MATSUMURA M, ABE O, MIYASHITA M, KANAMARU H, KARASAWA K, AYUSAWA M, FUKAMIZU S, NAGAOKA I, HORIE M,

- HARADA K, HIRAOKA M. ASSOCIATION OF ATRIAL ARRHYTHMIA AND SINUS NODE DYSFUNCTION IN PATIENTS WITH CATECHOLAMINERGIC POLYMORPHIC VENTRICULAR TACHYCARDIA. *CIRC J*. 2007;71:1606-1609
456. VAN DER WERF C, NEDEREND I, HOFMAN N, VAN GELOVEN N, EBINK C, FROHN-MULDER IM, ALINGS AM, BOSKER HA, BRACKE FA, VAN DEN HEUVEL F, WAALEWIJN RA, BIKKER H, VAN TINTELEN JP, BHUIYAN ZA, VAN DEN BERG MP, WILDE AA. FAMILIAL EVALUATION IN CATECHOLAMINERGIC POLYMORPHIC VENTRICULAR TACHYCARDIA: DISEASE PENETRANCE AND EXPRESSION IN CARDIAC RYANODINE RECEPTOR MUTATION-CARRYING RELATIVES. *CIRC ARRHYTHM ELECTROPHYSIOL*. 2012;5:748-756
457. DOMINGO D, NECO P, FERNANDEZ-PONS E, ZISSIMOPOULOS S, MOLINA P, OLAGUE J, SUAREZ-MIER MP, LAI FA, GOMEZ AM, ZORIO E. NON-VENTRICULAR, CLINICAL, AND FUNCTIONAL FEATURES OF THE RYR2(R420Q) MUTATION CAUSING CATECHOLAMINERGIC POLYMORPHIC VENTRICULAR TACHYCARDIA. *REV ESP CARDIOL (ENGL ED)*. 2015;68:398-407
458. NECO P, TORRENTE A, MESIRCA P, ZORIO E, LIU N, PRIORI S, NAPOLITANO C, RICHARD S, BENITAH J, MANGONI M, GÓMEZ A. PARADOXICAL EFFECT OF INCREASED DIASTOLIC CA<sup>2+</sup> RELEASE AND DECREASED SINOATRIAL NODE ACTIVITY IN A MOUSE MODEL OF CATECHOLAMINERGIC POLYMORPHIC VENTRICULAR TACHYCARDIA. *CIRCULATION*. 2012;126:392-401
459. GLUKHOV AV, KALYANASUNDARAM A, LOU Q, HAGE LT, HANSEN BJ, BELEVYCH AE, MOHLER PJ, KNOLLMANN BC, PERIASAMY M, GYORKE S, FEDOROV VV. CALSEQUESTRIN 2 DELETION CAUSES SINOATRIAL NODE DYSFUNCTION AND ATRIAL ARRHYTHMIAS ASSOCIATED WITH ALTERED SARCOPLASMIC RETICULUM CALCIUM CYCLING AND DEGENERATIVE FIBROSIS WITHIN THE MOUSE ATRIAL PACEMAKER COMPLEX1. *EUR HEART J*. 2015;36:686-697
460. YANO M, YAMAMOTO T, IKEDA Y, MATSUZAKI M. MECHANISMS OF DISEASE: RYANODINE RECEPTOR DEFECTS IN HEART FAILURE AND FATAL ARRHYTHMIA. *NAT CLIN PRACT CARDIOVASC MED*. 2006;3:43-52
461. XIAO Z, GUO W, YUEN SM, WANG R, ZHANG L, VAN PETEGEM F, CHEN SR. THE H29D MUTATION DOES NOT ENHANCE CYTOSOLIC CA<sup>2+</sup> ACTIVATION OF THE CARDIAC RYANODINE RECEPTOR. *PLOS ONE*. 2015;10:E0139058
462. BORKO L, BAUEROVA-HLINKOVA V, HOSTINOVA E, GASPERIK J, BECK K, LAI FA, ZHRADNIKOVA A, SEVCIK J. STRUCTURAL INSIGHTS INTO THE HUMAN RYR2 N-TERMINAL REGION INVOLVED IN CARDIAC ARRHYTHMIAS. *ACTA CRYSTALLOGRAPHICA. SECTION D, BIOLOGICAL CRYSTALLOGRAPHY*. 2014;70:2897-2912
463. BEZZINA CR, LAHROUCHI N, PRIORI SG. GENETICS OF SUDDEN CARDIAC DEATH. *CIRC RES*. 2015;116:1919-1936
464. ZHAO YT, VALDIVIA CR, GURROLA GB, POWERS PP, WILLIS BC, MOSS RL, JALIFE J, VALDIVIA HH. ARRHYTHMOGENESIS IN A CATECHOLAMINERGIC POLYMORPHIC VENTRICULAR TACHYCARDIA MUTATION THAT DEPRESSES RYANODINE RECEPTOR FUNCTION. *PROC NATL ACAD SCI U S A*. 2015;112:E1669-1677
465. LIU N, COLOMBI B, MEMMI M, ZISSIMOPOULOS S, RIZZI N, NEGRI S, IMBRIANI M, NAPOLITANO C, LAI FA, PRIORI SG. ARRHYTHMOGENESIS IN CATECHOLAMINERGIC POLYMORPHIC VENTRICULAR TACHYCARDIA: INSIGHTS FROM A RYR2 R4496C KNOCK-IN MOUSE MODEL. *CIRC RES*. 2006;99:292-298
466. KASHIMURA T, BRISTON SJ, TRAFFORD AW, NAPOLITANO C, PRIORI SG, EISNER DA, VENETUCCI LA. IN THE RYR2(R4496C) MOUSE MODEL OF CPVT, BETA-ADRENERGIC STIMULATION INDUCES CA WAVES BY INCREASING SR CA CONTENT AND NOT BY DECREASING THE THRESHOLD FOR CA WAVES. *CIRC RES*. 2010;107:1483-1489
467. WANG R, CHEN W, CAI S, ZHANG J, BOLSTAD J, WAGENKNECHT T, LIU Z, CHEN SR. LOCALIZATION OF AN NH<sub>2</sub>-TERMINAL DISEASE-CAUSING MUTATION HOT SPOT TO THE "CLAMP" REGION IN THE THREE-DIMENSIONAL STRUCTURE OF THE CARDIAC RYANODINE RECEPTOR. *J BIOL CHEM*. 2007;282:17785-17793
468. KANNANKERIL PJ, MITCHELL BM, GOONASEKERA SA, CHELU MG, ZHANG W, SOOD S, KEARNEY DL, DANILA CI, DE BIASI M, WEHRENS XH, PAUTLER RG, RODEN DM, TAFFET GE, DIRKSEN RT, ANDERSON ME, HAMILTON SL. MICE WITH THE R176Q CARDIAC RYANODINE RECEPTOR MUTATION EXHIBIT CATECHOLAMINE-INDUCED

- VENTRICULAR TACHYCARDIA AND CARDIOMYOPATHY. *PROC NATL ACAD SCI U S A*. 2006;103:12179-12184
469. CHENG H, LEDERER WJ. CALCIUM SPARKS. *PHYSIOL REV*. 2008;88:1491-1545
470. PESSAH IN, ZIMANYI I. CHARACTERIZATION OF MULTIPLE [3H]RYANODINE BINDING SITES ON THE CA<sup>2+</sup> RELEASE CHANNEL OF SARCOPLASMIC RETICULUM FROM SKELETAL AND CARDIAC MUSCLE: EVIDENCE FOR A SEQUENTIAL MECHANISM IN RYANODINE ACTION. *MOLECULAR PHARMACOLOGY*. 1991;39:679-689
471. OTSU K, WILLARD HF, KHANNA VK, ZORZATO F, GREEN NM, MACLENNAN DH. MOLECULAR CLONING OF CDNA ENCODING THE CA<sup>2+</sup> RELEASE CHANNEL (RYANODINE RECEPTOR) OF RABBIT CARDIAC MUSCLE SARCOPLASMIC RETICULUM. *J BIOL CHEM*. 1990;265:13472-13483
472. NIXON GF, MIGNERY GA, SOMLYO AV. IMMUNOGOLD LOCALIZATION OF INOSITOL 1,4,5-TRISPHOSPHATE RECEPTORS AND CHARACTERIZATION OF ULTRASTRUCTURAL FEATURES OF THE SARCOPLASMIC RETICULUM IN PHASIC AND TONIC SMOOTH MUSCLE. *J MUSCLE RES CELL MOTIL*. 1994;15:682-700
473. INUI M, SAITO A, FLEISCHER S. PURIFICATION OF THE RYANODINE RECEPTOR AND IDENTITY WITH FEET STRUCTURES OF JUNCTIONAL TERMINAL CISTERNAE OF SARCOPLASMIC RETICULUM FROM FAST SKELETAL MUSCLE. *J BIOL CHEM*. 1987;262:1740-1747
474. LAI FA, ERICKSON HP, ROUSSEAU E, LIU QY, MEISSNER G. PURIFICATION AND RECONSTITUTION OF THE CALCIUM RELEASE CHANNEL FROM SKELETAL MUSCLE. *NATURE*. 1988;331:315-319
475. VAN PETEGEM F. RYANODINE RECEPTORS: STRUCTURE AND FUNCTION. *J BIOL CHEM*. 2012;287:31624-31632
476. BASSANI JW, BASSANI RA, BERS DM. RELAXATION IN RABBIT AND RAT CARDIAC CELLS: SPECIES-DEPENDENT DIFFERENCES IN CELLULAR MECHANISMS. *J PHYSIOL*. 1994;476:279-293
477. LANNER JT, GEORGIU DK, JOSHI AD, HAMILTON SL. RYANODINE RECEPTORS: STRUCTURE, EXPRESSION, MOLECULAR DETAILS, AND FUNCTION IN CALCIUM RELEASE. *COLD SPRING HARBOR PERSPECTIVES IN BIOLOGY*. 2010;2:A003996
478. TAKESHIMA H, NISHIMURA S, MATSUMOTO T, ISHIDA H, KANGAWA K, MINAMINO N, MATSUO H, UEDA M, HANAOKA M, HIROSE T, ET AL. PRIMARY STRUCTURE AND EXPRESSION FROM COMPLEMENTARY DNA OF SKELETAL MUSCLE RYANODINE RECEPTOR. *NATURE*. 1989;339:439-445
479. ZORZATO F, FUJII J, OTSU K, PHILLIPS M, GREEN NM, LAI FA, MEISSNER G, MACLENNAN DH. MOLECULAR CLONING OF CDNA ENCODING HUMAN AND RABBIT FORMS OF THE CA<sup>2+</sup> RELEASE CHANNEL (RYANODINE RECEPTOR) OF SKELETAL MUSCLE SARCOPLASMIC RETICULUM. *J BIOL CHEM*. 1990;265:2244-2256
480. MATTEI MG, GIANNINI G, MOSCATELLI F, SORRENTINO V. CHROMOSOMAL LOCALIZATION OF MURINE RYANODINE RECEPTOR GENES RYR1, RYR2, AND RYR3 BY IN SITU HYBRIDIZATION. *GENOMICS*. 1994;22:202-204
481. NAKAI J, IMAGAWA T, HAKAMAT Y, SHIGEKAWA M, TAKESHIMA H, NUMA S. PRIMARY STRUCTURE AND FUNCTIONAL EXPRESSION FROM CDNA OF THE CARDIAC RYANODINE RECEPTOR/CALCIUM RELEASE CHANNEL. *FEBS LETTERS*. 1990;271:169-177
482. COUSSIN F, MACREZ N, MOREL JL, MIRONNEAU J. REQUIREMENT OF RYANODINE RECEPTOR SUBTYPES 1 AND 2 FOR CA(2+)-INDUCED CA(2+) RELEASE IN VASCULAR MYOCYTES. *J BIOL CHEM*. 2000;275:9596-9603
483. GIANNINI G, CONTI A, MAMMARELLA S, SCROBOGNA M, SORRENTINO V. THE RYANODINE RECEPTOR/CALCIUM CHANNEL GENES ARE WIDELY AND DIFFERENTIALLY EXPRESSED IN MURINE BRAIN AND PERIPHERAL TISSUES. *J CELL BIOL*. 1995;128:893-904
484. TAKESHIMA H, KOMAZAKI S, HIROSE K, NISHI M, NODA T, IINO M. EMBRYONIC LETHALITY AND ABNORMAL CARDIAC MYOCYTES IN MICE LACKING RYANODINE RECEPTOR TYPE 2. *EMBO J*. 1998;17:3309-3316
485. HAKAMATA Y, NAKAI J, TAKESHIMA H, IMOTO K. PRIMARY STRUCTURE AND DISTRIBUTION OF A NOVEL RYANODINE RECEPTOR/CALCIUM RELEASE CHANNEL FROM RABBIT BRAIN. *FEBS LETTERS*. 1992;312:229-235

486. DU GG, KHANNA VK, MACLENNAN DH. MUTATION OF DIVERGENT REGION 1 ALTERS CAFFEINE AND CA(2+) SENSITIVITY OF THE SKELETAL MUSCLE CA(2+) RELEASE CHANNEL (RYANODINE RECEPTOR). *J BIOL CHEM*. 2000;275:11778-11783
487. PEREZ CF, MUKHERJEE S, ALLEN PD. AMINO ACIDS 1-1,680 OF RYANODINE RECEPTOR TYPE 1 HOLD CRITICAL DETERMINANTS OF SKELETAL TYPE FOR EXCITATION-CONTRACTION COUPLING. ROLE OF DIVERGENCE DOMAIN D2. *J BIOL CHEM*. 2003;278:39644-39652
488. HAYEK SM, ZHAO J, BHAT M, XU X, NAGARAJ R, PAN Z, TAKESHIMA H, MA J. A NEGATIVELY CHARGED REGION OF THE SKELETAL MUSCLE RYANODINE RECEPTOR IS INVOLVED IN CA(2+)-DEPENDENT REGULATION OF THE CA(2+) RELEASE CHANNEL. *FEBS LETTERS*. 1999;461:157-164
489. SHARMA MR, PENCZEK P, GRASSUCCI R, XIN HB, FLEISCHER S, WAGENKNECHT T. CRYOELECTRON MICROSCOPY AND IMAGE ANALYSIS OF THE CARDIAC RYANODINE RECEPTOR. *J BIOL CHEM*. 1998;273:18429-18434
490. SHARMA MR, JEYAKUMAR LH, FLEISCHER S, WAGENKNECHT T. THREE-DIMENSIONAL STRUCTURE OF RYANODINE RECEPTOR ISOFORM THREE IN TWO CONFORMATIONAL STATES AS VISUALIZED BY CRYO-ELECTRON MICROSCOPY. *J BIOL CHEM*. 2000;275:9485-9491
491. LIU Z, ZHANG J, LI P, CHEN SR, WAGENKNECHT T. THREE-DIMENSIONAL RECONSTRUCTION OF THE RECOMBINANT TYPE 2 RYANODINE RECEPTOR AND LOCALIZATION OF ITS DIVERGENT REGION 1. *J BIOL CHEM*. 2002;277:46712-46719
492. WAGENKNECHT T, SAMSO M. THREE-DIMENSIONAL RECONSTRUCTION OF RYANODINE RECEPTORS. *FRONT BIOSCI*. 2002;7:D1464-1474
493. RADERMACHER M, RAO V, GRASSUCCI R, FRANK J, TIMERMAN AP, FLEISCHER S, WAGENKNECHT T. CRYO-ELECTRON MICROSCOPY AND THREE-DIMENSIONAL RECONSTRUCTION OF THE CALCIUM RELEASE CHANNEL/RYANODINE RECEPTOR FROM SKELETAL MUSCLE. *J CELL BIOL*. 1994;127:411-423
494. SAMSO M, WAGENKNECHT T, ALLEN PD. INTERNAL STRUCTURE AND VISUALIZATION OF TRANSMEMBRANE DOMAINS OF THE RYR1 CALCIUM RELEASE CHANNEL BY CRYO-EM. *NATURE STRUCTURAL & MOLECULAR BIOLOGY*. 2005;12:539-544
495. SAMSO M, FENG W, PESSAH IN, ALLEN PD. COORDINATED MOVEMENT OF CYTOPLASMIC AND TRANSMEMBRANE DOMAINS OF RYR1 UPON GATING. *PLOS BIOLOGY*. 2009;7:E85
496. LUDTKE SJ, SERYSHEVA, II, HAMILTON SL, CHIU W. THE PORE STRUCTURE OF THE CLOSED RYR1 CHANNEL. *STRUCTURE*. 2005;13:1203-1211
497. SERYSHEVA, II, ORLOVA EV, CHIU W, SHERMAN MB, HAMILTON SL, VAN HEEL M. ELECTRON CRYOMICROSCOPY AND ANGULAR RECONSTITUTION USED TO VISUALIZE THE SKELETAL MUSCLE CALCIUM RELEASE CHANNEL. *NATURE STRUCTURAL BIOLOGY*. 1995;2:18-24
498. SERYSHEVA, II, LUDTKE SJ, BAKER ML, CONG Y, TOPF M, ERAMIAN D, SALI A, HAMILTON SL, CHIU W. SUBNANOMETER-RESOLUTION ELECTRON CRYOMICROSCOPY-BASED DOMAIN MODELS FOR THE CYTOPLASMIC REGION OF SKELETAL MUSCLE RYR CHANNEL. *PROC NATL ACAD SCI U S A*. 2008;105:9610-9615
499. ORLOVA EV, SERYSHEVA, II, VAN HEEL M, HAMILTON SL, CHIU W. TWO STRUCTURAL CONFIGURATIONS OF THE SKELETAL MUSCLE CALCIUM RELEASE CHANNEL. *NATURE STRUCTURAL BIOLOGY*. 1996;3:547-552
500. ZALK R, CLARKE OB, DES GEORGES A, GRASSUCCI RA, REIKEN S, MANCIA F, HENDRICKSON WA, FRANK J, MARKS AR. STRUCTURE OF A MAMMALIAN RYANODINE RECEPTOR. *NATURE*. 2015;517:44-49
501. WELCH W, RHEAULT S, WEST DJ, WILLIAMS AJ. A MODEL OF THE PUTATIVE PORE REGION OF THE CARDIAC RYANODINE RECEPTOR CHANNEL. *BIOPHYS J*. 2004;87:2335-2351
502. JIANG Y, LEE A, CHEN J, RUTA V, CADENE M, CHAIT BT, MACKINNON R. X-RAY STRUCTURE OF A VOLTAGE-DEPENDENT K+ CHANNEL. *NATURE*. 2003;423:33-41
503. MEAD-SAVERY FC, WANG R, TANNA-TOPAN B, CHEN SR, WELCH W, WILLIAMS AJ. CHANGES IN NEGATIVE CHARGE AT THE LUMINAL MOUTH OF THE PORE ALTER ION HANDLING AND GATING IN THE CARDIAC RYANODINE-RECEPTOR. *BIOPHYS J*.

2009;96:1374-1387

504. ALTSCHAFL BA, ARVANITIS DA, FUENTES O, YUAN Q, KRANIAS EG, VALDIVIA HH. DUAL ROLE OF JUNCTIN IN THE REGULATION OF RYANODINE RECEPTORS AND CALCIUM RELEASE IN CARDIAC VENTRICULAR MYOCYTES. *J PHYSIOL*. 2011;589:6063-6080
505. GOONASEKERA SA, BEARD NA, GROOM L, KIMURA T, LYFENKO AD, ROSENFELD A, MARTY I, DULHUNTY AF, DIRKSEN RT. TRIADIN BINDING TO THE C-TERMINAL LUMINAL LOOP OF THE RYANODINE RECEPTOR IS IMPORTANT FOR SKELETAL MUSCLE EXCITATION CONTRACTION COUPLING. *J GEN PHYSIOL*. 2007;130:365-378
506. LEE JM, RHO SH, SHIN DW, CHO C, PARK WJ, EOM SH, MA J, KIM DH. NEGATIVELY CHARGED AMINO ACIDS WITHIN THE INTRALUMINAL LOOP OF RYANODINE RECEPTOR ARE INVOLVED IN THE INTERACTION WITH TRIADIN. *J BIOL CHEM*. 2004;279:6994-7000
507. CORONADO R, MORRISSETTE J, SUKHAREVA M, VAUGHAN DM. STRUCTURE AND FUNCTION OF RYANODINE RECEPTORS. *AM J PHYSIOL*. 1994;266:C1485-1504
508. TINKER A, WILLIAMS AJ. DIVALENT CATION CONDUCTION IN THE RYANODINE RECEPTOR CHANNEL OF SHEEP CARDIAC MUSCLE SARCOPLASMIC RETICULUM. *J GEN PHYSIOL*. 1992;100:479-493
509. MURAYAMA T, OBA T, KATAYAMA E, OYAMADA H, OGUCHI K, KOBAYASHI M, OTSUKA K, OGAWA Y. FURTHER CHARACTERIZATION OF THE TYPE 3 RYANODINE RECEPTOR (RYR3) PURIFIED FROM RABBIT DIAPHRAGM. *J BIOL CHEM*. 1999;274:17297-17308
510. LINDSAY AR, MANNING SD, WILLIAMS AJ. MONOVALENT CATION CONDUCTANCE IN THE RYANODINE RECEPTOR-CHANNEL OF SHEEP CARDIAC MUSCLE SARCOPLASMIC RETICULUM. *J PHYSIOL*. 1991;439:463-480
511. SMITH JS, IMAGAWA T, MA J, FILL M, CAMPBELL KP, CORONADO R. PURIFIED RYANODINE RECEPTOR FROM RABBIT SKELETAL MUSCLE IS THE CALCIUM-RELEASE CHANNEL OF SARCOPLASMIC RETICULUM. *J GEN PHYSIOL*. 1988;92:1-26
512. FILL M, COPELLO JA. RYANODINE RECEPTOR CALCIUM RELEASE CHANNELS. *PHYSIOL REV*. 2002;82:893-922
513. WILLIAMS AJ. ION CONDUCTION AND DISCRIMINATION IN THE SARCOPLASMIC RETICULUM RYANODINE RECEPTOR/CALCIUM-RELEASE CHANNEL. *J MUSCLE RES CELL MOTIL*. 1992;13:7-26
514. CORONADO R, AFFOLTER H. INSULATION OF THE CONDUCTION PATHWAY OF MUSCLE TRANSVERSE TUBULE CALCIUM CHANNELS FROM THE SURFACE CHARGE OF BILAYER PHOSPHOLIPID. *J GEN PHYSIOL*. 1986;87:933-953
515. KAGAYA Y, WEINBERG EO, ITO N, MOCHIZUKI T, BARRY WH, LORELL BH. GLYCOLYTIC INHIBITION: EFFECTS ON DIASTOLIC RELAXATION AND INTRACELLULAR CALCIUM HANDLING IN HYPERTROPHIED RAT VENTRICULAR MYOCYTES. *J CLIN INVEST*. 1995;95:2766-2776
516. SHANNON TR, GUO T, BERS DM. CA<sup>2+</sup> SCRAPES: LOCAL DEPLETIONS OF FREE [CA<sup>2+</sup>] IN CARDIAC SARCOPLASMIC RETICULUM DURING CONTRACTIONS LEAVE SUBSTANTIAL CA<sup>2+</sup> RESERVE. *CIRC RES*. 2003;93:40-45
517. VAN PETEGEM F. RYANODINE RECEPTORS: ALLOSTERIC ION CHANNEL GIANTS. *J MOL BIOL*. 2015;427:31-53
518. TATEISHI H, YANO M, MOCHIZUKI M, SUTOMI T, ONO M, XU X, UCHINOUMI H, OKUDA S, ODA T, KOBAYASHI S, YAMAMOTO T, IKEDA Y, OHKUSA T, IKEMOTO N, MATSUZAKI M. DEFECTIVE DOMAIN-DOMAIN INTERACTIONS WITHIN THE RYANODINE RECEPTOR AS A CRITICAL CAUSE OF DIASTOLIC CA<sup>2+</sup> LEAK IN FAILING HEARTS. *CARDIOVASC RES*. 2009;81:536-545
519. BAUEROVA-HLINKOVA V, HOSTINOVA E, GASPERIK J, BECK K, BORKO L, LAI FA, ZAHRADNIKOVA A, SEVCIK J. BIOINFORMATIC MAPPING AND PRODUCTION OF RECOMBINANT N-TERMINAL DOMAINS OF HUMAN CARDIAC RYANODINE RECEPTOR 2. *PROTEIN EXPRESSION AND PURIFICATION*. 2010;71:33-41
520. KIMLICKA L, TUNG CC, CARLSSON AC, LOBO PA, YUCHI Z, VAN PETEGEM F. THE CARDIAC RYANODINE RECEPTOR N-TERMINAL REGION CONTAINS AN ANION BINDING SITE THAT IS TARGETED BY DISEASE MUTATIONS. *STRUCTURE*. 2013;21:1440-1449



521. TANG Y, TIAN X, WANG R, FILL M, CHEN SR. ABNORMAL TERMINATION OF CA<sup>2+</sup> RELEASE IS A COMMON DEFECT OF RYR2 MUTATIONS ASSOCIATED WITH CARDIOMYOPATHIES. *CIRC RES*. 2012;110:968-977
522. HAGIWARA S, NAKAJIMA S. EFFECTS OF THE INTRACELLULAR CA ION CONCENTRATION UPON THE EXCITABILITY OF THE MUSCLE FIBER MEMBRANE OF A BARNACLE. *J GEN PHYSIOL*. 1966;49:807-818
523. GILKEY JC, JAFFE LF, RIDGWAY EB, REYNOLDS GT. A FREE CALCIUM WAVE TRAVERSES THE ACTIVATING EGG OF THE MEDAKA, ORYZIAS LATIPES. *J CELL BIOL*. 1978;76:448-466
524. RIDGWAY EB, GILKEY JC, JAFFE LF. FREE CALCIUM INCREASES EXPLOSIVELY IN ACTIVATING MEDAKA EGGS. *PROC NATL ACAD SCI U S A*. 1977;74:623-627
525. ALLEN DG, BLINKS JR. CALCIUM TRANSIENTS IN AEQUORIN-INJECTED FROG CARDIAC MUSCLE. *NATURE*. 1978;273:509-513
526. WIER WG. CALCIUM TRANSIENTS DURING EXCITATION-CONTRACTION COUPLING IN MAMMALIAN HEART: AEQUORIN SIGNALS OF CANINE PURKINJE FIBERS. *SCIENCE*. 1980;207:1085-1087
527. CHENG H, LEDERER WJ, CANNELL MB. CALCIUM SPARKS: ELEMENTARY EVENTS UNDERLYING EXCITATION-CONTRACTION COUPLING IN HEART MUSCLE. *SCIENCE*. 1993;262:740-744
528. BROCHET DX, YANG D, CHENG H, LEDERER WJ. ELEMENTARY CALCIUM RELEASE EVENTS FROM THE SARCOPLASMIC RETICULUM IN THE HEART. *ADV EXP MED BIOL*. 2012;740:499-509
529. SHEEHAN KA, ZIMA AV, BLATTER LA. REGIONAL DIFFERENCES IN SPONTANEOUS CA<sup>2+</sup> SPARK ACTIVITY AND REGULATION IN CAT ATRIAL MYOCYTES. *J PHYSIOL*. 2006;572:799-809
530. WOO SH, CLEEMANN L, MORAD M. SPATIOTEMPORAL CHARACTERISTICS OF JUNCTIONAL AND NONJUNCTIONAL FOCAL CA<sup>2+</sup> RELEASE IN RAT ATRIAL MYOCYTES. *CIRC RES*. 2003;92:E1-11
531. WOO SH, CLEEMANN L, MORAD M. DIVERSITY OF ATRIAL LOCAL CA<sup>2+</sup> SIGNALLING: EVIDENCE FROM 2-D CONFOCAL IMAGING IN CA<sup>2+</sup>-BUFFERED RAT ATRIAL MYOCYTES. *J PHYSIOL*. 2005;567:905-921
532. FABIATO A. TIME AND CALCIUM DEPENDENCE OF ACTIVATION AND INACTIVATION OF CALCIUM- INDUCED RELEASE OF CALCIUM FROM THE SARCOPLASMIC RETICULUM OF A SKINNED CANINE CARDIAC PURKINJE CELL. *J GEN PHYSIOL*. 1985;85:247-289
533. RIOS E, BRUM G. INVOLVEMENT OF DIHYDROPYRIDINE RECEPTORS IN EXCITATION-CONTRACTION COUPLING IN SKELETAL MUSCLE. *NATURE*. 1987;325:717-720
534. RIOS E, KARHANEK M, MA J, GONZALEZ A. AN ALLOSTERIC MODEL OF THE MOLECULAR INTERACTIONS OF EXCITATION-CONTRACTION COUPLING IN SKELETAL MUSCLE. *J GEN PHYSIOL*. 1993;102:449-481
535. MEISSNER G, DARLING E, EVELETH J. KINETICS OF RAPID CA<sup>2+</sup> RELEASE BY SARCOPLASMIC RETICULUM. EFFECTS OF CA<sup>2+</sup>, MG<sup>2+</sup>, AND ADENINE NUCLEOTIDES. *BIOCHEMISTRY*. 1986;25:236-244
536. PERCIVAL AL, WILLIAMS AJ, KENYON JL, GRINSELL MM, AIREY JA, SUTKO JL. CHICKEN SKELETAL MUSCLE RYANODINE RECEPTOR ISOFORMS: ION CHANNEL PROPERTIES. *BIOPHYS J*. 1994;67:1834-1850
537. LAVER DR, RODEN LD, AHERN GP, EAGER KR, JUNANKAR PR, DULHUNTY AF. CYTOPLASMIC CA<sup>2+</sup> INHIBITS THE RYANODINE RECEPTOR FROM CARDIAC MUSCLE. *THE JOURNAL OF MEMBRANE BIOLOGY*. 1995;147:7-22
538. JEYAKUMAR LH, COPELLO JA, O'MALLEY AM, WU GM, GRASSUCCI R, WAGENKNECHT T, FLEISCHER S. PURIFICATION AND CHARACTERIZATION OF RYANODINE RECEPTOR 3 FROM MAMMALIAN TISSUE. *J BIOL CHEM*. 1998;273:16011-16020
539. CHEN SR, LI X, EBISAWA K, ZHANG L. FUNCTIONAL CHARACTERIZATION OF THE RECOMBINANT TYPE 3 CA<sup>2+</sup> RELEASE CHANNEL (RYANODINE RECEPTOR) EXPRESSED IN HEK293 CELLS. *J BIOL CHEM*. 1997;272:24234-24246
540. SCHIEFER A, MEISSNER G, ISENBERG G. CA<sup>2+</sup> ACTIVATION AND CA<sup>2+</sup> INACTIVATION OF CANINE RECONSTITUTED CARDIAC SARCOPLASMIC RETICULUM CA(2+)-

- RELEASE CHANNELS. *J PHYSIOL*. 1995;489 ( PT 2):337-348
541. VELEZ P, GYORKE S, ESCOBAR AL, VERGARA J, FILL M. ADAPTATION OF SINGLE CARDIAC RYANODINE RECEPTOR CHANNELS. *BIOPHYS J*. 1997;72:691-697
542. ZAHRADNIKOVA A, ZAHRADNIK I, GYORKE I, GYORKE S. RAPID ACTIVATION OF THE CARDIAC RYANODINE RECEPTOR BY SUBMILLISECOND CALCIUM STIMULI. *J GEN PHYSIOL*. 1999;114:787-798
543. LAVER DR. CA<sup>2+</sup> STORES REGULATE RYANODINE RECEPTOR CA<sup>2+</sup> RELEASE CHANNELS VIA LUMINAL AND CYTOSOLIC CA<sup>2+</sup> SITES. *BIOPHYS J*. 2007;92:3541-3555
544. LAVER DR. LUMINAL CA(2+) ACTIVATION OF CARDIAC RYANODINE RECEPTORS BY LUMINAL AND CYTOPLASMIC DOMAINS. *EUROPEAN BIOPHYSICS JOURNAL : EBJ*. 2009;39:19-26
545. ZAHRADNIKOVA A, VALENT I, ZAHRADNIK I. FREQUENCY AND RELEASE FLUX OF CALCIUM SPARKS IN RAT CARDIAC MYOCYTES: A RELATION TO RYR GATING. *J GEN PHYSIOL*. 2010;136:101-116
546. LAVER DR. REGULATION OF RYR CHANNEL GATING BY CA(2+), MG(2+) AND ATP. *CURRENT TOPICS IN MEMBRANES*. 2010;66:69-89
547. XU L, MEISSNER G. REGULATION OF CARDIAC MUSCLE CA<sup>2+</sup> RELEASE CHANNEL BY SARCOPLASMIC RETICULUM LUMENAL CA<sup>2+</sup>. *BIOPHYS J*. 1998;75:2302-2312
548. GYORKE I, GYORKE S. REGULATION OF THE CARDIAC RYANODINE RECEPTOR CHANNEL BY LUMINAL CA<sup>2+</sup> INVOLVES LUMINAL CA<sup>2+</sup> SENSING SITES. *BIOPHYS J*. 1998;75:2801-2810
549. GYORKE S, GYORKE I, LUKYANENKO V, THERENTYEV D, VIATCHENKO-KARPINSKI S, WIESNER TF. REGULATION OF SARCOPLASMIC RETICULUM CALCIUM RELEASE BY LUMINAL CALCIUM IN CARDIAC MUSCLE. *FRONT BIOSCI*. 2002;7:D1454-1463
550. QIN J, VALLE G, NANI A, NORI A, RIZZI N, PRIORI SG, VOLPE P, FILL M. LUMINAL CA<sup>2+</sup> REGULATION OF SINGLE CARDIAC RYANODINE RECEPTORS: INSIGHTS PROVIDED BY CALSEQUESTRIN AND ITS MUTANTS. *J GEN PHYSIOL*. 2008;131:325-334
551. QIN J, VALLE G, NANI A, CHEN H, RAMOS-FRANCO J, NORI A, VOLPE P, FILL M. RYANODINE RECEPTOR LUMINAL CA<sup>2+</sup> REGULATION: SWAPPING CALSEQUESTRIN AND CHANNEL ISOFORMS. *BIOPHYS J*. 2009;97:1961-1970
552. CHEN H, VALLE G, FURLAN S, NANI A, GYORKE S, FILL M, VOLPE P. MECHANISM OF CALSEQUESTRIN REGULATION OF SINGLE CARDIAC RYANODINE RECEPTOR IN NORMAL AND PATHOLOGICAL CONDITIONS. *J GEN PHYSIOL*. 2013;142:127-136
553. COPELLO JA, BARG S, SONNLEITNER A, PORTA M, DIAZ-SYLVESTER P, FILL M, SCHINDLER H, FLEISCHER S. DIFFERENTIAL ACTIVATION BY CA<sup>2+</sup>, ATP AND CAFFEINE OF CARDIAC AND SKELETAL MUSCLE RYANODINE RECEPTORS AFTER BLOCK BY MG<sup>2+</sup>. *THE JOURNAL OF MEMBRANE BIOLOGY*. 2002;187:51-64
554. BURI A, MCGUIGAN JA. INTRACELLULAR FREE MAGNESIUM AND ITS REGULATION, STUDIED IN ISOLATED FERRET VENTRICULAR MUSCLE WITH ION-SELECTIVE MICROELECTRODES. *EXPERIMENTAL PHYSIOLOGY*. 1990;75:751-761
555. MEISSNER G. RYANODINE RECEPTOR/CA<sup>2+</sup> RELEASE CHANNELS AND THEIR REGULATION BY ENDOGENOUS EFFECTORS. *ANNU REV PHYSIOL*. 1994;56:485-508
556. LAVER DR, HONEN BN. LUMINAL MG<sup>2+</sup>, A KEY FACTOR CONTROLLING RYR2-MEDIATED CA<sup>2+</sup> RELEASE: CYTOPLASMIC AND LUMINAL REGULATION MODELED IN A TETRAMERIC CHANNEL. *J GEN PHYSIOL*. 2008;132:429-446
557. ZAHRADNIKOVA A, DURA M, GYORKE I, ESCOBAR AL, ZAHRADNIK I, GYORKE S. REGULATION OF DYNAMIC BEHAVIOR OF CARDIAC RYANODINE RECEPTOR BY MG<sup>2+</sup> UNDER SIMULATED PHYSIOLOGICAL CONDITIONS. *AMERICAN JOURNAL OF PHYSIOLOGY. CELL PHYSIOLOGY*. 2003;285:C1059-1070
558. LAVER DR, BAYNES TM, DULHUNTY AF. MAGNESIUM INHIBITION OF RYANODINE-RECEPTOR CALCIUM CHANNELS: EVIDENCE FOR TWO INDEPENDENT MECHANISMS. *THE JOURNAL OF MEMBRANE BIOLOGY*. 1997;156:213-229
559. MEISSNER G, HENDERSON JS. RAPID CALCIUM RELEASE FROM CARDIAC SARCOPLASMIC RETICULUM VESICLES IS DEPENDENT ON CA<sup>2+</sup> AND IS MODULATED BY MG<sup>2+</sup>, ADENINE NUCLEOTIDE, AND CALMODULIN. *J BIOL CHEM*. 1987;262:3065-3073
560. MEISSNER G. ADENINE NUCLEOTIDE STIMULATION OF CA<sup>2+</sup>-INDUCED CA<sup>2+</sup> RELEASE IN SARCOPLASMIC RETICULUM. *J BIOL CHEM*. 1984;259:2365-2374

561. LAVER DR, LENZ GK, LAMB GD. REGULATION OF THE CALCIUM RELEASE CHANNEL FROM RABBIT SKELETAL MUSCLE BY THE NUCLEOTIDES ATP, AMP, IMP AND ADENOSINE. *J PHYSIOL*. 2001;537:763-778
562. XU L, MANN G, MEISSNER G. REGULATION OF CARDIAC CA<sup>2+</sup> RELEASE CHANNEL (RYANODINE RECEPTOR) BY CA<sup>2+</sup>, H<sup>+</sup>, MG<sup>2+</sup>, AND ADENINE NUCLEOTIDES UNDER NORMAL AND SIMULATED ISCHEMIC CONDITIONS. *CIRC RES*. 1996;79:1100-1109
563. KERMODE H, WILLIAMS AJ, SITSAPESAN R. THE INTERACTIONS OF ATP, ADP, AND INORGANIC PHOSPHATE WITH THE SHEEP CARDIAC RYANODINE RECEPTOR. *BIOPHYS J*. 1998;74:1296-1304
564. MEISSNER G, ROUSSEAU E, LAI FA, LIU QY, ANDERSON KA. BIOCHEMICAL CHARACTERIZATION OF THE CA<sup>2+</sup> RELEASE CHANNEL OF SKELETAL AND CARDIAC SARCOPLASMIC RETICULUM. *MOLECULAR AND CELLULAR BIOCHEMISTRY*. 1988;82:59-65
565. CHAN WM, WELCH W, SITSAPESAN R. STRUCTURAL CHARACTERISTICS THAT GOVERN BINDING TO, AND MODULATION THROUGH, THE CARDIAC RYANODINE RECEPTOR NUCLEOTIDE BINDING SITE. *MOLECULAR PHARMACOLOGY*. 2003;63:174-182
566. CHAN WM, WELCH W, SITSAPESAN R. STRUCTURAL FACTORS THAT DETERMINE THE ABILITY OF ADENOSINE AND RELATED COMPOUNDS TO ACTIVATE THE CARDIAC RYANODINE RECEPTOR. *BR J PHARMACOL*. 2000;130:1618-1626
567. MEISSNER G. REGULATION OF MAMMALIAN RYANODINE RECEPTORS. *FRONT BIOSCI*. 2002;7:D2072-2080
568. NEUBAUER S. THE FAILING HEART--AN ENGINE OUT OF FUEL. *N ENGL J MED*. 2007;356:1140-1151
569. RUIZ-HURTADO G, LI L, FERNANDEZ-VELASCO M, RUEDA A, LEFEBVRE F, WANG Y, MATEO P, CASSAN C, GELLEN B, BENITAH JP, GOMEZ AM. RECONCILING DEPRESSED CA<sup>2+</sup> SPARKS OCCURRENCE WITH ENHANCED RYR2 ACTIVITY IN FAILING MICE CARDIOMYOCYTES. *J GEN PHYSIOL*. 2015;146:295-306
570. KENNEDY C. ATP AS A COTRANSMITTER IN THE AUTONOMIC NERVOUS SYSTEM. *AUTONOMIC NEUROSCIENCE : BASIC & CLINICAL*. 2015;191:2-15
571. CAMARA H, RODRIGUES JQ, ALVES GA, DA SILVA JUNIOR ED, CARICATI-NETO A, GARCIA AG, JURKIEWICZ A. WOULD CALCIUM OR POTASSIUM CHANNELS BE RESPONSIBLE FOR CARDIAC ARREST PRODUCED BY ADENOSINE AND ATP IN THE RIGHT ATRIA OF WISTAR RATS? *EUR J PHARMACOL*. 2015;768:199-206
572. CAMORS E, VALDIVIA HH. CAMKII REGULATION OF CARDIAC RYANODINE RECEPTORS AND INOSITOL TRIPHOSPHATE RECEPTORS. *FRONTIERS IN PHARMACOLOGY*. 2014;5:101
573. HUK S, BERS DM. RYANODINE RECEPTOR PHOSPHORYLATION AT SERINE 2030, 2808 AND 2814 IN RAT CARDIOMYOCYTES. *BIOCHEM BIOPHYS RES COMMUN*. 2008;376:80-85
574. RODRIGUEZ P, BHOGAL MS, COLYER J. STOICHIOMETRIC PHOSPHORYLATION OF CARDIAC RYANODINE RECEPTOR ON SERINE 2809 BY CALMODULIN-DEPENDENT KINASE II AND PROTEIN KINASE A. *J BIOL CHEM*. 2003;278:38593-38600
575. XIAO B, ZHONG G, OBAYASHI M, YANG D, CHEN K, WALSH MP, SHIMONI Y, CHENG H, TER KEURS H, CHEN SR. SER-2030, BUT NOT SER-2808, IS THE MAJOR PHOSPHORYLATION SITE IN CARDIAC RYANODINE RECEPTORS RESPONDING TO PROTEIN KINASE A ACTIVATION UPON BETA-ADRENERGIC STIMULATION IN NORMAL AND FAILING HEARTS. *BIOCHEM J*. 2006;396:7-16
576. XIAO B, JIANG MT, ZHAO M, YANG D, SUTHERLAND C, LAI FA, WALSH MP, WARLTIER DC, CHENG H, CHEN SR. CHARACTERIZATION OF A NOVEL PKA PHOSPHORYLATION SITE, SERINE-2030, REVEALS NO PKA HYPERPHOSPHORYLATION OF THE CARDIAC RYANODINE RECEPTOR IN CANINE HEART FAILURE. *CIRC RES*. 2005;96:847-855
577. WEHRENS XH, LEHNART SE, REIKEN S, VEST JA, WRONSKA A, MARKS AR. RYANODINE RECEPTOR/CALCIUM RELEASE CHANNEL PKA PHOSPHORYLATION: A CRITICAL MEDIATOR OF HEART FAILURE PROGRESSION. *PROC NATL ACAD SCI U S A*. 2006;103:511-518
578. JIANG MT, LOKUTA AJ, FARRELL EF, WOLFF MR, HAWORTH RA, VALDIVIA HH. ABNORMAL CA<sup>2+</sup> RELEASE, BUT NORMAL RYANODINE RECEPTORS, IN CANINE AND HUMAN HEART FAILURE. *CIRC RES*. 2002;91:1015-1022.
579. CARTER S, COLYER J, SITSAPESAN R. MAXIMUM PHOSPHORYLATION OF THE

- CARDIAC RYANODINE RECEPTOR AT SERINE-2809 BY PROTEIN KINASE A PRODUCES UNIQUE MODIFICATIONS TO CHANNEL GATING AND CONDUCTANCE NOT OBSERVED AT LOWER LEVELS OF PHOSPHORYLATION. *CIRC RES.* 2006;98:1506-1513
580. BENKUSKY NA, WEBER CS, SCHERMAN JA, FARRELL EF, HACKER TA, JOHN MC, POWERS PA, VALDIVIA HH. INTACT BETA-ADRENERGIC RESPONSE AND UNMODIFIED PROGRESSION TOWARD HEART FAILURE IN MICE WITH GENETIC ABLATION OF A MAJOR PROTEIN KINASE A PHOSPHORYLATION SITE IN THE CARDIAC RYANODINE RECEPTOR. *CIRC RES.* 2007;101:819-829
581. MACDONNELL SM, GARCIA-RIVAS G, SCHERMAN JA, KUBO H, CHEN X, VALDIVIA H, HOUSER SR. ADRENERGIC REGULATION OF CARDIAC CONTRACTILITY DOES NOT INVOLVE PHOSPHORYLATION OF THE CARDIAC RYANODINE RECEPTOR AT SERINE 2808. *CIRC RES.* 2008;102:E65-72
582. ZHANG H, MAKAREWICH CA, KUBO H, WANG W, DURAN JM, LI Y, BERRETTA RM, KOCH WJ, CHEN X, GAO E, VALDIVIA HH, HOUSER SR. HYPERPHOSPHORYLATION OF THE CARDIAC RYANODINE RECEPTOR AT SERINE 2808 IS NOT INVOLVED IN CARDIAC DYSFUNCTION AFTER MYOCARDIAL INFARCTION. *CIRC RES.* 2012;110:831-840
583. STANGE M, XU L, BALSHAW D, YAMAGUCHI N, MEISSNER G. CHARACTERIZATION OF RECOMBINANT SKELETAL MUSCLE (SER-2843) AND CARDIAC MUSCLE (SER-2809) RYANODINE RECEPTOR PHOSPHORYLATION MUTANTS. *J BIOL CHEM.* 2003;278:51693-51702
584. XIAO B, SUTHERLAND C, WALSH MP, CHEN SR. PROTEIN KINASE A PHOSPHORYLATION AT SERINE-2808 OF THE CARDIAC CA<sup>2+</sup>-RELEASE CHANNEL (RYANODINE RECEPTOR) DOES NOT DISSOCIATE 12.6-KDA FK506-BINDING PROTEIN (FKBP12.6). *CIRC RES.* 2004;94:487-495
585. GUO T, CORNEA RL, HUKU S, CAMORS E, YANG Y, PICT E, FRUEN BR, BERS DM. KINETICS OF FKBP12.6 BINDING TO RYANODINE RECEPTORS IN PERMEABILIZED CARDIAC MYOCYTES AND EFFECTS ON CA SPARKS. *CIRC RES.* 2010;106:1743-1752
586. XIAO J, TIAN X, JONES PP, BOLSTAD J, KONG H, WANG R, ZHANG L, DUFF HJ, GILLIS AM, FLEISCHER S, KOTLIKOFF M, COPELLO JA, CHEN SR. REMOVAL OF FKBP12.6 DOES NOT ALTER THE CONDUCTANCE AND ACTIVATION OF THE CARDIAC RYANODINE RECEPTOR OR THE SUSCEPTIBILITY TO STRESS-INDUCED VENTRICULAR ARRHYTHMIAS. *J BIOL CHEM.* 2007;282:34828-34838
587. TIMERMAN AP, ONOUE H, XIN HB, BARG S, COPELLO J, WIEDERRECHT G, FLEISCHER S. SELECTIVE BINDING OF FKBP12.6 BY THE CARDIAC RYANODINE RECEPTOR. *J BIOL CHEM.* 1996;271:20385-20391
588. RESPRESS JL, VAN OORT RJ, LI N, ROLIM N, DIXIT SS, DEALMEIDA A, VOIGT N, LAWRENCE WS, SKAPURA DG, SKARDAL K, WISLOFF U, WIELAND T, AI X, POGWIZD SM, DOBREV D, WEHRENS XH. ROLE OF RYR2 PHOSPHORYLATION AT S2814 DURING HEART FAILURE PROGRESSION. *CIRC RES.* 2012;110:1474-1483
589. DI CARLO MN, SAID M, LING H, VALVERDE CA, DE GIUSTI VC, SOMMESE L, PALOMEQUE J, AIELLO EA, SKAPURA DG, RINALDI G, RESPRESS JL, BROWN JH, WEHRENS XH, SALAS MA, MATTIAZZI A. CAMKII-DEPENDENT PHOSPHORYLATION OF CARDIAC RYANODINE RECEPTORS REGULATES CELL DEATH IN CARDIAC ISCHEMIA/REPERFUSION INJURY. *J MOL CELL CARDIOL.* 2014;74:274-283
590. GRIMM M, LING H, WILLEFORD A, PEREIRA L, GRAY CB, ERICKSON JR, SARMA S, RESPRESS JL, WEHRENS XH, BERS DM, BROWN JH. CAMKII DELTA MEDIATES BETA-ADRENERGIC EFFECTS ON RYR2 PHOSPHORYLATION AND SR CA(2+) LEAK AND THE PATHOPHYSIOLOGICAL RESPONSE TO CHRONIC BETA-ADRENERGIC STIMULATION. *J MOL CELL CARDIOL.* 2015;85:282-291
591. XIAO B, TIAN X, XIE W, JONES PP, CAI S, WANG X, JIANG D, KONG H, ZHANG L, CHEN K, WALSH MP, CHENG H, CHEN SR. FUNCTIONAL CONSEQUENCE OF PROTEIN KINASE A-DEPENDENT PHOSPHORYLATION OF THE CARDIAC RYANODINE RECEPTOR: SENSITIZATION OF STORE OVERLOAD-INDUCED CA<sup>2+</sup> RELEASE. *J BIOL CHEM.* 2007;282:30256-30264
592. ROKITA AG, ANDERSON ME. NEW THERAPEUTIC TARGETS IN CARDIOLOGY: ARRHYTHMIAS AND CA<sup>2+</sup>/CALMODULIN-DEPENDENT KINASE II (CAMKII). *CIRCULATION.* 2012;126:2125-2139

593. LEE LC, MAURICE DH, BAILLIE GS. TARGETING PROTEIN-PROTEIN INTERACTIONS WITHIN THE CYCLIC AMP SIGNALING SYSTEM AS A THERAPEUTIC STRATEGY FOR CARDIOVASCULAR DISEASE. *FUTURE MEDICINAL CHEMISTRY*. 2013;5:451-464
594. ESCHENHAGEN T. IS RYANODINE RECEPTOR PHOSPHORYLATION KEY TO THE FIGHT OR FLIGHT RESPONSE AND HEART FAILURE? *J CLIN INVEST*. 2010;120:4197-4203
595. CHELU MG, DANILA CI, GILMAN CP, HAMILTON SL. REGULATION OF RYANODINE RECEPTORS BY FK506 BINDING PROTEINS. *TRENDS CARDIOVASC MED*. 2004;14:227-234
596. JEYAKUMAR LH, BALLESTER L, CHENG DS, MCINTYRE JO, CHANG P, OLIVEY HE, ROLLINS-SMITH L, BARNETT JV, MURRAY K, XIN HB, FLEISCHER S. FKBP BINDING CHARACTERISTICS OF CARDIAC MICROSOMES FROM DIVERSE VERTEBRATES. *BIOCHEM BIOPHYS RES COMMUN*. 2001;281:979-986
597. MASUMIYA H, WANG R, ZHANG J, XIAO B, CHEN SR. LOCALIZATION OF THE 12.6-KDA FK506-BINDING PROTEIN (FKBP12.6) BINDING SITE TO THE NH<sub>2</sub>-TERMINAL DOMAIN OF THE CARDIAC CA<sup>2+</sup> RELEASE CHANNEL (RYANODINE RECEPTOR). *J BIOL CHEM*. 2003;278:3786-3792
598. ZISSIMOPOULOS S, LAI FA. INTERACTION OF FKBP12.6 WITH THE CARDIAC RYANODINE RECEPTOR C-TERMINAL DOMAIN. *J BIOL CHEM*. 2005;280:5475-5485
599. SHOU W, AGHDASI B, ARMSTRONG DL, GUO Q, BAO S, CHARNG MJ, MATHEWS LM, SCHNEIDER MD, HAMILTON SL, MATZUK MM. CARDIAC DEFECTS AND ALTERED RYANODINE RECEPTOR FUNCTION IN MICE LACKING FKBP12. *NATURE*. 1998;391:489-492
600. XIAO RP, VALDIVIA HH, BOGDANOV K, VALDIVIA C, LAKATTA EG, CHENG H. THE IMMUNOPHILIN FK506-BINDING PROTEIN MODULATES CA<sup>2+</sup> RELEASE CHANNEL CLOSURE IN RAT HEART. *J PHYSIOL (LOND)*. 1997;500:343-354
601. WEHRENS XH, LEHNART SE, HUANG F, VEST JA, REIKEN SR, MOHLER PJ, SUN J, GUATIMOSIM S, SONG LS, ROSEMBLIT N, D'ARMIENTO JM, NAPOLITANO C, MEMMI M, PRIORI SG, LEDERER WJ, MARKS AR. FKBP12.6 DEFICIENCY AND DEFECTIVE CALCIUM RELEASE CHANNEL (RYANODINE RECEPTOR) FUNCTION LINKED TO EXERCISE-INDUCED SUDDEN CARDIAC DEATH. *CELL*. 2003;113:829-840
602. LI N, WANG T, WANG W, CUTLER MJ, WANG Q, VOIGT N, ROSENBAUM DS, DOBREV D, WEHRENS XH. INHIBITION OF CAMKII PHOSPHORYLATION OF RYR2 PREVENTS INDUCTION OF ATRIAL FIBRILLATION IN FKBP12.6 KNOCKOUT MICE. *CIRC RES*. 2012;110:465-470
603. GOMEZ AM, SCHUSTER I, FAUCONNIER J, PRESTLE J, HASENFUSS G, RICHARD S. FKBP12.6 OVEREXPRESSION DECREASES CA<sup>2+</sup> SPARK AMPLITUDE BUT ENHANCES [CA<sup>2+</sup>]<sub>i</sub> TRANSIENT IN RAT CARDIAC MYOCYTES. *AMERICAN JOURNAL OF PHYSIOLOGY-HEART AND CIRCULATORY PHYSIOLOGY*. 2004;287:H1987-H1993
604. GELLEN B, FERNANDEZ-VELASCO M, BRIEC F, VINET L, LEQUANG K, ROUET-BENZINEB P, BENITAH JP, PEZET M, PALAIS G, PELLEGRIN N, ZHANG A, PERRIER R, ESCOUBET B, MARNIQUET X, RICHARD S, JAISSER F, GOMEZ AM, CHARPENTIER F, MERCADIER JJ. CONDITIONAL FKBP12.6 OVEREXPRESSION IN MOUSE CARDIAC MYOCYTES PREVENTS TRIGGERED VENTRICULAR TACHYCARDIA THROUGH SPECIFIC ALTERATIONS IN EXCITATION-CONTRACTION COUPLING. *CIRCULATION*. 2008;117:1778-1786
605. BARG S, COPELLO JA, FLEISCHER S. DIFFERENT INTERACTIONS OF CARDIAC AND SKELETAL MUSCLE RYANODINE RECEPTORS WITH FK-506 BINDING PROTEIN ISOFORMS. *AM J PHYSIOL*. 1997;272:C1726-1733
606. MARUYAMA M, LI BY, CHEN H, XU X, SONG LS, GUATIMOSIM S, ZHU W, YONG W, ZHANG W, BU G, LIN SF, FISHBEIN MC, LEDERER WJ, SCHILD JH, FIELD LJ, RUBART M, CHEN PS, SHOU W. FKBP12 IS A CRITICAL REGULATOR OF THE HEART RHYTHM AND THE CARDIAC VOLTAGE-GATED SODIUM CURRENT IN MICE. *CIRC RES*. 2011;108:1042-1052
607. BALSHAW DM, XU L, YAMAGUCHI N, PASEK DA, MEISSNER G. CALMODULIN BINDING AND INHIBITION OF CARDIAC MUSCLE CALCIUM RELEASE CHANNEL (RYANODINE RECEPTOR). *J BIOL CHEM*. 2001;276:20144-20153
608. RODNEY GG, WILLIAMS BY, STRASBURG GM, BECKINGHAM K, HAMILTON SL. REGULATION OF RYR1 ACTIVITY BY CA<sup>(2+)</sup> AND CALMODULIN. *BIOCHEMISTRY*. 2000;39:7807-7812

609. FRUEN BR, BARDY JM, BYREM TM, STRASBURG GM, LOUIS CF. DIFFERENTIAL CA(2+) SENSITIVITY OF SKELETAL AND CARDIAC MUSCLE RYANODINE RECEPTORS IN THE PRESENCE OF CALMODULIN. *AMERICAN JOURNAL OF PHYSIOLOGY. CELL PHYSIOLOGY*. 2000;279:C724-733
610. MOORE CP, RODNEY G, ZHANG JZ, SANTACRUZ-TOLOZA L, STRASBURG G, HAMILTON SL. APOCALMODULIN AND CA<sup>2+</sup> CALMODULIN BIND TO THE SAME REGION ON THE SKELETAL MUSCLE CA<sup>2+</sup> RELEASE CHANNEL. *BIOCHEMISTRY*. 1999;38:8532-8537
611. YAMAGUCHI N, XU L, PASEK DA, EVANS KE, CHEN SR, MEISSNER G. CALMODULIN REGULATION AND IDENTIFICATION OF CALMODULIN BINDING REGION OF TYPE-3 RYANODINE RECEPTOR CALCIUM RELEASE CHANNEL. *BIOCHEMISTRY*. 2005;44:15074-15081
612. SONDERGAARD MT, SORENSEN AB, SKOV LL, KJAER-SORENSEN K, BAUER MC, NYEGAARD M, LINSE S, OXVIG C, OVERGAARD MT. CALMODULIN MUTATIONS CAUSING CATECHOLAMINERGIC POLYMORPHIC VENTRICULAR TACHYCARDIA CONFER OPPOSING FUNCTIONAL AND BIOPHYSICAL MOLECULAR CHANGES. *THE FEBS JOURNAL*. 2015;282:803-816
613. MARSMAN RF, BARC J, BEEKMAN L, ALDERS M, DOOIJES D, VAN DEN WIJNGAARD A, RATBI I, SEFIANI A, BHUIYAN ZA, WILDE AA, BEZZINA CR. A MUTATION IN CALM1 ENCODING CALMODULIN IN FAMILIAL IDIOPATHIC VENTRICULAR FIBRILLATION IN CHILDHOOD AND ADOLESCENCE. *J AM COLL CARDIOL*. 2014;63:259-266
614. SONDERGAARD MT, TIAN X, LIU Y, WANG R, CHAZIN WJ, CHEN SR, OVERGAARD MT. ARRHYTHMOGENIC CALMODULIN MUTATIONS AFFECT THE ACTIVATION AND TERMINATION OF CARDIAC RYANODINE RECEPTOR-MEDIATED CA<sup>2+</sup> RELEASE. *J BIOL CHEM*. 2015;290:26151-26162
615. FUKUDA M, YAMAMOTO T, NISHIMURA S, KATO T, MURAKAMI W, HINO A, ONO M, TATEISHI H, ODA T, OKUDA S, KOBAYASHI S, KOSEKI N, KYUSHIKI H, YANO M. ENHANCED BINDING OF CALMODULIN TO RYR2 CORRECTS ARRHYTHMOGENIC CHANNEL DISORDER IN CPVT-ASSOCIATED MYOCYTES. *BIOCHEM BIOPHYS RES COMMUN*. 2014;448:1-7
616. ANDERSON ME. CALMODULIN AND THE PHILOSOPHER'S STONE: CHANGING CA<sup>2+</sup> INTO ARRHYTHMIAS. *J CARDIOVASC ELECTROPHYSIOL*. 2002;13:195-197
617. BEARD NA, LAVER DR, DULHUNTY AF. CALSEQUESTRIN AND THE CALCIUM RELEASE CHANNEL OF SKELETAL AND CARDIAC MUSCLE. *PROG BIOPHYS MOL BIOL*. 2004;85:33-69
618. WANG S, TRUMBLE WR, LIAO H, WESSON CR, DUNKER AK, KANG CH. CRYSTAL STRUCTURE OF CALSEQUESTRIN FROM RABBIT SKELETAL MUSCLE SARCOPLASMIC RETICULUM. *NATURE STRUCTURAL BIOLOGY*. 1998;5:476-483
619. WEI L, HANNA AD, BEARD NA, DULHUNTY AF. UNIQUE ISOFORM-SPECIFIC PROPERTIES OF CALSEQUESTRIN IN THE HEART AND SKELETAL MUSCLE. *CELL CALCIUM*. 2009;45:474-484
620. DE LA FUENTE S, VAN LANGEN IM, POSTMA AV, BIKKER H, MEIJER A. A CASE OF CATECHOLAMINERGIC POLYMORPHIC VENTRICULAR TACHYCARDIA CAUSED BY TWO CALSEQUESTRIN 2 MUTATIONS. *PACING CLIN ELECTROPHYSIOL*. 2008;31:916-919
621. CHOPRA N, KANNANKERIL PJ, YANG T, HLAING T, HOLINSTAT I, ETTENSOHN K, PFEIFER K, AKIN B, JONES LR, FRANZINI-ARMSTRONG C, KNOLLMANN BC. MODEST REDUCTIONS OF CARDIAC CALSEQUESTRIN INCREASE SARCOPLASMIC RETICULUM CA<sup>2+</sup> LEAK INDEPENDENT OF LUMINAL CA<sup>2+</sup> AND TRIGGER VENTRICULAR ARRHYTHMIAS IN MICE. *CIRC RES*. 2007;101:617-626
622. KNOLLMANN BC, CHOPRA N, HLAING T, AKIN B, YANG T, ETTENSOHN K, KNOLLMANN BE, HORTON KD, WEISSMAN NJ, HOLINSTAT I, ZHANG W, RODEN DM, JONES LR, FRANZINI-ARMSTRONG C, PFEIFER K. CASQ2 DELETION CAUSES SARCOPLASMIC RETICULUM VOLUME INCREASE, PREMATURE CA<sup>2+</sup> RELEASE, AND CATECHOLAMINERGIC POLYMORPHIC VENTRICULAR TACHYCARDIA. *J CLIN INVEST*. 2006;116:2510-2520
623. SONG L, ALCALAI R, ARAD M, WOLF CM, TOKA O, CONNER DA, BERUL CI, ELДАР M, SEIDMAN CE, SEIDMAN JG. CALSEQUESTRIN 2 (CASQ2) MUTATIONS INCREASE EXPRESSION OF CALRETICULIN AND RYANODINE RECEPTORS, CAUSING

- CATECHOLAMINERGIC POLYMORPHIC VENTRICULAR TACHYCARDIA. *J CLIN INVEST*. 2007;117:1814-1823
624. RIZZI N, LIU N, NAPOLITANO C, NORI A, TURCATO F, COLOMBI B, BICCIATO S, ARCELLI D, SPEDITO A, SCELMI M, VILLANI L, ESPOSITO G, BONCOMPAGNI S, PROTASI F, VOLPE P, PRIORI SG. UNEXPECTED STRUCTURAL AND FUNCTIONAL CONSEQUENCES OF THE R33Q HOMOZYGOUS MUTATION IN CARDIAC CALSEQUESTRIN: A COMPLEX ARRHYTHMOGENIC CASCADE IN A KNOCK IN MOUSE MODEL. *CIRC RES*. 2008;103:298-306
625. TERYTYEV D, NORI A, SANTORO M, VIATCHENKO-KARPINSKI S, KUBALOVA Z, GYORKE I, TERYTYEVA R, VEDAMOORTHYRAO S, BLOM NA, VALLE G, NAPOLITANO C, WILLIAMS SC, VOLPE P, PRIORI SG, GYORKE S. ABNORMAL INTERACTIONS OF CALSEQUESTRIN WITH THE RYANODINE RECEPTOR CALCIUM RELEASE CHANNEL COMPLEX LINKED TO EXERCISE-INDUCED SUDDEN CARDIAC DEATH. *CIRC RES*. 2006;98:1151-1158
626. KORNIEYEV D, PETROSKY AD, ZEPEDA B, FERREIRO M, KNOLLMANN B, ESCOBAR AL. CALSEQUESTRIN 2 DELETION SHORTENS THE REFRACTORINESS OF CA(2)(+) RELEASE AND REDUCES RATE-DEPENDENT CA(2)(+)-ALTERNANS IN INTACT MOUSE HEARTS. *J MOL CELL CARDIOL*. 2012;52:21-31
627. MITCHELL GF, JERON A, KOREN G. MEASUREMENT OF HEART RATE AND Q-T INTERVAL IN THE CONSCIOUS MOUSE. *AM J PHYSIOL*. 1998;274:H747-751
628. PONNUSAMY A, MARQUES JL, REUBER M. COMPARISON OF HEART RATE VARIABILITY PARAMETERS DURING COMPLEX PARTIAL SEIZURES AND PSYCHOGENIC NONEPILEPTIC SEIZURES. *EPILEPSIA*. 2012;53:1314-1321
629. THIREAU J, ZHANG BL, POISSON D, BABUTY D. HEART RATE VARIABILITY IN MICE: A THEORETICAL AND PRACTICAL GUIDE. *EXPERIMENTAL PHYSIOLOGY*. 2008;93:83-94
630. WANG HM, HUANG SC. SDNN/RMSSD AS A SURROGATE FOR LF/HF: A REVISED INVESTIGATION. . *MODEL AND SIMUL ENGIN. ARTICLE ID 931943*, [HTTP://DX.DOI.ORG.GATE2.INIST.FR/10.1155/2012/931943](http://dx.doi.org/gate2.inist.fr/10.1155/2012/931943). 2012;2012
631. HAMIL OP, MARTY A, NEHER E, SAKMANN B, SIGWORTH FJ. IMPROVED PATCH-CLAMP TECHNIQUES FOR HIGH-RESOLUTION CURRENT RECORDING FROM CELLS AND CELL-FREE MEMBRANE PATCHES. *PFLUGERS ARCH*. 1981;391:85-100
632. FAGGIONI M, VAN DER WERF C, KNOLLMANN BC. SINUS NODE DYSFUNCTION IN CATECHOLAMINERGIC POLYMORPHIC VENTRICULAR TACHYCARDIA: RISK FACTOR AND POTENTIAL THERAPEUTIC TARGET? *TRENDS CARDIOVASC MED*. 2014
633. JIANG D, XIAO B, ZHANG L, CHEN SR. ENHANCED BASAL ACTIVITY OF A CARDIAC CA<sup>2+</sup> RELEASE CHANNEL (RYANODINE RECEPTOR) MUTANT ASSOCIATED WITH VENTRICULAR TACHYCARDIA AND SUDDEN DEATH. *CIRC RES*. 2002;91:218-225
634. FERNÁNDEZ-VELASCO M, RUEDA A, RIZZI N, BENITAH JP, COLOMBI B, NAPOLITANO C, PRIORI SG, RICHARD S, GÓMEZ AM. INCREASED CA<sup>2+</sup> SENSITIVITY OF THE RYANODINE RECEPTOR MUTANT RYR2R4496C UNDERLIES CATECHOLAMINERGIC POLYMORPHIC VENTRICULAR TACHYCARDIA. *CIRC RES*. 2009;104:201-209, 212P FOLLOWING 209
635. GEORGE CH, JUNDI H, THOMAS NL, SCOOTE M, WALTERS N, WILLIAMS AJ, LAI FA. RYANODINE RECEPTOR REGULATION BY INTRAMOLECULAR INTERACTION BETWEEN CYTOPLASMIC AND TRANSMEMBRANE DOMAINS. *MOL BIOL CELL*. 2004;15:2627-2638
636. IKEMOTO N, YAMAMOTO T. REGULATION OF CALCIUM RELEASE BY INTERDOMAIN INTERACTION WITHIN RYANODINE RECEPTORS. *FRONT BIOSCI*. 2002;7:D671-683
637. GOMEZ AM, RICHARD S. MUTANT CARDIAC RYANODINE RECEPTORS AND VENTRICULAR ARRHYTHMIAS: IS 'GAIN-OF-FUNCTION' OBLIGATORY? *CARDIOVASC RES*. 2004;64:3-5
638. THOMAS NL, GEORGE CH, LAI FA. FUNCTIONAL HETEROGENEITY OF RYANODINE RECEPTOR MUTATIONS ASSOCIATED WITH SUDDEN CARDIAC DEATH. *CARDIOVASC RES*. 2004;64:52-60
639. OKUDAIRA N, KUWAHARA M, HIRATA Y, OKU Y, NISHIO H. A KNOCK-IN MOUSE MODEL OF N-TERMINAL R420W MUTATION OF CARDIAC RYANODINE RECEPTOR EXHIBITS ARRHYTHMOGENESIS WITH ABNORMAL CALCIUM DYNAMICS IN CARDIOMYOCYTES. *BIOCHEM BIOPHYS RES COMMUN*. 2014;452:665-668

640. SATOH H. POSITIVE AND NEGATIVE CHRONOTROPIC EFFECTS OF CAFFEINE IN SPONTANEOUSLY BEATING RABBIT SINO-ATRIAL NODE CELLS. *GEN PHARMACOL.* 1993;24:1223-1230
641. SATOH H. CAFFEINE DEPRESSION OF SPONTANEOUS ACTIVITY IN RABBIT SINO-ATRIAL NODE CELLS. *GEN PHARMACOL.* 1993;24:555-563
642. PEREIRA L, RUIZ-HURTADO G, RUEDA A, MERCADIER JJ, BENITAH JP, GOMEZ AM. CALCIUM SIGNALING IN DIABETIC CARDIOMYOCYTES. *CELL CALCIUM.* 2014;56:372-380
643. FERNANDEZ-VELASCO M, RUIZ-HURTADO G, GOMEZ AM, RUEDA A. CA(2+) HANDLING ALTERATIONS AND VASCULAR DYSFUNCTION IN DIABETES. *CELL CALCIUM.* 2014;56:397-407



## **Anexe**

**Reconciling depressed Ca<sup>2+</sup> sparks occurrence with enhanced RyR<sub>2</sub> activity in failing mice cardiomyocytes**

# Reconciling depressed $\text{Ca}^{2+}$ sparks occurrence with enhanced RyR2 activity in failing mice cardiomyocytes

Gema Ruiz-Hurtado,<sup>1,2,3\*</sup> Linwei Li,<sup>1,2\*</sup> María Fernández-Velasco,<sup>4</sup> Angélica Rueda,<sup>5</sup> Florence Lefebvre,<sup>1,2</sup> Yueyi Wang,<sup>1,2</sup> Philippe Mateo,<sup>1,2</sup> Cécile Cassan,<sup>6</sup> Barnabas Gellen,<sup>7,8</sup> Jean Pierre Benitah,<sup>1,2</sup> and Ana María Gómez<sup>1,2</sup>

<sup>1</sup>Institut National de la Santé et de la Recherche Médicale (INSERM), UMR-S 1180, LabEx LERMIT, DHU TORINO, and <sup>2</sup>Faculté de Pharmacie, Université Paris Sud, Université Paris-Saclay, 92296 Châtenay-Malabry, France

<sup>3</sup>Instituto de Investigación, Hospital 12 de Octubre, 28041 Madrid, Spain

<sup>4</sup>Instituto de Investigación Hospital Universitario La Paz, 28046 Madrid, Spain

<sup>5</sup>Departamento de Bioquímica, Centro de Investigación y de Estudios Avanzados del IPN, 07360 México City, D.F., México

<sup>6</sup>Maladies infectieuses et vecteurs: écologie, génétique, évolution et contrôle, Institut de recherche pour le développement, 34394 Montpellier, France

<sup>7</sup>INSERM U955 and <sup>8</sup>Department of Cardiology, AP-HP, Henri Mondor Hospital, Université Paris-Est Créteil, 94010 Créteil, France

Abnormalities in cardiomyocyte  $\text{Ca}^{2+}$  handling contribute to impaired contractile function in heart failure (HF). Experiments on single ryanodine receptors (RyRs) incorporated into lipid bilayers have indicated that RyRs from failing hearts are more active than those from healthy hearts. Here, we analyzed spontaneous  $\text{Ca}^{2+}$  sparks (brief, localized increased in  $[\text{Ca}^{2+}]_i$ ) to evaluate RyR cluster activity in situ in a mouse post-myocardial infarction (PMI) model of HF. The cardiac ejection fraction of PMI mice was reduced to  $\sim 30\%$  of that of sham-operated (sham) mice, and their cardiomyocytes were hypertrophied. The  $[\text{Ca}^{2+}]_i$  transient amplitude and sarcoplasmic reticulum (SR)  $\text{Ca}^{2+}$  load were decreased in intact PMI cardiomyocytes compared with those from sham mice, and spontaneous  $\text{Ca}^{2+}$  sparks were less frequent, whereas the fractional release and the frequency of  $\text{Ca}^{2+}$  waves were both increased, suggesting higher RyR activity. In permeabilized cardiomyocytes, in which the internal solution can be controlled,  $\text{Ca}^{2+}$  sparks were more frequent in PMI cells (under conditions of similar SR  $\text{Ca}^{2+}$  load), confirming the enhanced RyR activity. However, in intact cells from PMI mice, the  $\text{Ca}^{2+}$  sparks frequency normalized by the SR  $\text{Ca}^{2+}$  load in that cell were reduced compared with those in sham mice, indicating that the cytosolic environment in intact cells contributes to the decrease in  $\text{Ca}^{2+}$  spark frequency. Indeed, using an internal “failing solution” with less ATP (as found in HF), we observed a dramatic decrease in  $\text{Ca}^{2+}$  spark frequency in permeabilized PMI and sham myocytes. In conclusion, our data show that, even if isolated RyR channels show more activity in HF, concomitant alterations in intracellular media composition and SR  $\text{Ca}^{2+}$  load may mask these effects at the  $\text{Ca}^{2+}$  spark level in intact cells. Nonetheless, in this scenario, the probability of arrhythmogenic  $\text{Ca}^{2+}$  waves is enhanced, and they play a potential role in the increase in arrhythmia events in HF patients.

## INTRODUCTION

Cardiovascular disease is the leading cause of death in the world (Dahlöf, 2010; Lloyd-Jones, 2010). Heart failure (HF) supports an important percentage of the cardiovascular diseases with serious clinical complications including cardiac arrhythmias, in many cases derived from calcium ( $\text{Ca}^{2+}$ )-handling impairment. Among others,  $\text{Ca}^{2+}$  is a key factor of electrical activation, ion channel gating, and excitation–contraction (EC) coupling in the cardiac muscle. During cardiac EC coupling,  $\text{Ca}^{2+}$  influx via sarcolemmal L-type  $\text{Ca}^{2+}$  channels triggers  $\text{Ca}^{2+}$

release from the SR by RyRs, increasing the cytosolic  $\text{Ca}^{2+}$  concentration ( $[\text{Ca}^{2+}]_i$ ), which activates myocyte contraction (Fabiato and Fabiato, 1975; Bers, 2002). Cytosolic  $[\text{Ca}^{2+}]_i$  transient results from spatial and temporal summation of elementary  $\text{Ca}^{2+}$  events named  $\text{Ca}^{2+}$  sparks (Cheng et al., 1993). This  $[\text{Ca}^{2+}]_i$  elevation is transient, because  $\text{Ca}^{2+}$  is promptly extruded to the extracellular medium by the sodium–calcium exchanger (NCX) and pumped back to the SR by the sarco-endoplasmic reticulum  $\text{Ca}^{2+}$  ATPase (SERCA), whose activity is controlled by phospholamban (PLB). Other systems participate in regaining diastolic  $[\text{Ca}^{2+}]_i$  but to a minor degree (Bers, 2002).

\*G. Ruiz-Hurtado and L. Li contributed equally to this paper.

Correspondence to Ana María Gómez: ana-maria.gomez@inserm.fr; or Gema Ruiz-Hurtado: gemaruiz@h12o.es

Abbreviations used in this paper: EC, excitation–contraction; FDHM, full duration at half-maximum; FWHM, full width at half-maximum; HF, heart failure; NCX, sodium–calcium exchanger; PLB, phospholamban; PMI, post-myocardial infarction; SERCA, sarco-endoplasmic reticulum  $\text{Ca}^{2+}$  ATPase.

© 2015 Ruiz-Hurtado et al. This article is distributed under the terms of an Attribution–Noncommercial–Share Alike–No Mirror Sites license for the first six months after the publication date (see <http://www.rupress.org/terms>). After six months it is available under a Creative Commons License (Attribution–Noncommercial–Share Alike 3.0 Unported license, as described at <http://creativecommons.org/licenses/by-nc-sa/3.0/>).

A significant decrease in the  $[Ca^{2+}]_i$  transient amplitude is a common feature observed in human and animal models of HF and contributes to depressed contractile function (Beuckelmann et al., 1992; Kubo et al., 2001; Piacentino et al., 2003). The global  $[Ca^{2+}]_i$  transient depends on several factors: the trigger L-type  $Ca^{2+}$  current ( $I_{CaL}$ ), the amount of  $Ca^{2+}$  stored in the SR, and the RyR function.  $I_{CaL}$  density has been found unaltered in human (Beuckelmann et al., 1992; Piacentino et al., 2003) and most experimental models of HF (Bénitah et al., 2002). However, a defect in the efficacy of  $I_{CaL}$  to release  $Ca^{2+}$  has been manifested as a significant reduction in the amount of  $Ca^{2+}$  sparks triggered by  $I_{CaL}$  (Gómez et al., 1997, 2001). This defect in EC coupling can be related to structural alteration of the remodeled cardiomyocyte, which effectively increases the distance between the L-type  $Ca^{2+}$  channels and RyRs, as it was first suggested (Gómez et al., 1997), and lately supported by alteration of T-tubular structure and increase in the orphaned RyRs (Wagner et al., 2012). Concomitantly, the reduction in SR  $Ca^{2+}$  load in the failing myocyte is an important determinant for the reduced amplitude of the  $[Ca^{2+}]_i$  transient amplitude in systole. This reduction has been ascribed to an impairment in the SR  $Ca^{2+}$  uptake, related to depressed SERCA function and expression in HF (Mercadier et al., 1990; Meyer et al., 1995; Gaughan et al., 1999) and increased ratio of PLB/SERCA expression and/or PLB hypophosphorylation (Reiken et al., 2003). The NCX expression has also been found to be increased in many HF models, and although its contribution to unload the SR  $Ca^{2+}$  is unclear (Bénitah et al., 2002; Gómez et al., 2002; Piacentino et al., 2003), it may participate to deplete  $Ca^{2+}$  stores. The reduction in the SR  $Ca^{2+}$  load in HF could also be caused by an increase in the  $Ca^{2+}$  leak during diastole (Fischer et al., 2013), which has been related to an increase in the RyR phosphorylation status by PKA (Marx et al., 2000; Reiken et al., 2003) or  $Ca^{2+}$ /calmodulin-dependent protein kinase II (Ai et al., 2005).

Diastolic  $Ca^{2+}$  leak occurs in several forms: as  $Ca^{2+}$  sparks,  $Ca^{2+}$  waves, or even as image-imperceptible RyR openings (Zima et al., 2010). What remains unclear today is how HF might affect  $Ca^{2+}$  spark occurrence in quiescent myocytes. If all other elements of EC coupling were unaffected, enhanced RyR activity might be viewed as an increased occurrence of spontaneous  $Ca^{2+}$  sparks. For example, the frequency of  $Ca^{2+}$  sparks is greatly enhanced in a pro-arrhythmogenic model caused by RyR point mutation (Fernández-Velasco et al., 2009). In healthy cardiomyocytes, an acute increase in RyR activity only produces transient effects: in a few twitches, the SR  $Ca^{2+}$  load is depressed so the  $[Ca^{2+}]_i$  transient returns to control values (Trafford et al., 1998). However, in HF, with numerous concomitants alterations, no consensus data have been reported regarding spontaneous  $Ca^{2+}$  spark frequency. In fact, the frequency of  $Ca^{2+}$  sparks is also dependent on the SR  $Ca^{2+}$  load (Györke and Terentyev, 2008). Thus,

even if RyRs were more active, this would decrease the SR  $Ca^{2+}$  load, depressing RyR activity, until reaching new equilibrium. Moreover, higher activity of RyRs does not exclusively mean more  $Ca^{2+}$  sparks. Some authors have reported an increase in the  $Ca^{2+}$  spark frequency in HF animal models (Belevych et al., 2011), whereas others demonstrated a significant decrease in the  $Ca^{2+}$  spark frequency of isolated cardiomyocytes from patients with terminal HF compared with non-failing individuals (Lindner et al., 2002). But the RyR activity not only depends on its phosphorylation state, but also on its environment, which can be altered in HF. For example, ATP level, which activates the RyR (Laver, 2006), is depressed in HF (Neubauer, 2007). To clarify this point, we hypothesize that the increased activity of RyRs may be masked in intact cardiomyocytes by other alterations, but might be unmasked in permeabilized myocytes where the cytosolic environment is tightly controlled by the used internal solution. Here we show, for the first time, a comparison between  $Ca^{2+}$  spark recordings in intact versus permeabilized cardiomyocytes in a mouse model of cardiac dysfunction post-myocardial infarction (PMI).

## MATERIALS AND METHODS

All experiments were performed according to the ethical principles laid down by the French Ministry of Agriculture and the European Union Council Directives (2010/63/EU) for the care of laboratory animals.

### Induction of myocardial infarction

Myocardial infarction was induced by left coronary artery ligation under anesthesia (2% isoflurane/ $O_2$ ; AErrane; Baxter) in 16 male C57BL/6J mice (9 wk of age) placed under mechanical ventilation. Left anterior descending coronary artery was visualized and ligated 1–2 mm from the top of the left atrium. A subcutaneous injection of buprenorphine (0.3 mg/ml) was administered for post-operative analgesia. Sham mice ( $n = 14$ ) were subjected to the same surgical procedure but without coronary artery ligation. 4–6 wk after surgery, cardiac contractile function was assessed by M-mode echocardiography. Only PMI hearts that showed a transmural scar greater than four (number of parts occupied by the scar from a total of six, as assessed by visual division of the left ventricle–free wall, as we did before) were used (Perrier et al., 2004).

### Echocardiography

Transthoracic echocardiography was performed using a 15-MHz transducer (Vivid 9; GE Healthcare) under 3% isoflurane gas anesthesia. Two-dimensional echocardiography was used to determine left ventricular ejection fraction using a modified version of Simpson's monoplane analysis (Milliez et al., 2009).

### Ventricular myocytes isolation

Ventricular myocytes from sham and PMI mice were isolated using an enzymatic perfusion method (Ruiz-Hurtado et al., 2007; Fernández-Velasco et al., 2011). In brief, mice pretreated with 1,000 U/kg heparin were anaesthetized with 50 mg/kg sodium pentobarbital administered intraperitoneally. Hearts were removed and placed in ice-cold oxygenated Tyrode's solution containing (in mmol/liter): 130 NaCl, 0.4  $NaH_2PO_4$ , 5.8  $NaHCO_3$ , 0.5  $MgCl_2$ , 5.4 KCl, 22 glucose, 25 HEPES, and  $10^{-3}$  insulin, pH 7.4 with NaOH. The aorta was cannulated above the aortic valve and perfused by

gravity at 37°C with preoxygenated Tyrode's solution containing 0.1 mmol/liter EGTA for 2 min. Enzyme solution with 1 g/liter collagenase Type II (Worthington Biochemical Corporation) or 5 g/liter Liberase (TM Research Grade; Roche) in Tyrode's solution supplemented with 0.1 mmol/liter CaCl<sub>2</sub> was then perfused until the aortic valve was digested, as assessed by increased efflux. Hearts were removed, cut in small pieces, and gently shaken in enzyme solution supplemented with 2 g/liter BSA for 2 min at 37°C to disperse individual myocytes. Myocytes were then filtered through a 250- $\mu$ m nylon mesh and centrifuged at 20 *g* for 2 min. A pellet containing myocytes was resuspended in Tyrode's solution supplemented with 0.5 mmol/liter CaCl<sub>2</sub> and 2 g/liter BSA, and then centrifuged again. The final pellet was resuspended in storage solution containing Tyrode's solution supplemented with 1 mmol/liter CaCl<sub>2</sub>.

#### [Ca<sup>2+</sup>]<sub>i</sub> transients and SR Ca<sup>2+</sup> load

We used 14 control mice and 16 PMI animals. Isolated ventricular myocytes were loaded with the membrane-permeant Fluo-3 AM, as described previously (Pereira et al., 2012; Ruiz-Hurtado et al., 2012b). Confocal Ca<sup>2+</sup> images were obtained by exciting the cell at 488 nm, and emission was collected at >505 nm using a laser scanning confocal microscope (LSM510; Carl Zeiss, or SP5; Leica) equipped with a 63 $\times$  N.A. 1.2 water-immersion objective in the line-scan mode. To record intracellular Ca<sup>2+</sup> ([Ca<sup>2+</sup>]<sub>i</sub>) transients, myocytes were electrically field stimulated by two Pt electrodes at 2 Hz. Before recording, Fluo-3-loaded myocytes were stimulated for 1 min to reach steady state. The fluorescence values (*F*) were normalized by the basal fluorescence (*F*<sub>0</sub>) to obtain *F*/*F*<sub>0</sub>. For SR Ca<sup>2+</sup> load estimation, intact ventricular myocytes were rapidly perfused with 10 mmol/liter caffeine just after field stimulation. The amplitude of caffeine-evoked Ca<sup>2+</sup> transients was used to assess SR

Ca<sup>2+</sup> load. Fractional SR release was measured by normalizing the steady state of the Ca<sup>2+</sup> transient (peak *F*/*F*<sub>0</sub>) by the caffeine-evoked intracellular Ca<sup>2+</sup> transient (peak *F*/*F*<sub>0</sub> evoked by 10 mmol/liter of rapid caffeine application). Post-rest potentiation was calculated by normalizing the first intracellular Ca<sup>2+</sup> transient (peak *F*/*F*<sub>0</sub>) after a period of rest from ~2 min to reach the steady-state [Ca<sup>2+</sup>]<sub>i</sub> transient (Ruiz-Hurtado et al., 2012a).

#### Ca<sup>2+</sup> spark recording

To record spontaneous Ca<sup>2+</sup> sparks and Ca<sup>2+</sup> waves in intact quiescent cells, after [Ca<sup>2+</sup>]<sub>i</sub> transient recordings, each myocyte was scanned 12 times for 1.5 s at 1.5 ms per line. Ca<sup>2+</sup> sparks were detected as localized, rapid, and brief elevations in Ca<sup>2+</sup> fluorescence. Ca<sup>2+</sup> sparks were detected using an automated detection system (homemade in IDL; Exelis Visual Information Solutions) and a criterion that limited the detection of false events while detecting most Ca<sup>2+</sup> sparks (Fernández-Velasco et al., 2009). Abnormal spontaneous Ca<sup>2+</sup> release manifested as Ca<sup>2+</sup> waves were quantified by the percentage of occurrence. Ca<sup>2+</sup> wave was identified as an increase in the Ca<sup>2+</sup> fluorescence starting locally and propagated to one or both sides of the cell (Fernández-Velasco et al., 2009).

In permeabilized myocytes, the basic control internal solution used contained (in mmol/liter): 120 K-aspartate, 10 HEPES, 3 MgATP, 0.5 EGTA, 10 Na phosphocreatine, 5 U/ml creatine phosphokinase, and 0.75 MgCl<sub>2</sub>, and 8% dextran, pH 7.2. After permeabilization with saponin (0.01% wt/vol for 60 s), this solution was supplemented with 50  $\mu$ mol/liter K<sub>5</sub>-Fluo-3 and enough CaCl<sub>2</sub> to reach 50 nmol/liter of free Ca<sup>2+</sup>, calculated with MAXCHELATOR. Ca<sup>2+</sup> sparks were recorded after a period of 1 min of stabilization in this internal solution.

In a set of experiments to mimic the pathological conditions of a failing heart, a "failing" internal solution was used, of similar

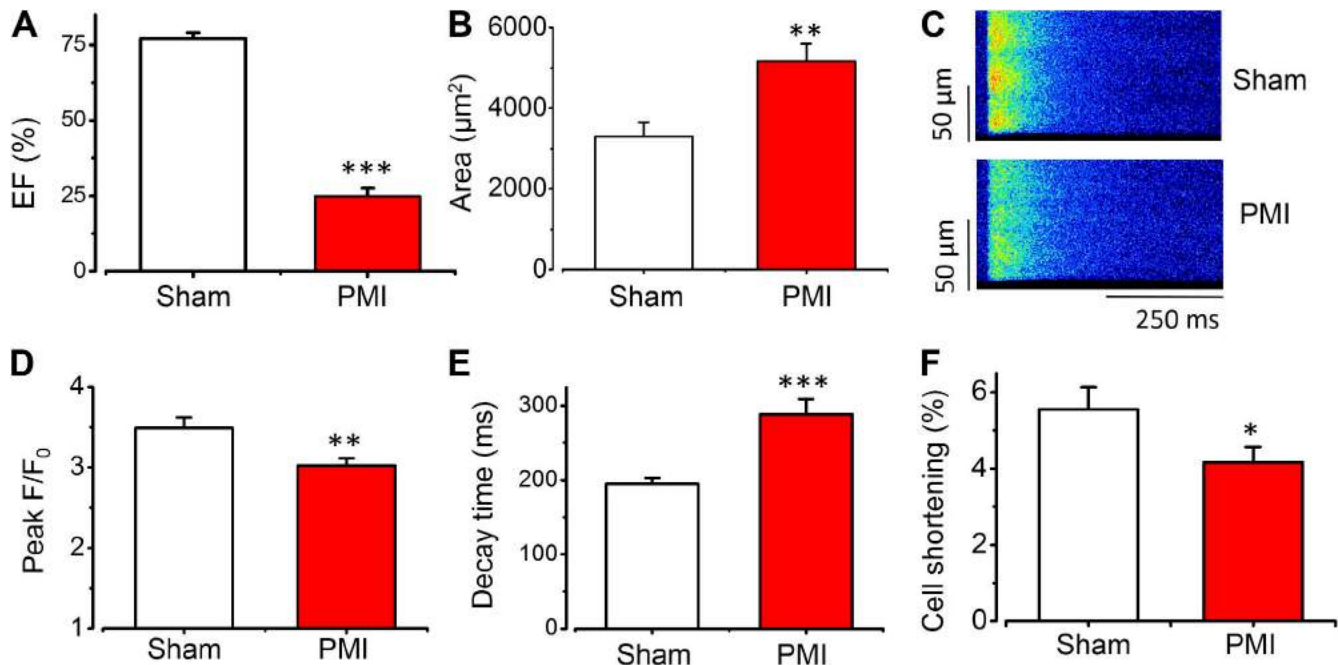


**Figure 1.** Myocardial infarction induces a decrease in [Ca<sup>2+</sup>]<sub>i</sub> transients. (A) Ejection fraction measured by echocardiography in control (white bar; *n* = 12) and coronary artery occlusion (PMI; red bar; *n* = 12)-operated mice. (B) Cardiomyocyte area expressed in square micrometers for sham (white bar; *n* = 14 cells from three animals) and PMI (red bar; *n* = 11 cells from three animals). (C) Line-scan images during field stimulation at 2 Hz of one ventricular myocyte from sham (top) or PMI (bottom) mice. (D–F) Intracellular [Ca<sup>2+</sup>]<sub>i</sub> transient peak (D), decay time (E), and cell shortening (F; 34 cells from eight sham mice and 30 cells from eight PMI mice) in ventricular myocytes. Peak expressed as maximum *F*/*F*<sub>0</sub>, where *F* is the fluorescence trace and *F*<sub>0</sub> is the fluorescence during the diastolic period. \*, *P* < 0.05; \*\*, *P* < 0.01; \*\*\*, *P* < 0.001 versus myocytes from sham mice. Error bars represent the SEM.

composition to the basic control solution, but ATP and creatine phosphokinase were reduced by half, and inorganic phosphates were added (6.5 mmol/liter  $K_2HPO_4$ ) (Ingwall, 2006, 2009). To maintain the total amount of Mg, while reducing MgATP concentrations, the amount of  $MgCl_2$  was increased to 2.25 mmol/liter.

SR  $Ca^{2+}$  load in permeabilized myocytes was estimated by rapid 20-mmol/liter caffeine application (solved in basic or failing solution) after  $Ca^{2+}$  spark recording.

#### Statistical analyses

Data are presented as means  $\pm$  SEM. Statistical significance was evaluated by Student's *t* test. For statistical comparison of occurrence,  $Ca^{2+}$  waves and triggered activity Gaussian Fisher's  $\chi^2$  test was used. Preliminary descriptive analyses included frequencies for categorical variables and mean  $\pm$  SD for continuous variables. A conditional hierarchical linear model was used (SAS/UNIX statistical software; PROC MIXED; SAS Institute) to compare continuous variables between groups to take into account the multiple observations per animal. The group was a fixed effect, and animals were a random effect nested in the group; in the case of repeated measurements on cells, we added a random effect for cells in animals.

## RESULTS

### $Ca^{2+}$ release and SR $Ca^{2+}$ load after myocardial infarction

Hearts from PMI mice showed a significant reduction in the ejection fraction, measured by echocardiography,

compared with hearts from sham mice (Fig. 1 A). Cellular hypertrophy was assessed by cardiomyocyte area measured by confocal microscopy images of isolated ventricular myocytes. Cardiomyocytes from PMI mice showed significantly higher cellular area than myocytes from sham-operated animals, indicating hypertrophy at the cellular level (Fig. 1 B). To determine whether intracellular  $Ca^{2+}$  handling was altered in hypertrophied myocytes from PMI mice, we analyzed  $[Ca^{2+}]_i$  transients. Fig. 1 C shows representative line-scan images of evoked  $[Ca^{2+}]_i$  transients from sham (top) and PMI (bottom) cardiomyocytes. The  $[Ca^{2+}]_i$  transients recorded in PMI myocytes were smaller in amplitude than those recorded in control myocytes. The average amplitude of  $[Ca^{2+}]_i$  transients showed a significant reduction in myocytes from PMI mice compared with myocytes from sham-operated mice (Fig. 1 D).  $[Ca^{2+}]_i$  transient decay time (Fig. 1 E) was significantly prolonged in myocytes from PMI mice compared with those from sham-operated mice, suggesting slower  $Ca^{2+}$  uptake by the SERCA pump. Cellular shortening was also significantly decreased in myocytes from PMI mice (Fig. 1 F). Because SR  $Ca^{2+}$  load is determinant in  $[Ca^{2+}]_i$  transient amplitude, we measured SR  $Ca^{2+}$  content by rapid caffeine application, as

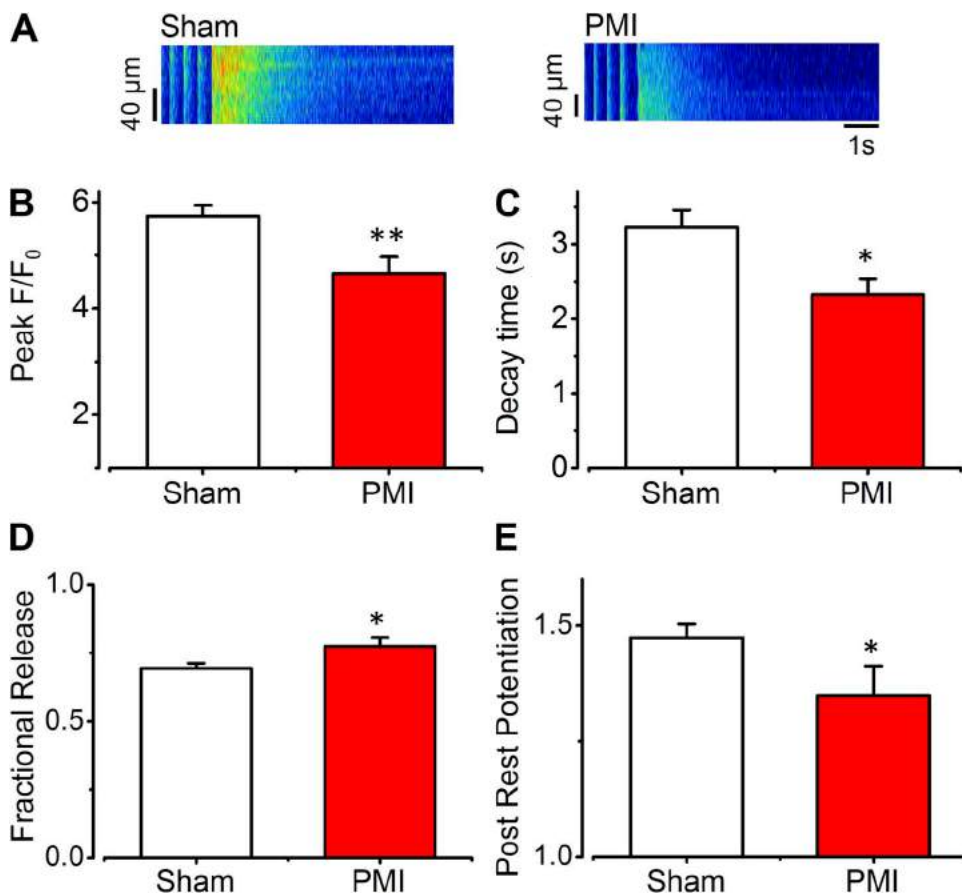


**Figure 2.** Myocardial infarction induces a decrease in SR  $Ca^{2+}$  load. (A) Line-scan images of caffeine-evoked intracellular  $Ca^{2+}$  transients after field stimulation at 2 Hz in one ventricular myocyte from sham (left) or PMI (right) mice obtained by the application of 10 mmol/liter caffeine. (B) Averaged caffeine-evoked  $Ca^{2+}$  transient peak ( $F/F_0$ ) of myocytes from sham (white bar;  $n = 43$  cells from six animals) and PMI (red bar;  $n = 21$  cells from five animals) mice. (C) Averaged decay time constant of the caffeine-evoked  $Ca^{2+}$  transient (34 cells from six sham animals; 13 cells from five PMI animals). (D) Fractional SR  $Ca^{2+}$  release during field stimulation at 2 Hz in control myocytes (white bar;  $n = 36$  cells from three animals) and in cells from PMI mice (red bar;  $n = 20$  cells from three animals). (E) Post-rest potentiation (white bar;  $n = 36$  cells from three animals) and in cells from PMI mice (red bar;  $n = 20$  cells from three animals). Error bars represent the SEM. \*,  $P < 0.05$ ; \*\*,  $P < 0.001$  PMI versus sham.



exemplified in Fig. 2 for one sham myocyte (left) and one hypertrophied myocyte from PMI mouse (right). The averaged caffeine-evoked  $[Ca^{2+}]_i$  transients were smaller in PMI myocytes compared with sham myocytes (Fig. 2 B). Thus, the decrease in  $[Ca^{2+}]_i$  transient amplitude might be related, at least in part, to the decrease in SR  $Ca^{2+}$  load. Caffeine-evoked  $[Ca^{2+}]_i$  transient decay was significantly accelerated in myocytes from PMI mice (Fig. 2 C), suggesting faster  $Ca^{2+}$  extrusion through the NCX. We also estimated the fractional release in electrically evoked beats by normalizing  $[Ca^{2+}]_i$  transient amplitude by the SR  $Ca^{2+}$  load (see Materials and methods). We observed that myocytes from PMI mice showed increased fractional release compared with sham myocytes (Fig. 2 D), suggesting higher RyR activity, even if the  $[Ca^{2+}]_i$  transient is depressed. However, the capacity of the SR to accumulate  $Ca^{2+}$  during rest, as estimated by the post-rest potentiation, was decreased in PMI cardiomyocytes (Fig. 2 E).

**Opposite effect in spark-mediated  $Ca^{2+}$  leak in intact versus permeabilized myocytes after myocardial infarction**  
The increase in fractional release may reflect a higher sensitivity of RyRs to  $Ca^{2+}$  in PMI mice. The opening of a RyR cluster induces rapid, local, and brief  $[Ca^{2+}]_i$  elevation

known as  $Ca^{2+}$  spark (Cheng et al., 1993). We therefore recorded  $Ca^{2+}$  sparks in quiescent cells, as exemplified in Fig. 3 A in cardiac myocytes from sham (left) and PMI mice (right). Surprisingly, contrary to the supposed increased activity of RyR based on the fractional release data (Fig. 2 D), cardiomyocytes from PMI hearts showed a significant decrease in  $Ca^{2+}$  spark frequency (Fig. 3 A, bottom).

However, single-channel data have shown higher activity of RyR in failing hearts (Marx et al., 2000), so an increase in  $Ca^{2+}$  sparks was expected. To resolve this discrepancy, we analyzed  $Ca^{2+}$  sparks in permeabilized myocytes (Pereira et al., 2006). Under these conditions, sarcolemmal fluxes (NCX,  $I_{CaL}$ ) are invalidated. Moreover, this maneuver allows us to analyze  $Ca^{2+}$  sparks in the same cytoplasmic environment for both cell types (same ATP,  $Ca^{2+}$ , Mg concentration). Fig. 3 B illustrates  $Ca^{2+}$  spark occurrence in myocytes from the sham mouse (left) and PMI mouse (right). After permeabilization, myocytes from PMI mice did exhibit significantly higher  $Ca^{2+}$  spark frequency than control myocytes (Fig. 3 B, bottom).

To assess biophysical characteristics of  $Ca^{2+}$  sparks, we analyzed their amplitude (measured as the peak  $F/F_0$ ), full duration at half-maximum (FDHM), and full width

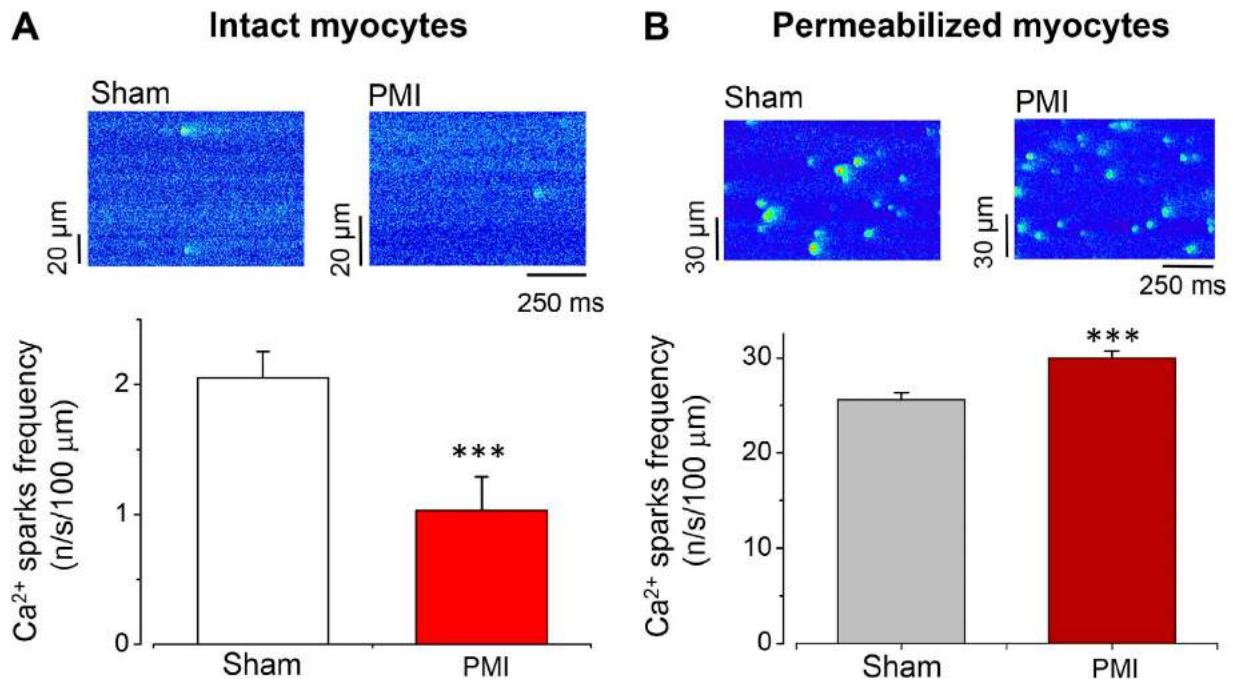


**Figure 3.**  $Ca^{2+}$  spark frequency in intact versus permeabilized myocytes after myocardial infarction. (A; top) Line-scan images obtained in intact myocytes from sham (left) or from PMI (right) mice. (Bottom) Bar graph showing the  $Ca^{2+}$  spark frequency in intact cells from sham ( $n = 59$  from five animals) and PMI mice ( $n = 41$  from seven animals). (B; top) Line-scan images obtained in permeabilized at 50 nmol/liter  $[Ca^{2+}]_i$  myocytes from sham (left) or from PMI (right) mice. (Bottom) Bar graph showing the increased  $Ca^{2+}$  spark frequency in permeabilized cells from PMI mice ( $n = 27$  cells from three animals) compared with myocytes from sham mice ( $n = 26$  cells from three animals). \*\*\*,  $P < 0.001$  versus myocytes from sham mice. Error bars represent the SEM.

at half-maximum (FWHM) in intact and permeabilized myocytes from sham and PMI mice. Fig. 4 A shows that  $\text{Ca}^{2+}$  spark amplitudes were smaller in intact PMI myocytes than in intact sham myocytes. Duration was also considerably reduced in intact PMI myocytes (Fig. 4 B), whereas no significant change was observed with respect to half-width (Fig. 4 C). A similar trend was observed in  $\text{Ca}^{2+}$  spark characteristics in permeabilized cardiomyocytes (Fig. 4, D–F), suggesting that alteration in the intrinsic RyR cluster activity or structural organization is behind alterations of  $\text{Ca}^{2+}$  spark characteristics in HF.

#### RyR environment in intact cells reduces probability of $\text{Ca}^{2+}$ sparks

To investigate the discrepancy between  $\text{Ca}^{2+}$  spark occurrence in intact versus permeabilized PMI myocytes, we addressed two possible mechanisms. It is well known that the amount of  $\text{Ca}^{2+}$  stored in the SR influences  $\text{Ca}^{2+}$  spark frequency (Györke and Terentyev, 2008). We found that the SR  $\text{Ca}^{2+}$  load is significantly reduced in intact PMI cells (Fig. 2). However, as shown in Fig. 5 A, in permeabilized myocytes, the SR load was not significantly different ( $P = 0.08$ ) between myocytes isolated from sham or PMI mice, suggesting that the SR  $\text{Ca}^{2+}$  load depletion

contributes to depression of  $\text{Ca}^{2+}$  spark rate in intact PMI cells. In fact, normalizing in each cell the  $\text{Ca}^{2+}$  spark occurrence by the amount of  $\text{Ca}^{2+}$  stored in the SR, we found in permeabilized myocytes that the frequency of  $\text{Ca}^{2+}$  spark by a given amount of  $\text{Ca}^{2+}$  stored in the SR is significantly higher in PMI than in sham myocytes (Fig. 5 B), whereas similar analysis in intact cells showed that the  $\text{Ca}^{2+}$  spark frequency remains decreased in PMI intact myocytes, even after normalizing it to the SR load (Fig. 5 C). This suggested that even if the SR  $\text{Ca}^{2+}$  load decrease may participate in the reduced  $\text{Ca}^{2+}$  spark occurrence, other mechanisms might also contribute. As ATP modifies RyR function (Meissner et al., 1986; Laver, 2010; Tencerová et al., 2012), and its levels are known to be decreased in HF (Ingwall, 2006, 2009), we repeated the  $\text{Ca}^{2+}$  spark measurements in permeabilized cardiomyocytes first with control intracellular media and then with a decreased energetic source media, which mimicked failing status (see Materials and methods). Fig. 6 A shows examples of the same cells from sham (left) and PMI heart (right) in control (top) and “failing” (bottom) solutions, illustrating that  $\text{Ca}^{2+}$  sparks were reduced in failing solution. On average (Fig. 6 B), the modified internal solution to mimic HF environment significantly reduced  $\text{Ca}^{2+}$  spark frequency in both sham and

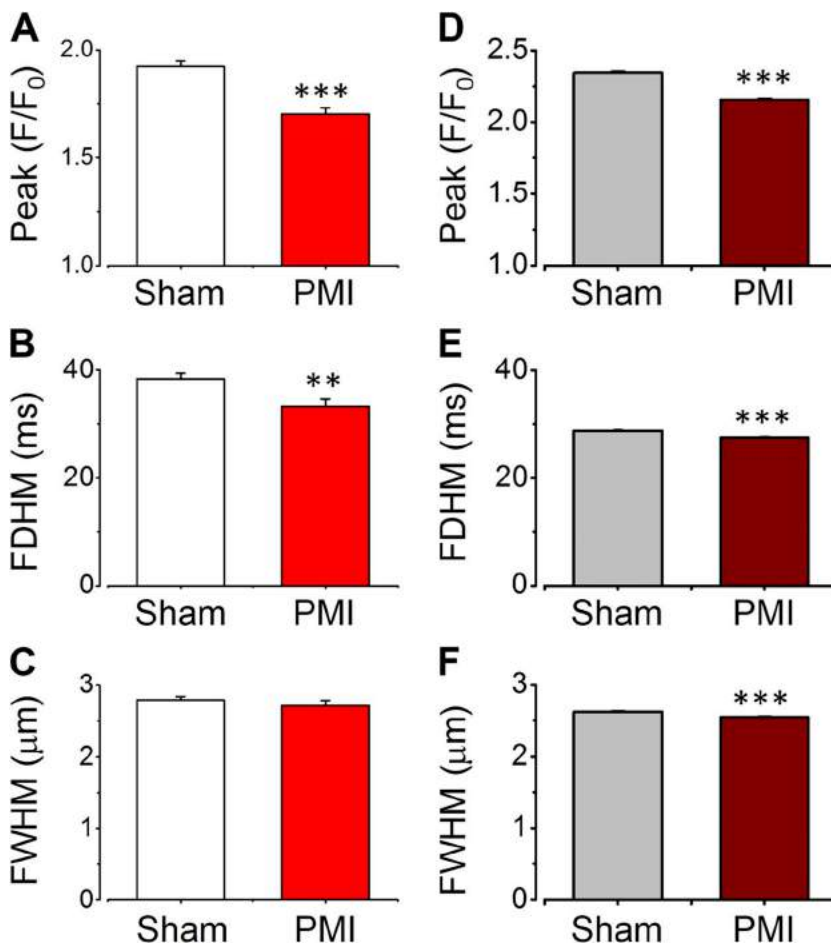


**Figure 4.** Difference in the  $\text{Ca}^{2+}$  spark characteristics between intact versus permeabilized myocytes after myocardial infarction. (A–C)  $\text{Ca}^{2+}$  spark amplitude (A; peak  $F/F_0$ ), duration at half-peak amplitude (B; FDHM), and width at half-peak amplitude (C; FWHM) in intact myocytes from sham ( $n = 442$   $\text{Ca}^{2+}$  sparks, from 22 cells, from three hearts) and PMI mice ( $n = 160$   $\text{Ca}^{2+}$  sparks, from 24 cells, from three hearts). (D–F) Same as A–C but in permeabilized myocytes from sham ( $n = 7,806$   $\text{Ca}^{2+}$  sparks, from 26 cells, from three hearts) and PMI ( $n = 9,783$   $\text{Ca}^{2+}$  sparks, from 27 cells, from three hearts) mice. \*\*,  $P < 0.01$ ; \*\*\*,  $P < 0.001$  versus myocytes from sham mice. Error bars represent the SEM.

PMI myocytes. In this condition, the SR  $\text{Ca}^{2+}$  load was unchanged between permeabilized cells from sham and PMI heart (Fig. 6 B). In addition, biophysical characteristics of  $\text{Ca}^{2+}$  sparks, namely amplitude (Fig. 6 C), duration (Fig. 6 D), and spatial spread (Fig. 6 E), remained reduced in PMI cells compared with sham cells in the failing solution.

#### $\text{Ca}^{2+}$ waves and triggered activity after myocardial infarction

To determine whether the depressed  $\text{Ca}^{2+}$  spark occurrence in intact cells may be protective of the cells from arrhythmia, we checked for  $\text{Ca}^{2+}$  waves and triggered activity during the rest period after one stimulation train (at 2 Hz) in the absence or presence of  $\beta$ -adrenergic stimulation (1  $\mu\text{mol/liter}$  isoproterenol). Fig. 7 A shows that the occurrence of  $\text{Ca}^{2+}$  waves was significantly higher in myocytes from PMI mice compared with those from sham-operated mice during the diastolic period. Moreover, myocytes from PMI showed a higher occurrence

of triggered activity than myocytes from sham mice, and this effect was enhanced by  $\beta$ -adrenergic stimulation (Fig. 7 B).

## DISCUSSION

In this paper, we have analyzed  $\text{Ca}^{2+}$  sparks in a mouse model of HF after myocardial infarction and demonstrated that even if RyRs showed signs of enhanced activity,  $\text{Ca}^{2+}$  sparks in intact cardiomyocytes were less frequent in PMI myocytes, although more  $\text{Ca}^{2+}$  waves were formed. Cell permeabilization unmasked the defect, unveiling enhanced  $\text{Ca}^{2+}$  spark occurrence in failing cardiomyocytes. The alterations in the SR  $\text{Ca}^{2+}$  load and cytosolic environment contributed to the depression in  $\text{Ca}^{2+}$  spark occurrence in intact myocytes from HF mice.

In the model we used herein, the hearts presented big transmural infarctions, ventricular myocytes were hypertrophied, and echocardiography measurements showed a depressed contractile function of the heart

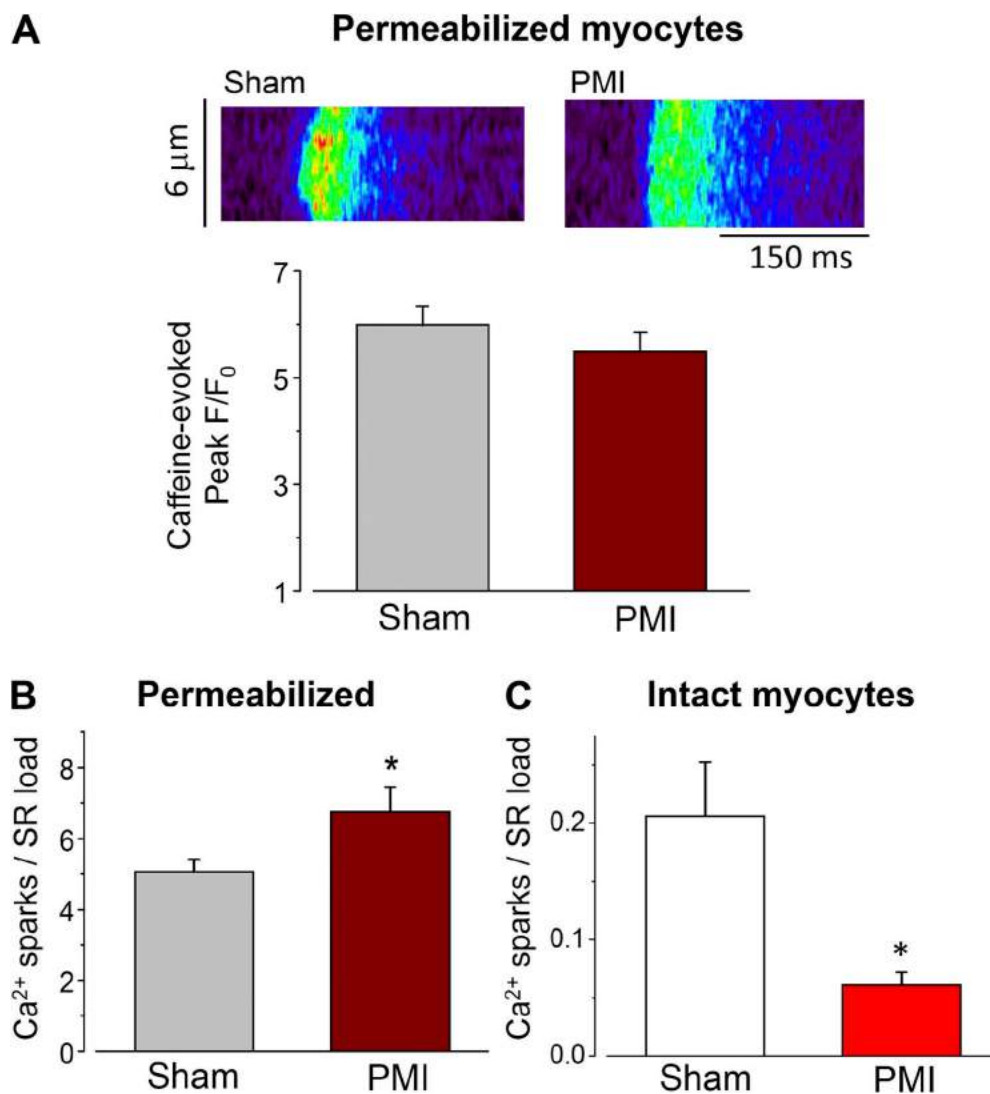


**Figure 5.** Permeabilized myocytes from PMIs show similar  $\text{Ca}^{2+}$  load but higher  $\text{Ca}^{2+}$  sparks per load unit than sham cells. (A; top) Line-scan images of representative caffeine-evoked  $\text{Ca}^{2+}$  release in permeabilized myocytes from sham (left) or from PMI (right) mice. (Bottom) Caffeine-evoked  $\text{Ca}^{2+}$  transient peak ( $F/F_0$ ) of permeabilized myocytes from sham (gray bar;  $n = 14$  cells from three animals) and PMI (dark red bar;  $n = 15$  cells from three animals) mice. (B)  $\text{Ca}^{2+}$  spark frequency normalized to SR load in permeabilized cells from sham (gray bar;  $n = 13$  from three animals) and PMI mice (dark red bar;  $n = 12$  cells from three animals). (C)  $\text{Ca}^{2+}$  spark frequency normalized to SR load in intact cells from sham (white bar;  $n = 10$  from four animals) and PMI mice (red bar;  $n = 9$  cells from four animals). \*,  $P < 0.05$  versus myocytes from sham mice. Error bars represent the SEM.



(Fig. 1). At the cellular level, the amplitude of the  $[Ca^{2+}]_i$  transient was reduced, and the decay time prolonged, in agreement with decreased SR  $Ca^{2+}$  load (Fig. 2). Interestingly, spontaneous  $Ca^{2+}$  sparks recorded during rest period were less frequent in PMI than in control cells (Fig. 3), which is consistent with the depressed SR  $Ca^{2+}$  load but inconsistent with the reported higher RyR2 activity (Marx et al., 2000).

Since the first report on  $Ca^{2+}$  sparks in an animal model of HF (Gómez et al., 1997), conflicting results have been reported regarding the  $Ca^{2+}$  sparks. Although the first study found a decrease in evoked  $Ca^{2+}$  sparks in two rat HF models (Gómez et al., 1997), a later one showed an increase (Shorofsky et al., 1999). However, the latter study concerned a model of compensated cardiac hypertrophy,

where the cardiac function was normal, thus without signs of HF. The confounding results regarding the occurrence on  $Ca^{2+}$  sparks was further complicated by the observation that single RyR channel activity, measured in isolated RyR incorporated into lipid bilayers, showed higher activity in failing hearts (Marx et al., 2000).  $Ca^{2+}$  sparks are described as the elementary events of SR  $Ca^{2+}$  release through RyRs, which can be visualized using appropriated techniques. Thus, an increase in RyR activity by either PKA (Marx et al., 2000) or calmodulin-dependent protein kinase II (Ai et al., 2005) phosphorylation, FKBP12.6 down-regulation (Marx et al., 2000), or RyR oxidation (Terentyev et al., 2008), among others, should be translated into a higher than normal  $Ca^{2+}$  spark frequency. In our experiments, we did not find increased,

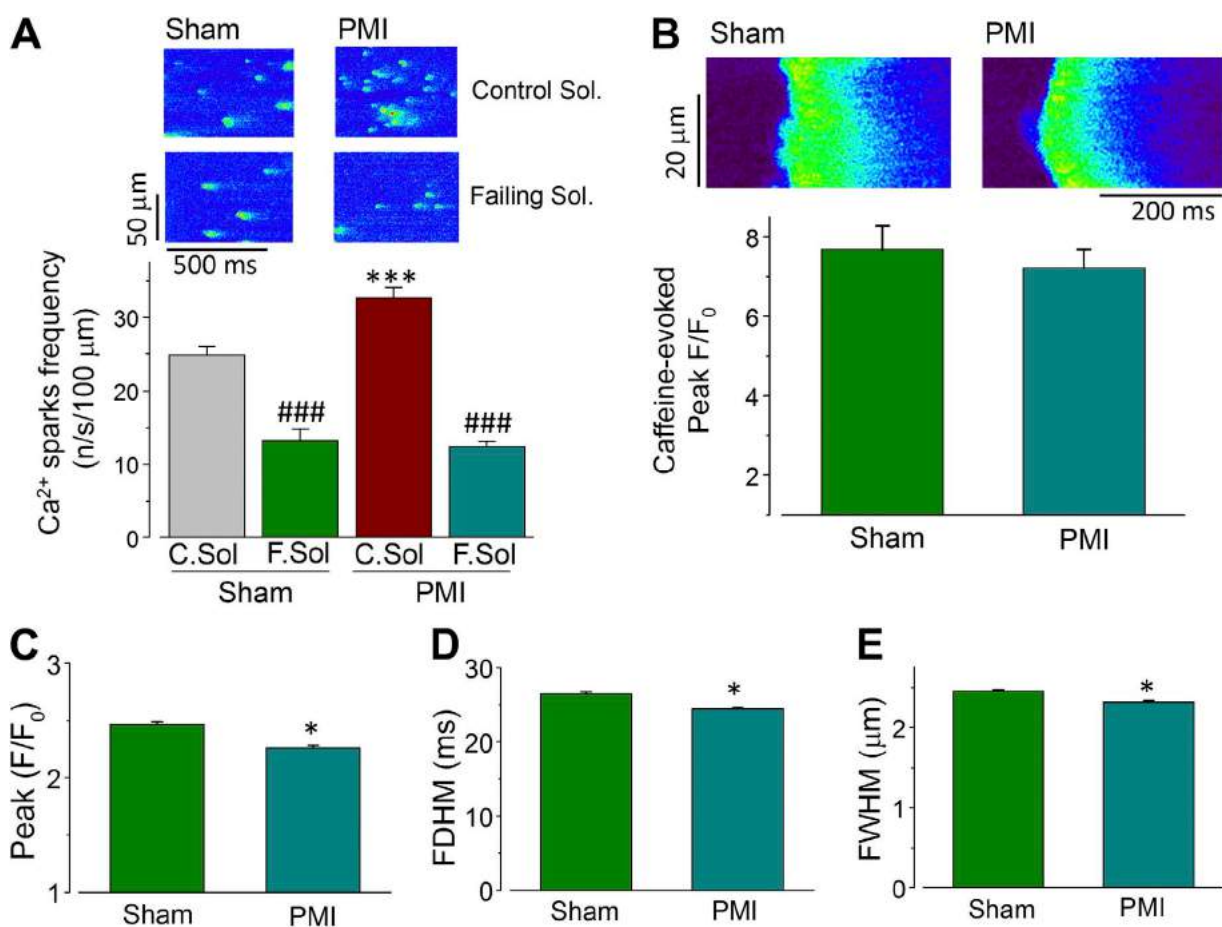


**Figure 6.** RyR metabolic environment influences  $Ca^{2+}$  spark release in PMI mice. (A; top) Representative line-scan images of  $Ca^{2+}$  sparks obtained in permeabilized myocytes from sham (left) or from PMI (right) mice, with the same cell first in control (C.Sol.; top) and then “failing” (F.Sol.; bottom) solutions. (Bottom) Bar graph showing the average data of  $Ca^{2+}$  spark frequency in permeabilized cells from sham ( $n = 6$ ) and PMI mice ( $n = 8$ ) in control (Ct.Sol.; gray and dark red bars for sham and PMI, respectively) and failing solutions (F.Sol.; dark green for sham and dark cyan bar for PMI). (B; top) Line-scan examples of caffeine-evoked  $Ca^{2+}$  release in permeabilized myocytes in failing solution from sham (left) or from PMI (right) mice. (Bottom) Averaged caffeine-evoked  $Ca^{2+}$  transient peak ( $F/F_0$ ) of permeabilized myocytes from sham (dark green bar;  $n = 6$  cells from two animals) and PMI (blue bar;  $n = 8$  cells from two animals) mice. (C–E)  $Ca^{2+}$  spark characteristics,  $Ca^{2+}$  spark amplitude (peak  $F/F_0$ ; C),  $Ca^{2+}$  spark duration at half-peak amplitude (FDHM; D), and  $Ca^{2+}$  spark width at half-peak amplitude (FWHM; E) of permeabilized myocytes from sham (dark green bar;  $n = 1,263$   $Ca^{2+}$  sparks, from six cells, from two hearts) and PMI (dark cyan bar;  $n = 1,391$  sparks, from eight cells, from two hearts) mice in failing solutions. \*,  $P < 0.05$  versus myocytes from sham mice; \*\*\*,  $P < 0.001$  versus Sham cells in control solution; ###,  $P < 0.001$  versus the same group of myocytes in control solution. Error bars represent the SEM.

but rather decreased,  $\text{Ca}^{2+}$  spark frequency, which is consistent with the depression in SR  $\text{Ca}^{2+}$  content (Fig. 2). In fact,  $\text{Ca}^{2+}$  spark frequency is highly dependent on  $\text{Ca}^{2+}$  content in the SR (Zima et al., 2010). However, our data did show hints indicating that the RyR is more active in HF cardiomyocytes. In fact, in Fig. 7 we evidenced an enhanced diastolic leak in the form of  $\text{Ca}^{2+}$  waves in PMI myocytes. This indicates a higher propensity for  $\text{Ca}^{2+}$  released in a RyR cluster to activate neighboring clusters and propagate throughout the cell in arrhythmogenic  $\text{Ca}^{2+}$  waves. Thus, diastolic  $\text{Ca}^{2+}$  release is higher in PMI cells, although  $\text{Ca}^{2+}$  sparks are not. Moreover, the fractional release (calculated as the amount of  $\text{Ca}^{2+}$  released in each twitch normalized to the amount of  $\text{Ca}^{2+}$  stored

in the SR) is significantly higher in PMI cells, indicating favored  $\text{Ca}^{2+}$  release when triggered. Cells from small rodents such as mice accumulate  $\text{Ca}^{2+}$  inside the SR during resting periods, which depend, among others factors, on the balance between  $\text{Ca}^{2+}$  leak and SERCA activity. We have measured this property as post-rest potentiation, a measurement of the enhancement of the  $[\text{Ca}^{2+}]_i$  transient amplitude after a rest period compared with the average  $[\text{Ca}^{2+}]_i$  transient amplitude in steady state during continued electrical stimulation. We found that the post-rest potentiation is less important in PMI cardiomyocytes, suggesting that the  $\text{Ca}^{2+}$  leak during rest may be more important. This is not incompatible with the decreased frequency of  $\text{Ca}^{2+}$  sparks in intact PMI

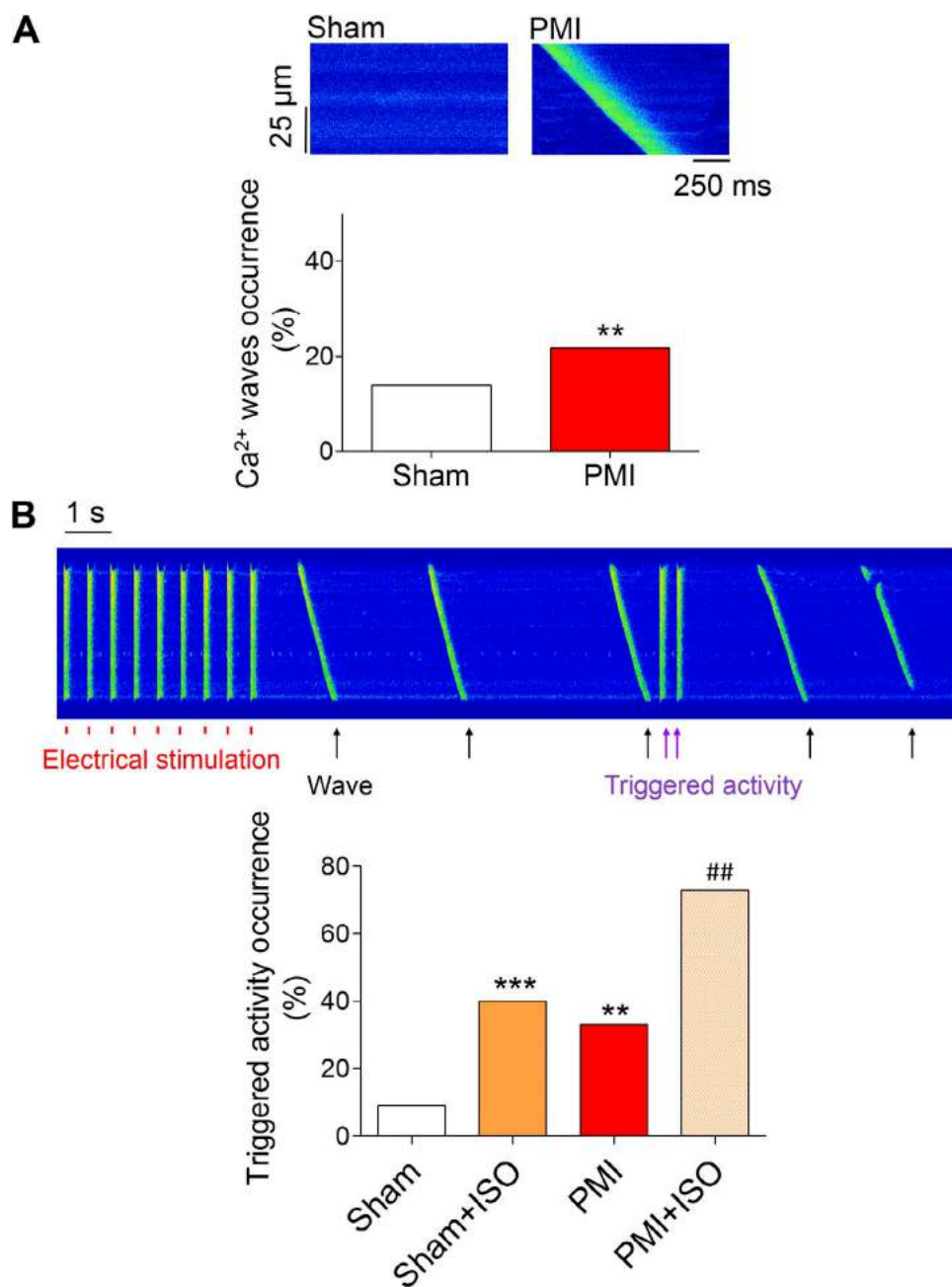


**Figure 7.** Myocardial infarction induces pro-arrhythmogenic  $\text{Ca}^{2+}$  release. (A; top) Line-scan images of representative spontaneous  $\text{Ca}^{2+}$  wave release during diastole (top) in one ventricular myocyte from sham (left) or PMI (right) mice. (Bottom) Occurrence of  $\text{Ca}^{2+}$  waves expressed as percentage (bottom) in cells from sham mice (white bar;  $n = 22$ ) and in cells from PMI mice (red bar;  $n = 24$ ). (B; top) Line-scan image of one ventricular myocyte isolated from PMI mice during electric stimulation at 2 Hz and during isoproterenol application. Red lines indicate electrical stimulation, and violet arrows indicate spontaneous triggered activity during diastole. (Bottom) Occurrence of abnormal triggered activity in myocytes from sham (white bar;  $n = 10$ ) or PMI (red bar;  $n = 13$ ) mice, and in myocytes from sham or PMI mice in the presence of 1  $\mu\text{mol/liter}$  isoproterenol (orange bar for sham,  $n = 10$ ; cross-hatched orange bar for PMI,  $n = 13$ ).  $n = 3$  hearts per group. \*\*,  $P < 0.01$ ; \*\*\*,  $P < 0.001$  versus myocytes from sham mice; ##,  $P < 0.01$  versus myocytes from PMI mice.

cardiomyocytes. In fact, although  $\text{Ca}^{2+}$  sparks were first described as the elementary event of  $\text{Ca}^{2+}$  release through RyRs, nonspark  $\text{Ca}^{2+}$  release can happen through RyRs (Lipp and Niggli, 1996; Zima et al., 2010), and the dependency of this release on the SR  $\text{Ca}^{2+}$  load is less steep than that of  $\text{Ca}^{2+}$  sparks (Lipp and Niggli, 1996). Moreover, PMI cells showed more diastolic  $\text{Ca}^{2+}$  release measured as  $\text{Ca}^{2+}$  waves (Fig. 7). Because HF is a complex process, where other  $\text{Ca}^{2+}$ -handling proteins show altered expression or function, and also the cytosolic environment around the RyR may be altered, an enhanced RyR activity may not be visualized as an elevated occurrence of  $\text{Ca}^{2+}$  sparks. This is extremely important regarding the amount of  $\text{Ca}^{2+}$  stored in the SR, as the RyR is also sensitive to luminal  $\text{Ca}^{2+}$  and below a certain threshold,  $\text{Ca}^{2+}$  sparks are shut down (Zima et al., 2010). Thus, in the setting of decreased SR  $\text{Ca}^{2+}$  load or depressed levels of ATP, as in HF, spontaneous  $\text{Ca}^{2+}$  sparks can be depressed. In permeabilized myocytes, we avoid this by controlling the intracellular solution. Using this maneuver, we unmasked the enhanced RyR activity in PMI myocytes, showing a marked increase in the  $\text{Ca}^{2+}$  spark frequency (Fig. 3). Under these conditions, the SR  $\text{Ca}^{2+}$  load was not significantly different from sham and PMI cells (Fig. 5 A), indicating that SR  $\text{Ca}^{2+}$  depletion in HF contributes to the depressed  $\text{Ca}^{2+}$  spark occurrence in PMI mice cardiomyocytes, but this may not be a unique mechanism. In fact, HF is a highly compromised metabolic state where substances that influence RyR activity, like ATP concentration, are altered (Meissner et al., 1986; Ingwall, 2006, 2009; Laver, 2010; Tencerová et al., 2012). In fact, in a subset of experiments, we tested the effect on  $\text{Ca}^{2+}$  sparks of a metabolically altered intracellular solution (similar to what could be found in HF; see Materials and methods) in the same cardiomyocyte by perfusing first with the basic control solution and then with the failing solution (Fig. 6 A). The results unequivocally show that the “failing” solution drastically reduces  $\text{Ca}^{2+}$  spark occurrence, even in the cells isolated from PMI mice, where the  $\text{Ca}^{2+}$  spark frequency was enhanced, demonstrating that the intracellular environment around the RyR can contribute to mask the otherwise enhanced  $\text{Ca}^{2+}$  spark frequency. Moreover, the effects of luminal  $\text{Ca}^{2+}$  on RyR modulation by ATP are synergistic (Tencerová et al., 2012). But once the  $\text{Ca}^{2+}$  spark happens (stochastically and/or under  $\beta$ -adrenergic stimulation, which also increases SR load), the probability of this  $\text{Ca}^{2+}$  spark initiating a  $\text{Ca}^{2+}$  wave is higher in PMI cells, likely because of RyR hyperactivity and SERCA depression. The differences in  $\text{Ca}^{2+}$  spark properties between sham and PMI cells were maintained in every condition tested, suggesting alterations in the RyR gating and/or rearrangement of clusters.

Thus, our data show that although the RyR is more active and may induce more leak in HF, this may occur preferably in nonspark form. However, the enhanced

sensitivity to  $\text{Ca}^{2+}$  of the RyR in HF may favor propagation of  $\text{Ca}^{2+}$  sparks into  $\text{Ca}^{2+}$  waves, which contrary to  $\text{Ca}^{2+}$  sparks, are arrhythmogenic by activating NCX current.

We are grateful to the ANIMEX platform for animal care, Renée Ventura-Clapier for discussions about intracellular metabolic alterations in HF, and Françoise Boussac for secretarial assistance.

This study was supported by grants from Agence Nationale de la Recherche (ANR-13-BSV1-0023-01), Fondation pour la Recherche Medicale (program cardiovasculaire 2011), Fundación Mutua Madrileña and Fundación Eugenio Rodríguez Pascual (to G. Ruiz-Hurtado). G. Ruiz-Hurtado was funded by a Servier contract and by the Ministerio de Economía y Competitividad in the Juan de la Cierva postdoctoral program from Spain.

The authors declare no competing financial interests.

Author contributions: G. Ruiz-Hurtado and L. Li did most of the collection, analysis, and interpretation of data. A. Rueda, M. Fernández-Velasco and Y.Y. Wang participated in collection, analysis, and interpretation. C. Cassan, B. Gellen, and F. Lefebvre performed the animal surgery. C. Cassan and P. Mateo recorded and analyzed echocardiograms. J.-P. Benitah and A.M. Gomez did the conception, design of the experiments, and some analyses. G. Ruiz-Hurtado and A.M. Gomez did the first drafting of the article, and all other authors revised it critically for important intellectual content. All authors approved the final version of the manuscript. All persons designated as authors qualify for authorship, and all those who qualify for authorship are listed.

Eduardo Rios served as editor.

Submitted: 18 January 2015

Accepted: 19 August 2015

## REFERENCES

- Ai, X., J.W. Curran, T.R. Shannon, D.M. Bers, and S.M. Pogwizd. 2005.  $\text{Ca}^{2+}$ /calmodulin-dependent protein kinase modulates cardiac ryanodine receptor phosphorylation and sarcoplasmic reticulum  $\text{Ca}^{2+}$  leak in heart failure. *Circ. Res.* 97:1314–1322. <http://dx.doi.org/10.1161/01.RES.0000194329.41863.89>
- Belevych, A.E., D. Terentyev, R. Terentyeva, Y. Nishijima, A. Sridhar, R.L. Hamlin, C.A. Carnes, and S. Györke. 2011. The relationship between arrhythmogenesis and impaired contractility in heart failure: role of altered ryanodine receptor function. *Cardiovasc. Res.* 90:493–502. <http://dx.doi.org/10.1093/cvr/cvr025>
- Bénitah, J.P., B.G. Kerfant, G. Vassort, S. Richard, and A.M. Gómez. 2002. Altered communication between L-type calcium channels and ryanodine receptors in heart failure. *Front. Biosci.* 7:e263–e275. <http://dx.doi.org/10.2741/benitah>
- Bers, D.M. 2002. Cardiac excitation-contraction coupling. *Nature.* 415:198–205. <http://dx.doi.org/10.1038/415198a>
- Beuckelmann, D.J., M. Näbauer, and E. Erdmann. 1992. Intracellular calcium handling in isolated ventricular myocytes from patients with terminal heart failure. *Circulation.* 85:1046–1055. <http://dx.doi.org/10.1161/01.CIR.85.3.1046>
- Cheng, H., W.J. Lederer, and M.B. Cannell. 1993. Calcium sparks: elementary events underlying excitation-contraction coupling in heart muscle. *Science.* 262:740–744. <http://dx.doi.org/10.1126/science.8235594>
- Dahlöf, B. 2010. Cardiovascular disease risk factors: Epidemiology and risk assessment. *Am. J. Cardiol.* 105:3A–9A. <http://dx.doi.org/10.1016/j.amjcard.2009.10.007>
- Fabiato, A., and F. Fabiato. 1975. Contractions induced by a calcium-triggered release of calcium from the sarcoplasmic reticulum of single skinned cardiac cells. *J. Physiol.* 249:469–495. <http://dx.doi.org/10.1113/jphysiol.1975.sp011026>



- Fernández-Velasco, M., A. Rueda, N. Rizzi, J.P. Benitah, B. Colombi, C. Napolitano, S.G. Priori, S. Richard, and A.M. Gómez. 2009. Increased  $\text{Ca}^{2+}$  sensitivity of the ryanodine receptor mutant RyR2R4496C underlies catecholaminergic polymorphic ventricular tachycardia. *Circ. Res.* 104:201–209. <http://dx.doi.org/10.1161/CIRCRESAHA.108.177493>
- Fernández-Velasco, M., G. Ruiz-Hurtado, A. Rueda, P. Neco, M. Mercado-Morales, C. Delgado, C. Napolitano, S.G. Priori, S. Richard, A.M. Gómez, and J.P. Benitah. 2011. RyR $\text{Ca}^{2+}$  leak limits cardiac  $\text{Ca}^{2+}$  window current overcoming the tonic effect of calmodulin mice. *PLoS ONE*. 6:e20863. <http://dx.doi.org/10.1371/journal.pone.0020863>
- Fischer, T.H., J. Herting, T. Tirilomis, A. Renner, S. Neef, K. Toischer, D. Ellenberger, A. Förster, J.D. Schmitto, J. Gummert, et al. 2013.  $\text{Ca}^{2+}$ /calmodulin-dependent protein kinase II and protein kinase A differentially regulate sarcoplasmic reticulum  $\text{Ca}^{2+}$  leak in human cardiac pathology. *Circulation*. 128:970–981. <http://dx.doi.org/10.1161/CIRCULATIONAHA.113.001746>
- Gaughan, J.P., S. Furukawa, V. Jeevanandam, C.A. Hefner, H. Kubo, K.B. Margulies, B.S. McGowan, J.A. Mattiello, K. Dipla, V. Piacentino III, et al. 1999. Sodium/calcium exchange contributes to contraction and relaxation in failed human ventricular myocytes. *Am. J. Physiol.* 277:H714–H724.
- Gómez, A.M., H.H. Valdivia, H. Cheng, M.R. Lederer, L.F. Santana, M.B. Cannell, S.A. McCune, R.A. Altschuld, and W.J. Lederer. 1997. Defective excitation-contraction coupling in experimental cardiac hypertrophy and heart failure. *Science*. 276:800–806. <http://dx.doi.org/10.1126/science.276.5313.800>
- Gómez, A.M., S. Guatimosim, K.W. Dilly, G. Vassort, and W.J. Lederer. 2001. Heart failure after myocardial infarction: Altered excitation-contraction coupling. *Circulation*. 104:688–693. <http://dx.doi.org/10.1161/hc3201.092285>
- Gómez, A.M., B. Schwaller, H. Porzig, G. Vassort, E. Niggli, and M. Egger. 2002. Increased exchange current but normal  $\text{Ca}^{2+}$  transport via  $\text{Na}^+\text{-Ca}^{2+}$  exchange during cardiac hypertrophy after myocardial infarction. *Circ. Res.* 91:323–330. <http://dx.doi.org/10.1161/01.RES.0000031384.55006.DB>
- Györke, S., and D. Terentyev. 2008. Modulation of ryanodine receptor by luminal calcium and accessory proteins in health and cardiac disease. *Cardiovasc. Res.* 77:245–255. <http://dx.doi.org/10.1093/cvr/cvm038>
- Ingwall, J.S. 2006. On the hypothesis that the failing heart is energy starved: Lessons learned from the metabolism of ATP and creatine. *Curr. Hypertens. Rep.* 8:457–464. <http://dx.doi.org/10.1007/s11906-006-0023-x>
- Ingwall, J.S. 2009. Energy metabolism in heart failure and remodeling. *Cardiovasc. Res.* 81:412–419. <http://dx.doi.org/10.1093/cvr/cvn301>
- Kubo, H., K.B. Margulies, V. Piacentino III, J.P. Gaughan, and S.R. Houser. 2001. Patients with end-stage congestive heart failure treated with beta-adrenergic receptor antagonists have improved ventricular myocyte calcium regulatory protein abundance. *Circulation*. 104:1012–1018. <http://dx.doi.org/10.1161/hc3401.095073>
- Laver, D.R. 2006. Regulation of ryanodine receptors from skeletal and cardiac muscle during rest and excitation. *Clin. Exp. Pharmacol. Physiol.* 33:1107–1113. <http://dx.doi.org/10.1111/j.1440-1681.2006.04500.x>
- Laver, D.R. 2010. Regulation of RyR channel gating by  $\text{Ca}^{2+}$ ,  $\text{Mg}^{2+}$  and ATP. *Curr Top Membr.* 66:69–89. [http://dx.doi.org/10.1016/S1063-5823\(10\)66004-8](http://dx.doi.org/10.1016/S1063-5823(10)66004-8)
- Lindner, M., M.C. Brandt, H. Sauer, J. Hescheler, T. Böhle, and D.J. Beuckelmann. 2002. Calcium sparks in human ventricular cardiomyocytes from patients with terminal heart failure. *Cell Calcium*. 31:175–182. <http://dx.doi.org/10.1054/ceca.2002.0272>
- Lipp, P., and E. Niggli. 1996. Submicroscopic calcium signals as fundamental events of excitation–contraction coupling in guinea-pig cardiac myocytes. *J. Physiol.* 492:31–38. <http://dx.doi.org/10.1113/jphysiol.1996.sp021286>
- Lloyd-Jones, D.M. 2010. Cardiovascular risk prediction: Basic concepts, current status, and future directions. *Circulation*. 121:1768–1777. <http://dx.doi.org/10.1161/CIRCULATIONAHA.109.849166>
- Marx, S.O., S. Reiken, Y. Hisamatsu, T. Jayaraman, D. Burkhoff, N. Rosemblyt, and A.R. Marks. 2000. PKA phosphorylation dissociates FKBP12.6 from the calcium release channel (ryanodine receptor): Defective regulation in failing hearts. *Cell*. 101:365–376. [http://dx.doi.org/10.1016/S0092-8674\(00\)80847-8](http://dx.doi.org/10.1016/S0092-8674(00)80847-8)
- Meissner, G., E. Darling, and J. Eveleth. 1986. Kinetics of rapid calcium release by sarcoplasmic reticulum. Effects of calcium, magnesium, and adenine nucleotides. *Biochemistry*. 25:236–244. <http://dx.doi.org/10.1021/bi00349a033>
- Mercadier, J.J., A.M. Lompré, P. Duc, K.R. Boheler, J.B. Fraysse, C. Wisnewsky, P.D. Allen, M. Komajda, and K. Schwartz. 1990. Altered sarcoplasmic reticulum  $\text{Ca}^{2+}$ -ATPase gene expression in the human ventricle during end-stage heart failure. *J. Clin. Invest.* 85:305–309. <http://dx.doi.org/10.1172/JCI114429>
- Meyer, M., W. Schillinger, B. Pieske, C. Holubarsch, C. Heilmann, H. Posival, G. Kuwajima, K. Mikoshiba, H. Just, G. Hasenfuss, et al. 1995. Alterations of sarcoplasmic reticulum proteins in failing human dilated cardiomyopathy. *Circulation*. 92:778–784. <http://dx.doi.org/10.1161/01.CIR.92.4.778>
- Milliez, P., S. Messaoudi, J. Nehme, C. Rodriguez, J.L. Samuel, and C. Delcayre. 2009. Beneficial effects of delayed ivabradine treatment on cardiac anatomical and electrical remodeling in rat severe chronic heart failure. *Am. J. Physiol. Heart Circ. Physiol.* 296:H435–H441. <http://dx.doi.org/10.1152/ajpheart.00591.2008>
- Neubauer, S. 2007. The failing heart—an engine out of fuel. *N. Engl. J. Med.* 356:1140–1151. <http://dx.doi.org/10.1056/NEJMra063052>
- Pereira, L., J. Matthes, I. Schuster, H.H. Valdivia, S. Herzig, S. Richard, and A.M. Gómez. 2006. Mechanisms of  $[\text{Ca}^{2+}]_i$  transient decrease in cardiomyopathy of *db/db* type 2 diabetic mice. *Diabetes*. 55:608–615. <http://dx.doi.org/10.2337/diabetes.55.03.06.db05-1284>
- Pereira, L., G. Ruiz-Hurtado, E. Morel, A.C. Laurent, M. Métrich, A. Domínguez-Rodríguez, S. Lauton-Santos, A. Lucas, J.P. Benitah, D.M. Bers, et al. 2012. Epac enhances excitation–transcription coupling in cardiac myocytes. *J. Mol. Cell. Cardiol.* 52:283–291. <http://dx.doi.org/10.1016/j.yjmcc.2011.10.016>
- Perrier, E., B.G. Kerfant, N. Lalevee, P. Bideaux, M.F. Rossier, S. Richard, A.M. Gómez, and J.P. Benitah. 2004. Mineralocorticoid receptor antagonism prevents the electrical remodeling that precedes cellular hypertrophy after myocardial infarction. *Circulation*. 110:776–783. <http://dx.doi.org/10.1161/01.CIR.0000138973.55605.38>
- Piacentino, V., III, C.R. Weber, X. Chen, J. Weisser-Thomas, K.B. Margulies, D.M. Bers, and S.R. Houser. 2003. Cellular basis of abnormal calcium transients of failing human ventricular myocytes. *Circ. Res.* 92:651–658. <http://dx.doi.org/10.1161/01.RES.0000062469.83985.9B>
- Reiken, S., M. Gaburjakova, S. Guatimosim, A.M. Gómez, J. D’Armiento, D. Burkhoff, J. Wang, G. Vassort, W.J. Lederer, and A.R. Marks. 2003. Protein kinase A phosphorylation of the cardiac calcium release channel (ryanodine receptor) in normal and failing hearts. Role of phosphatases and response to isoproterenol. *J. Biol. Chem.* 278:444–453. <http://dx.doi.org/10.1074/jbc.M207028200>
- Ruiz-Hurtado, G., M. Fernández-Velasco, M. Mourelle, and C. Delgado. 2007. LA419, a novel nitric oxide donor, prevents pathological cardiac remodeling in pressure-overloaded rats via endothelial nitric oxide synthase pathway regulation. *Hypertension*. 50:1049–1056. <http://dx.doi.org/10.1161/HYPERTENSIONAHA.107.093666>

- Ruiz-Hurtado, G., A. Domínguez-Rodríguez, L. Pereira, M. Fernández-Velasco, C. Cassan, F. Lezoualc'h, J.P. Benitah, and A.M. Gómez. 2012a. Sustained Epac activation induces calmodulin dependent positive inotropic effect in adult cardiomyocytes. *J. Mol. Cell. Cardiol.* 53:617–625. <http://dx.doi.org/10.1016/j.yjmcc.2012.08.004>
- Ruiz-Hurtado, G., N. Gómez-Hurtado, M. Fernández-Velasco, E. Calderón, T. Smani, A. Ordoñez, V. Cachofeiro, L. Boscá, J. Díez, A.M. Gómez, and C. Delgado. 2012b. Cardiotrophin-1 induces sarcoplasmic reticulum Ca<sup>2+</sup> leak and arrhythmogenesis in adult rat ventricular myocytes. *Cardiovasc. Res.* 96:81–89. <http://dx.doi.org/10.1093/cvr/cvs234>
- Shorofsky, S.R., R. Aggarwal, M. Corretti, J.M. Baffa, J.M. Strum, B.A. Al-Seikhan, Y.M. Kobayashi, L.R. Jones, W.G. Wier, and C.W. Balke. 1999. Cellular mechanisms of altered contractility in the hypertrophied heart: Big hearts, big sparks. *Circ. Res.* 84:424–434. <http://dx.doi.org/10.1161/01.RES.84.4.424>
- Tencerová, B., A. Zahradníková, J. Gaburjáková, and M. Gaburjáková. 2012. Luminal Ca<sup>2+</sup> controls activation of the cardiac ryanodine receptor by ATP. *J. Gen. Physiol.* 140:93–108. <http://dx.doi.org/10.1085/jgp.201110708>
- Terentyev, D., I. Györke, A.E. Belevych, R. Terentyeva, A. Sridhar, Y. Nishijima, E.C. de Blanco, S. Khanna, C.K. Sen, A.J. Cardounel, et al. 2008. Redox modification of ryanodine receptors contributes to sarcoplasmic reticulum Ca<sup>2+</sup> leak in chronic heart failure. *Circ. Res.* 103:1466–1472. <http://dx.doi.org/10.1161/CIRCRESAHA.108.184457>
- Trafford, A.W., M.E. Díaz, and D.A. Eisner. 1998. Measurement of sarcoplasmic reticulum Ca content and sarcolemmal fluxes during the transient stimulation of the systolic Ca transient produced by caffeine. *Ann. NY Acad. Sci.* 853:368–371. <http://dx.doi.org/10.1111/j.1749-6632.1998.tb08302.x>
- Wagner, E., M.A. Lauterbach, T. Kohl, V. Westphal, G.S. Williams, J.H. Steinbrecher, J.H. Streich, B. Korff, H.T. Tuan, B. Hagen, et al. 2012. Stimulated emission depletion live-cell super-resolution imaging shows proliferative remodeling of T-tubule membrane structures after myocardial infarction. *Circ. Res.* 111:402–414. <http://dx.doi.org/10.1161/CIRCRESAHA.112.274530>
- Zima, A.V., E. Bovo, D.M. Bers, and L.A. Blatter. 2010. Ca<sup>2+</sup> spark-dependent and -independent sarcoplasmic reticulum Ca<sup>2+</sup> leak in normal and failing rabbit ventricular myocytes. *J. Physiol.* 588:4743–4757. <http://dx.doi.org/10.1113/jphysiol.2010.197913>

**Titre :** titre (en français)  $\text{Ca}^{2+}$  manutention dans un model de souris de CPVT

**Mots clés :** CPVT, RyR<sub>2</sub>, nœud sino-auriculaire

**Résumé :**

Le canal calcique de libération du  $\text{Ca}^{2+}$ , appelé récepteur à la ryanodine (RyR) est localisé dans la membrane du réticulum sarcoplasmique des cardiomyocytes, en incluant ceux du pacemaker, et a un rôle important dans le couplage excitation contraction et la génération du rythme cardiaque. Des mutations dans leur gène sont responsables de la tachycardie catécholergique (CPVT), qui est une maladie létale, manifestée par des syncopes ou mort subite lors de stress émotionnel ou physique. Au repos, ces patients ont un électrocardiogramme normal, mais une tendance plus importante à la bradycardie.

Nos collaborateurs ont identifié la mutation RyR<sub>2</sub><sup>R420Q</sup> dans une famille espagnole atteinte de CPVT. Nous avons construit une souris portant cette mutation et étudié l'activité du nœud sinoatrial (NSA, pacemaker principale) afin d'élucider les mécanismes.

Nous avons trouvé que les cellules du NSA présentent une activité spontanée plus lente que les souris sauvages (WT). Dans la cellule in situ, on peut étudier l'activité des RyRs par l'analyse des « sparks »  $\text{Ca}^{2+}$ , qui sont des événements élémentaires produits par l'activation d'un cluster des RyRs. Nos analyses en microscopie confocale sur des NSA disséquées on montré que la fréquence des sparks  $\text{Ca}^{2+}$  était légèrement augmentée. Par contre, la longueur de ces sparks est fortement prolongée dans les cellules KI. Ceci produit une libération plus importante de  $\text{Ca}^{2+}$  pendant la diastole dans les cellules KI qui réduit l'automatisme, en réduisant la charge en  $\text{Ca}^{2+}$  du réticulum sarcoplasmique et en inactivant le courant calcique type L. Donc les thérapies en étude qi favoriseraient la stabilisation du RyR2 en état fermé pourraient ne pas Être efficaces, et il faudra plutôt essayer des thérapies qui faciliteraient la fermeture du canal, une fois il est ouvert.

**Title :** Titre (en anglais)  $\text{Ca}^{2+}$  handling in a mice model of CPVT

**Keywords :** CPVT, RyR<sub>2</sub>, sinoatrial node

**Abstract :**

The cardiac type-2 ryanodine receptor (RyR2) encodes a  $\text{Ca}^{2+}$  release channel on sarcoplasmic reticulum (SR) membrane in cardiomyocytes, including sinoatrial node (SAN) myocytes, and releases  $\text{Ca}^{2+}$  required for contraction and SAN spontaneous rhythm. Its genetic defects are related to catecholaminergic polymorphic ventricular tachycardia (CPVT), which is a lethal heritable disease characterized by exercise/stress-induced syncope and/or sudden cardiac death. Interestingly, CPVT patients frequently present SAN dysfunction as bradycardia at rest.

In a previous study, a novel CPVT-related RyR<sub>2</sub> mutation (RyR<sub>2</sub><sup>R420Q</sup>) in a Spanish family, associated with SAN dysfunction was reported. R420 is located at the N-terminal portion of the channel and seems to be an important site for maintaining a stable A/B/C domain of N-terminus in RyR<sub>2</sub>. As N-terminal

mutation resultant RyR<sub>2</sub> behaviour and SAN function are never analyzed before, we created the KI mice model bearing mutation R420Q to understand the underlying mechanism.

In this thesis, we found increased  $\text{Ca}^{2+}$  release during diastole, indicating a gain-of-function effect of RyR<sub>2</sub> N-terminal mutation R420Q. Interestingly, this defect may not be only an enhanced activity, as the  $\text{Ca}^{2+}$  sparks frequency was only slightly increased in KI, but also the closing mechanism, producing longer  $\text{Ca}^{2+}$  sparks. That is, the number of  $\text{Ca}^{2+}$  sparks is increased by the RyR<sub>2</sub><sup>R420Q</sup> mutation, and meanwhile the amount of  $\text{Ca}^{2+}$  released in each  $\text{Ca}^{2+}$  spark is also dramatically enhanced. This increased  $\text{Ca}^{2+}$  release retards SR  $\text{Ca}^{2+}$  replenishment, disrupting the  $\text{Ca}^{2+}$  clock and the coupled clock, resulting in the slower SAN function. Thus favouring RyR stabilization in the closing state might not be an adequate therapy but accelerating its closure.